

ELUCIDATING THE FUNCTIONAL IMPLICATIONS OF HISTONE ACYLATION IN ADIPOGENESIS AND HEPATIC STEATOSIS

A Thesis Submitted for the Degree of

Doctor of Philosophy

By

Aditya Bhattacharya



To

Molecular Biology and Genetics Unit,
Jawaharlal Nehru Centre for Advanced Scientific Research,
(A Deemed University)
Jakkur, Bangalore-560064, India.

March 2022

DECLARATION

I hereby declare that this thesis entitled “**Elucidating the functional implications of histone acylation in adipogenesis and hepatic steatosis**” is an authentic record of research work carried out by me under the supervision of Prof. Tapas K. Kundu at the Molecular Biology and Genetics Unit, Jawaharlal Nehru Centre for Advanced Scientific Research, Bangalore- 560064, India and this work has not been submitted elsewhere for the award of any other degree.

In keeping with the general practice of reporting scientific observations, due acknowledgements have been made wherever the work described was based on the findings of other investigators. Any omission, which might have occurred by oversight or misjudgment, is regretted.

Place – Bangalore

Date: 21/3/2022

Aditya Bhattacharya

Aditya Bhattacharya



जवाहरलाल नेहरु उन्नत वैज्ञानिक अनुसंधान केन्द्र
(मान्यता प्राप्त विश्वविद्यालय)
JAWAHARLAL NEHRU CENTRE FOR ADVANCED SCIENTIFIC RESEARCH
(A Deemed University)
जक्कूर, बेंगलूर - 560 064, भारत / Jakkur P.O., Bengaluru - 560 064. INDIA

Prof. Tapas K Kundu
Transcription and Disease Laboratory,
Molecular Biology and Genetics Unit,
Jawaharlal Nehru Centre for Advanced Scientific Research,
Bangalore-560064, India

CERTIFICATE

This is to certify that the work described in this thesis entitled, “**Elucidating the functional implications of histone acylation in adipogenesis and hepatic steatosis**” is a result of the investigations carried out by Mr. Aditya Bhattacharya in Molecular Biology and Genetics Unit, Jawaharlal Nehru Centre for Advanced Scientific Research (A Deemed University), Bangalore-560064, India, under my supervision, and the results presented in this thesis have not previously formed the basis for the award of any other diploma, degree or fellowship.

Date: March 9, 2022

Place: Bangalore 560064

Prof. Tapas K Kundu

Acknowledgements

I am grateful to my mentor Prof. Tapas Kumar Kundu for his guidance throughout this long journey of my PhD. He has been a visionary with great ambition that led to the initiation of this challenging new project in the laboratory. While the project was at its incipient stage, there were several obstacles that came up and the hurdles never stopped coming along the way. However, his unwavering belief in me along with his continuous encouragement enabled me to overcome the obstacles and reach the point where I am today.

I would like to thank Prof. M.R.S. Rao, Prof. Maneesha Inamdar, Prof. Uday Kumar Ranga, Prof. Anuranjan Anand, Prof. Namita Surolia, Prof. Hemalatha Balaram, Prof. Ravi Manjithaya, Prof. James Cheliah and Dr. Kushagra Bansal for their constructive criticism and inputs related to my work that helped to improve several aspects of the project. A special vote of thanks needs to be given to Prof. Umesh Varshney, IISc along with Prof. Ranga, Prof. Manjithaya and Prof. Cheliah for the ideas generated from our discussion in my comprehensive examination that had ultimately led me towards the path of studying adipogenesis.

I am thankful to Prof. K.V. Sashidhara, Dr. Rajdeep Guha and Prof. Amir Nazir from CSIR, CDRI for their valuable assistance in my project. I would also like to thank Dr. R.G. Prakash for his help regarding animal experiments and Suma madam and Keerthana of imaging facility for their help in confocal microscopy related work. I thank Mr. Madavan Vasudevan for his help in bioinformatics related analysis and Dr. Nagashayana Natesh for providing the raw materials that formed the basis of my research work.

During this long and challenge riddled journey, I have had the opportunity of being taught by some highly knowledgeable seniors in the laboratory. I am especially thankful to Dr. Parijat Senapati, under whose tutelage I started work in the laboratory; Dr. Sourav Chatterjee, who has remained a constant source of support for my work; Dr. Amit Kumar Behera, who generously got me involved in his own work and introduced me to the field of adipogenesis; and Dr. Sadhan Das, who I was fortunate to work with in a serendipitous turn of events. He has been a

huge inspiration for me due to his ability to balance a disciplined hard work ethic with an attitude to enjoy the “researcher’s” life for whatever it throws at you. I am also thankful to Dr. Amrutha Swaminathan, Dr. Stephanie Kaypee, Dr. Sweta Sikder, Dr. Arnab Bose, Dr. Suchismita Dey, Dr. Sharmistha Halder Sinha and Dr. Shrinka Sen, Deepthi and Dr. Surabhi Sudevan for their advice about my work. Moreover, I am grateful to my laboratory colleagues Dr. Pallabi Mustafi, Siddharth, Akash, Smitha, Moumita, Dharaneeswar, Ila and Vinay for all the good times we had together. Special mention needs to be made of Mune Gowda, Sunil, Kruthi and Salauddin without whose help; the laboratory would not remain functional.

I am thankful to University Grants Commission and J.C. Bose fellowship for the financial assistance, without which this journey would have remained highly improbable.

During my stay in JNCASR, I have also been able to make friends with several people from outside the laboratory. I shall cherish the good memories I had with Dr. Arindam Ray, Utsa, Kajal, Disha, Asutosh, Srilaxmi, Arun, Raktim, Dr. Iyer Aditya Mahadevan, Dr. Gaurav Barve, Dr. Krishnendu Guin, Dr. Vijay Jayraman, Sambhavi, Dr. Saloni Sinha, Rajarshi, Preeti, Alice, Arijit, Dr. Abhilash Laxman, Monoj, Anaranya, Monodeep and Dr. Sourav Mondal.

Finally, I thank my parents Baba and Ma who were always supportive of me for whatever decision I have made till date. Their moral support enabled me to persist through the most difficult times, for which I shall forever be indebted to them.

CONTENTS

Declaration	i
Certificate	ii
Acknowledgements	iii
Chapter 1: Introduction	1
1.1 Post-translational modifications of histones	3
1.2 Histone modifications dependent on metabolite flux	5
1.3 Chromatin methylation	8
1.3.1 Lysine methylation	8
1.3.2 Lysine demethylation	9
1.3.3 Metabolic regulation of lysine methylation	9
1.3.4 DNA methylation and demethylation	13
1.3.5 Arginine methylation	14
1.3.6 Gene expression regulation by chromatin methylation and their physiological consequences	17
1.4 Reversible acetylation of chromatin	19
1.4.1 Histone acetylation	19
1.4.2 Histone deacetylation	21
1.4.3 Family of KATs	23
1.4.4 Molecular mechanism of acetylation	24
1.4.5 Structural organization of master epigenetic enzyme p300/KAT3B	26
1.4.6 Dynamicity of acetylation-deacetylation	27
1.4.7 Gene expression regulation by chromatin acetylation and its physiological consequences	28
1.5 Other emerging epigenetic modifications	30
1.5.1 Histone homocysteinylation	31
1.5.2 Histone monoaminylation	32
1.5.3 Histone O-GlcNacylation	33
1.5.4 Histone ADP-ribosylation	34
1.5.5 Non-enzymatic modifications of histones	35
1.5.6 RNA modifications	37
1.6 Paradigm shift in histone modifications- discovery of acylation	39
1.7 Methods for identification of new acylation modifications	40
1.8 The epigenetic processors of acylation	41

1.8.1 Acylation writers	41
1.8.2 Acylation readers	44
1.8.3 Acylation erasers	46
1.9 Physiological significance of histone acylation	47
1.10 Possible metabolic sources for acylation	52
1.10.1 Competition of other acyl CoA derivatives with acetyl CoA	53
1.10.2 Possible pathways for increased generation of acyl CoAs	54
1.11 Background and rationale of the study	56
1.12 Objectives of the Study	57
Chapter 2: Materials and Methods	59
2.1 General methods	62
2.2 Protein expression and purification	65
2.2.1 Purification of full length hexa histidine-tagged p300 from Sf21 insect cells infected with baculovirus of recombinant p300	65
2.2.2 Purification of hexa histidine-tagged p300 catalytic domain from E. coli	66
2.2.3 Generation of point mutant of p300 catalytic domain C1438A	67
2.3 In vitro enzymatic assays	68
2.3.1 In vitro acetylation and filter binding assay	68
2.3.2 In vitro butyrylation assay	69
2.4 Adipogenesis assay	69
2.5 Hepatic steatosis assay	71
2.6 MTT assay	72
2.7 RNA expression analysis	72
2.7.1 Total RNA isolation	72
2.7.2 cDNA synthesis	73
2.7.3 Quantitative real time PCR	74
2.7.4 Transcriptomics analysis by RNA sequencing	74
2.8 Histone extraction	76
2.8.1 Acid extraction of histones from cultured mammalian cells	76
2.8.2 Acid extraction of histones from mice epididymal fat pads	76
2.9 Chromatin immunoprecipitation	77
2.10 Isolation and derivatization of compounds from Garcinia indica	79
2.10.1 Isolation of garcinol from Garcinia indica	79

2.10.2 Synthesis of isogarcinol	79
2.10.3 Synthesis of LTK-14 and LTK-14A	80
2.10.4 X-ray crystal structure determination of LTK-14A	82
2.11 Molecular docking analysis	84
2.12 Animal experiments	84
2.12.1 High fat diet induced obesity in mice	84
2.12.2 Genetically obese mice (db/db)	85
2.12.3 Hematoxylin and eosin staining of liver and adipose tissue	86
2.12.4 Picrosirius Red staining of liver	87
2.12.5 Immunofluorescence staining of liver	88
2.13 Mass spectrometry	88
2.13.1 Targeted analysis of butyryl CoA by Ultra performance liquid chromatography coupled with time-of-flight mass spectrometer (Q-TOF LC/MS)	88
2.13.2 Untargeted analysis of intracellular metabolites by Ultra-performance liquid chromatography coupled with time-of-flight mass spectrometer (Q-TOF LC/MS)	90
2.14 Generation and characterization of H4K5 butyrylation antibody	91
Chapter 3: p300 mediated histone butyrylation is critical for adipogenesis	94
3.1 Background	96
3.1.1 Adipose tissue and obesity	96
3.1.2 Molecular origins of adipose tissue	100
3.1.3 Chromatin landscape of adipogenesis	102
3.1.4 Inhibitors of p300 acetyltransferase activity	107
3.1.4.1 Bisubstrate inhibitors	108
3.1.4.2 Inhibitors from natural sources (semisynthetic modulators of p300)	109
3.1.4.3 Synthetic inhibitors	112
3.1.4.4 Bromodomain inhibitors	114
3.2 Results	115
3.2.1 Search for a selective inhibitor of p300 butyryltransferase activity	115
3.2.2 Understanding the structural basis for selective inhibition of EP300 catalysed butyrylation by LTK-14A by molecular docking	119
3.2.3 Validation of molecular docking by site directed mutagenesis	122
3.2.4 Butyryl CoA levels are higher in adipocytes compared to pre-adipocytes	126

3.2.5 Histone butyrylation increases during adipogenesis	127
3.2.6 Histone butyrylation increases in the promoters of pro-adipogenic genes during adipogenesis	129
3.2.7 LTK-14A is metabolically stable, cell permeable and inhibits adipogenesis without causing toxic effects	130
3.2.8 LTK-14A inhibits adipogenesis by mainly repressing the expression of lipogenic genes including the master regulators of adipogenesis	132
3.2.9 LTK-14A represses gene expression by specific inhibition of histone butyrylation without affecting acetylation	139
3.2.10 LTK-14A prevents obesity and adipocyte hypertrophy in mice fed with high fat diet by specific inhibition of histone butyrylation without affecting acetylation in adipose tissues	141
3.2.11 LTK-14A reverses obesity and adipocyte hypertrophy in genetically obese mice by specific inhibition of histone butyrylation without affecting acetylation in adipose tissues	146
3.2.12 LTK-14A prevents adipocyte hypertrophy by repression of lipogenic genes and not by browning of fat	150
Chapter 4: p300 mediated histone butyrylation is critical for hepatic steatosis	157
4.1 Background	159
4.1.1 Non-alcoholic fatty liver disease	159
4.1.2 Pathways leading to fatty liver disease manifestation	161
4.1.2.1 Increased release of fatty acids into liver from direct excessive food consumption and from adipose tissue stores	161
4.1.2.2 Increased de novo synthesis of fatty acids and triacylglycerides	162
4.1.2.3 Impaired export of lipids	162
4.1.2.4 Impaired β oxidation of fatty acids	162
4.1.2.5 Oxidative stress and inflammatory response	163
4.1.3 Epigenetic regulation of NAFLD	165
4.1.3.1 Lysine methylation and demethylation in hepatic steatosis	166
4.1.3.2 Lysine acetylation in hepatic steatosis	167
4.1.3.3 Lysine deacetylation in hepatic steatosis	171
4.2 Results	172
4.2.1 Histone butyrylation increases with hepatic steatosis in HepG2	172
4.2.2 LTK-14A inhibits glucose induced steatosis in HepG2 cells without having any toxic effect	174

4.2.3 LTK-14A inhibits steatosis of HepG2 by repressing the expression of lipogenic genes	176
4.2.4 LTK-14A represses gene expression by specific inhibition of histone butyrylation without affecting acetylation in HepG2	177
4.2.5 LTK-14A prevents hepatic steatosis in mice fed with high fat diet by specific inhibition of histone butyrylation without affecting acetylation in liver	178
4.2.6 LTK-14A prevents hepatic steatosis in genetically obese mice by specific inhibition of histone butyrylation without affecting acetylation in liver	181
4.2.7 LTK-14A is metabolically stable and is bio-available in its intact form in liver	185
4.2.8 Application of LTK-14A for prevention of liver fibrosis	187
Discussion	190
Publications and Patents	205
References	206
Annexure	247

Acknowledgements

I am grateful to my mentor Prof. Tapas Kumar Kundu for his guidance throughout this long journey of my PhD. He has been a visionary with great ambition that led to the initiation of this challenging new project in the laboratory. While the project was at its incipient stage, there were several obstacles that came up and the hurdles never stopped coming along the way. However, his unwavering belief in me along with his continuous encouragement enabled me to overcome the obstacles and reach the point where I am today.

I would like to thank Prof. M.R.S. Rao, Prof. Maneesha Inamdar, Prof. Uday Kumar Ranga, Prof. Anuranjan Anand, Prof. Namita Surolia, Prof. Hemalatha Balaram, Prof. Ravi Manjithaya, Prof. James Cheliah and Dr. Kushagra Bansal for their constructive criticism and inputs related to my work that helped to improve several aspects of the project. A special vote of thanks needs to be given to Prof. Umesh Varshney, IISc along with Prof. Ranga, Prof. Manjithaya and Prof. Cheliah for the ideas generated from our discussion in my comprehensive examination that had ultimately led me towards the path of studying adipogenesis.

I am thankful to Prof. K.V. Sashidhara, Dr. Rajdeep Guha and Prof. Amir Nazir from CSIR, CDRI for their valuable assistance in my project. I would also like to thank Dr. R.G. Prakash for his help regarding animal experiments and Suma madam and Keerthana of imaging facility for their help in confocal microscopy related work. I thank Mr. Madavan Vasudevan for his help in bioinformatics related analysis and Dr. Nagashayana Natesh for providing the raw materials that formed the basis of my research work.

During this long and challenge riddled journey, I have had the opportunity of being taught by some highly knowledgeable seniors in the laboratory. I am especially thankful to Dr. Parijat Senapati, under whose tutelage I started work in the laboratory; Dr. Sourav Chatterjee, who has remained a constant source of support for my work; Dr. Amit Kumar Behera, who generously got me involved in his own work and introduced me to the field of adipogenesis; and Dr. Sadhan Das, who I was fortunate to work with in a serendipitous turn of events. He has been a

huge inspiration for me due to his ability to balance a disciplined hard work ethic with an attitude to enjoy the “researcher’s” life for whatever it throws at you. I am also thankful to Dr. Amrutha Swaminathan, Dr. Stephanie Kaypee, Dr. Sweta Sikder, Dr. Arnab Bose, Dr. Suchismita Dey, Dr. Sharmistha Halder Sinha and Dr. Shrinka Sen, Deepthi and Dr. Surabhi Sudevan for their advice about my work. Moreover, I am grateful to my laboratory colleagues Dr. Pallabi Mustafi, Siddharth, Akash, Smitha, Moumita, Dharaneeswar, Ila and Vinay for all the good times we had together. Special mention needs to be made of Mune Gowda, Sunil, Kruthi and Salauddin without whose help; the laboratory would not remain functional.

I am thankful to University Grants Commission and J.C. Bose fellowship for the financial assistance, without which this journey would have remained highly improbable.

During my stay in JNCASR, I have also been able to make friends with several people from outside the laboratory. I shall cherish the good memories I had with Dr. Arindam Ray, Utsa, Kajal, Disha, Asutosh, Srilaxmi, Arun, Raktim, Dr. Iyer Aditya Mahadevan, Dr. Gaurav Barve, Dr. Krishnendu Guin, Dr. Vijay Jayraman, Sambhavi, Dr. Saloni Sinha, Rajarshi, Preeti, Alice, Arijit, Dr. Abhilash Laxman, Monoj, Anaranya, Monodeep and Dr. Sourav Mondal.

Finally, I thank my parents Baba and Ma who were always supportive of me for whatever decision I have made till date. Their moral support enabled me to persist through the most difficult times, for which I shall forever be indebted to them.

INTRODUCTION

Introduction

The following chapter introduces basic concepts on the most well characterized post-translational modifications of histones and their association with cellular metabolism. It also discusses in detail the new acylation modifications that have been recently discovered along with their physiological relevance with respect to gene expression regulation.

1.1 Post-translational modifications of histones

1.2 Histone modifications dependent on metabolite flux

1.3 Chromatin methylation

1.3.1 Lysine methylation

1.3.2 Lysine demethylation

1.3.3 Metabolic regulation of lysine methylation

1.3.4 DNA methylation and demethylation

1.3.5 Arginine methylation

1.3.6 Gene expression regulation by chromatin methylation and its physiological consequences

1.4 Chromatin acetylation

1.4.1 Histone acetylation

1.4.2 Histone deacetylation

1.4.3 Family of KATs

1.4.4 Molecular mechanism of acetylation

1.4.5 Structural organization of master epigenetic enzyme p300/KAT3B

1.4.6 Dynamicity of acetylation-deacetylation

1.4.7 Gene expression regulation by chromatin acetylation and its physiological consequences

1.5 Other emerging epigenetic modifications

1.5.1 Histone homocysteinylation

1.5.2 Histone monoaminylation

1.5.3 Histone O-GlcNacylation

1.5.4 Histone ADP-ribosylation

1.5.5 Non-enzymatic modifications of histones

1.5.6 RNA modifications

1.6 Paradigm shift in histone modifications- discovery of acylation

1.7 Methods for identification of new acylation modifications

1.8 The epigenetic processors of acylation

1.8.1 Acylation writers

1.8.2 Acylation readers

1.8.3 Acylation erasers

1.9 Physiological significance of histone acylation

1.10 Possible metabolic sources for acylation

1.10.1 Competition of other acyl CoA derivatives with acetyl CoA

1.10.2 Possible pathways for increased generation of acyl CoAs

1.11 Background and rationale of the study

1.12 Objectives of the Study

1.1 Post-translational modifications of histones

All the cells of any living organism consist of near-identical DNA. However, these cells have different morphology and functions because the genetic information encoded within the DNA gets processed and expressed differently in different cells. This is because the genomic DNA resides within a nucleoprotein complex called chromatin that packages and organizes the genome. The functional subunit of chromatin is called the nucleosome. Each nucleosome core particle is composed of 147 base pairs of DNA wrapped around positively charged proteins called histones by forming electrostatic interactions (Luger *et al*, 1997). There are four canonical histones H2A, H2B, H3 and H4 that are present as two functional copies apiece in each nucleosome. These histones dimerize through histone fold domains that stabilize the structure of the nucleosome octamer (Kornberg *et al*, 1974). A subset of nucleosome further associates with the linker histone H1 to form the chromatosome (Figure 1) (Simpson *et al*, 1978). The histones are small globular proteins whose N-terminal extensions protrude out from the larger nucleosome structure. These extensions are commonly referred to as histone tails, which due to their amino acid composition and accessibility can serve as a platform for several reversible chemical modifications called post-translational modifications (Allis *et al*, 2016). The packaging state of the chromatin can serve as a barrier that can restrict the access of different molecular factors to the genome. The post-translational modifications can regulate the chromatin architecture by two ways. Firstly, they can change the intrinsic chemical properties of the chromatin by charge neutralization or imparting a different charge. Secondly, these modifications can serve as docking sites for several proteins that can further recruit effectors such as transcription factors, histone chaperones, chromatin modifiers and chromatin remodelers. All these processes can individually or synergistically influence the local and global structure of the genome organization.

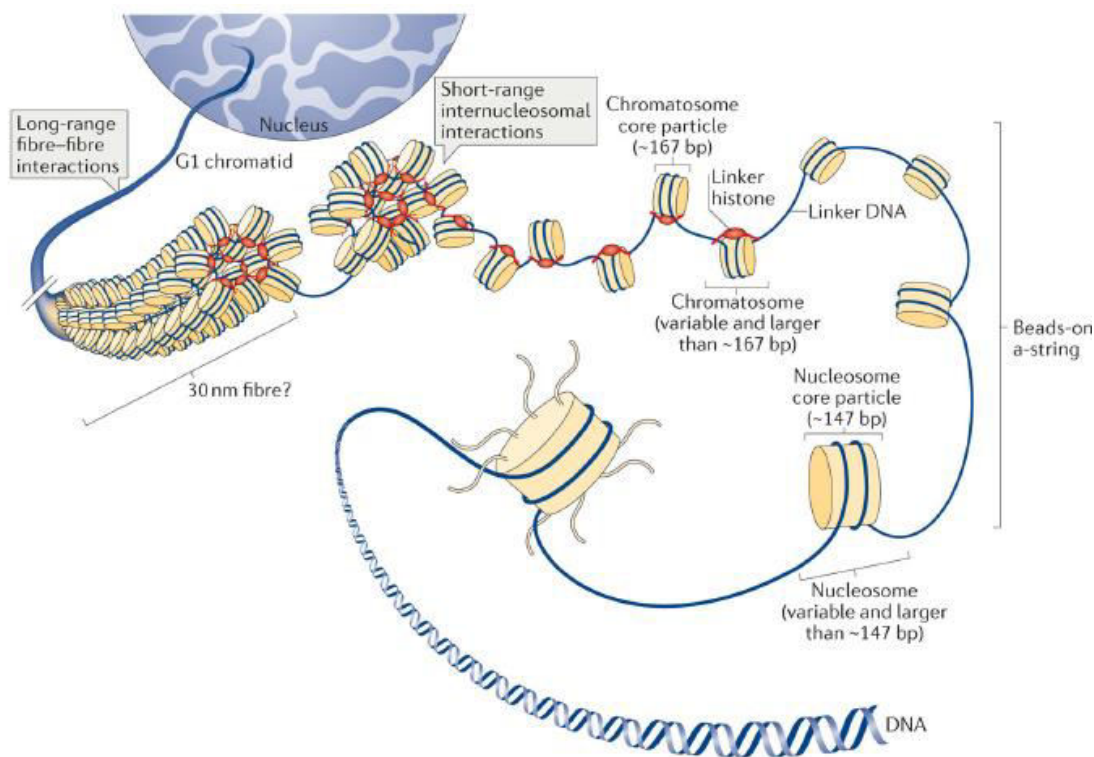


Figure 1: Cartoon diagram illustrating the different levels of chromatin organization in the interphase nucleus. It begins with the association of the core histones and DNA to form the nucleosome, followed by the association of linker histone H1 to form the chromatosome, “beads on a string arrangement” of the core particles, further folding to form the debatable 30 nm fibre and long range interactions between fibres to form chromatin territories. (Adapted from Fyodorov *et al*, Nat Rev Mol Cell Biol, 2018).

The histones have been known to undergo a vast number of post-translational modifications which include acetylation, acylation, methylation, phosphorylation, ubiquitylation, hydroxylation, seronylation, glycation, glycosylation, sumoylation and ADP-ribosylation (Li, X. *et al*, 2018) (Figure 2). Similar to histones, the DNA can also be chemically modified in the form of methylation at cytosine and adenine residues (Wu *et al*, 2016). The modifications could be brought about by enzymes, or they could happen non-enzymatically by covalent addition of electrophilic moieties, derived from different metabolic pathways. Interestingly, RNA can also get methylated and acetylated that regulates RNA processing, half-life and translation and these are called epitranscriptomic modifications (Arango

et al, 2018; Yue *et al*, 2015). Collectively, all these modifications are known as the chemical epigenome which play diverse roles in regulation of gene expression.

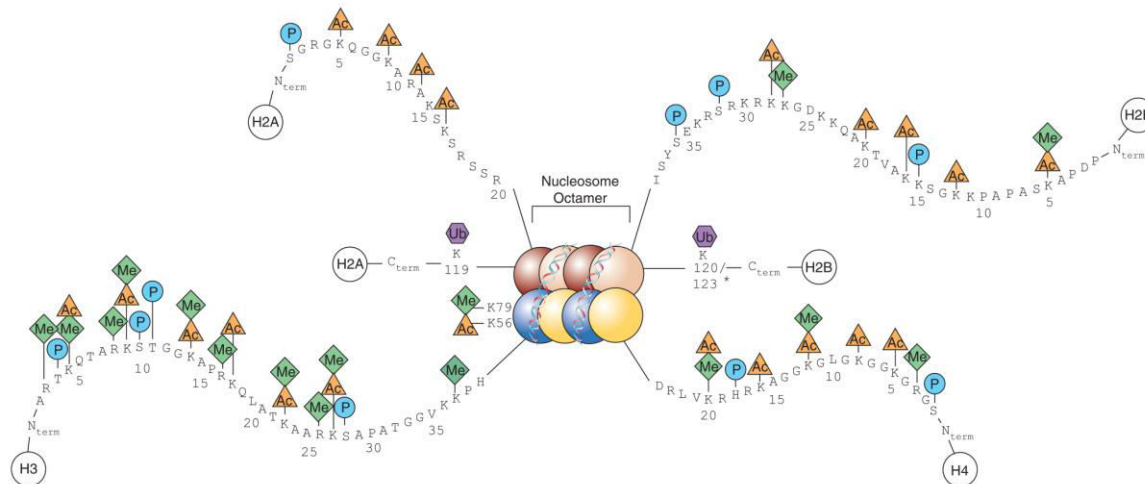


Figure 2: Cartoon diagram depicting the different well known and characterized post-translational modifications of canonical core histones. Abbreviations: Ac – Acetylation, Me – Methylation, P – Phosphorylation, Ub – Ubiquitination. (Adapted from Keppler *et al*, Expert Opin Ther Targets, 2008)

The enzymes that catalyze modifications on the chromatin are commonly termed as ‘writers’ and the proteins that recognize these groups are called ‘readers’. The ‘reader’ proteins have domains that impart specificity for recognizing different chemical groups and they in turn recruit downstream factors to carry out specific functions at the genomic loci marked by the modifications. Playing an antagonistic role is another group of enzymes called ‘erasers’ which remove the groups deposited by the ‘writers’. A dynamic interplay exists between the two groups which shape the chromatin landscape by establishing permissive and repressive regions in the genome, orchestrating transcription of genes.

1.2 Histone modifications dependent on metabolite flux

Histone modifications are carried out by a plethora of metabolites, the intracellular abundance of which can directly impact the extent of the modifications. Metabolites that directly enter the cells could actively or passively diffuse through the nuclear membrane and modify the chromatin. Alternatively,

different intermediates of several metabolic reactions catalyzed by metabolic enzymes could serve as cofactors for chromatin modifications (Figure 3, Table 1). Under certain circumstances, the metabolic enzymes could themselves translocate into the nucleus and regulate transcription of genes at specific loci by modifying histones (Nagaraj *et al*, 2017). The metabolites whose cellular concentrations are either close to or less than the Michaelis Menten constant (K_m) values of their corresponding enzymes are more susceptible to be used in metabolically driven epigenetic modification reactions (Reid *et al*, 2017). The thermodynamic and kinetic properties of acetyltransferases and methyltransferases are responsible for making them the most suitable enzymes whose catalytic activities are dictated by metabolite flux.

Since the metabolites can serve as cofactors for different histone modifications, they are indirectly responsible for regulating the gene expression pattern which ultimately has a significant effect on the physiological state of the cells.

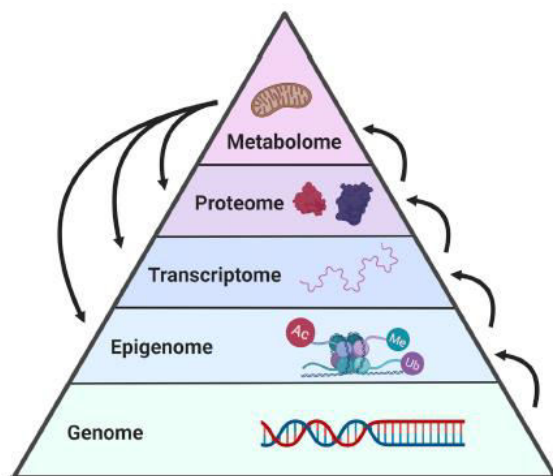


Figure 3: Traditional dogma of molecular biology depicting the hierarchy of regulatory processes inside the cell. As each process from the bottom dictates the fate of each process immediately above, new evidences are emerging of feedback mechanisms, further complicating the network. (Adapted from Ly *et al*, Cell Metabolism, 2020)

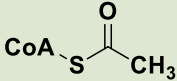
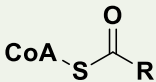
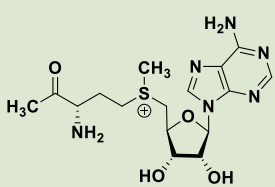
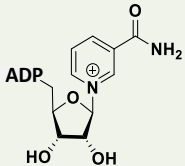
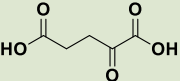
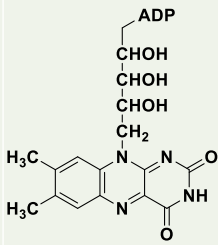
Cofactor	Structure	Associated metabolic pathways	Protein modification	Reader proteins
Acetyl CoA		Glycolysis, TCA cycle, fatty acid oxidation, amino acid metabolism, acetate metabolism	Lysine acetylation	Bromodomain, YEATS, DPF
Acyl CoA		Fatty acid metabolism, ketogenesis, Warburg effect, amino acid catabolism	Lysine acylation	YEATS, DPF
SAM		One carbon metabolism (methionine and folate cycle), phospholipid biosynthesis	Lysine methylation, DNA methylation	Chromodomain, PHD, Tudor, PWWP, TTD, MBD
NAD+		Amino acid catabolism, Preiss-Handler pathway, NAM salvage pathway	Lysine deacetylation, lysine deacylation, lysine ADP-ribosylation	Bromodomain, YEATS, DPF, PBZ, WWE, Macrodomain
Alpha-ketoglutarate		TCA cycle, amino acid metabolism	Histone demethylation, DNA demethylation	Chromodomain, PHD, Tudor, PWWP, TTD, MBD
FAD		TCA cycle, oxidative phosphorylation	Lysine demethylation	Chromodomain, PHD

Table 1: List of different cofactors, derived from various metabolic pathways, that drive epigenetic modifications.

1.3 Chromatin methylation

1.3.1 Lysine methylation

Histones can be methylated on two amino acid residues- lysine and arginine. Unlike acetyl group, the methyl group is too small to cause chromatin decompaction on its own. However, there can be multiple combinations of methylation that gives rise to a much greater complexity in gene regulation, because there are different reader proteins with different effector functions for different methylation patterns and neighboring amino acid combinations. Each lysine residue can be mono-, di- or trimethylated and considering that there are 8 lysine residues known to be methylated, there could be a possible 4.3×10^9 permutations for this sole modification, with different downstream consequences (Figure 4). As for example, H3K4me3 is considered as an activation mark because it gets recognized by PHD containing transcription factors which promote chromatin remodeling and pre-initiation complex formation in transcription start sites (Li *et al*, 2006; Wysocka *et al*, 2006; Lauberth *et al*, 2013). On the other hand, H3K9me2/3 is considered as a repression mark because it gets recognized by chromodomain containing heterochromatin protein 1 alpha (HP1 α) that induces transcriptional silencing by establishment of constitutive heterochromatin (Eissenberg *et al*, 2014). Lysine trimethylation is usually associated with transcriptional activation while mono- and dimethylation could lead to either activation or repression. In general, methylation at H3K4, H3K36 and H3K79 are taken as signatures for activation while methylation at H3K9, H3K27 and H4K20 are signatures for repression, even though there are a few exceptions.

All lysine methyltransferases are characterized by the presence of the SET domain (Suppressor of Variegation, Enhancer of Zeste, Trithorax) (Lachner *et al*, 2002), except for DOT 1L (Feng *et al*, 2002). This enzyme methylates histone at H3K79 residue that has implications in telomere silencing (Lacoste *et al*, 2002). This is also a case of exception from histone modifications occurring usually on N-terminus of histone tails.

1.3.2 Lysine demethylation

Based on their cofactor usage, there are two groups of lysine demethylases that are responsible for active removal of methyl groups from lysine residues. They are lysine specific demethylase (LSD) and jumonji C (JmjC) domain containing demethylase (Figure 4) (Kooistra *et al*, 2012). LSDs require FAD as a cofactor for oxidation dependant removal of methyl group from the ϵ -amine, leading to reduction of FAD to FADH₂ and release of the methyl group as formaldehyde (Shi *et al*, 2004). As this type of reaction requires the presence of lone pair electrons on the amine group, LSDs can only bring about demethylation of mono- and dimethylated amines. JmjC demethylases on the other hand require alpha-ketoglutarate (α -KG) and iron (II) for dioxygenase type removal of methyl groups. They are capable of demethylating all three methylated states of amine groups (Anand *et al*, 2007).

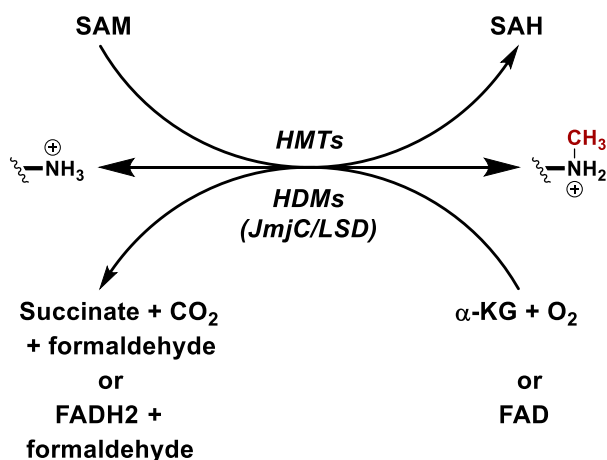


Figure 4: Enzyme reaction diagram of reversible lysine methylation and demethylation in histones. Abbreviations: SAM – S-Adenosyl methionine, SAH – S-Adenosyl homocysteine, HMT- Histone methyltransferase, HDM- Histone demethylase, FAD – Flavin adenine dinucleotide. (Adapted from Haws *et al*, Trends Biochem Sci, 2020)

1.3.3 Metabolic regulation of lysine methylation

Methylation in mammals is dependent on the supply of methyl groups in the form of the essential amino acid methionine, which is obtained solely from diet. In fact,

methionine is abundant in protein rich food items such as meat, fish and eggs while it is present in far lower amounts in plants. Therefore, people on plant based diets have lower circulating methionine levels in their blood leading to reduced methylation of the genome. Surprisingly, despite the correlative changes in methylation patterns, there does not seem to be too much adverse effects on the concerned individuals. This has led to the proposition of the hypothesis that the chromatin is flexible enough to accommodate these metabolite-linked perturbations in methyl group supply by ensuring methylation of the critical regions of the genome in all kinds of conditions (Haws *et al*, 2020). Besides restriction based diets (eg. diets with low methionine content), high energy diets (rich in fat and sugar) can also drastically alter the methylation pattern as has been seen in the liver of SM/J mice made obese on high fat diet (Keleher *et al*, 2018). Moreover, in type 2 diabetes mellitus, associated with chronic energy intake, there occurs hypermethylation in the promoters of genes required for proper functioning of pancreatic β cells which leads to abnormally high expression of glycated hemoglobin A1c, a signature of high glucose levels in blood of diabetic individuals (Davegårdh *et al*, 2018).

The cofactor used for chromatin methylation is S-Adenosyl Methionine (SAM) which is produced from methionine by ATP dependant methyladenosine transferases (MATs) (Markham *et al*, 2018). There are mainly two known MATs – MATI α which is expressed only in liver and MATII α which is ubiquitously expressed in all tissues (Markham *et al*, 2018). There exists a third enzyme MATII β which is the regulatory partner of MATII α (Halim *et al*, 1999; LeGros *et al*, 2000). It reduces the binding affinity of MATII α for methionine and also makes it susceptible to product inhibition. The synthesis of SAM by the MAT enzymes forms the core of once carbon metabolism where folate and methionine metabolic pathways converge, making it a focal point for regulation of chromatin methylation via metabolism (Figure 5A) (Sanderson *et al*, 2019). Limiting the availability of SAM by disrupting the catabolism of threonine to glycine, a SAM precursor, causes widespread reduction of H3K4 di/trimethylation in mouse embryonic stem cells (Shyh-Chang *et al*, 2013). Similar perturbations in SAM availability leading to changes in methylation pattern have been observed in the

cases of H3K4me3 in human embryonic stem cells (Shiraki *et al*, 2014), mouse liver and human colon cancer cells (Dai *et al*, 2018; Mentch *et al*, 2015) and *C. elegans* (Ding *et al*, 2018); H3K9me1/2/3 in human colon cancer cells and mouse liver (Haws *et al*, 2020); H3K27me3 in mouse embryonic stem cells (Sperber *et al*, 2015), H3K36me3 in macrophages (Sinclair *et al*, 2019) and T cells (Roy *et al*, 2020) along with several methylation marks in yeast (Ye *et al*, 2017; Ye *et al*, 2019). All these alterations in methylation levels led to changes in gene expression. Another way by which metabolism affects lysine methylation is by regulation of activities of different epigenetic enzymes. JmjC demethylases require alpha-ketoglutarate as a cofactor. Therefore, structural analogues of this molecule which could competitively bind with the enzyme would reduce its activity leading to dysregulated chromatin methylation. In different types of cancer (glioma, melanoma and acute myeloid leukemia) there have been occurrences of mutations in isocitrate dehydrogenase genes *IDH1* and *IDH2*, as a result of which the enzymes convert alpha-ketoglutarate to 2-hydroxyglutarate (Xu *et al*, 2011). This molecule binds to the same site of the demethylases as alpha-ketoglutarate and brings about genome wide changes in methylation patterns. Moreover, loss of function mutations in succinate and fumarate dehydrogenases, which are enzymes downstream of isocitrate dehydrogenase in the TCA cycle, lead to accumulation of succinate and fumarate that have the same effect on the demethylases as the oncometabolite 2-hydroxyglutarate (Figure 5B) (Xiao *et al*, 2012; Letouzé *et al*, 2013; Cervera *et al*, 2009). Since iron is another cofactor used by these demethylases, the activity of these enzymes and downstream methylation can also be affected by iron deficiency (Jiang *et al*, 2019).

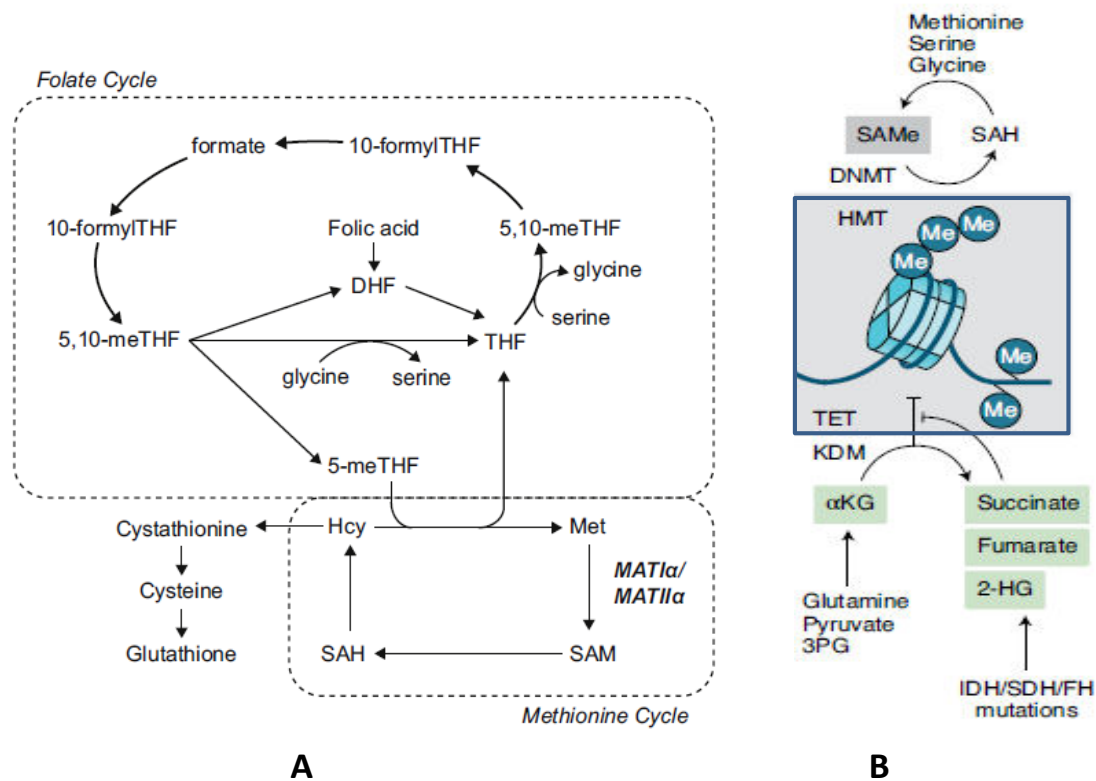


Figure 5: (A) Basic scheme of the metabolic reactions involved in SAM biosynthesis and utilization (Adapted from Haws *et al*, Trends Biochem Sci, 2020). (B) Metabolite driven epigenetic regulation by lysine methylation of histones (Adapted from Boon *et al* Nat Metab, 2020).

Oxygen levels in the cells have also been found to regulate methylation pattern although the detailed underlying mechanisms are still not clear. In *C. elegans*, during early stages of development there is generation of reactive oxygen species (ROS) which modulates the expression of several genes required for long term survival by inhibiting the H3K4 methyltransferase MLL1, 2, 3 and 4 activities leading to reduced H3K4 trimethylation levels (Bazopoulou *et al*, 2019). It has been assumed that the ROS generation affects the activity of enzyme methionine synthase, further affecting downstream methylation. Hypoxia has been found to affect the activity of JmjC demethylases KDM5A, KDM6A and KDM6B resulting in increased methylation of chromatin (Chakraborty *et al*, 2019; Batie *et al*, 2019).

1.3.4 DNA methylation and demethylation

In addition to histone proteins, the nitrogenous bases of DNA can also be methylated. The most observed and studied among them in the eukaryotic systems is cytosine methylation at sixth carbon position. In recent times, another base modification – N⁶ adenine methylation has also been gaining importance in the mammalian system as an important regulatory epigenetic mark. DNA methylation is carried out by DNA methyltransferases 3A and 3B (DNMT3A and DNMT3B) at promoters of actively transcribed genes as well as repetitive DNA elements (Figure 5) (Greenberg *et al*, 2019). In the promoter regions, DNA methylation mainly occurs at CpG islands – which are regions in the genome with high abundance of CpG dinucleotides (Deaton *et al*, 2011). It is usually associated with repression of gene expression whereby DNA methylation marks serve as recruitment sites for proteins that promote heterochromatinization (H3K9 methyltransferases and histone deacetylases) (Yin *et al*, 2017; Estève *et al*, 2006; Myant *et al*, 2011; Deplus *et al*, 2002; Fuks *et al*, 2000; Hendrich *et al*, 1998; Meehan *et al*, 1989). There are also exceptional instances of DNA methylation serving as a derepressor whereby DNA methylation displaces PRC2 (polycomb repressor complex) and promotes gene expression (Holoch *et al*, 2017).

DNA methylation can be passively removed in due course of time through serial rounds of replication but there is a class of enzymes called TETs (ten eleven translocation DNA demethylase) that are responsible for active removal of methylation marks from DNA (Figure 6). These enzymes require iron (II) and alpha-ketoglutarate for performing their dioxygenase type demethylation reactions. These TETs catalyze several rounds of 5-methyl cytosine oxidation before thymine DNA glycosylase (TDG) and base excision repair pathways completely remove the base and replace it with a new unmodified cytosine in the DNA sequence (Wu *et al*, 2017).

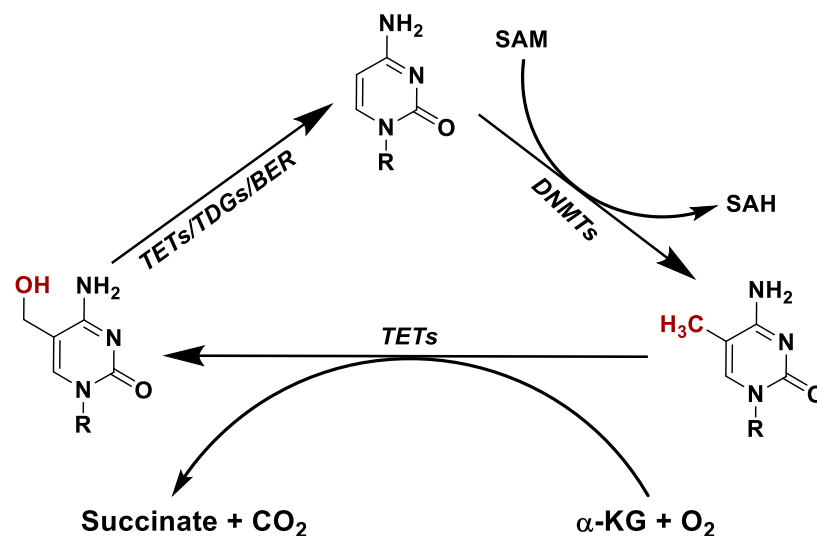


Figure 6: Enzyme reaction diagram of reversible DNA methylation and demethylation. Abbreviations: TET- Ten eleven translocation DNA demethylase, TDG- Thymine DNA glycosylase, BER- Base excision repair. (Adapted from Haws *et al*, Trends Biochem Sci, 2020)

1.3.5 Arginine methylation

Arginine methylation has been found to occur on a vast number of proteins and is highly unique because of the presence of five potential hydrogen bond donors in the guanidinium group that can form hydrogen bond with various partners in different orientations. In fact, arginine residues are the most frequent hydrogen bond donors to the phosphate backbone of DNA as well as to the bases thymine, guanine and adenine (Luscombe *et al*, 2001). Methylation of any of the donors could influence the interaction of histones with certain binding partners by not only changing the shape of the modified residue but also by blocking hydrogen bond formation (Bedford *et al*, 2000). Methylation of arginine could also increase its binding affinity with reader proteins having an aromatic cage by cationic pi-pi interactions (Hughes *et al*, 2006).

Three distinct types of arginine methylation are found in nature (Figure 7). The most common is asymmetric dimethylation in which two methyl groups are added to a single terminal nitrogen atom in the guanidinium group (omega-N^G, N^G-dimethyl arginine). The other two are symmetric dimethylation, in which a methyl group is added to each of the two terminal nitrogen atoms (omega-N^G,N^{G'}-

dimethyl arginine); and monomethylation, in which a single methyl group is added to one of the terminal nitrogen atoms (omega-N^G-monomethyl arginine). Depending on the type of methylation catalyzed by the enzyme, arginine methyltransferases have been classified into four groups- Type I, II, III and IV. All these enzymes are commonly known as PRMTs (Protein Arginine Methyltransferase) and are characterized by the presence of a motif containing seven beta strands (Katz *et al*, 2003) as well as the additional “double E” and “CHW” motifs (Cheng *et al*, 2005). Type I, II and III PRMTs can all catalyze monomethylation of terminal (ω) nitrogen atoms in the guanidinium groups. Additionally, type I PRMTs can induce asymmetric dimethylation, type II PRMTs induce symmetric dimethylation and type III can only monomethylate. A fourth type of monomethylation has been reported in yeast in which an internal (δ) nitrogen atom of the guanidinium group gets methylated. The enzyme RMT2 performs this reaction (Nieumierzycka *et al*, 1999) and is the only known methyltransferase to do so, making it the sole type IV PRMT.

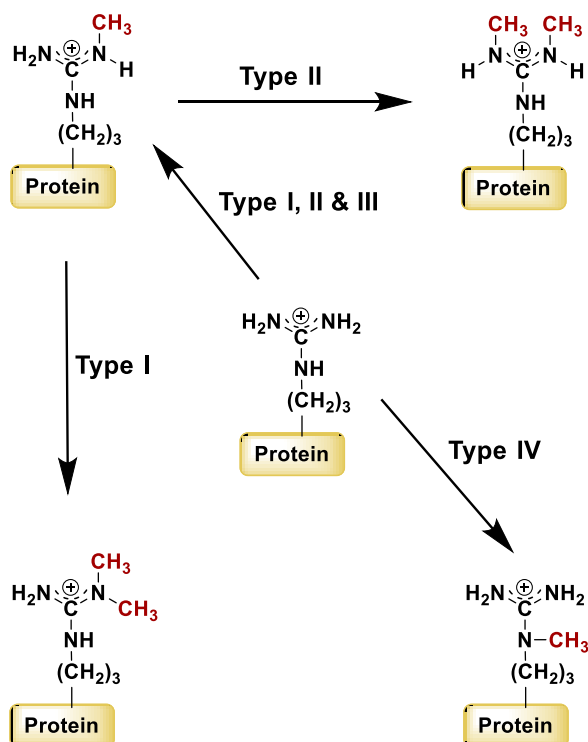


Figure 7: Enzyme reaction diagram of different types of arginine methylation. (Adapted from Bedford *et al*, Mol Cell, 2009)

Till date, there are no known arginine demethylases capable of catalyzing reversible removal of methyl groups from arginine, but there are some lysine specific demethylases that have also exhibited arginine demethylase activity (Walport *et al*, 2016; Li, S. *et al*, 2018). Arginine methylation can also be permanently removed by peptidylarginine deiminase to form citrulline (Figure 8) (Raijmakers *et al*, 2007). In recent times, a third mechanism for this modification removal has been discovered which involves proteolytic cleavage of histone tails. The Jumonji C domain containing proteins JMJD5 and JMJD7 can cleave the histone tails in a cation dependant manner and then chop up the released fragments containing the methyl arginine groups (Liu, H. *et al*, 2017).

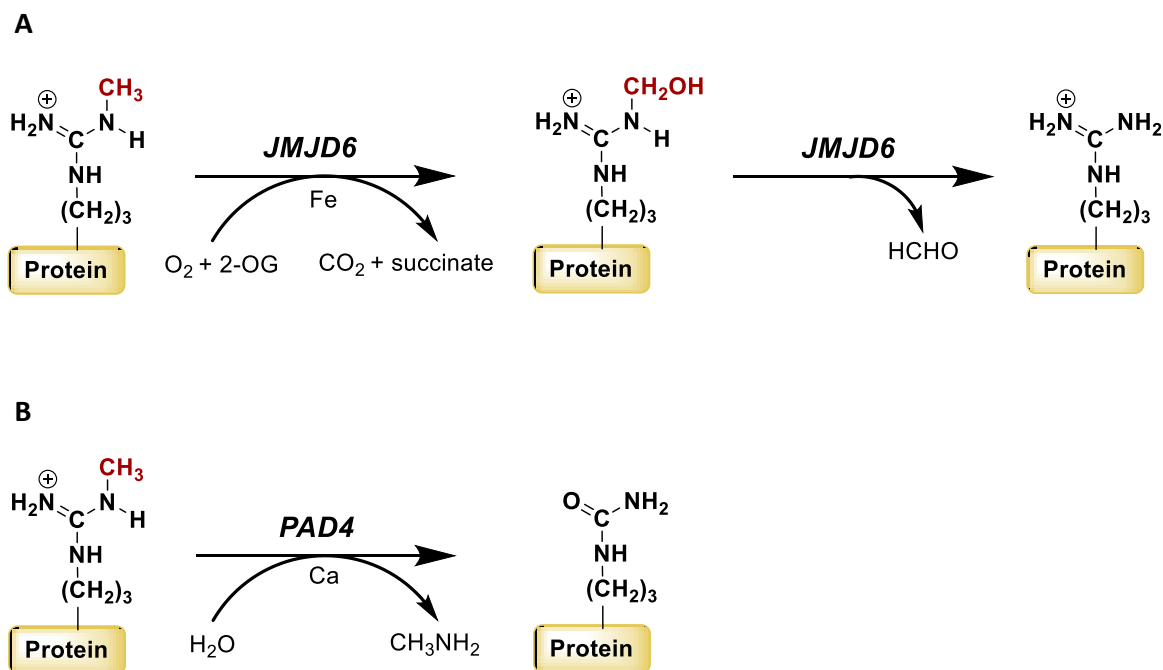


Figure 8: Enzyme reaction diagram of different types of arginine demethylation. Abbreviations: JMJD- Jumonji C domain containing demethylase, PAD4- Peptidylarginine deiminase.

Removal of arginine methylation releases monomethyl arginine (MMA) and asymmetric dimethylarginine (ADMA) which can serve as competitive inhibitors

for nitric oxide synthase and arginase (Liu *et al*, Nitric Oxide, 2018). Both these enzymes utilize L-arginine as a substrate to produce nitric oxide and L-citrulline or ornithine and urea respectively. Treatment of patients with type I PRMT inhibitors reduces global levels of mono- and asymmetric dimethylation. As a result, there are fewer amounts of MMA and ADMA generated by demethylation and the activities of NO synthase and arginase can go on unhindered. On the other hand, treatment with type II PRMT inhibitors leads to higher generation of MMA and ADMA due to greater utilization of SAM by type I PRMTs (Dhar *et al*, 2013). The excess load of MMA and ADMA can be a risk factor for cardiovascular and renal diseases. The molecule nitric oxide has been found to play important regulatory roles in cancer as well as immune systems (Inoue *et al*, 2018; Infantino *et al*, 2010; Geoghegan *et al*, 2015; Infantino *et al*, 2017; Litzler *et al*, 2019; Somasundaram *et al*, 2019). Therefore, there could be interesting link between the metabolic regulation of arginine methylation and these physiological processes with NO serving as the connecting factor.

1.3.6 Gene expression regulation by chromatin methylation and its physiological consequences

The nutritional status of the cells can have an impact on their lineage determination in cells by modulating the expression of genes involved in induced pluripotency (Folmes *et al*, 2011), maintenance of stemness (Tsogetbaatar *et al*, 2020) or commitment to differentiation into particular cell types (Takubo *et al*, 203). Disruption of one carbon metabolism can affect the intracellular levels of SAM which leads to changes in the pattern of histone and DNA methylation. Such changes have been found to drastically alter the expression pattern of stemness related genes in both cell line (Shyh-Chang *et al*, 2013) and mice models (Tang *et al*, 2017). Moreover, the activity of the demethylases JHDM and TET is dependent on alpha Ketoglutarate/succinate ratio, any fluctuation in which can also change the chromatin methylation pattern and modulate gene expression, resulting in changes in cell lineage fate (Carey *et al*, 2015; TeSlaa *et al*, 2016).

A large number of immune cells can undergo metabolic reprogramming upon activation which is also associated with changes in chromatin methylation state.

Antigen receptor engagement in T cells increases their metabolic flux which alters the methylation state of the chromatin. Elevated levels of SAM leads to increased H3K4 trimethylation in the promoters of immune response related genes in CD4+ T cells (Roy *et al*, 2020). Lipopolysachharide induced inflammation activated macrophages also exhibit elevated SAM levels with increased H3K36 trimethylation associated with increased IL-1 β synthesis (Yu *et al*, 2019). Glutaminolysis generates alpha Ketoglutarate which is utilized by JHDM demethylase for removal of repressive methylation marks in specific activation loci of the genome within M2 macrophages for endotoxin clearance (Liu, P.S. *et al*, 2017). Conversely, tumor cells have been found to secrete glutamate which immunologically suppresses the activity of the neighboring T cells. JHDM activity is also dependant on iron availability and it has been observed that iron supplementation improves B cell dependent humoral response in vaccinated patients while iron deficiency suppresses the response due to reduced JHDM activity resulting in enhanced levels of repressive H3K9 methylation in the promoter of cyclin E, an important player in the process of B cell proliferation (Jiang *et al*, 2019).

Histone methylation regulated gene expression has been studied in the context of several diseases, especially cancer. Cancer is associated with increased glycolytic flux due Warburg effect, hypoxia and dysregulated amino acid metabolism, all of which can impact SAM levels (Chakraborty *et al*, 2019; Thienpont *et al*, 2016). Tumor initiating cells exhibit the property of enhanced methionine cycle activity with increased H3K4 trimethylation and activation of cancer associated genes (Dai *et al*, 2018). Oncogenic driver mutations have been observed in the genes encoding isocitrate dehydrogenase *IDH1* and *IDH2* in at least seven types of cancer which depletes alpha Ketoglutarate levels and thereby affects the activity of JHDM demethylases resulting in hypermethylation and repression of genes responsible for maintaining tumor suppression (Bailey *et al*, 2018).

1.4 Reversible acetylation of chromatin

1.4.1 Histone acetylation

Histone acetylation takes place on the ϵ amino group of lysine residues. The enzymes that catalyse acetylation were commonly known as HATs (histone acetyltransferases). As a large number of non-histone proteins also get acetylated by them, the new nomenclature refers to these enzymes as lysine acetyltransferases (KAT). The HATs/KATs have been broadly divided into two classes based on their subcellular localization and have been numbered from KAT1 to KAT13D. Class A consists of the most abundant nuclear KATs which modify histones and chromatin associated proteins. Based on structural homology to yeast orthologues, substrate specificity and catalytic mechanism these enzymes are further subdivided into the following classes- GNAT superfamily, MYST family, p300/CBP family, TFIIC family and Nuclear receptor coactivator family (Sterner *et al*, 2000). There are a few additional proteins that have been found to possess acetyltransferase activity but they do not belong to any particular group. These include transcription factor associated complexes, nuclear receptor coactivators and circadian rhythm related protein CLOCK. All these KATs are characterized by the presence of a bromodomain that enables them to recognize acetylated lysines. The class B consists of cytosolic KATs which lack a bromodomain and acetylate newly synthesized histones within the cytoplasm. Once these acetylated histones enter the nucleus, they are incorporated within the chromatin after their acetylation marks are removed. Hat1 and Hat2 are two well known examples of type B KATs (Roth *et al*, 2001).

Histone acetylation has usually been associated in promoting gene transcription. It does so by two distinct yet complementary mechanisms – (1) by neutralizing the positive charge of lysine residues, thereby reducing the electrostatic interaction between positively charged histones and negatively charged phosphate backbone of DNA which makes the chromatin less densely packaged and more suitable for transcription factor recruitment; and (2) by serving as a ligand for acetylation reader proteins.

The cofactor required for acetylation is the high energy metabolite acetyl CoA. It consists of an acetyl group linked to Coenzyme A through an energy rich thioester bond, providing the chemical basis for it to take part in several anabolic reactions like fatty acid synthesis and steroidogenesis, along with histone acetylation. In fed state, the primary source of acetyl CoA within the cells is glucose which undergoes glycolysis to produce pyruvate that enters the mitochondria for TCA cycle. There, acetyl CoA is produced from pyruvate by the pyruvate dehydrogenase multienzyme complex (PDC) (Figure 9). Besides this, acetyl CoA can also be generated within the mitochondria by fatty acid oxidation, amino acid degradation and also from free acetate by acyl coenzyme A synthetase short chain family members 1 and 3 (ACSS 1 and 3) (Fan, J. *et al*, 2015). The mitochondria do not have their own acetyl CoA exporter. So, at first it is combined with oxaloacetate to produce citrate that escapes the mitochondria via the citrate shuttle. Inside the cytoplasm, acetyl CoA is regenerated by ATP citrate lyase and this is one of the major contributing pathways contributing to nucleocytosolic pool of acetyl CoA (Sivanand *et al*, 2017). In addition, ACSS2 and PDC (pyruvate dehydrogenase complex) can also contribute to generation of nuclear pool of acetyl CoA (Sivanand *et al* 2018; Sutendra *et al*, 2014; Mews *et al*, 2017). During starvation conditions, free fatty acids are converted to their corresponding CoAs which enter the mitochondria via the carnitine shuttle and then undergo β oxidation to produce acetyl CoA (Sebastián *et al*, 2017; Bose *et al*, 2019; McDonnell *et al*, 2016). Short chain fatty acid acetate can directly be used in the nucleus by ACSS2 to produce acetyl CoA (Liu *et al*, Cell, 2018). Both acetate and acetyl CoA have also been found to be produced from ethanol metabolism within the liver that leads to enhanced acetylation in the brain (Mews *et al*, 2019).

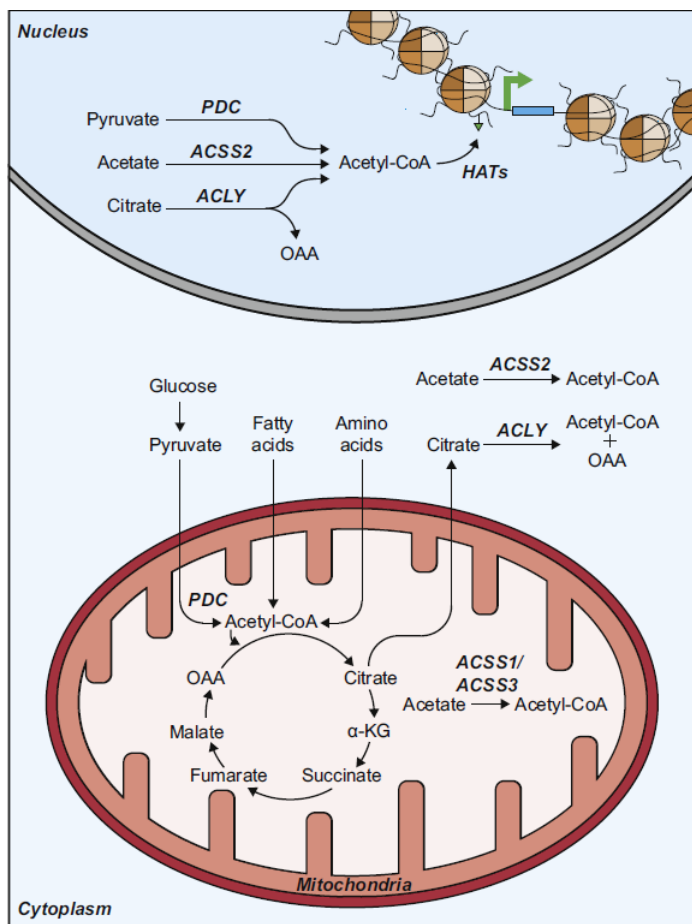


Figure 9: Basic scheme of the metabolic reactions involved in generation of acetyl CoA within the cell. Abbreviations: PDC- Pyruvate dehydrogenase complex, ACSS2- Acyl coenzyme A synthetase short chain family member 2, ACLY- ATP citrate lyase, HAT- Histone acetyltransferase. (Adapted from Haws *et al*, Trends Biochem Sci, 2020)

1.4.2 Histone deacetylation

Histone acetylation is a reversible modification which is removed by a class of enzymes called HDACs (histone deacetylases). Based on structural organization, they are divided into four classes – Class I, II, III and IV (Figure 10). Only class III HDACs, also known as sirtuins, utilize NAD^+ as a metabolic cofactor; while the other three classes are zinc (Zn^{2+}) ion dependant. Sirtuins have been so named for their sequence homology to the yeast HDAC silent information regulator 2 (Sir2). There are seven mammalian sirtuins in total that perform diverse biological functions. Sirtuins 3-5 play important roles within the mitochondria. SIRT1, SIRT2,

SIRT6 and SIRT7 can induce deacetylation of histones within the nucleus (Feldman *et al*, 2012; Jing *et al*, 2015).

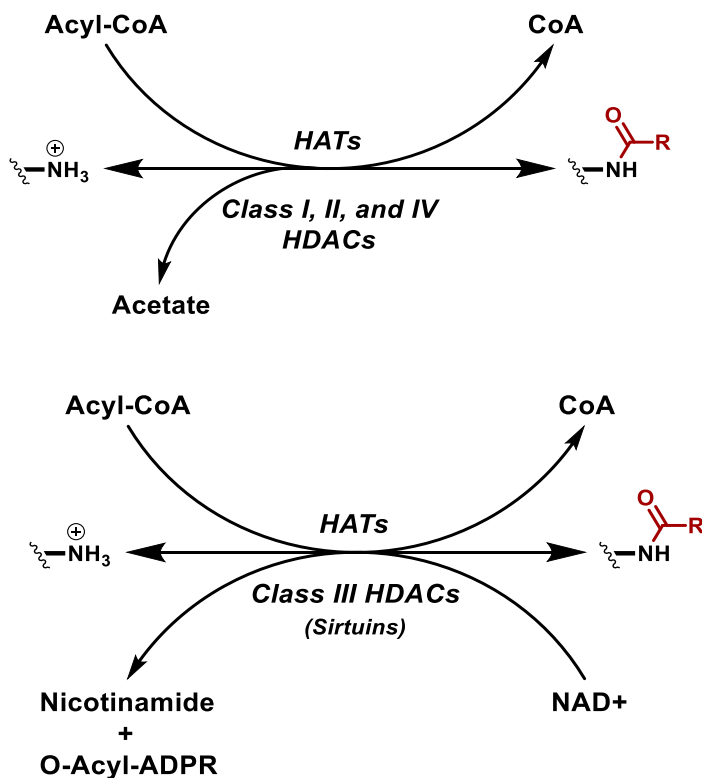


Figure 10: Enzyme reaction diagram showing reversible acetylation and deacetylation. Abbreviations: HAT- Histone acyltransferase, HDAC- Histone deacetylase. (Adapted from Haws *et al*, Trends Biochem Sci, 2020)

The sirtuin activity is not determined by the oxidation state of the cells reflected by the NAD⁺:NADH ratio, but it is rather dependant directly on the NAD⁺ levels (Mouchiroud *et al*, 2013; Belenky *et al*, 2007; Ho *et al*, 2009; Brown *et al*, 2014). NAD⁺ is produced within the cells by three pathways- (1) *de novo* synthesis from tryptophan, (2) Preiss-Handler pathway, both of which are minor contributors; and (3) salvage pathway from NAM (produced due to cleavage of nicotinamide glycosidic bond of NAD during deacetylation), which is the major contributor for NAD⁺ pools (Verdin *et al*, 2015; Revollo *et al*, 2004).

There are emerging evidences indicating that besides NAD, there could be other metabolites which could regulate Sirtuin activity in a context dependant manner.

Long chain fatty acids have been shown to stimulate deacetylase activities (Feldman *et al*, 2013). Mono-unsaturated fatty acids are transported by the carrier protein perilipin to the nucleus where they can enhance the deacetylase activity of SIRT1 leading to activation of its co-regulator PGC1 α (peroxisome proliferator activated receptor gamma coactivator 1 alpha) (Najt *et al*, 2020). In addition, non-fatty acid small molecules have also been found to promote activities of SIRT1 and SIRT6 (Hubbard *et al*, 2014).

Interestingly, the Zn²⁺ dependant Class I and II HDACs are susceptible to inhibition by short chain fatty acids butyrate and β -hydroxybutyrate which are produced from fatty acid oxidation/synthesis, ketogenesis and also from fermentation of fibres by intestinal microbiota (den Besten *et al*, 2013; Krautkramer *et al*, 2016).

1.4.3 Family of KATs

The best understood amongst the different acetyltransferases is the GNAT (GCN5 related N-acetyltransferase) superfamily. It is so named after the founding member of the family GCN5. It was first discovered in ciliate *Tetrahymena thermophila* by performing in gel assay with nuclear extracts wherein a 55 kDa polypeptide was found to acetylate histones (Brownell *et al*, 1995). Subsequent protein sequencing revealed it to be a homolog of yeast Gcn5 (General Control Nonderepressible 5) which was previously known as a transcriptional adaptor, mediating interaction between several activators and transcription complexes. Other important and well-studied members of this group include PCAF (p300/CBP associated factor), Hat1, Hpa2 and Elp3. The next family is the p300/CREB-binding protein family which is the most versatile and potent among the acetyltransferases. These proteins are regarded as master regulators of gene expression with well documented functions in various cellular processes such as differentiation, disease, transcription, replication, repair, apoptosis cell survival and death (Kalkhoven *et al*, 2004). The third group is the MYST family, named after its founding members MOZ, Ybf2/Sas3, Sas2 and Tip60. Each of these enzymes has important roles in differentiation and disease. The nuclear receptor coactivator family includes acetyltransferases that are implicated in transcriptional activation involving hormonal signals. Its best studied member is

SRC- 1 (Steroid Receptor Coactivator 1) which brings about ligand induced activation in association with several hormonal receptors, namely progesterone receptor, glucocorticoid receptor, estrogen receptor and thyroid hormone receptor (Spencer *et al*, 1997). Other two members of this family are ACTR and TIF2, both of which share many structural features with SRC-1, although acetyltransferase activity of the later has not been proven yet. There are two groups of acetyltransferases that are transcription factor related. One of the TAF_{II} (TATA-Binding Protein [TBP] associated factor) subunits of TFIID (a general factor required for the assembly of RNA polymerase II) itself possesses acetyltransferase activity (Mizzen *et al*, 1996). The homologues of this protein TAF_{II}250 in humans, TAF_{II}230 in *Drosophila* and Taf_{II}145/130 in *Saccharomyces cerevisiae*, have all been shown to have acetyltransferase activity. TFIIC is a general transcription factor of RNA polymerase III that has acetyltransferase ability. Three of its nine subunits- TFIIC90, TFIIC110 and TFIIC220 have been confirmed to possess this catalytic activity (Hsieh *et al*, 1999). In addition, the circadian rhythm associated protein CLOCK has also been found to possess acetyltransferase activity (Doi *et al*, 2006).

Histones H3 and H4 are predominantly acetylated by these enzymes, although there are evidences of p300/CBP acetylating all four canonical core histones.

1.4.4 Molecular mechanism of acetylation

Histone acetylation is essentially a bi-substrate reaction involving the transfer of acetyl group from the pseudo-substrate acetyl CoA to the ϵ amino group of lysine residue on histone substrate (Figure 11). The kinetics of acetylation reaction varies among the different enzymes. Among them, GCN5 and PCAF follow a sequential bi-bi kinetic mechanism whereby the enzyme binds first to the acetyl CoA and then the histone peptide, which is followed by the release of the acetylated histone and finally the CoA molecule (CoASH) (Tanner *et al*, Biochemistry, 2000; Tanner *et al*, J Biol Chem, 2000). On the other hand, p300/CBP family proteins follow a ping-pong bi-bi mechanism in which it binds to the acetyl CoA, releases the CoASH, then binds to the histone, transfers the acetyl group to its lysine residue and finally releases the acetylated histone (Thompson

et al, 2001). However, X-ray crystallographic studies with supporting biochemical evidences proved that p300 too forms a very short-lived ternary complex with histone and acetyl CoA (Liu *et al*, 2008). This unique mode of catalysis is called Theorell-Chance mechanism. The yeast acetyltransferase Rtt109 has been found to follow random ternary kinetics as it has no preference in binding first to any particular substrate (Albaugh *et al*, 2010).

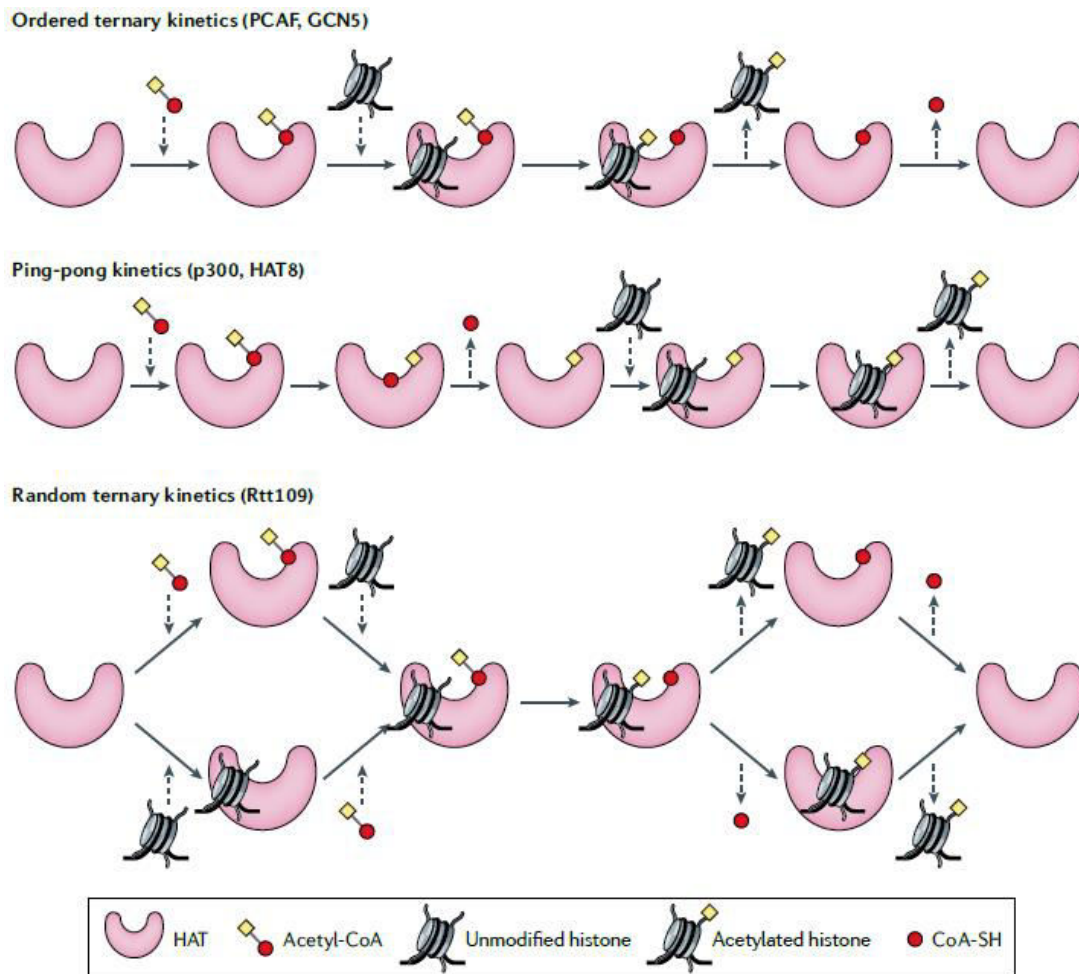


Figure 11: Cartoon diagram depicting different types of acetylation reaction mechanisms (Adapted from Dai *et al*, Nat Rev Genet. 2020)

1.4.5 Structural organization of master epigenetic enzyme p300/KAT3B

Pharmacological targeting of epigenetic enzymes for regulating gene expression and thereby the related physiological processes, has remained an attractive strategy to treat diseases. The master epigenetic enzyme p300 plays diverse roles in several biological processes by interacting with a plethora of transcription factors and coactivators. p300 is a modular protein with several well defined domains from the amino to carboxy terminus – nuclear receptor interaction domain (NRID), kinase-inducible domain of CREB-interacting domain (KIX), bromodomain (Bd), really interesting new gene (RING), plant homeodomain (PHD), histone acetyltransferase domain (HAT), ZZ-type zinc finger domain (ZZ), transcription adaptor zinc finger domain 2 (TAZ2) and IRF3 binding domain (IBiD) (Figure 12) (Goodman *et al*, 2000). The polypeptide segment encompassing RING-PHD domain is also collectively called CH2 domain and the ZZ-TAZ2 region is called CH3 domain. These domains are responsible for mediating interaction of p300 with its binding partners. They are interlinked by long stretches of intrinsically disordered residues to the catalytic core of p300 that is comprised of the bromodomain, CH2 region and the HAT domain. This central core of p300 is involved in binding with the acetyl CoA cofactor and is structurally similar to the core of other members of acetyltransferase families of GNAT (Trievel *et al*, 1999) and MYST (Yan *et al*, 2002). The flanking regions are relatively more diverse in terms of structural organization. The HAT domain performs the function of acetylating p300 substrates while bromodomain helps in recognition of already acetylated substrates (Zeng *et al*, 2008; Mujtaba *et al*, 2004). Besides, the bromodomain is also required for binding with unmodified substrates as loss of this domain impairs p300 catalytic activity and specificity (Ragvin *et al*, 2004; Manning *et al*, 2001). The CH2 region contains a PHD domain that helps in recognition of trimethylated histone (H3K4me3) as well as unmodified histone tails (Ragvin *et al*, 2004; Sanchez *et al*, 2011).

There are two interesting structural features of p300 that distinguish it from the rest of the KATs (lysine acetyltransferases). The first one is its acetyl CoA binding pocket that is buried much deeper inside compared to other KATs. This is mainly

because of an L1 loop that is unique to p300 and covers one side of acetyl CoA and contributes almost one-third of the protein-cofactor interactions (Wang *et al*, 2008). The second feature is the largely electronegative nature of the substrate binding site compared to a more neutral nature of the corresponding region in other KATs for interacting with the lysine to be modified (Wang *et al*, 2008). Another interesting property of p300 is the presence of a highly basic autoinhibitory loop that sits in the electronegative substrate binding site and prevents interaction with substrate (Ddelvecchio *et al*, 2013). The RING domain has also been found to orient itself towards the substrate binding groove of p300 and prevent its catalytic activity. For p300 to adopt its active confirmation, more than one copy of the protein need to assemble near each other so that one protein can acetylate the other's autoacetylation loop – a phenomenon known as trans-autoacetylation. The autoacetylation disrupts the interaction between the active site and the loop and also re-orientes the RING domain away from the active site. This now frees the active site of p300 to bind with the substrate and promote acetylation of the histones and other substrates.

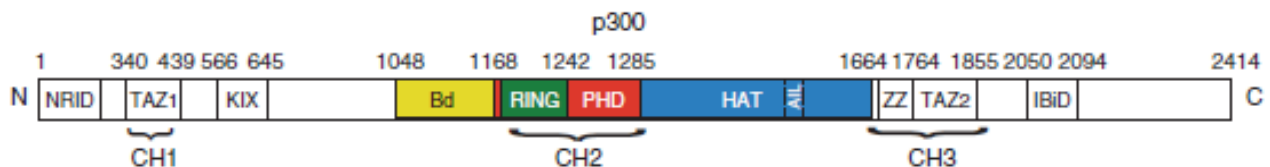


Figure 12: Domain organization of p300. Abbreviations: NRID- Nuclear receptor interaction domain, TAZ- Transcription adaptor zinc finger domain, KIX- Kinase-inducible domain of CREB-interacting domain, Bd- Bromodomain, RING- Really interesting new gene, PHD- Plant homeodomain, HAT- histone acetyltransferase domain, ZZ- ZZ-type zinc finger domain, IBiD- IRF3 binding domain. (Source- Delvecchio *et al*, Nat Struct Mol Biol, 2013)

1.4.6 Dynamicity of acetylation-deacetylation

The thermodynamic and kinetic properties of epigenetic modifications depend on the type of modification, corresponding chromatin modifier, specific genomic locus and the availability of cofactors and allosteric regulators. Due to this

diversity, the histone modification deposition and turnover varies from one metabolic condition to another.

It has been estimated that each histone octamer for every nucleosome could harbor upto 100 acetyl groups which translates to 4 billion acetyl units across the entire human genome (Ye *et al*, 2018). If 0.1 percent of the histone residues were involved in acetylation-deacetylation process, then around 3 μ M of acetyl CoA would be consumed out of the total 20 μ M present usually inside the cells (Shurubor *et al*, 2017). Upon deacetylation of histones, acetate is generated which can once again be used to generate acetyl CoA for further acetylation. The consumption pattern of acetylation itself varies according to physiological conditions. The dynamics of histone acetylation and deacetylation is much faster than other epigenetic modifications such as methylation. While the half-life of acetylation is generally 2-3 minutes *in vivo* (Jackson *et al*, 1975), that of methylation is in the range of 0.3-4 days (Zee *et al*, 2010). This makes methylation more stable and it constitutes a type of epigenetic memory in response to stronger but transient perturbations. On the other hand, due to its high turnover rate, acetylation is a much more dynamic modification. This turnover rate is especially quite high in the vicinity of active transcription start sites. The functional implications of this dynamicity are an interesting aspect of study that still remains elusive.

1.4.7 Gene expression regulation by chromatin acetylation and its physiological consequences

Histone acetylation by various KATs has been implicated in maintaining pluripotency as well as dictating lineage commitment by differentiation in different contexts. H3K56 acetylation mark has been found to be enriched in the promoters of three of the Yamanaka factors OCT4, SOX2 and Nanog for maintaining pluripotency of embryonic stem cells. Several members of the MYST family of KATs viz. Mof, HBO1 and Tip60 regulate the expression of these pluripotency inducing genes by acetylation of histones in their gene promoters (Li *et al*, 2012; Kim *et al*, 2015; Chen *et al*, eLife, 2013). Other important KATs playing similar roles include GCN5 which deposits H3K9 acetylation mark in the

promoters of OCT4 and Nanog, and p300 which directly interacts with Nanog and helps in activation of Nanog target genes via histone acetylation (Fang *et al*, 2014).

KATs also play important regulatory roles in cellular differentiation as well as maintenance of cell lineage. In hematopoietic stem cells p300 and CBP help in maintain the stemness of the cells by acetylation of histones across several genomic loci (Cabal-Hierro *et al*, 2020). Knockdown of MYST family member MORF leads to differentiation of hematopoietic stem cells to myeloid lineage as well as reduced erythropoiesis (Khokhar *et al*, 2020). p300 plays a crucial role in muscle differentiation by promoting the expression of master transcription factor MyoD through acetylation of its gene regulatory elements (Hamed *et al*, 2013). Moreover, p300 also acetylates MyoD itself that is necessary for activating its ability to induce expression of genes required for myotube formation (Puri *et al*, 1997). p300 also helps in neurogenesis by H3K9 acetylation in the promoters of genes required for neuronal cell differentiation (Qiao *et al*, 2015). CBP plays an equally important role in this aspect as loss of this protein leads to impaired neurogenesis as well as reduced neuron density in certain regions of the mouse brain (Schoof *et al*, 2019). Member of MYST family MORF also helps in neuronal differentiation by H4K16 acetylation (Merson *et al*, 2006).

Histone acetylation is also critical for immunological functioning of T cells. Upon antigen recognition, the T cells get activated which is accompanied by increased glucose uptake for fuelling the high metabolic rate of the cells. The enhanced glycolysis leads to induction of activity of lactate dehydrogenase resulting in Warburg effect and fast generation of acetyl CoA. The elevated levels of acetyl CoA are utilized for acetylation of histones to increase the expression of proinflammatory cytokine IFN γ . In a tumor microenvironment, the cancer cells can out-compete the T cells for utilization of glucose. Reduction in glucose uptake further decreases the histone acetylation, thereby suppressing the activity of the T cells (Peng *et al*, 2016). This could be reversed by acetate supplementation which rescues the T cell activity by replenishing them with the required acetyl CoA (Qiu *et al*, 2019).

Histone acetylation plays an important role in carcinogenesis. Enzymes responsible for acetyl CoA generation within the cells – ATP citrate lyase and pyruvate dehydrogenase complex, translocate to the nucleus upon growth factor stimulation and increase the nuclear pool of acetyl CoA to promote histone acetylation (Welln *et al*, 2009; Sutendra *et al*, 2014). The oncogenic protein KRAS or AKT can stimulate the activity of ATP citrate lyase to further promote histone acetylation (Lee *et al*, 2014). Moreover, in different types of cancers altered expression pattern and mutations have been discovered in several class I and II HDACs, which leads to aberrant expression of genes responsible for cell proliferation, cell cycle progression, differentiation and apoptosis (Glozak *et al*, 2007).

1.5 Other emerging histone modifications

With the passage of time, there has been continuous discovery and addition of new posttranslational modifications to the already known canonical ones. There are also supporting evidences indicating that these modifications and metabolic pathways inside the cells are intimately intertwined (Figure 13).

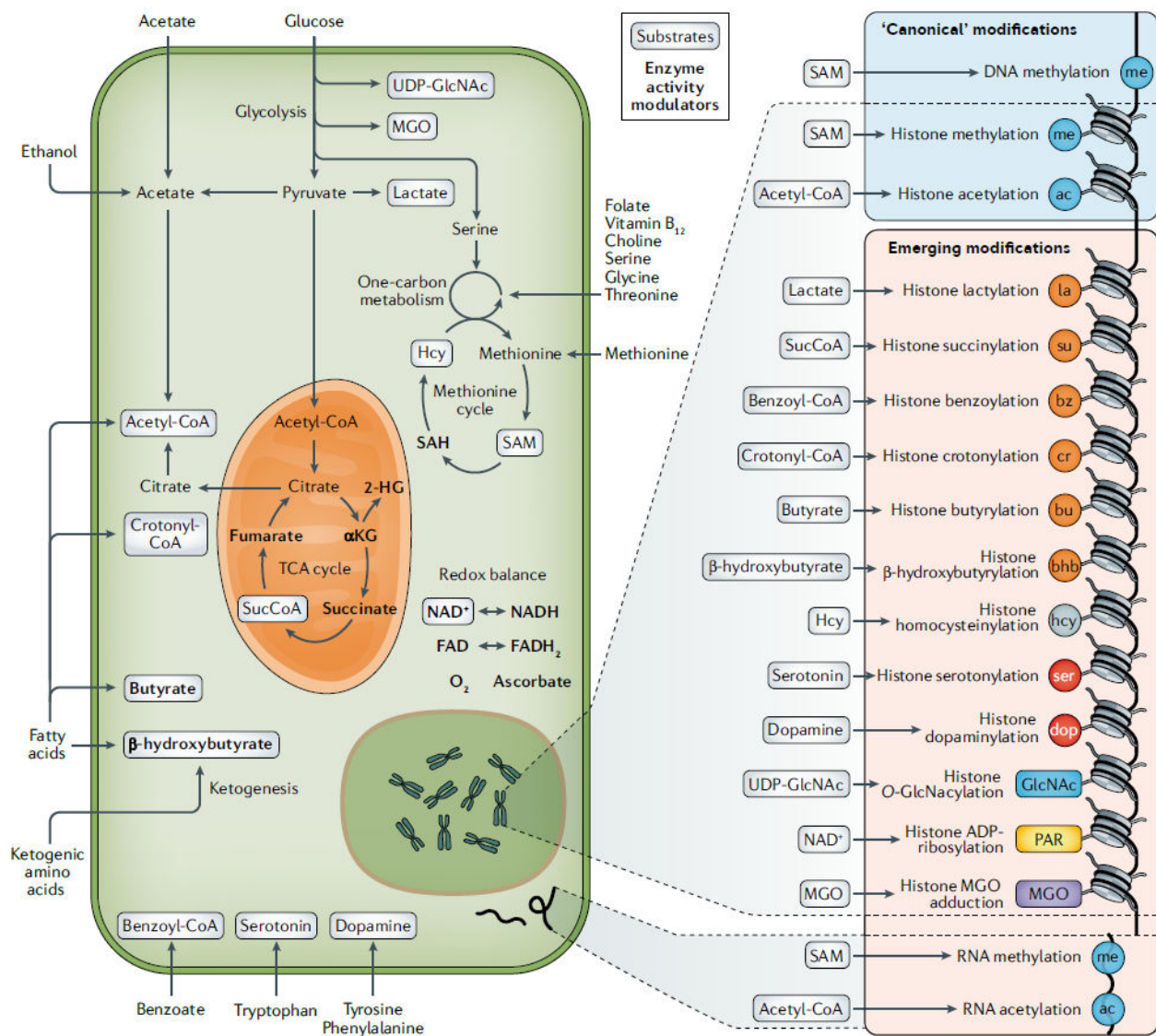


Figure 13: Different metabolic pathways generating intermediates that are used as cofactors for modifying histones (Adapted from Dai *et al*, Nat Rev Genet. 2020)

1.5.1 Histone homocysteinylation

Histones have been found to be modified by homocysteine (Figure 14) in their lysine residues in cases of elevated homocysteine levels in the brain of fetuses within pregnant mothers (Zhang *et al*, 2018). Homocysteine production is linked with folate based one carbon metabolism and there have been observations of neural tube defects in infants due to folate deficiency in their mothers. In fact, homocysteinylation at H3K79 position has been found to be negatively correlated

with expression of genes associated with neural tube closure, indicating a possible role of the metabolite homocysteine in epigenetic regulation of neural tube formation.

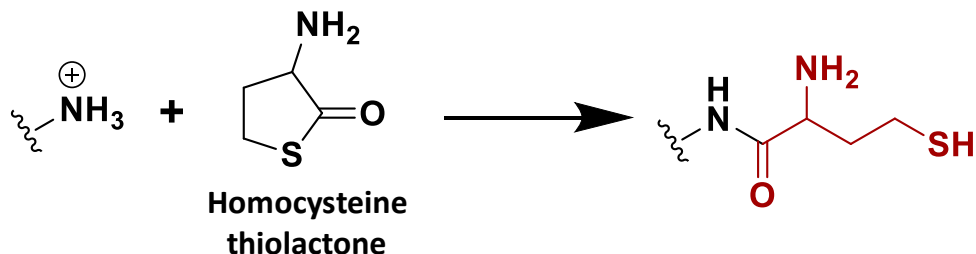


Figure 14: Reaction diagram of lysine homocysteinylation. Lysine is the substrate and homocysteine thiolactone is the cofactor.

1.5.2 Histone monoaminylation

Monoaminylation of histones is a very recently discovered phenomenon wherein glutamine residues in histones get modified by monoamine neurotransmitters like serotonin and dopamine. (Figure 15) Both these neurotransmitters are synthesized from different amino acids- tryptophan is required for serotonin biosynthesis, while tyrosine and phenylalanine for dopamine. Therefore, their production within the body could get hindered due to limitation in availability of these precursor amino acids. Serotonin is an important neurotransmitter required for maintaining neuronal circuit functions. Histone serotonylation has been observed not only in the brain, but also in other tissues where bulk production of serotonin takes place. It has been specifically found to co-occur at the glutamine residue H3Q5 along with H3K4me3 mark to promote euchromatinisation of the genome and induce transcription required for neuronal cell differentiation and development (Farrelly *et al*, 2019). Dopamine is a neurotransmitter associated with reward circuit and it has been found to modify histones at the same position- H3Q5 in the regions of brain rich in dopaminergic neurons (Lepack *et al*, 2020). Histone dopaminylation has been found to decrease upon exposure to the narcotic cocaine but its levels increase upon cocaine withdrawal. Enforced reduction in histone dopaminylation by overexpression of dopaminylation defective histone mutants leads to a reversal in the expression of genes associated with addictive behavior. This proves that histone dopaminylation could

regulate mood of the individuals through gene expression regulation. Both these modifications are catalysed by transglutaminase 2.

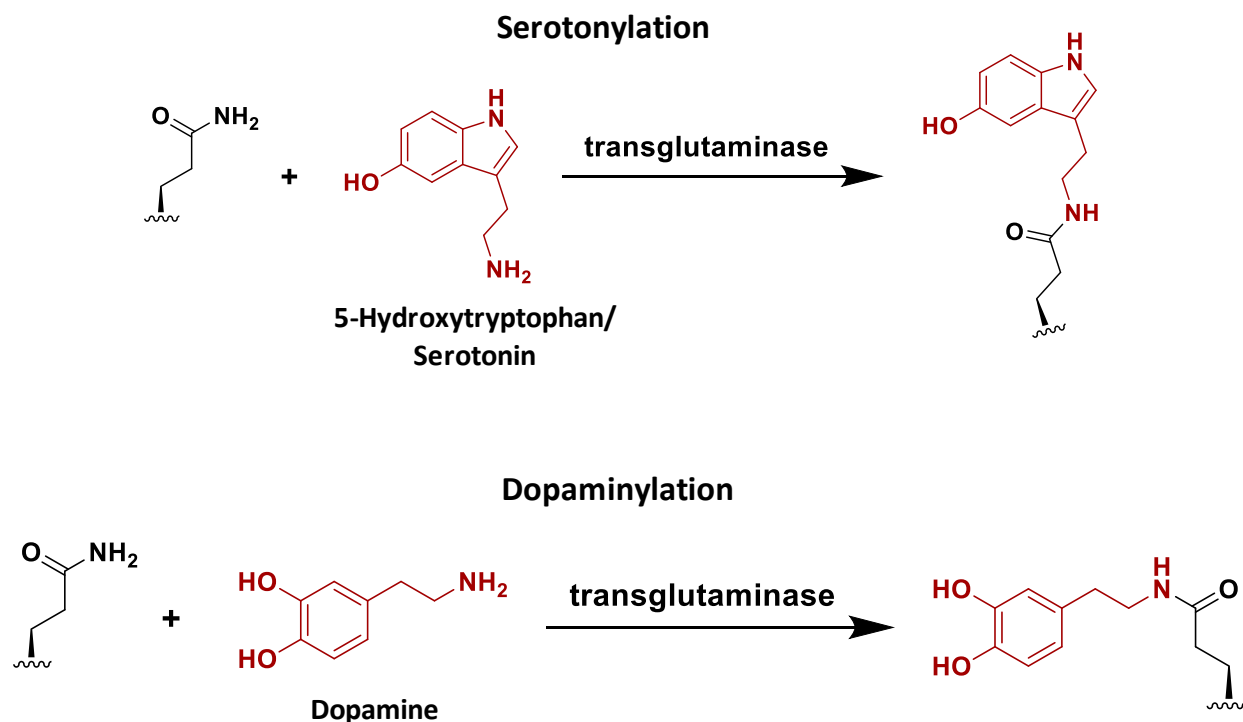


Figure 15: Reaction diagram of glutamine monoaminylation. Glutamine is the substrate and serotonin and dopamine are the cofactors.

1.5.3 Histone O-GlcNacylation

O-GlcNacylation of histones is carried out using UDP-GlcNac as a substrate, which is a byproduct of hexosamine synthesis pathway that utilizes intermediates of fatty acid, carbohydrate and nucleotide biosynthetic pathways to generate substrates for glycosylation of proteins at serine and threonine residues (Figure 16). It requires O-linked GlcNac transferase (OGT) as the enzyme to deposit the modification, while O-linked GlcNac hydrolase (OGA) is responsible for removal of this group (Zhang *et al*, 2011). OGT can associate with the enzymes TET2 and TET3 and promote O-GlcNacylation of histones to induce transcription (Chen *et al*,

Nature, 2013) and regulate chromatin structure during DNA replication (Zhang *et al*, 2011).

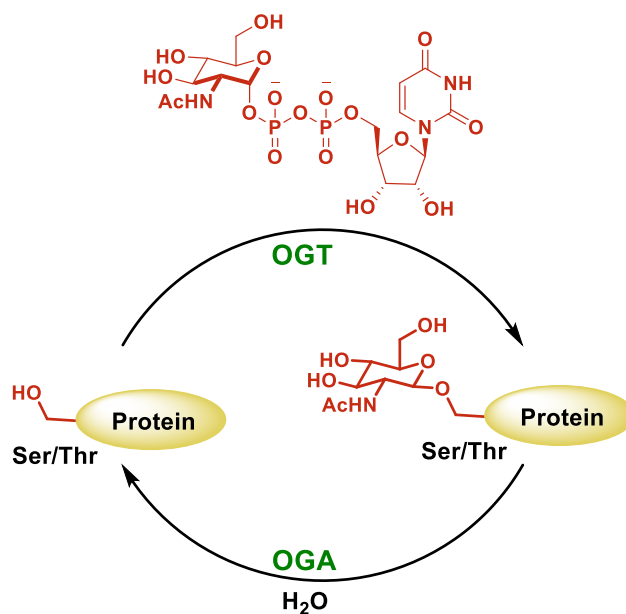


Figure 16: Reaction diagram of serine/threonine O-GlcNacylation. Abbreviations: Ser—Serine, Thr- Threonine, OGT- O-linked GlcNac transferase, OGA- O-linked GlcNac transferase.

1.5.4 Histone ADP-ribosylation

Histones have been found to undergo ADP-ribosylation which involves the addition of a single or multiple units of ADP ribose derived from NAD onto lysine residues (Figure 17) (Messner *et al*, 2011). The reaction is catalysed by poly (ADP-ribose) polymerase or PARP. ADP-ribosylation can not only alter the packaging state of the chromatin but also act as downstream effectors for regulation of transcription (Ciccarone *et al*, 2017). This modification has been found to be enriched in various regions of the genome in several stress related responses like DNA damage, oxidative stress, ageing and high fat diet consumption (Bai *et al*, 2012).

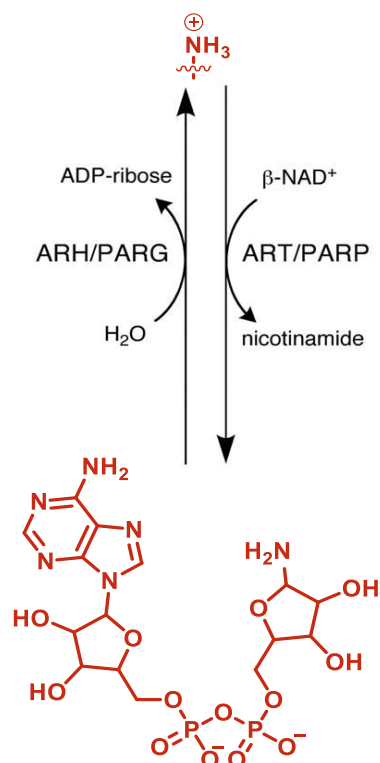


Figure 17: Reaction diagram of lysine ADP-ribosylation.

1.5.5 Non-enzymatic modifications of histones

Besides the well studied enzyme catalysed modifications, histones and DNA have also been found to be chemically modified without the participation of any enzyme. These non-enzymatic modifications usually follow the law of mass action whereby a significant rise in the stoichiometric levels of the metabolites could lead to their addition onto nucleophilic residues on histones and DNA. Both acetylation (Wagner *et al*, 2014) and methylation (Paik *et al*, 1975; Rydberg *et al*, 1982) have been reported to occur non-enzymatically under rarer special circumstances. The probability for these modifications to occur on the histones varies across the different sites as it depends on biophysical factors like surface exposure of the site to be modified and local electrostatic interactions with neighboring residues (Rydberg *et al*, 1982)..

Besides the canonical modifications, there are certain electrophilic molecules that have also been found to form adducts with DNA and histones. There are certain

ketoamides such as malondialdehyde, 4-hydroxy-2-nonenal and 4-oxo-2-nonenal that are formed due to lipid peroxidation by free radicals, reactive oxygen species and endogenous enzymes (Figure 18) (Long *et al*, 2013). Mass spectrometry experiments in macrophages and colon cancer cell lines have revealed that these molecules can also modify lysine residues on histones (Galligan *et al*, 2014). *In vitro* biochemical assays indicate that these modifications could open up the chromatin by disrupting the interactions between DNA and histones and thereby have a similar effect as acetylation. It has also been observed that SIRT2 has the ability to remove these modifications from histones (Jin *et al*, 2016). Levuglandins are another type of ketoamide, formed by the peroxidation of arachidonic acid by cyclooxygenase (Boutaud *et al*, 2005) that can modify lysines on histones (Figure 16) (Carrier *et al*, 2014; Mont *et al*, 2016). It is still not known whether there are any deacylases committed for removal of these modifications or whether they are simply replaced by histone turnover.

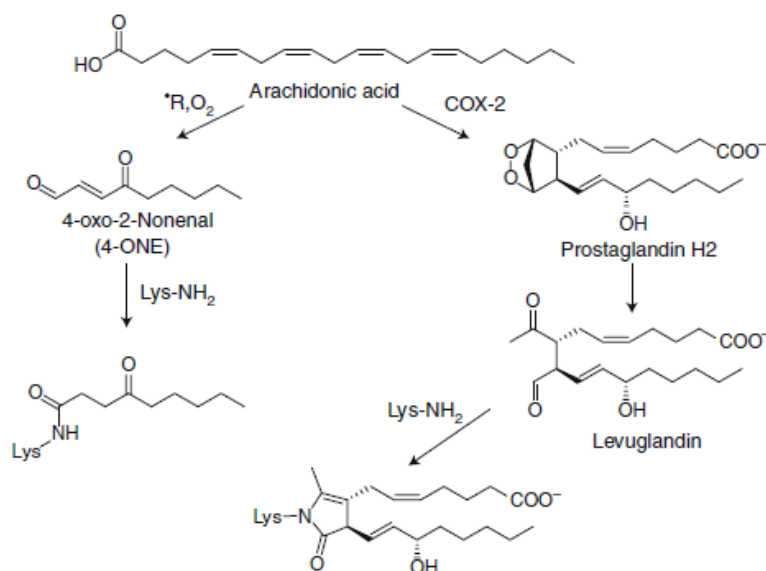


Figure 18: Reaction diagram of ketoamidation of lysine. Abbreviations: COX2- Cyclooxygenase 2. (Adapted from Diehl *et al*, Nat Chem Biol, 2020)

Several reducing sugars such as fructose, glucose-6-phosphate as well as glycolytic byproducts such as glyoxal, methylglyoxal and 3-deoxyglucosone can also be subjected to nucleophilic addition by lysine and arginine residues on histones

(Figure 19) (Singh *et al*, 2001). These molecules are produced upon degradation of certain glycolytic intermediates and therefore their levels rise during increased glycolytic flux as well as in cases where downstream steps of glycolysis are impaired (Singh *et al*, 2001; Allaman *et al*, 2015). The adducts they form with histones and other proteins upon rearrangement are known as advanced glycation end products (AGEs) such as carboxyl-methyllysine, carboxylethyllysine and pentosidine. These AGEs can compete with lysine acetylation and methylation of histones leading to diverse outcomes. The formation of AGEs with histones has been found to increase during aging, diabetes, cardiovascular diseases, cancer and neurodegenerative diseases (Singh *et al*, 2001; Allaman *et al*, 2015; Schröter *et al*, 2018). There are certain enzymes such as DJ-1 and GLO-I/II (Cao *et al*, 2015) along with the ketone body acetoacetate which are responsible for buffering the effect of AGE formation by removing the modifications or preventing their formation (178).

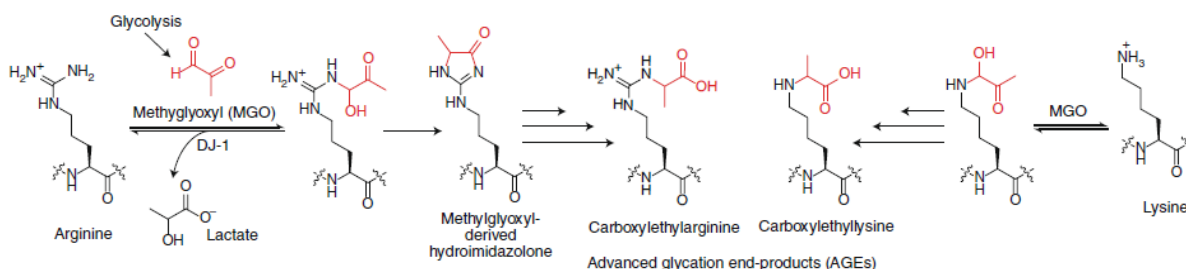


Figure 19: Reaction diagram of advanced glycation of lysine. Abbreviations: MGO- Methyl glyoxal, AGE- Advanced glycation end product. (Adapted from Diehl *et al*, Nat Chem Biol, 2020)

1.5.6 RNA modifications

Besides proteins and DNA, the RNA has also been found to undergo chemical modifications. The discovery of RNA modifications is relatively more recent and till date, methylation and acetylation of RNA has been mostly reported. These modifications are collectively known as the epitranscriptome and their formation and removal are also regulated by enzymes dependent on different metabolic pathways. RNA modifications have been found to regulate the stability,

translation as well as splicing of mRNA (Arango *et al*, 2018; Shi *et al*, 2019; Zaccara *et al*, 2019).

RNA is methylated mainly at adenine residues at the sixth position (m^6A). The methylation is carried out by METTL3-METTL14 complex as well as METTL16. An interesting case of RNA methylation is that of *MAT2A* gene that encodes MATI α which is responsible for generation of SAM. It has been observed that reduced m^6A methylation of *MAT2A* increases its stability leading to more SAM generation and methylation of targets. Therefore *MAT2A* methylation serves as a negative feedback loop for SAM biosynthesis inside the cells (Pendleton *et al*, 2017; Shima *et al*, 2017). Methyl groups on RNA are removed by the enzymes FTO and ALKBH5, both of which are dioxygenases using alpha-ketoglutarate as a cofactor. Therefore these enzymes can be competitively inhibited by structurally similar metabolites citrate, succinate, fumarate and the oncometabolite 2-hydroxyglutarate (Aik *et al*, 2013; Gerken *et al*, 2007). The increased levels of 2-hydroxyglutarate due to IDH1 in leukemia has been found to reduce the activity of FTO which leads to enhanced global m^6A methylation and decreased stability of the transcripts encoding *MYC* and *CEBPA*, both of which are known to positively regulate FTO (Su *et al*, 2018). Moreover, impairment in FTO activity also increases methylation of several small nuclear RNAs (snRNAs) and modulate mRNA splicing (Mauer *et al*, 2019).

mRNA is acetylated at fourth position of cytosine to generate N^4 acetylcytidine. The enzyme responsible for catalyzing this modification is NAT10 acetyltransferase, the activity of which is dependent on the abundance levels of the metabolite ATP (Ito *et al*, 2014). Acetylation of mRNA can increase the translation efficiency of the RNA (Arango *et al*, 2018). Till date, no deacetylase has been found performing the role of removing acetyl groups from RNA.

1.6 Paradigm shift in histone modifications- discovery of acylation

Owing to advancements made in the field of high sensitivity mass spectrometry, the current list of histone modifications has grown and is still growing. A large number of modifications have been discovered that are clubbed together under the name of acylation modifications (Figure 20). These modifications, just like the well-characterized acetylation, can also occur on lysine ϵ amino groups. They differ from acetylation with respect to size, hydrophobicity and charge. Based on chemical properties, these acylation modifications have been further subdivided into three groups- the hydrophobic group, polar group and acidic group. The hydrophobic group consists of propionyl, butyryl, isobutyryl and crotonyl groups that have differences in chain length. Propionyl and butyryl groups have an additional one and two carbon atoms compared to acetyl group. Crotonyl group is actually a butyryl group with an additional unsaturation. This C-C π bond brings a rigid planar configuration to the crotonyl group, making it structurally unique. All these groups are bigger and bulkier than acetyl group which could further decompact the chromatin and enhance the transcriptional output. Moreover, it might also lead to newer protein-protein interactions due to larger Van der Waal's radii of the groups. The polar group includes 2-hydroxyisobutyryl group and β -hydroxybutyryl group which could form additional hydrogen bonds with other molecules. The acidic group consists of malonyl, glutaryl, succinyl and lactyl groups. These groups can change the overall charge of the modified lysine residue from +1 to -1 depending on the physiological pH.

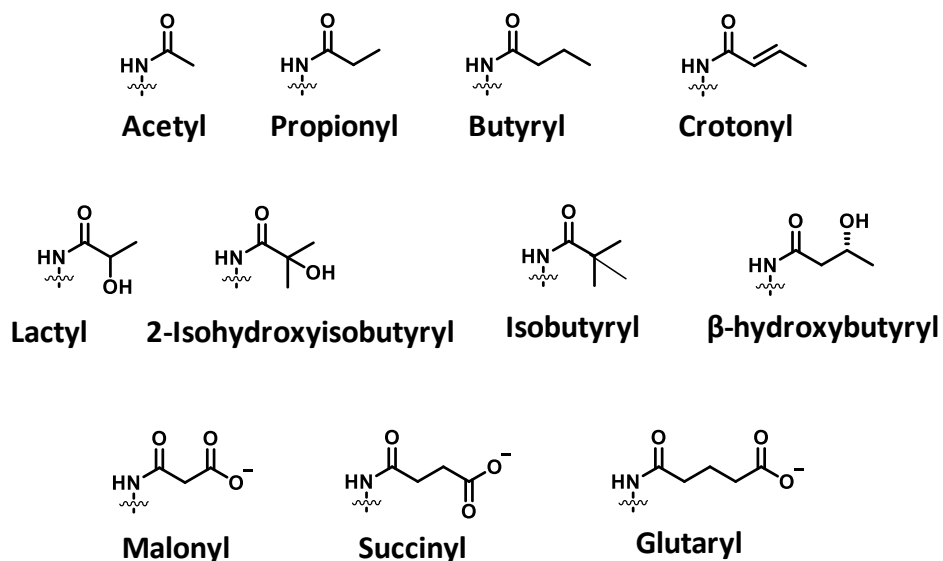


Figure 20: Structures of different acylation groups that have been known to modify lysine till date.

1.7 Methods for identification of new acylation modifications

The discovery of new post-translational modifications of histones has taken place with the help of techniques involving mass spectrometry. Structurally, the propionyl, butyryl and crotonyl groups are quite similar to acetyl group with differences mainly in chain length. These groups were first identified by tandem mass spectrometry analysis of trypsin digested peptides that were enriched for acetylation by immune-affinity isolation with a pan-acetyllysine antibody. The hypothesis was that due to structural similarity of the non-polar acyl groups with acetyl group, the pan-acetyllysine antibody could also cross-react and bind to some of the acylated peptides in addition to the acetylated ones. Indeed this particular approach led to the discovery of propionylation and butyrylation on histone H4 (Kim *et al*, 2006; Chen *et al*, 2007). Similar approaches subsequently led to the discovery of lysine succinylation, malonylation and glutarylation (Peng *et al*, 2011; Tan *et al*, 2014).

There exists a second approach for identification of new post-translational modifications, which is based on unbiased systematic screening of peptides for previously uncharacterized modifications. The particular residues getting modified could be found out by aligning the tandem mass spectrometry data with

existent protein sequence database. Algorithms have been developed to conduct unbiased search for mass shifts at specific residues due to previously uncharacterized modifications. Once such mass shifts are detected, the possible structure of these chemical groups is predicted and peptides are synthesized carrying similar groups. The existence of the predicted modifications are verified by performing high performance liquid chromatography coupled with tandem mass spectrometry with the trypsin digested peptides and the artificially synthesized ones to look for co-elution of the peptides carrying the same predicted modification at same residues. This is then followed by further downstream experiments which include isotopic labeling studies and immunocytochemistry with modification specific antibodies. This strategy has been used for the successful identification of lysine succinylation, crotonylation, betahydroxybutyrylation, 2-isohydroxybutyrylation and lactylation (Chick *et al*, 2015; Tan *et al*, 2011; Xie *et al*, 2006; Dai *et al*, 2014).

1.8 The epigenetic processors of acylation

1.8.1 Acylation writers

Till date, no enzyme has been identified that has exclusively specific acyltransferase activity. Some of the previously discovered and characterized acetyltransferases have been found to possess an enhanced repertoire of catalyzing additional acylation reactions. These include members of GNAT, p300/CBP and MYST family. The rates of acylation reactions catalyzed by these enzymes have been found to gradually decrease with increasing length of the variable acyl chain.

The GNAT family members GCN5 (KAT2A) and PCAF (p300-CBP associated factor or KAT2B) and yeast MYST family member Esa1 (Tip60 or KAT5 in mammals) have been shown to catalyze lysine propionylation *in vitro* albeit at a slower rate than acetylation (Berndsen *et al*, 2007; Leemhuis *et al*, 2008; Ringel *et al*, 2016; Kaczmarska *et al*, 2016). GCN5 and PCAF can also perform butyrylation *in vitro* but the rate is even slower and so their contribution to this modification in nature could be negligible (Leemhuis *et al*, 2008; Ringel *et al*, 2016). Structural studies of GCN5 in complex with different acyl CoA derivatives have shown the reason

behind the ability of this enzyme to catalyze the acylation reactions. GCN5 binds to the invariant Coenzyme A portion of acyl CoAs as a result of which it can bind to all acyl CoAs with equal affinity. However, while the acetyl group is positioned within the active site perfectly for its transfer to the lysine residue, the presence of a catalytic water molecule blocks the addition of more methyl groups to the acyl chain as a result of which longer acyl chains need to undergo rotation to fit inside the active site, thereby reducing the efficiency of the reaction. While propionyl and butyryl groups can still be oriented to fit inside the active site, the rigid planar conformation of crotonyl group makes it very difficult to be accommodated (Ringel *et al*, 2016). Therefore even in vitro, GCN5 cannot catalyze crotonylation of its substrates.

The KAT p300 (EP300) has been found to exhibit the greatest degree of promiscuity with respect to perform diverse acylation reactions. It can not only catalyze propionylation, butyrylation, crotonylation, betahydroxybutyrylation, succinylation, glutarylation and lactylation reactions, but it has also been found to accommodate within its active site large artificial acyl CoA analogues such as 4-pentenoyl CoA. EP300 possesses a deep aliphatic pocket within its active site, a structural feature absent in other acetyltransferases that enables it to accommodate different acyl CoAs (Figure 21) (Kaczmarek *et al*, 2016). Despite this structural advantage, the ability of EP300 to catalyze the different acylation reactions decreases with increasing chain length. Mutagenesis studies have shown that an isoleucine residue at 1395th position within the active site serves as a gatekeeper for entry of different acyl chains. Mutating this isoleucine to methionine increased the size of the cavity within the hydrophobic tunnel which led to faster catalysis of butyrylation and crotonylation reactions. In contrast, mutating the isoleucine to phenylalanine reduced the cavity size that further impaired the acylation reactions. These studies highlight the importance of the unique pocket in EP300 active site that confers it the ability to perform multiple acylation reactions.

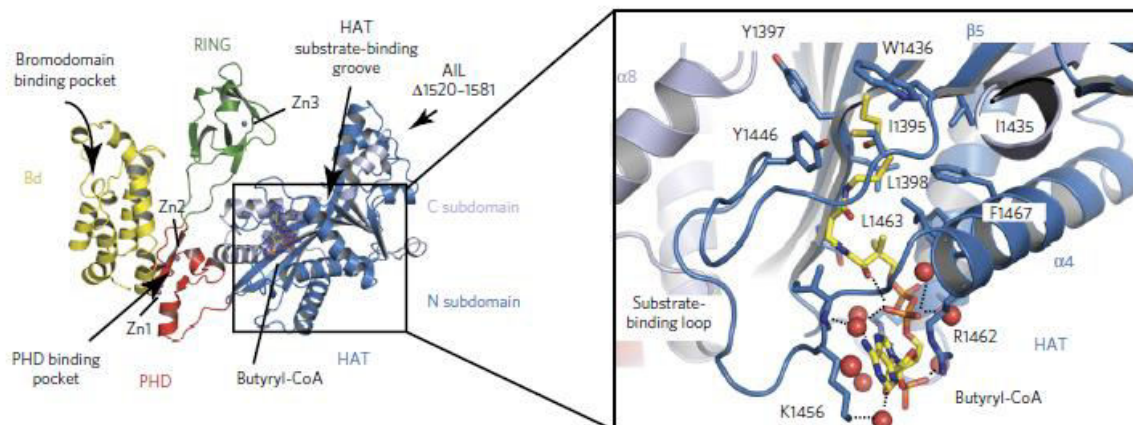


Figure 21: X-ray crystal structure shown in ribbon representation of p300 active site with the butyryl CoA inside the catalytic pocket. (Adapted from Kaczmarska *et al*, Nat Chem Biol, 2016)

In recent times, new evidences have begun emerging on the ability of members of MYST family of KATs to catalyse different acylation modifications. MOF can carry out both histone propionylation and crotonylation (Liu, X. *et al*, 2017; Han *et al*, 2018), while MOZ and MORF can only perform propionylation (Yan *et al*, 2020). Another member of this family, HBO1 has been shown to perform propionylation, butyrylation as well as crotonylation reactions by forming functionally active complexes with its binding partners inside the cells (Xiao *et al*, 2021). Structural analysis revealed that the functional complex of HBO1 can nicely accommodate the invariable portion of the acyl CoAs within its active site while the variable acyl chain was located adjacent to the hydrophobic residues Pro 507 and Val 472 (Figure 22).

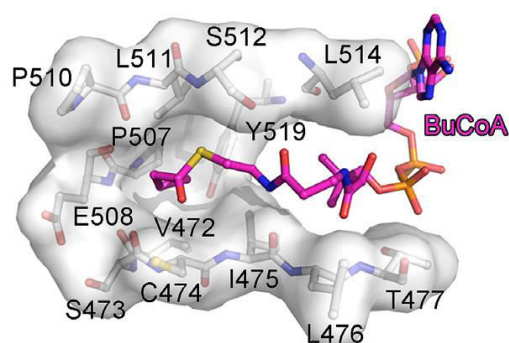


Figure 22: Representative image of butyryl CoA within the acyl CoA binding pocket of HBO1 (Adapted from Xiao *et al*, Nucleic Acids Res, 2021)

Recently, the non-histone protein EB1 was reported to be crotonylated at Lys 66 residue by another MYST family member Tip60 (Song *et al*, 2021). This modification is required for fine tuning the accurate spindle positioning during the metaphase. Mechanistically, the crotonylation of EB1 is required for forming a link between astral microtubules and the polar cortex with the help of NuMA. The crotonylation mark is then removed by the HDAC3 for ensuring proper separation of the sister chromatids.

1.8.2 Acylation readers

There are three major families of histone acylation readers discovered till date. They are bromodomain, YEATS (Yaf9, ENL, Af9, Taf14 and Sas5) domain and double plant homeodomain (PHD) finger proteins.

An earlier study had shown that bromodomain containing protein 4 (BRD4) could recognize and bind propionylated and butyrylated lysine, albeit with reduced affinity (Vollmuth *et al*, 2010). Another extensive survey with 49 different different bromodomains revealed that while all of them could bind propionyl group only three bound to butyryl group, one bound to crotonyl group and none to succinyl group (Flynn *et al*, 2015). A more interesting observation has been made in the context of spermatogenesis wherein, the testes specific bromodomain testis-associated protein (BRDT) was found to simultaneously bind peptides carrying H4K5Ac and H4K8Bu in addition to the canonical recognition sites of H4K5Ac and H4K8Ac (Goudarzi *et al*, 2016). It was however unable to recognize peptides having the modification combination of H4K5Bu and H4K8Ac as well as butyrylation at both sites i.e. H4K5Bu and H4K8Bu. This indicates that the propensity of bromodomain to bind to certain acylated residues could not only depend on the modification of that site itself, but also on the modification pattern of neighboring residues.

Unlike bromodomain containing proteins, the YEATS domain proteins have been found to exhibit greater binding affinity for longer acylations compared to acetylation (Li, Y. *et al*, 2016; Zhao *et al*, 2016; Andrews *et al*, 2016; Zhang *et al*, 2016). In fact, the binding affinity increases with increasing chain length with the

highest affinity for crotonyl group. X-ray crystal structural study of AF9 YEATS domain in complex with H3K9Ac has revealed that the binding site of the domain has an open ended pocket that snugly fits inside it the acetyl group and still has more space left in which extended acyl chains could be accommodated (Figure 23). As a result, propionyl and butyryl groups can also be fitted inside the reader domain and the interaction is further stabilized by hydrophobic interactions between the amino acids and the extended hydrocarbon chains. Crotonyl group is accommodated inside with minor changes in the conformation. It has been observed in the crystal structure of the Af9 with H3K9cr that the crotonyl group, due to the presence of an additional unsaturation, can form π - π stacking interactions with two sandwiching aromatic amino acid side chains. This kind of π -stacking interaction has also been observed in YEATS2 and Taf14 with crotonylated lysine.

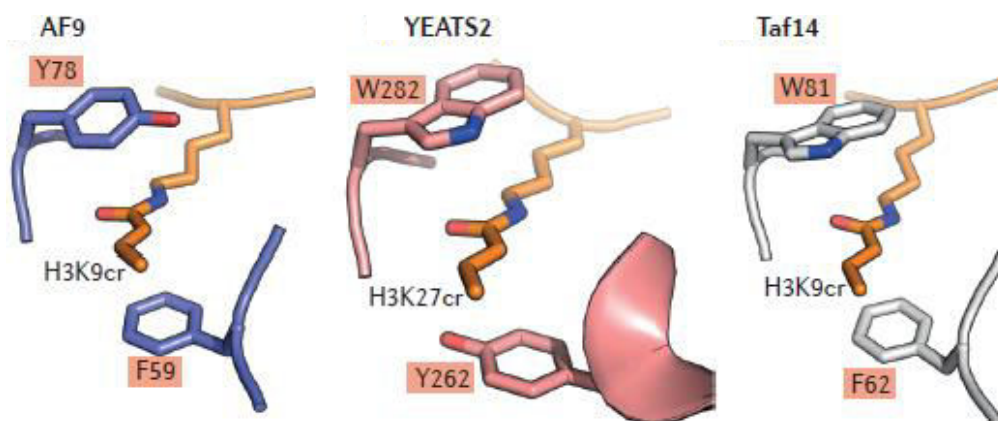


Figure 23: Representative images of different YEATS domain proteins- AF9, YEATS2 and Taf14 forming sandwiching interactions with crotonyllysine. (Adapted from Sabari et al, Nat Rev Mol Cell Biol, 2017)

PHD finger proteins were previously known to be methyllysine readers, but tandem PHD fingers (or double PHD finger domains) have been found to be able to bind with acetylated lysines as well (Lange *et al*, 2008). Till date, DPF domains from five human proteins have been characterized as lysine acylation readers. They include the two paralogues from MYST family- monocytic leukemia zinc-finger protein (MOZ, also known as KAT6A) and MOZ-related factor (MORF); and DPF1, DPF2 and DPF3 which are all subunits of the BRG1-associated factor (BAF)

chromatin remodeling complex (Qiu *et al*, 2012, Dreveny *et al*, 2014; Zeng *et al*, 2010; Ali *et al*, 2012). Isothermal titration calorimetry studies with MOZ and DPF2 have shown that just like YEATS domain, these PHD finger proteins also show an increasing binding affinity with acyl groups with increasing chain length (Xiong *et al*, 2016). The greatest preference of binding again lies for lysine crotonylation, but in these cases, instead of π -stacking interactions, the crotonyl group is stabilized by encapsulation with hydrophobic amino acids and coordinated hydrogen bonding with polar amino acids.

1.8.3 Acylation erasers

Since the discovery of existence of new acylation modifications, an extensive search has been performed for enzymes responsible for removing these chemical moieties. Just as in the case of writers, in this case also, the pre-existent pool of known deacetylases has served as the main source for screening for possible deacylases. Amongst the two principal classes of HDACs, the NAD dependent sirtuins have shown more efficiency and diversity at removal of different types of acylation groups. Sirtuins 1, 2 and 3 have shown the ability to remove uncharged short chain acylations – propionylation, butyrylation and crotonylation *in vitro* (Feldman *et al*, 2013). Their efficiency for removal of these groups is less than their deacetylation activity. Surprisingly, SIRT5 can remove negatively charged succinyl, malonyl and glutaryl groups, even though it has low canonical deacetylase activity (Tan *et al*, 2014; Peng *et al*, 2011; Du *et al*, 2011; Park *et al*, 2013). SIRT7 has also shown desuccinylase activity in the context of DNA damage response (Li, L. *et al*, 2016). Further long chain fatty acid groups have been found to be removed by SIRT6 and zinc ion dependant deacetylase HDAC11 (Feldman *et al*, 2013; Cao *et al*, 2019). Recently, HDAC3 has been shown to bring about decrotonylation of microtubule plus end trafficking protein EB1 which is required for proper spindle positioning during mitosis (Song *et al*, 2021). Three more members of class I histone deacetylases- HDAC1, HDAC2 and HDAC3 have been found to be the major decrotonylases for histone crotonylation in intestinal epithelium (Fellows *et al*, 2018).

ENZYMES	Lysine acylations										
	Kpr	Kbu	Kcr	Kla	Khib	Kib	Kbhb	Kmal	Ksuc	Kglu	Kben
Writers											
p300/CBP	+	+	+	+	+	+	+	NA	-	+	NA
GCN5	+	-/+	-	NA	NA	-	NA	NA	+	+	NA
HAT1	NA	NA	NA	NA	NA	+	NA	NA	NA	NA	NA
MOF	+	-	+	NA	NA	NA	NA	NA	NA	NA	NA
MOZ	+	-	-	NA	NA	NA	NA	NA	NA	NA	NA
MORF	+	-	-	NA	NA	NA	NA	NA	NA	NA	NA
HBO1	+	+	+	NA	NA	NA	NA	NA	NA	NA	NA
Tip60	-	-	+	NA	NA	NA	NA	NA	NA	NA	NA
Erasers											
NAD ⁺ dependent Sirtuins	SIRT1-3	SIRT1-3	SIRT1-3	NA	NA	NA	NA	SIRT5	SIRT3-5,7	SIRT5	SIRT2
Zn ²⁺ dependent HDACs	NA	NA	HDAC 1-3	NA	NA	NA	NA	NA	NA	NA	-

Table 2: List of known writers and erasers of different histone acylation modifications (NA- No available information yet)

1.9 Physiological significance of histone acylation

Genome wide ChIP sequencing analysis for lysine propionylation, crotonylation, butyrylation, isobutyrylation and beta hydroxybutyrylation have shown that all these modifications are enriched in various enhancer elements and therefore could play important roles in regulating gene expression.

p300 catalysed histone crotonylation has been found to be increased upon lipopolysaccharide induced inflammation (Sabari *et al*, 2015). This leads to activation of TLR4 (Toll-like receptor 4) based signaling along with enhanced expression of genes involved with inflammatory response. The increased transcription of inflammation associated genes is dependent on elevated levels of crotonylation reader Af9-YEATS domain that has a higher affinity for crotonylation over acetylation and further helps in chromatin decompaction after binding to the crotonylation sites. Histone crotonylation is highly enriched in the small intestine

of mice due to production of short chain fatty acids like butyrate by the gut microbiota. Butyrate can serve as an HDAC inhibitor as a result of which it reduces histone deacetylation, creating the opportunity for enhanced crotonylation of histones. Acute kidney injury caused by folic acid and cisplatin treatment (Ruiz-Andres *et al*, 2016) also leads to increased histone crotonylation in the promoters of tissue stress associated genes that are upregulated. These genes confer protection against further tissue damage and are dependent on the enhanced histone crotonylation for their upregulation in expression. Histone crotonylation has also been found to be important in the context of meiotic sex chromosome inactivation (Tan *et al*, 2011; Sin *et al*, 2012). This process involves the depletion of histone acetylation, butyrylation and isohydroxybutyrylation but histone crotonylation marks remain retained in a fraction of the sex chromosomes escaping meiotic sex chromosome inactivation in post-meiotic round spermatids. This indicates that histone crotonylation might still be able to sustain transcription in spermatids even in regions of chromatin that does not favour transcription.

There have been a number of interesting instances of intracellular metabolites that get converted to their corresponding acyl CoA derivatives and bring about modification of lysine residues of histones. Upon bacterial infection, M1 macrophages enter a highly active metabolic state to combat the infection by recruiting other immune cells. This pro-inflammatory state has a high energetic cost and so in order to meet the energy demand anaerobic glycolysis becomes predominant for quick ATP generation. This induces the Warburg effect leading to high production of lactate. With time, the lactate concentration builds up, a fraction of which gets converted to lactyl CoA which causes lactylation of histones, catalysed by p300 (Zhang *et al*, 2019). This results in the expression of homeostatic genes responsible for switching of the M1 macrophages to the less aggressive M2 phenotype for the recovery of the host tissues from the collateral damage caused by the pro-inflammatory response to the bacterial infection.

The ketone body beta-hydroxybutyrate is generated inside the mitochondria of liver and gets released into the bloodstream under conditions of starvation, low carbohydrate diet and high exercise. While it may serve as a metabolic fuel for

other tissues under nutrient deprived conditions, beta-hydroxybutyrate can also modify histone lysine residues through conversion to its acyl CoA derivative (Xie *et al*, 2016). Gene ontology analysis of the promoters enriched in beta-hydroxybutyrylation at H3K9 show that this modification is enriched in the promoters of a different set of genes compared to H3K9 acetylation, further highlighting the fact that this modification has distinct regulatory roles from acetylation. Previously, beta-hydroxybutyrate has been considered more as an HDAC inhibitor, but new evidences indicate that it should be regarded as a possible source for chromatin modification.

H3K9 betahydroxybutyrylation has also been found to be essential for maintaining the redox balance in the CD8⁺ T cells which are involved in immune cell memory formation (Zhang *et al*, 2020). Within these T cells the metabolic processes of gluconeogenesis and glycogenesis are highly predominant, this is necessary for NADPH and glutathione formation that prevent buildup of reactive oxygen species. One of the critical enzymes

for this process is phosphoenolpyruvate carboxykinase (Pck1) that generates phosphoglucose from oxaloacetate. The high expression and enzymatic activity of Pck1 causes the oxaloacetate in the mitochondria to be shunted away from TCA cycle and instead produce ketone bodies like betahydroxybutyrate. This leads to modification of histones in the promoters of *Foxo1* and *Ppargc1a* by betahydroxybutyryl CoA and upregulated expression of these genes. The transcription factors encoded by these genes, in turn further promote *Pck1* expression thereby forming a feedforward loop of carbon flow along gluconeogenesis to glycogen synthesis.

Succinylation of histones is carried out by KAT2A/GCN5 which utilizes succinyl CoA generated by alpha-ketoglutarate dehydrogenase localized within the nucleus. Specifically H3K79 gets succinylated and marks important transcription start sites of various genes (Wang *et al*, 2017). Benzoylation of histones have been reported in cell lines upon treatment with sodium benzoate, an FDA approved food preservative (Huang *et al*, 2018). The modification can be removed by the deacetylase SIRT2. YEATS and DPF are the corresponding readers.

Glutarylation of histones is catalysed mainly by p300 (Tan *et al*, 2014) and GCN5 (234) while removal of this group is carried out by SIRT5 (Ishiguro *et al*, 2018; Peng *et al*, 2011; Du *et al*, 2011; Park *et al*, 2013) and SIRT7 (Li *et al*, 2016). *In vitro* assays have demonstrated that glutarylation leads to decompaction of chromatin and increase in transcription. Functional significance of this modification has been seen in the context of cell division, wherein H4K91 glutarylation peaks during the S phase and gradually drops during mitosis (Bao *et al*, 2019).

Till date no acyltransferase has been discovered that is capable of depositing malonylation marks on histones. Since malonyl group is the most electrophilic among all the acylations discovered, it has been hypothesized that this modification could even happen non-enzymatically. Malonylation at H2AK119 position has been found to regulate chromosome segregation by cross-talk with nearby phosphorylation at H2AS121 (Ishiguro *et al*, 2018). Because malonyl CoA is an important player in the fatty acid biosynthesis pathway, there could be a mechanistic link between fatty acid metabolism and cell division through the mediation of H2AK119 malonylation.

The physiological significance of histone butyrylation was first observed in the case of spermatogenesis (Goudarzi *et al*, 2016). Butyrylation on histones was retained at late stages of spermatogenesis even when histone acetylation was removed. Moreover, BRDT- a testes specific bromodomain containing protein was found to have reduced ability to bind with histones carrying H4K5 butyrylation. BRDT is responsible for docking onto histones at acetylation marks and bring about replacement of histones with protamines. The inability of BRDT to bind with H4K5 butyrylated histones indicate that histones carrying butyrylation may be retained in the genomic loci of sperm chromatin throughout the developmental process. The importance of this butyrylation modification at the same site i.e. H4K5 has also been highlighted in acute lymphoblastic leukemia (ALL) (Gao *et al*, 2021). Using patient samples as well as cell line based studies it has been shown that increased mitochondrial activity of fatty acid synthesis or breakdown would lead to enhanced histone butyrylation and crotonylation levels especially at H4K5 position. This can have wider consequences on genome wide

distribution of the bromodomain containing protein BRD4 which preferentially binds to acetylated histones and promotes transcription. The genome wide increase in H4K5 butyrylation lowers the binding affinity of BRD4 towards histones and it gets redistributed to specific transcription start sites harbouring acetylated histones for inducing transcription of carcinogenesis associated genes in ALL.

There are also a few interesting observations on diverse histone butyrylation patterns due to various kinds of metabolic stress in different tissues. Just like beta-hydroxybutyrylation, starvation also leads to increased histone butyrylation in mice liver (Goudarzi *et al*, 2020). Interestingly the basal level of histone butyrylation in the liver of female mice is high and so the enhanced butyrylation upon starvation is only observed in male mice liver. This indicates that there could be sex specific variation in levels of histone acylation due to differences in hormone influenced metabolism. Cardiac muscles of mice maintained on high fat diet for 4 days exhibit lower levels of H3K9 butyrylation compared to mice on normal diet, while H3K18 butyrylation levels remain unchanged (Yang *et al*, 2021). The stress induced in heart muscles due to high lipid intake is responsible for increase in expression of Acyl CoA dehydrogenase (ACADS) that is responsible for conversion of butyryl CoA to crotonyl CoA. The increased activity of ACADS leads to reduced butyryl CoA accumulation resulting in decreased H3K9 butyrylation. On the other hand, upon fat free normal diet consumption, acetyl CoA derived from glucose gets converted to fatty acids by fatty acid synthase (FASN) which may be responsible for elevated butyrylation of histones under normal conditions. Conversely, unlike in the heart muscles, the liver in mice maintained on high fat diet over a prolonged period of time exhibited a reduction in H3K18 butyrylation (Nie *et al*, 2017).

The effect of these kinds of metabolic stress could be global or site specific and vary temporally across different tissues. More investigations would be needed in this aspect for a clearer understanding of how acylation pattern changes in different physiological conditions.

Recently another new acylation modification has been discovered- the branched chain version of straight chain butyrylation i.e. isobutyrylation (Zhu *et al*, 2021).

Isobutyryl CoA is generated from valine catabolism and branched chain fatty acid oxidation, indicating that the metabolic processes involved in its generation is different from that of butyryl CoA. The nuclear acetyltransferase p300 and cytoplasmic acetyltransferase HAT1 have shown high propensity to isobutyrylate histones. It would be interesting to investigate under which cellular contexts this new version of histone acylation might play important roles in regulating gene expression.

1.10 Possible metabolic sources for acylation

In most of the common physiological scenarios, the abundance of acetyl CoA is in the micromolar range (Langer *et al*, 2002) which is much higher than that of the other acyl CoAs and the cellular concentration of acetyl CoA is more or less close to the Michaelis Menten constant (K_m) of the different acetyltransferases for acetyl CoA (Huang *et al*, 2015). Therefore fluctuations in acetyl CoA levels do not drastically affect global acetylation levels (Sabari *et al*, 2015) and if there are any changes in acetylation pattern, they are usually at specific genomic loci. On the other hand, the concentrations of other rarer acyl CoA derivatives are far lower than the K_m of most acetyltransferases like p300 (Meier *et al*, 2013). Hence, even slight changes in their stoichiometric levels could be detected by the enzymes, which become nutritional sensors for the acyl CoA derivatives (Xie *et al*, 2016; Sabari *et al*, 2015). Yet, since acetyl CoA is much more predominant than acyl CoA and both modifications are competing for the same lysine residues, the former would predictably out-compete the latter for modifying histones.

It has been speculated that there could be two possible scenarios under which acylation of histones may become relevant. They are-

- 1) Conditions in which the stoichiometric levels of acetyl CoA get reduced, giving opportunity to the other rarer acyl CoAs to modify histones.
- 2) Conditions in which there is an increased production of a specific acyl CoA which would modify histones by competing with acetyl CoA.

1.10.1 Competition of other acyl CoA derivatives with acetyl CoA

Initially certain observations made in cell line based studies had indicated that perturbing the cellular concentration of acetyl CoA by genetic means could reduce the histone acetylation and in turn promote other forms of acylation. The enzyme mainly responsible for generation of nucleocytoplasmic pool of acetyl CoA is ATP citrate lyase (ACL) and knockdown of ACL leads to a drastic reduction in acetylation of histones due to depletion of acetyl CoA pools (Wellen *et al*, 2009). Moreover, under similar conditions the histone H3K18 crotonylation levels were markedly increased, further highlighting the fact that reducing the competition with acetyl CoA could be the key to increase acylation levels in histones (Sabari *et al*, 2015). This gave rise to the speculation that since acetyl CoA is mainly derived from glucose by glycolysis; any condition under which cells are depleted of glucose might also create the opportunity for other acyl CoAs to bring about acylation. Separately performed studies in various cell culture systems have shown that histone crotonylation is higher in cells cultured under low glucose conditions compared to high glucose conditions (Bhanu *et al*, 2013; Tweedie-Cullen *et al*, 2012). Surprisingly, depletion of glucose by different means such as treatment with glycolysis inhibitor 2-deoxyglucose or culturing cells in low glucose containing media, led to not only a reduction of acetylation but also other acylation modifications such as propionylation, butyrylation and crotonylation (Cluntun *et al*, 2015; Jo *et al*, 2020). In fact acylation modifications seemed to be even more negatively affected under such conditions. Similar reduction in the acylation marks especially at H3K23 position was observed upon depletion of acetyl CoA pools within the cells by knockdown of different acetyl CoA producing enzymes ATP citrate lyase (ACL), Acetyl Coenzyme A Synthetase Short Chain Family Member 2 (ACSS2) and Carnitine Acetyltransferase (CRAT). Since histone acylation has also been generally associated with transcriptional activation due to opening up of the chromatin, it may be assumed that nutrient deficient conditions become non-conducive for the transcription of genes usually expressed when cells are metabolically more active. As a result, acylation of histones also get reduced along with acetylation. The mechanisms behind how the acyltransferase activity of the enzymes like p300 is regulated under these conditions have not

been investigated yet, and could hold a key for understanding why this contradictory pattern in histone modification takes place.

1.10.2 Possible pathways for increased generation of acyl CoAs

One of the most probable sources of acyl CoA has been speculated to be short chain fatty acids. When cells were flooded with radioisotope labeled short chain fatty acids, there was a concomitant increase in corresponding acylation levels of histones, corroborating this hypothesis (Tan *et al*, 2011; Xie *et al*, 2016; Peng *et al*, 2011). The enzyme that might be responsible for converting the fatty acids to their corresponding acyl CoA derivatives is Acyl Coenzyme A Synthetase Short Chain Family Member 2 (ACSS2) (Sabari *et al*, 2015). The activity of this enzyme could be modulated by enhanced substrate availability because it has been observed that cells treated with increased doses of crotonate showed increased histone crotonylation, a phenomenon that was abolished by knockdown of the enzyme (Sabari *et al*, 2015). Moreover, the redox state and energy availability might also affect ACSS2 activity. In depleted nutrient conditions when glycolytic flux is low, the NAD⁺/NADH ratio will be increased. This could activate the NAD⁺ dependent sirtuin enzymes like SIRT1 leading to deacetylation of substrates like ACSS2. Upon undergoing deacetylation, the activity of ACSS2 is increased which could lead to enhance production of acyl CoA derivatives resulting in increased acylation of histones. These are still speculative hypotheses, and till date no investigation has been carried out to validate them.

The idea that increased fatty acid availability could increase acylation of histones has gained pace in recent times (Figure 24). Experiments have been performed using chemical biology based methods to inhibit different steps of fatty acid synthesis as well as oxidation by treatment with a variety of inhibitors. It was observed that in both cases, histone butyrylation especially at H4K5 position was reduced while acetylation remained relatively unaffected (Gao *et al*, 2021). Fatty acid synthesis takes place in the cytoplasm and small metabolites such as short chain fatty acids in the cytoplasm can permeate into the nucleus. On the other hand, beta oxidation of fatty acids takes place in the mitochondria and there are

still no mechanisms known by which fatty acids produced in the mitochondria can directly enter the nucleus. Still, the mitochondrial activity has been found to be high in patient samples of acute lymphoblastic leukemia, exhibiting high butyrylation levels in histones (Gao *et al*, 2021). All these point to some hitherto unknown mechanism by which fatty acid oxidation can also promote nuclear histone acylation.

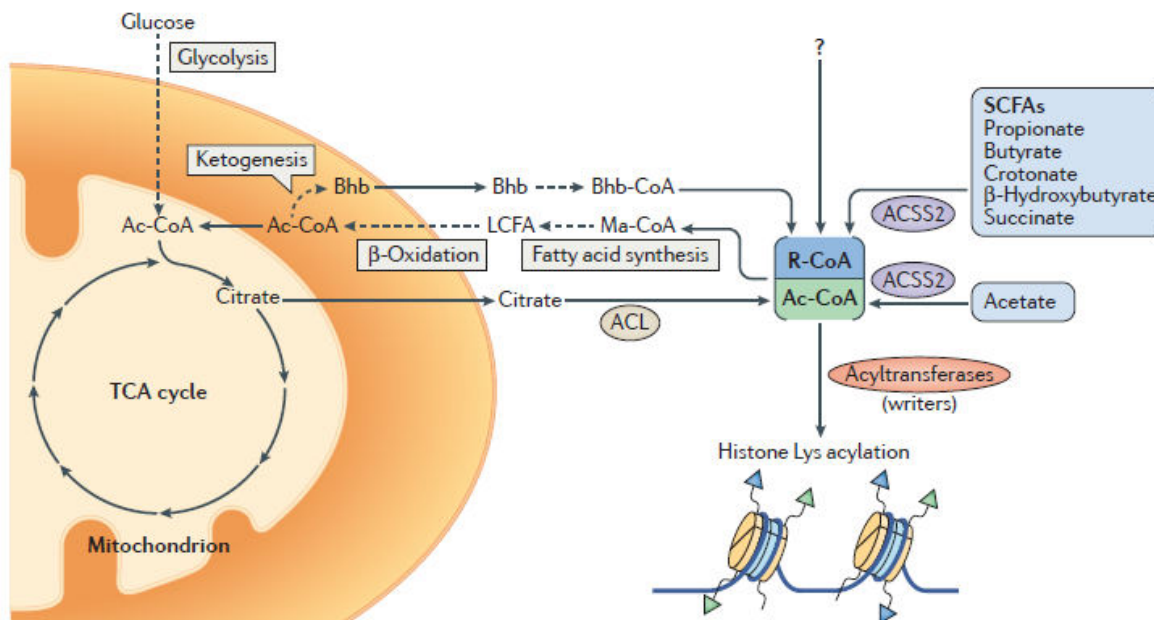


Figure 24: Metabolic reactions showing possible sources of acyl CoA derivatives for histone acylation (Adapted from Sabari et al, Nat Rev Mol Cell Biol, 2017)

Another artificial approach to induce histone acylation was thought to be via perturbation of the enzymes responsible for acyl CoA catabolism. Complete ablation of propionyl CoA carboxylase alpha subunit leads to a drastic reduction in propionyl CoA catabolism leading to accumulation of propionyl CoA and increased histone propionylation at H3K14 (Kebede *et al*, 2017). Surprisingly, the same effect is not seen in mice in which the catabolic enzyme for butyryl CoA i.e. acyl CoA dehydrogenase short chain is ablated, despite there being increased levels of butyryl CoA (Kebede *et al*, 2017). These observations indicate that acylation of histones does not simply follow the law of mass action in which only the stoichiometric levels of the acyl CoA derivatives would be directing the

modification of histones. Instead, there are probably several layers of regulatory mechanisms modulating the activities of different enzymes and transcription factors that influence the histone acylation patterns.

1.11 Background and rationale of the study

There are a myriad of cellular processes and diseases in which histone acylation could be studied for their significance. We speculated that a process in which fatty acid production is high might serve as a good candidate for a case study of histone acylation. One such process in which fatty acids are prominent is adipogenesis i.e. the process by which fat laden cells or adipocytes develop and accumulate as adipose tissues at various sites within the body both as subcutaneous and visceral depots. From the perspective of epigenetics, p300 plays an important role as a chromatin modifier by promoting expression of pro-adipogenic genes. Studies performed in cellular models of adipogenesis have demonstrated that during adipocyte development there is an increase in protein levels of p300, decrease in expression of histone deacetylases that perform antagonistic functions and a concomitant increase in global acetylation of histones (Yoo *et al*, 2006). Moreover, the importance of histone acetylation for adipogenesis has been further underlined by the finding that knockdown of ATP citrate lyase, an enzyme responsible for regeneration of acetyl CoA in the cytoplasm and nucleus, leads to decrease in histone acetylation and also suppression of adipogenesis (Wellen *et al*, 2009).

When dietary intake of energy exceeds energy expenditure, the adipose tissue serves as a conduit for storing the excess energy in the form of lipids. This leads to enlarged adipose tissue due to increased adipocyte number (hyperplasia) by differentiation of pre-adipocytes to adipocytes, and increased size of pre-existent adipocytes (hypertrophy). The enhanced adipose tissue mass is a symptom for the onset of obesity.

Besides adipose tissue, the liver also serves as an important organ for lipid metabolism. Inside the hepatocytes, p300 serves as a key nutritional sensor, which helps in conversion of excess carbohydrates into lipids by promoting lipogenic gene expression. Mechanistically, p300 acetylates and recruits transcription factors such as ChREBP and SREBP1c to the promoters of lipogenic genes that encode proteins required for lipid synthesis (Giandomenica *et al*, 2003; Ponugoti *et al*, 2010; Jang *et al*, 2017; Bricambert *et al*, 2010). With the progression of lipid dysbiosis, lipids are also released from the adipose tissue by the action of hormone sensitive lipase into the portal circulation and begin to accumulate inside the liver. The overall process by which excessive lipid deposition takes place in the liver, either through *de novo* biosynthesis or through excessive intake, is known as hepatic steatosis. Uncontrolled steatosis could lead to inflammation and lipid peroxidation, causing damage to the hepatocytes that are replaced by collagen secreting cells resulting in liver fibrosis.

Collectively, there exists a functional cross-talk between the adipose tissue and liver with respect to lipid metabolism and p300 plays a very important role at the molecular level in both the organs. We took butyrylation as the representative example of acylation to explore a possible role of this modification in adipogenesis and hepatic steatosis. Since p300 catalysed acetylation is a well established phenomenon in these two processes, our hypothesis was that an increased generation of short chain fatty acids could also promote increased histone butyrylation by p300. Due to rapid turnover of histone acetylation, especially in the promoters of highly transcribed genes, p300 might utilize butyryl CoA, derived from butyric acid, to butyrylate histones and keep the lipid biosynthesis related genes transcriptionally active.

1.12 Objectives of the Study

Due to the possibility of redundancy in the functionality of histone butyrylation with acetylation in regulation of adipogenesis and liver steatosis, we adopted a pharmacological approach for establishing the importance of butyrylation. Our aim was to screen for a small molecule modulator that could selectively inhibit p300 catalysed butyrylation without affecting acetylation. This molecule could

therefore be used as a chemical biology based tool to specially highlight the significance of butyrylation in any of our selected processes.

We had two principle objectives of our study:

1) **Understanding the importance of histone butyrylation in adipogenesis**

We aimed to investigate the pattern of histone butyrylation in adipogenesis and also address its importance using the selective inhibitor of butyrylation. With this compound, we would test our hypothesis in a cellular model of adipogenesis. We would further validate our findings in two mouse models of obesity – one high fat diet induced, the other genetic.

2) **Understanding the importance of histone butyrylation in hepatic steatosis**

The same mice models of obesity would serve the purpose of studying the importance of histone butyrylation in hepatic steatosis. Depending on our observations, we would adopt a top-down approach to cross-verify the findings in a cellular model of steatohepatitis.

MATERIALS AND METHODS

Materials and Methods

2.1 General methods

2.2 Protein expression and purification

2.2.1 Purification of full length hexa histidine-tagged p300 from Sf21 insect cells infected with baculovirus of recombinant p300

2.2.2 Purification of hexa histidine-tagged p300 catalytic domain from *E. coli*

2.2.3 Generation of point mutant of p300 catalytic domain C1438A

2.3 *In vitro* enzymatic assays

2.3.1 *In vitro* acetylation assay

2.3.2 *In vitro* butyrylation assay

2.4 Adipogenesis assay

2.5 Hepatic steatosis assay

2.6 MTT assay

2.7 RNA expression analysis

2.7.1 Total RNA isolation

2.7.2 cDNA synthesis

2.7.3 Quantitative real time PCR

2.7.4 Transcriptomics analysis by RNA sequencing

2.8 Histone extraction

2.8.1 Acid extraction of histones from cultured mammalian cells

2.8.2 Acid extraction of histones from mice epididymal fat pads

2.9 Chromatin immunoprecipitation

2.10 Isolation and derivatization of compounds from *Garcinia indica*

2.10.1 Isolation of garcinol from *Garcinia indica*

2.10.2 Synthesis of isogarcinol

2.10.3 Synthesis of LTK-14 and LTK-14A

2.10.4 X-ray crystal structure determination of LTK-14A

2.11 Molecular docking analysis

2.12 Animal experiments

2.12.1 High fat diet induced obesity in mice

2.12.2 Genetically obese mice (db/db)

2.12.3 Hematoxylin and eosin staining of liver and adipose tissue

2.12.4 Picrosirius Red staining of liver

2.12.5 Immunofluorescence staining of liver

2.13 Mass spectrometry

2.13.1 Targeted analysis of butyryl CoA by Ultra-performance liquid chromatography coupled with time-of-flight mass spectrometer (Q-TOF LC/MS)

2.13.2 Untargeted analysis of intracellular metabolites by Ultra-performance liquid chromatography coupled with time-of-flight mass spectrometer (Q-TOF LC/MS)

2.14 Generation and characterization of H4K5 butyrylation antibody

2.1 General methods

2.1.1 Competent cell preparation

Escherichia coli strains BL21 DE3, DH5 α and XL10 Gold were used as competent cells. These were grown overnight in Luria Bertini (LB) medium containing 10 gm/L trypton, 5 gm/L yeast extract and 10 gm/L NaCl (Himedia) at 37°C, 160 rpm. The next day 1% of the inoculum was added to 200 ml LB medium in a 2 L flask and the culture was grown at 37°C, 160 rpm till O.D.₆₀₀ reached a value of 0.35. The culture was spun at 3500 rpm for 7 minutes. Then it was resuspended in 4 ml TSS buffer (a filter sterilized solution of 5 ml 2X LB, 4 ml 25% PEG 43350, 0.5 ml 1M MgCl₂ and 0.5 ml DMSO) and stored at -80°C as 100 μ l aliquots.

2.1.2 Bacterial transformation

Frozen aliquot of competent cells were thawed on ice for 5 minutes before addition of 100 ng of DNA to be transformed, followed by incubation on ice for 30 minutes. Heat shock was given for 90 seconds in a water bath at 42°C and the cells were immediately incubated on ice again for 5 minutes. 1 ml of LB media was added and the cells were kept for 1 hour at 37°C in a shaker incubator at 180 rpm. The cells were then spun down, resuspended in 100 μ l of warmed LB media, spread on LB agar plate containing the appropriate antibiotic for selection and grown overnight at 37°C.

2.1.3 Plasmid purification

DNA was purified from DH5 α cells that were transformed with different plasmids using Mini prep kits according to the protocol supplied by Macherey-Nagel.

2.1.4 Estimation of nucleic acids and proteins

The concentration of nucleic acids was estimated using nanodrop spectrophotometer following the Lambert-Beer's law-

$$A = \epsilon C l$$

Where, A = absorbance, ϵ = molar absorption coefficient in litres/mole-cm, C = concentration (in the units corresponding to ϵ) and l = length of the light path in cm.

Considering absorbance maxima for nucleic acids to be at 260 nm, the corresponding value of ϵ is 50 ng-cm/ μ l for double stranded DNA, 33 ng-cm/ μ l for single stranded DNA and 40 ng-cm/ μ l for RNA.

The concentration of proteins was estimated by Bradford assay using Biorad protein estimation reagent following the protocol supplied by the manufacturers using BSA as a standard.

2.1.5 Agarose gel electrophoresis

Agarose gel electrophoresis was used to detect, visualize, segregate and isolate nucleic acids (RNA and DNA) for different purposes. For preparation of 1% agarose gel, 1 gm of agarose (Sigma) was weighed and mixed with 100 ml of 1X TBE buffer (27 gm Tris, 12.75 gm Boric acid and 8 ml 0.5 M EDTA in 1L) and heated in a microwave oven until agarose was completely dissolved. The melted agarose was allowed to cool for 5 minutes after which ethidium bromide was added (0.5 μ g/ml) and thoroughly mixed. The agarose was then poured in a horizontal casting tray with the well comb in place to further cool and polymerize. The nucleic acid samples were mixed with 6X loading dye (1X: 0.25% Bromophenol blue, 0.25% Xylene cyanol in 40% sucrose) and loaded into the wells with micropipettes. The samples were run at 150 Volts in 1X TBE. The stained gel was subjected to ultraviolet (UV) light illumination in Gel documentation system instrument (Biorad) and nucleic acids were detected upon EtBr fluorescence.

2.1.6 SDS polyacrylamide gel electrophoresis

The resolving gel was prepared with addition of 12% acrylamide: bis-acrylamide (29:1) mix, 375 mM Tris-Cl (pH 8.8), 0.1% SDS, 0.1% APS and 0.05% TEMED and poured into vertical casting apparatus. After solidification of resolving gel, it was layered with a 5% stacking gel (5% acrylamide: bis-acrylamide (29:1) mix, 100 mM

Tris-Cl (pH 6.8), 0.1% SDS, 0.1% APS, 0.1% TEMED with well comb in place. The recombinant proteins and extracted histones were mixed with 5X sample buffer (1X: 50 mM Tris-Cl pH 6.8, 0.1% Bromophenol blue, 2% SDS, 10% glycerol, 100 mM β -mercaptoethanol), heated at 90°C for 5 minutes and loaded into the wells. The samples were run in Tris-Glycine running buffer (1X: 25 mM Tris pH 8.3, 250 mM glycine, 0.1% SDS) at 150 Volts for 1 hour. The gel was stained with coomassie brilliant blue stain (0.25% CBB, 45% methanol, 10% glacial acetic acid) followed by destaining with destaining solution (30% methanol, 10% glacial acetic acid) to visualize the proteins.

2.1.7 Immunoblotting

The protein samples were run in 15% SDS-PAGE, transferred onto PVDF membrane (Milipore) in transfer buffer (25 mM Tris, 192 mM glycine, 0.036% SDS in 20% methanol), blocked with 5% skimmed milk solution to prevent non-specific antibody binding and finally probed with antibodies against acetylation and butyrylation marks prepared in 1% skimmed milk or FBS solution (5% BSA, 1x TBS, 0.1% Tween-20). HRP-conjugated secondary antibodies (Abcam) were used against the primary antibodies to obtain a chemiluminiscent signal in the presence of SuperSignal West Pico Chemiluminiscent Substrate (Thermo Scientific) which was developed using the VersaDoc imaging system (Biorad).

2.1.8 Dot blot assay

Unconjugated peptide was reconstituted with water to a final concentration of 1 microgram/microlitre. Different dilutions of the peptide were prepared. Nitrocellulose membrane was cut (2 cm X 10 cm) and placed over an aluminium foil. A sharp pencil was used to fix the points for different peptide concentrations with a gap of 1.5 cm. At each point, 4 microlitres of peptide solution were added and allowed to dry. The membrane was washed in PBS and then kept in 5% skimmed milk solution for 30 minutes. After that the membrane was kept in a plastic sheet along with the antibody solution and sealed and then kept at 4°C on a rocker overnight. The next day the membrane was incubated with the

corresponding HRP-conjugated secondary antibody followed by development of chemiluminiscent signal using SuperSignal West Pico Chemiluminiscent Substrate (Thermo Scientific) and image collection using the VersaDoc imaging system (Biorad).

2.1.9 Cell culture

The mammalian cell lines used in this study, namely 3T3L1, HepG2 and insect cell line Sf21 were obtained from ATCC (American Type Culture Collection). 3T3L1 was grown in DMEM-High Glucose (Dulbecco's Modified Eagle's Medium containing 25 mM Glucose). HepG2 was grown in DMEM-No Glucose (Dulbecco's Modified Eagle's Medium without any glucose and pyruvate) supplemented with 5MM glucose under normal culture conditions. Insect cell line Sf21 was grown in Grace's Insect Medium. In all cases the growth medium was supplemented with 10% FBS (Fetal Bovine Serum). Mammalian cells were grown in 37°C incubator with 5% CO₂ and 90% relative humidity while the insect cells were grown in 25°C incubator.

2.2 Protein expression and purification

2.2.1 Purification of full length hexa histidine-tagged p300 from Sf21 insect cells infected with baculovirus of recombinant p300

Polyhistidine tagged recombinant p300 was purified from Sf21 insect cells by Ni-NTA based affinity chromatography. These cells were infected by the baculovirus containing p300 for 72 hours. Once the cells showed signs of infection, they were scraped off and centrifuged to separate the spent media. The cell pellets were resuspended in ice cold homogenisation buffer (20 mM Tris, pH 7.5; 20 mM imidazole, 10% glycerol, 0.2 mM EDTA, 300 mM KCl, 0.1%NP-40, 2 mM PMSF, 2 mM βmercaptoethanol) and then homogenised using a Dounce homogeniser (5 cycles, 6 strokes per cycle with 5 minutes interval between each cycle). The cell debris was separated by centrifugation and then the lysate was incubated with pre-equilibrated Ni-NTA slurry for 2.5 hours at 4°C on an end-to-end rotor. Then

the beads were washed with wash buffer (20 mM Tris, pH 7.5; 40 mM imidazole) nine times to remove unwanted contaminants. Finally p300 was eluted using elution buffer (20 mM Tris, pH 7.5; 250 mM imidazole).

2.2.2 Purification of hexa histidine-tagged p300 catalytic domain from *E. coli*

Polyhistidine tagged p300 catalytic domain cloned in pET28b plasmid and Sirt2 were used for co-transforming BL21(DE3) cells. At first, 50 ml primary culture was prepared in Luria broth containing kanamycin (50 µg/ml) and ampicillin (100 µg/ml) (HIMEDIA) and then it was scaled up 10 times to prepare secondary culture. Incubation was done at 37°C, 180 rpm till O.D. reached 0.37 followed by induction with 0.2 mM IPTG and a further incubation at 30°C for 4 hours. Cells were pelleted at 6000 rpm, 4°C for 10 minutes and stored at -80°C. Resuspension and homogenisation of the pellet was carried out in homogenisation buffer (20 mM Tris, pH 7.5; 20 mM imidazole, 10% glycerol, 0.2 mM EDTA, 300 mM KCl, 0.1%NP-40, 2 mM PMSF, 2 mM βmercaptoethanol). 3 cycles of sonication were done for 3 minutes at 35% amplitude with 5 minutes interval between each cycle. The cell debris were separated by pelleting at 12000 rpm for 30 minutes at 4°C. The supernatant was equilibrated with Ni-NTA beads slurry (Novagen) in an end-to-end rotor for 3 hours at 4 C. Eight washes were given with wash buffer (20 mM Tris, pH 7.5; 40 mM imidazole). Elution was carried out in batches with elution buffer (20 mM Tris, pH 7.5; 250 mM imidazole).

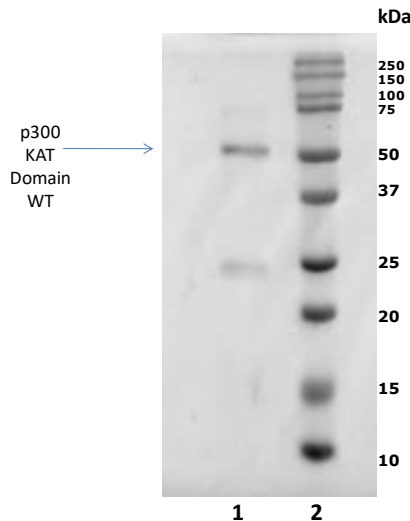


Figure 1: Purification profile of wild type p300 KAT domain.

2.2.3 Generation of point mutant of p300 catalytic domain C1438A

Point mutation was introduced into the p300 catalytic domain sequence cloned within pET-28b plasmid by using the Quikchange site directed mutagenesis kit (Agilent). Briefly, the template was mixed with *Pfutura* DNA polymerase, designed forward and reverse primers and dNTPs for PCR (Initial denaturation for 30 seconds at 95°C; Cycles: 95°C for 30'', 55°C for 60'', 68°C for 7'; final elongation at 68°C for 5'.) The mixture was then incubated with DpnI enzyme for 2.5 hours for removal of the parent wild type sequence followed by transformation of competent XL10Gold cells and kanamycin selection of positive transformants. The inserted mutation was verified by sequencing and alignment with the wild type sequence using ClustalOmega software.

The sequences of the primers used are as follows:

Forward primer- 5'- CCTCACTTGGTGGAGCTGCCCAAATATGCCCTGTTGTG – 3'

Reverse primer- 5'- CACAACAGGGCATATTTGGGCAGCTCCACCAAGTGAGG -3'

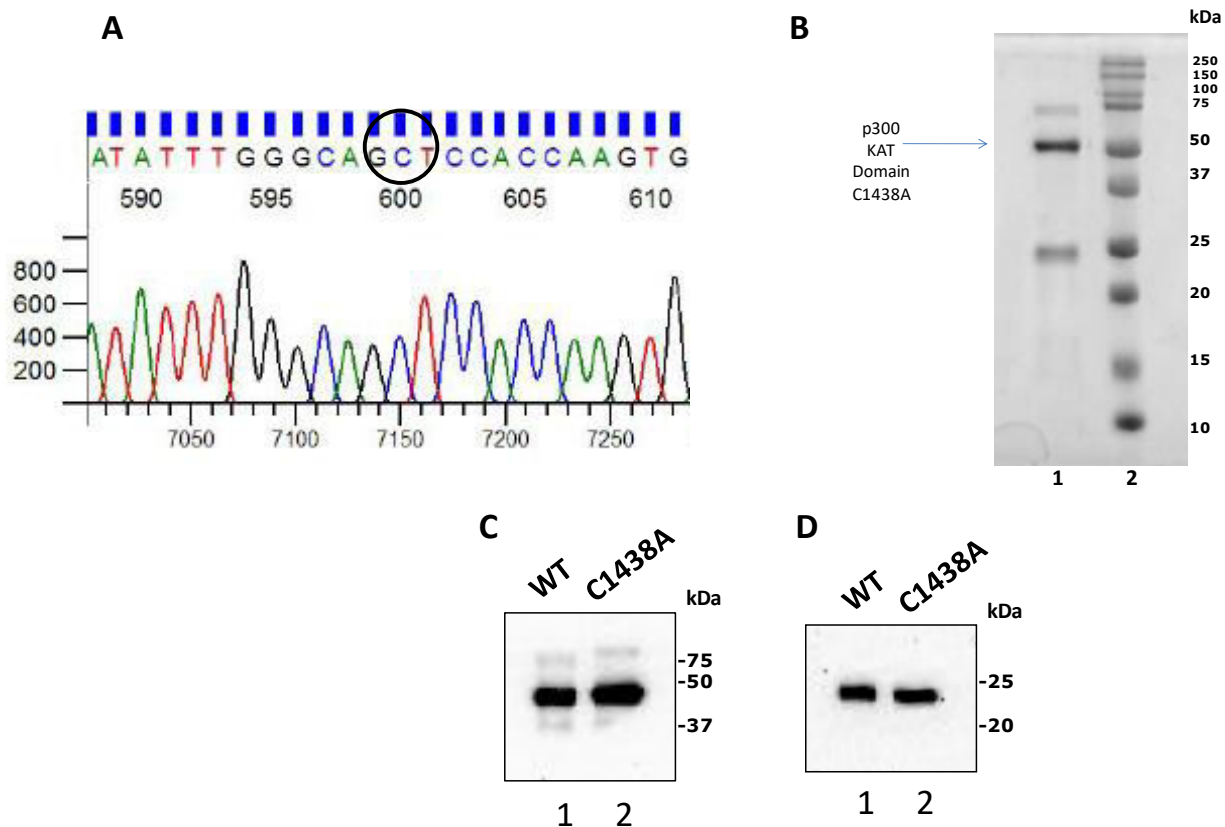


Figure 2: (A) Sequence chromatogram of mutated C1438A p300 KAT domain. Three mutated residues are encircled. (B) Purification profile of C1438A p300 KAT domain mutant. Immunoblotting image of wild type and mutant C1438A p300 KAT domain with antibody against p300 catalytic domain, demonstrating similar migration properties of the two full length proteins in polyacrylamide gel electrophoresis (C). The lower band at 25 kDa position corresponds to a degraded fragment for both proteins that also was recognized by the antibody (D).

2.3 *In vitro* enzymatic assays

2.3.1 *In vitro* acetylation and filter binding assay

Different dilutions of purified enzyme were incubated in reaction buffer (50 mM Tris-HCl pH 7.5, 1 mM DTT, 10 % Glycerol, 2 mM PMSF) with 10 mM NaBu, tritiated acetyl CoA (50 μ Ci) (PerkinElmer, Part No: NET290050UC) and *Xenopus* histone H3 (500 ng) for 30 minutes at 30°C. The reaction mixture was then spotted on P81 filter paper and the paper was allowed to dry at room

temperature. The paper was washed in wash buffer (50 mM sodium bicarbonate and 50 mM sodium carbonate), dried at 90°C and immersed in enhancing solution (2.5% PPO and 0.25% POPOP in toluene) for taking radioactive counts using liquid scintillation counter (Perkin Elmer, MicroBeta2 system).

2.3.2 *In vitro* acylation assay

Acylation reactions were performed in reaction buffer (25 mM Tris-HCl pH 7.5, 100 mM NaCl, 0.1 mM EDTA, 1 mM DTT, 10 % Glycerol, 1x PIC) with 100 ng/mL TSA, and 50 μM Butyryl-CoA/Acetyl CoA. *Xenopus* histone H3 (1 μg) was used as the substrate and full length p300 or p300 catalytic domain (10,000 cpm activity) was used as the enzyme. Reactions were incubated in presence or absence of butyrylation inhibitor for 10 minutes at 30 °C, followed by initiation of the acetylation/butyrylation reaction by the addition of acetyl CoA/butyryl CoA. After a further 10 minutes, reactions were stopped by addition of Laemmli buffer and samples were used for immunoblotting.

2.4 Adipogenesis assay

3T3L1 preadipocytes were grown to confluency and 24 hours post-confluence, cells were incubated with differentiation medium (growth medium containing 1μM Dexamethasone, 0.5 mM IBMX and 1 μg/ml insulin) for 2 days. Then the cells were supplemented with maintenance medium (growth medium with 1 μg/ml insulin only) every alternate day. On the 6th / 7th day post induction of differentiation, the cells were stained with Oil Red-O to estimate the extent of adipogenesis. At first, the cells were fixed with 3.7% formaldehyde solution followed by a brief wash in phosphate buffered saline (PBS). Then the cells were pre-incubated in 60% isopropanol for 5 minutes followed by staining with Oil Red-O dye (Sigma-Aldrich) (prepared in 60% isopropanol) for 1 hour at room temperature. Excess background stain was removed by giving multiple washes

with water. The incorporated dye was extracted using isopropanol and absorbance values were determined spectrophotometrically at 510 nm to estimate total amount of lipid accumulation under different experimental conditions.

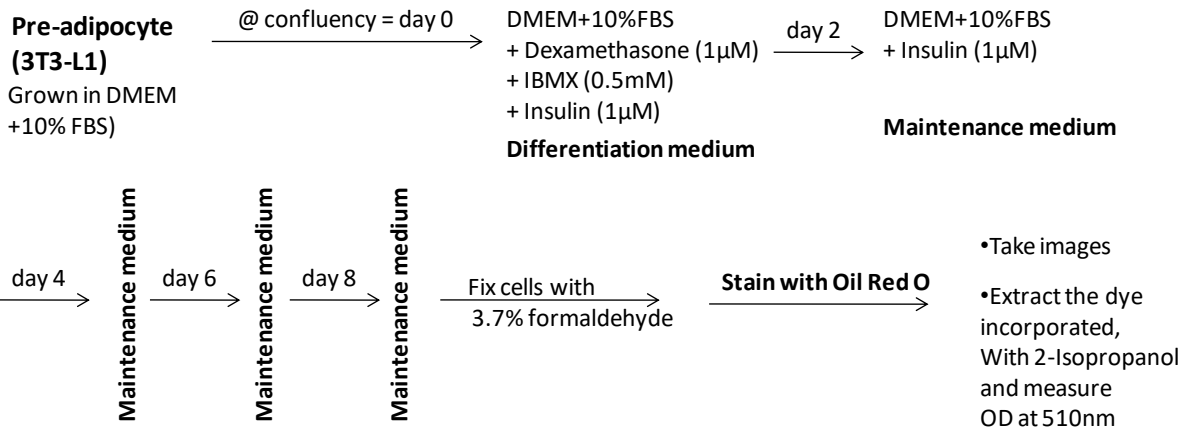
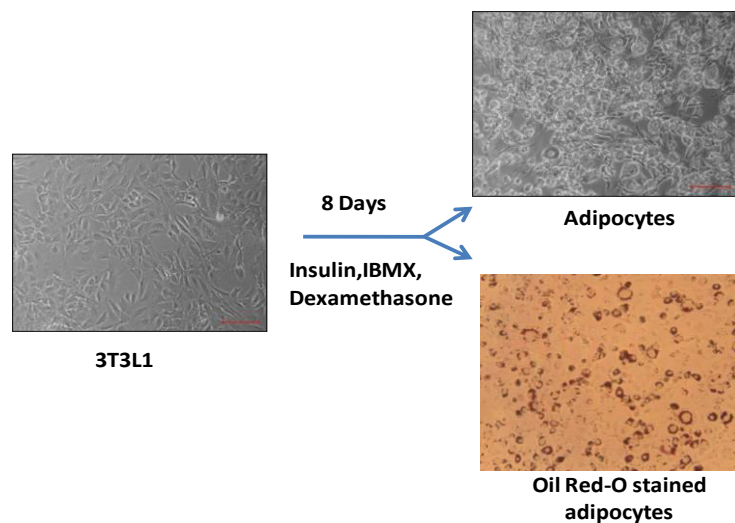
A**B**

Figure 3: (A) Schematic representation of the steps followed for inducing adipogenesis in 3T3L1 cells. (B) Phase contrast images of 3T3L1 cells exhibiting fibroblast like morphology in

their pre-adipocyte state and accumulation of lipid droplets in their adipocyte state. The lipid droplets can be stained using Oil Red-O dye.

2.5 Hepatic steatosis assay

HepG2 cells were grown in DMEM with low glucose (5 mM) till they reached around 70 percent confluent state. Steatosis was induced by changing the media to DMEM with high glucose (25 mM) along with the addition of 100 nM insulin. 24 hours later, the cells were stained with Oil Red-O to estimate the extent of steatosis. At first, the cells were fixed with 3.7% formaldehyde solution followed by a brief wash in phosphate buffered saline (PBS). Then the cells were pre-incubated in 60% isopropanol for 5 minutes followed by staining with Oil Red-O dye (Sigma-Aldrich) (prepared in 60% isopropanol) for 10 minutes at room temperature. Excess background stain was removed by giving multiple washes with water. The incorporated dye was extracted using isopropanol and absorbance values were determined spectrophotometrically at 510 nm to estimate total amount of lipid accumulation under different experimental conditions.

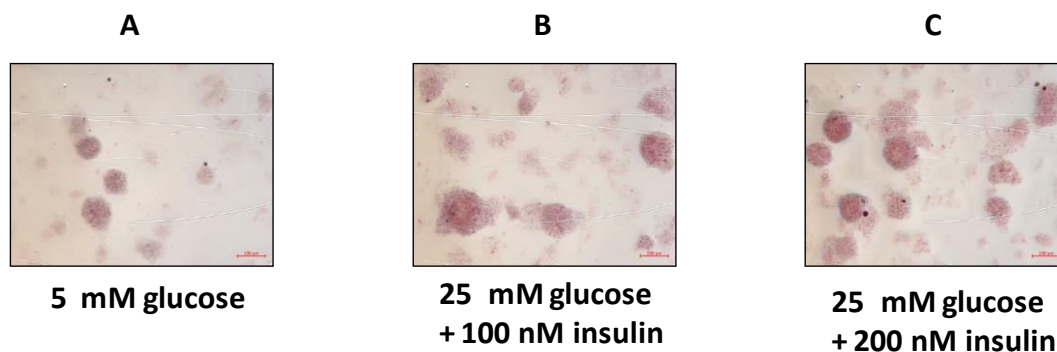


Figure 4: Representative images (10X magnification) of Oil Red-O stained HepG2 cells cultured under low glucose conditions (A) and also upon exposure to high glucose concentration and different doses of insulin for 24 hours (B,C).

2.6 MTT assay

Cells were seeded in 96 well plates (12500 cells/ ml) and maintained under desired conditions. On the respective days they were treated with 1/10th volume of 5mg/ml MTT solution [3-(4,5-dimethylthiazol-2-yl)-2,5-diphenyltetrazolium bromide] by incubation at 37 °C for 3 hours. During this time the yellow coloured tetrazolium dye would be reduced by intracellular oxidoreductase enzymes to produce insoluble purple coloured formazan crystals. The media was aspirated and the formed crystals were dissolved using DMSO (Dimethyl Sulfoxide). The absorbance of the colored solution was measured spectrophotometrically at 570 nm.

2.7 RNA expression analysis

2.7.1 Total RNA isolation

Cultured cells were lysed using Trizol solution (Ambion Life Technologies). For RNA isolation from mice fat pads, the adipose tissues were homogenized in Trizol with a mechanical homogenizer. Chloroform was added to the sample (1/5 th volume of Trizol i.e. 0.2 ml to 1 ml sample) and mixed by shaking and inverting for 15 seconds followed by incubation at room temperature for 5 minutes. Samples were centrifuged at 13000 rpm for 15 minutes at 4°C. The aqueous phase containing the RNA was aspirated and to it an equal volume of isopropanol was added followed by incubation at room temperature for 10 minutes. The RNA was precipitated by centrifugation of the samples at 13000 rpm for 10 minutes at 4°C. The RNA pellets were washed twice with 75% ethanol and air-dried. The RNA pellets were dissolved in RNase free water, which was facilitated by incubation at 60°C for 10 minutes. The concentration of RNA was determined using nanodrop spectrophotometer. 10 microgram of the RNA was taken and incubated with DNase I (4 International Units) for 20 minutes at 37°C. The enzyme was inactivated by addition of 5mM EDTA and heating for 10 minutes at 70°C. To the samples, 1/10th volume of 3 M sodium acetate and 250 microlitres of absolute

ethanol were added followed by overnight precipitation at -80°C . The next day, RNA was precipitated by centrifugation at 13000 rpm for 30 minutes at 4°C , and then twice washed with 75% ethanol. After air drying, the RNA was again dissolved in RNase free water by heating at 60°C for 10 minutes.

The purified RNA samples were run in 1% agarose gel to assess the quality of RNA where 28S rRNA and 18S rRNA appeared as two distinct bands with intensity of 2:1 ratio. The samples were stored at -80°C until further use.

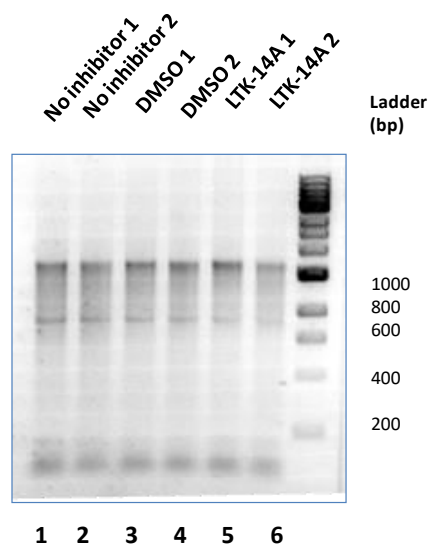


Figure 5: Ethidium bromide stained 1% agarose gel showing integrity of RNA isolated from 3T3L1 cells. Lanes 1 to 6 correspond to cells under different treatment conditions.

2.7.2 cDNA synthesis

1-2 μg of RNA was taken as template and incubated with 40 picomoles of oligo dT and 1 mM dNTPs in a 10 microlitre reaction volume at 70°C for 10 minutes followed by immediate incubation in ice for 10 minutes. The reaction was initiated by addition of MMLV Reverse Transcriptase (MMLV RT) and RT buffer making up the volume to 20 microlitres and then incubation at 37°C for 50 minutes. Finally the enzyme was inactivated by incubating the reaction mixture at 90°C for 10 minutes.

2.7.3 Quantitative real time PCR

QRT-PCR amplification was done in kappa SYBR green reagent (Biosystems) (Initial denaturation for 10 minutes at 95°C; Cycles: 95°C 15'', 65°C for 30'', 72°C for 30'') with the help of Real time PCR instrument (Applied Biosystems). For estimation of relative fold change in RNA expression, the following calculation was done: Relative fold change = $2^{-\Delta\Delta Ct}$, where $\Delta\Delta Ct = \Delta Ct$ value of sample – ΔCt value of control and $\Delta Ct = Ct$ value of target – Ct value of internal control eg. actin for individual sample. The sequences of primers are provided in Table 1 (Annexure).

2.7.5 Transcriptomics analysis by RNA sequencing

RNA integrity was checked by Agilent Bioanalyzer 2100, only samples with clean rRNA peaks were used. Libraries for RNA-seq were prepared according to KAPA Stranded RNA-Seq Kit with RiboErase (KAPA Biosystems, Wilmington, MA) system. Final library quality and quantity were analyzed by Agilent Bioanalyzer 2100 and Life Technologies Qubit3.0 Fluorometer, respectively. 150 bp Paired-end sequencing was performed on Illumina HiSeq 4000 (Illumina Inc., San Diego, CA).

House mouse (*Mus musculus*, strain C57BL/6J) genome (mm10) was downloaded from GENCODE and indexed using Bowtie2-build with default parameters. Adapter removal was done using Trim Galore (v 0.4.4) and each of the raw Fastq files were passed through a quality check using FastQC. PCR duplicates were removed using the Samtools 1.3.1 with the help of 'rmdup' option. Each of the raw files was then aligned to mm10 genome assembly using TopHat2 with default parameters for paired-end sequencing as described in (Trapnell *et al*, 2012). After aligning, quantification of transcripts was performed using Cufflinks and then Cuffmerge was used to create merged transcriptome annotation. Finally differentially expressed (DE) genes were identified using Cuffdiff. The threshold for DE genes was \log_2 (fold change) >1.5 for up regulated genes and \log_2 (fold change) <1.5 for down regulated genes with p-value <0.05.

Gene Ontology (GO) analysis was performed in PANTHER (Thomaset *et al*, 2003). Significant enrichment test was performed with the set of differentially expressed genes in PANTHER and Bonferroni correction method was applied to get the best result of significantly enriched biological processes.

Fisher's exact test was performed in PANTHER Gene Ontology (GO) where p-value significance was calculated based on the ratio of obtained number of genes to the expected number of genes (O/E) considering the total number of genes for the respective pathway in *Mus musculus* with a FDR of <0.05.

Unsupervised hierarchical clustering method was performed using Cluster 3.0 (de Hoon *et al*, 2003) with Pearson Correlation and average linkage rule. Gene expression data (FPKM of all samples) was taken and log₂ transformed. Low expressed (FPKM<0.05) and invariant genes were removed. Then genes were centered and clustering was performed based on differential expression pattern of genes and fold change. Finally, the heatmap was visualized in Java TreeView 3.0.

Statistically significant differentially expressed transcripts were subjected to GO and Pathway enrichment using DAVID tool. Only those GO and pathways with a FDR score of ≤ 0.05 was considered for further downstream analysis. Key biologically dysregulated GO and Pathways along with the differentially expressed genes was provided as an input to Pathreg algorithm from Theomics International Pvt Ltd, Bangalore, India for gene regulatory network modeling. The result (nodes and edges) of the Pathreg algorithm was provided as an input to Cytoscape v2.8.2 to identify key nodes and edges that could be representative of the gene regulatory changes upon treatment.

Identification of pro-adipogenic and anti-adipogenic factors was performed by manual curation of candidate genes from previously published reports and Mouse Genome Informatics international database of genes involved in fat cell differentiation.

2.8 Histone extraction

2.8.1 Acid extraction of histones from cultured mammalian cells

Cells were washed with ice-cold PBS and then resuspended in Triton extraction buffer (PBS containing 0.5% Triton X-100 (v/v) and 2 mM PMSF). The cells were allowed to lyse on ice for 10 minutes, spun down, washed with PBS and the process was repeated another time. Then the proteins were acid extracted with 0.2 N HCl for two hours on ice. The debris was spun down and then histones were precipitated by incubating the supernatant with 33% trichloroacetic acid (Sigma-Aldrich) at 4°C for 30 minutes. The histones were then pelleted down and then given two washes with acetone. The pellet was allowed to air-dry for 10 minutes and then resuspended with 50 mM Tris-Cl, pH 7.4.

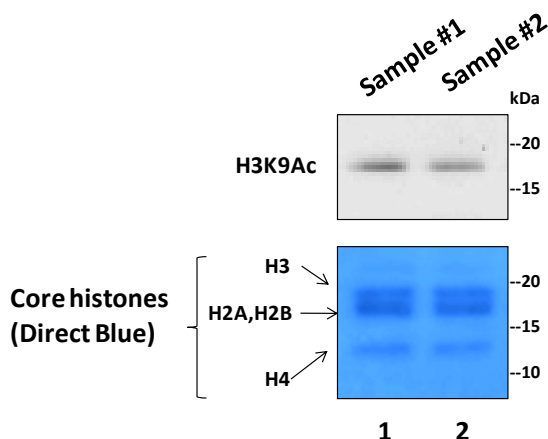


Figure 6: Direct blue stained PVDF membrane showing all four core histones acid extracted from cultured HEK293 (from two dishes). The suitability of these samples for immunoblotting was verified by probing with H3K9 acetylation specific antibody.

2.8.2 Acid extraction of histones from mice fat pads

Extraction of histones from fat pads was performed by mechanically homogenizing the adipose tissues in Triton extraction buffer (PBS containing 0.5%

Triton X-100 (v/v) and 2 mM PMSF). The homogenate was transferred to a different tube and the nuclear pellet was spun down. The upper phase containing the lipids were removed as much as possible by aspiration using gel loading tips and then proteins were acid extracted from the pellet with 0.2 N HCl for four hours on ice. The debris was spun down and then histones were precipitated by incubating the supernatant with 33% trichloroacetic acid (Sigma-Aldrich) at 4°C for 30 minutes. The histones were then pelleted down and then given two washes with acetone. The pellet was allowed to air-dry for 10 minutes and then resuspended with Tris Glycine buffer / 1X SDS running buffer (1 L of 5X buffer contains 15.1 gm Tris, 94 gm glycine and 50 ml 10% SDS).

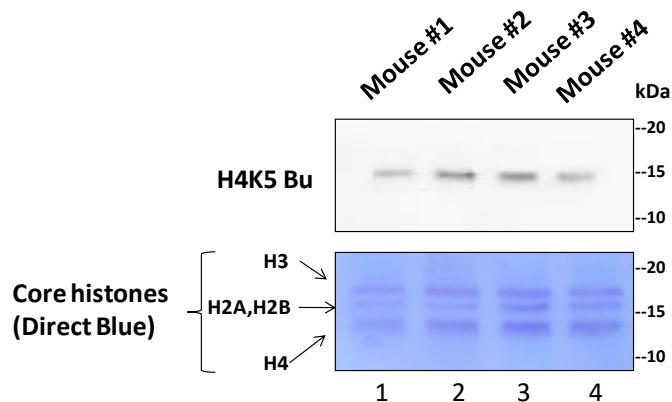


Figure 7: Direct blue stained PVDF membrane showing all four core histones acid extracted from epididymal fat pads of four different mice. The suitability of these samples for immunoblotting was verified by probing with H4K5 butyrylation specific antibody.

2.9 Chromatin Immunoprecipitation

Nuclear ChIP was performed using intact nuclei from cells for removal of lipids. 3T3L1 that were either undifferentiated or differentiated for 3 to 6 days were cross-linked using 1% formaldehyde. Nuclear fractions were obtained by sequentially lysing the cells in two buffers- lysis buffer 1 (140 mM NaCl, 1 mM EDTA, 50 mM HEPES, 10% Glycerol, 0.5% NP-40, 0.25% Triton X-100) and lysis buffer 2 (10 mM Tris pH 8, 200 mM NaCl, 1 mM EDTA, 0.5 mM EGTA). This was followed by lysis in SDS lysis buffer (1% SDS, 10 mM EDTA, 50 mM Tris-HCl pH 8).

Lysates were sonicated in a Diagenode Bioruptor (Liège, Belgium) to produce 200 to 1000 bp DNA fragments. The cell lysates were incubated with H4K5 Bu antibody (PTM Biolabs) or preimmune IgG per sample and 25 μ l of magnetic protein G Dynabeads (catalog no. 10003D; Novex, Waltham, MA) overnight at 4°C. Beads were then washed successively with low-salt buffer (0.1% SDS, 1% Triton X-100, 2 mM EDTA, 20 mM Tris-HCl pH 8, and 150 mM NaCl), high-salt buffer (0.1% SDS, 1% Triton X-100, 2 mM EDTA, 20 mM Tris-HCl pH 8, and 500 mM NaCl), LiCl buffer (250 mM LiCl, 1% NP-40, 1% NaDOC, 1 mM EDTA, and 10 mM Tris-HCl, pH 8), and TE (10 mM Tris-HCl pH 8 and 1 mM EDTA). DNA-protein complexes were recovered from beads in elution buffer (0.1% SDS and 100 mM NaHCO₃). The CHIP eluates and input samples in the elution buffer were then reverse cross-linked by adding 200 mM NaCl and 20 μ g proteinase K (Sigma) and incubating at 65°C for 4 h. Subsequently, 20 μ g of RNase A (Sigma) were added and the samples were further incubated for 15 min at 37°C. The immunoprecipitated DNA was extracted using phenol-chloroform, ethanol precipitated, and used for quantitative PCR. The region-specific primer sets used for the CHIP-qPCR analysis have been mentioned in Table 2 (Annexure).

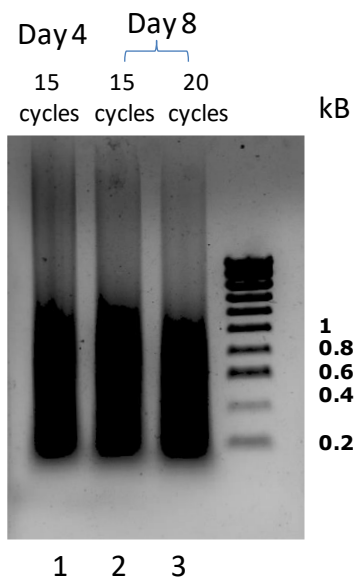


Figure 8: Standardisation of sonication of chromatin from 3T3L1 cells differentiated for 4 to 8 days. The extracted DNA was run in 1% agarose gel and stained with Ethidium Bromide to check for sonicated DNA fragments. Lane 1 - 3T3L1 differentiated for 4 days and sonicated for 15 cycles; Lane 2 - 3T3L1 differentiated for 8 days and sonicated for 15 cycles; Lane 3 - 3T3L1 differentiated for 8 days and sonicated for 20 cycles.

2.10 Isolation and derivatization of compounds from *Garcinia indica*

2.10.1 Isolation of garcinol from *Garcinia indica*

Garcinia Indica fruit rinds were sun dried and powdered by a grinder. 100 gm dry powder was taken in a one liter beaker and 300 ml methanol was added to it. The entire mass was then stirred at room temperature for 24 hours. It was then filtered through Buchner funnel and washed with additional 100 ml methanol. The residue was taken into 150 ml methanol and allowed to stir at room temperature for another 24 hours. It was again filtered, and the combined filtrates were evaporated to dryness to obtain 53 gm wine red colored thick syrup as crude mass. The dry mass was washed with 300 ml water and extracted with ethyl acetate (150 ml × 3). The combined organic layers were washed with brine, dried over anhydrous sodium sulfate and evaporated to dryness under reduced pressure to obtain 35 gm crude thick liquid. Garcinol was further isolated by column chromatography using 8-10% ethyl acetate in hexane as eluting solvent. 900 mg garcinol was isolated after which further trituration in hexane ultimately produced 730 mg pure garcinol as pale yellow solid. Spectral analysis was consistent with pure garcinol and also matched with the literature report.

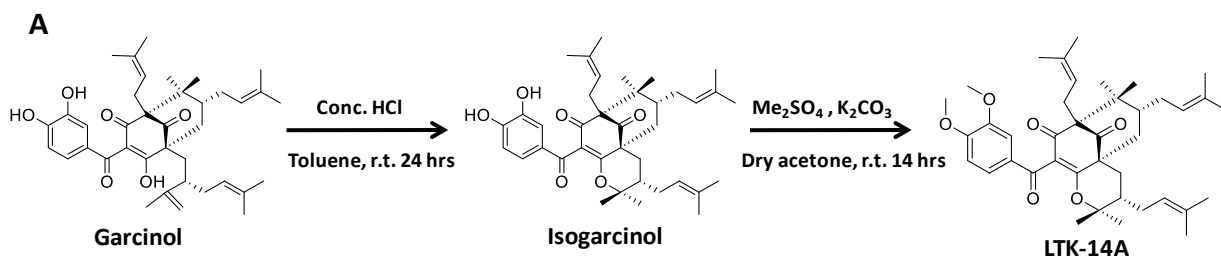
2.10.2 Synthesis of isogarcinol

To a stirred solution of garcinol (200 mg, 0.33 mmol) in toluene, concentrated HCl was added dropwise (11.5 N, 100 µl). The resulting solution was stirred for 24 hours at room temperature. Toluene was evaporated from the reaction mass followed by addition of ice. A heavy white precipitate was observed which further filtered and washed with cold water. The residue was dried and the dry mass was

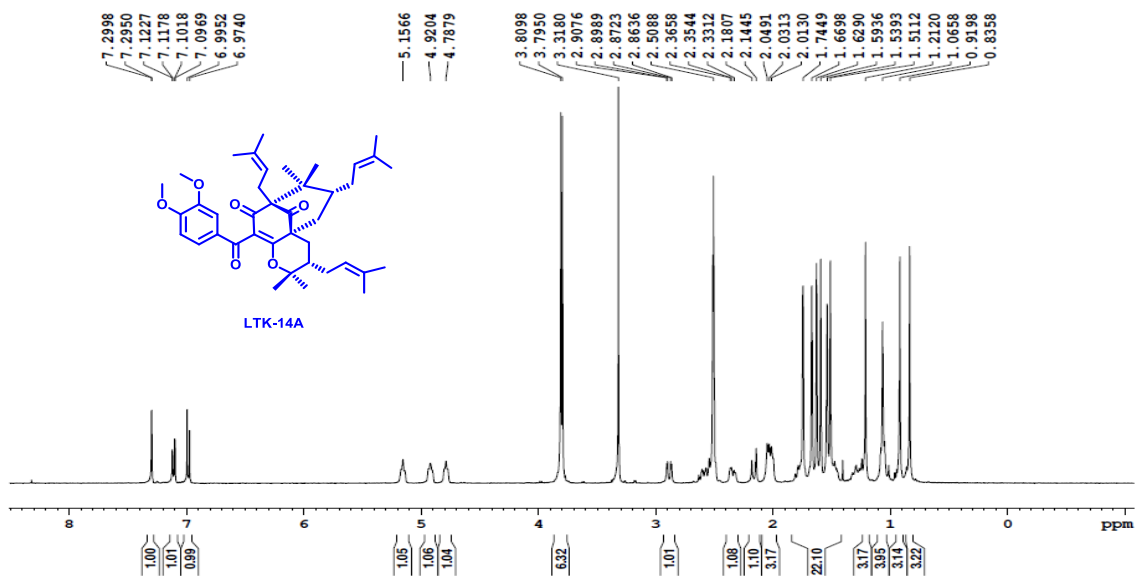
further purified by crystallization in. Spectral analysis was consistent with isogarcinol and also matched with the literature report.

2.10.3 Synthesis of LTK-14A

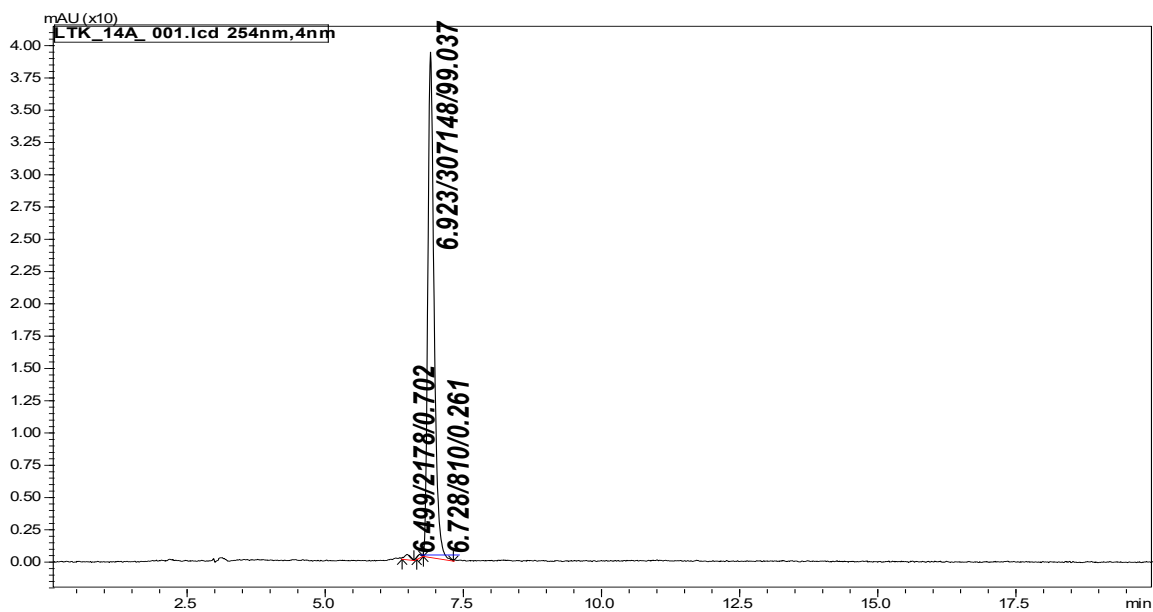
Anhydrous potassium carbonate (0.41 mmol) was added to a stirred solution of isogarcinol (100 mg, 0.16 mmol) in dry acetone. The mixture was stirred for 1 hour at room temperature followed by dropwise addition of dimethyl sulfate (0.41 mmol) under nitrogen gas atmosphere. The resulting reaction mixture was further stirred at room temperature for 14 hours. Progress of the reaction was monitored through thin layer chromatography. Acetone was evaporated from the reaction mass, ice was added and acidified with 5% aqueous HCl (pH ~ 5-6). A pale brown precipitate was observed, which was filtered and washed with cold water. The dry mass was then chromatographed on silica gel using 5-6% ethyl acetate in hexane as eluting solvent mixture. 720 mg (69%) LTK14A was isolated as white solid. NMR spectral analysis was consistent with the desired product. A 20 mg sample was dissolved in hot methanol and placed in a flat surface glass vial with access to very slow solvent evaporation. Crystals as colorless needles were isolated. The purity of the synthesized LTK-14A was found to be more than 98% as verified by HPLC and only the protonated species of LTK-14A were observed in the ESI spectra of the corresponding fraction.



B



C



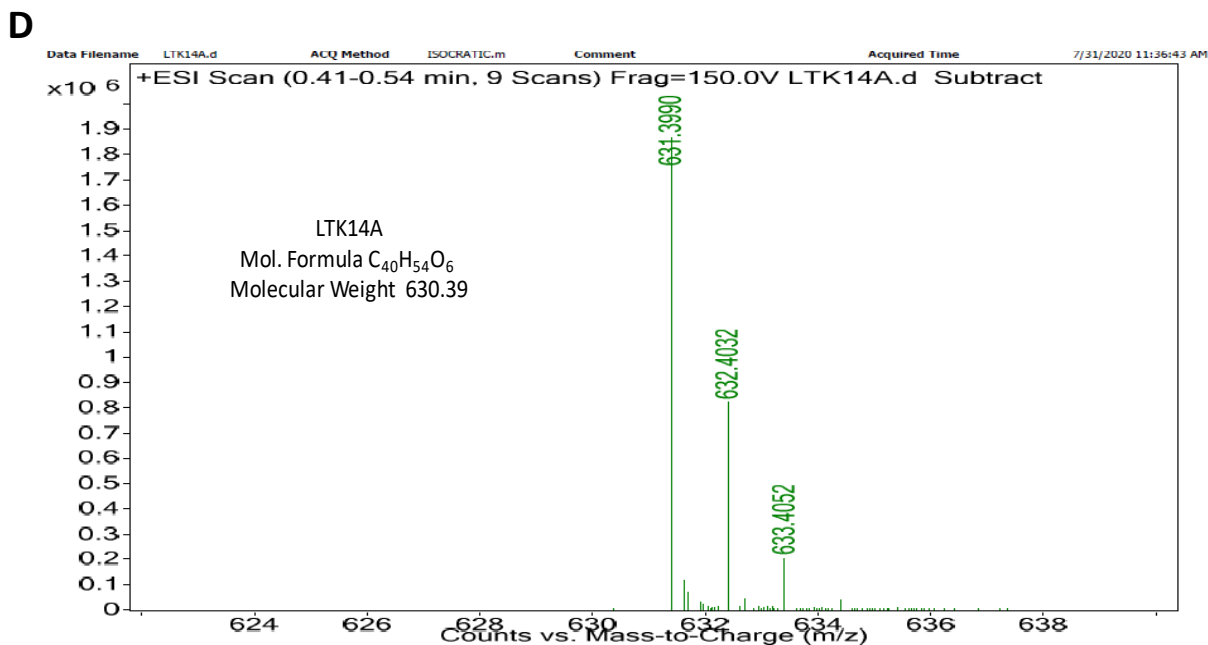


Figure 9: (A) Outline of synthetic route of LTK-14A. (B) Proton NMR spectra of LTK-14A for its structural confirmation. (C) HPLC chromatogram to demonstrate >98% purity of synthesized LTK-14A. (D) HR-MS spectra of purified LTK-14A for verification of its presence in the sample used for HPLC.

2.10.4 X-ray crystal structure determination of LTK-14A

Suitable single crystal with approximate dimensions of $0.35 \times 0.18 \times 0.15$ mm³ was used for X-ray diffraction analyses by mounting on the tip of a glass fibre in air. Data were collected on a Bruker kappa apex 2 with Mo K α ($\lambda=0.71073$ Å) at 296 (2) K. The structure was solved by direct method using program SHELXL-97 and subsequent Fast Fourier Transform technique. Crystallographic for LTK14A have been deposited in Cambridge Crystallographic Data Centre (CCDC: 1969185). The relevant details of the crystal structure are summarized below-

Empirical formula	$C_{40}H_{54}O_6$
Formula weight	630.86
Temperature/K	296 (2)

Crystal system	monoclinic
Space group	C2
a/Å	19.1677(11)
b/Å	11.5860(7)
c/Å	16.8399(11)
α /°	90
β /°	90
γ /°	90
Volume/Å ³	3739.8(4)
Z	110
ρ_{calc} /cm ³	1.417
μ /mm ⁻¹	0.131
F(000)	1650
Crystal size/mm ³	0.35 × 0.18 × 0.15
Radiation	MoK α (λ = 0.71073)
2 θ range for data collection/°	0.995 to 25.75
Index ranges	-23 ≤ h ≤ 23, -14 ≤ k ≤ 14, -20 ≤ l ≤ 20
Reflections collected	108274
Independent reflections	108274 [R _{int} = 0.0811, R _{sigma} = 0.0325]
Data/restraints/parameters	7123/3/415
Goodness-of-fit on F ²	1.045
Final R indexes [I >= 2 σ (I)]	R ₁ = 0.1038, wR ₂ = 0.2797
Final R indexes [all data]	R ₁ = 0.1362, wR ₂ = 0.3157

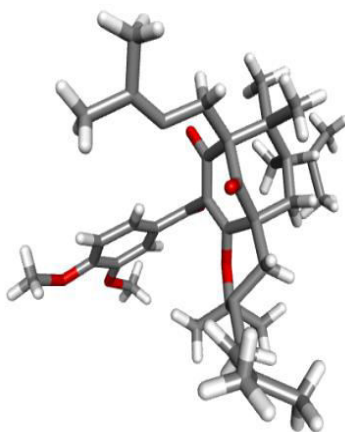


Figure 10: Crystal structure of LTK-14A (CCDC: 1969185)

2.11 Molecular docking analysis

Glide module of Schrodinger suite was used to dock LTK-14 and LTK-14A to p300 catalytic domain (PDB: 3BIY). Chimera was used as visualizing software. The protein was prepared using the wizard tool in Maestro version 10.2. The crystal structure of LTK-14A (CCDC 1969185) and LTK-14 (CCDC 645420) were used as the most optimized and energy minimized ligand structures. The receptor grid for p300 catalytic domain was generated by specifying the binding (active) site residues using Receptor grid generation in the Schrodinger Glide application. Once the receptor grid was generated, the ligands LTK-14 and LTK-14A were docked to the p300 catalytic domain using Glide version 5.8 molecular docking.

2.12 Animal experiments

2.12.1 High fat diet induced obesity in mice

Male C57BL/6J mice (8 weeks old) were bred in house and acclimatized for 1 week prior to experiments. Mice were maintained on a 12 hour light/dark cycle and given ad libitum access to food and water. Experiments were carried out in accordance with the Committee for the Purpose of Control and Supervision of Experiments on Animals (CPCSEA) guidelines and were approved by the Institutional Animal Ethics Committee of JNCASR (201/GO/Re/S/2000/CPCSEA dated 1st June, 2000 Renewed in Aug 2015). The age-matched animals were maintained on a standard laboratory chow diet (AMRUT M/s Krishna Valley Agrotech, Maharashtra) or high fat diet (60 kcal% fat) (Research Diets, Cat. No. D12492) with or without LTK-14A (50 mg/Kg body weight) and water. LTK-14A was mixed in high fat diet by at first dissolving it in optimal volume of corn oil (Sigma Aldrich, Cat. N. C8267) which was then added dropwise to crushed diet pellets. After thoroughly mixing everything, the pellets were reformed and provided to the mice. Body weight and food intake of the mice was measured twice every week.

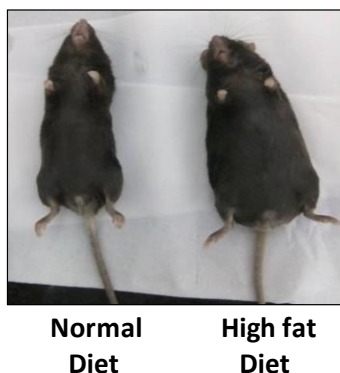


Figure 11: Representative images of mice maintained on normal chow diet and high fat diet; exhibiting lean and obese phenotype respectively.

2.12.2 Genetically obese mice (db/db)

Male db/db mice and db+/- mice (8-10 weeks old) bred in house were obtained and acclimatized for 1 week prior to experiments. Mice were maintained on a 12-hour light/dark cycle at 22+/-3 oC and a relative humidity of 55% and given ad libitum access to food and water. The experiments were carried out in accordance with the Committee for the Purpose of Control and Supervision of Experiments on Animals (CPCSEA) guidelines, Government of India and were approved by the Institutional Animal Ethics Committee of CSIR-CDRI, Lucknow (IAEC/2020/115/Renew-0/Sl.No.09). The age-matched animals were maintained on a standard laboratory pelleted diet (Altromin International, Cat. No. 1320) and water. db/db mice were oral gavaged (50 mg/kg) with LTK14A in 0.5% carboxymethyl cellulose, equal volume of the vehicle was orally gavaged to control db/db mice for a total period of 30 days. db+/- animals were kept as untreated normal control group. The body weights and feed intake was recorded every week throughout the experimental period. The lean and fat mass of the mice were determined using Echo MRI in live mice on day 15th and day 30th.



Figure 12: Representative images of heterozygous mutant *db +/-* mice and homozygous mutant *db/db* mice, exhibiting lean and obese phenotype respectively.

2.12.3 Hematoxylin and eosin staining of liver and adipose tissue

Staining was performed on paraffin embedded sections of liver and epididymal fat pads having the thickness of 5 μm and 10 μm respectively. Briefly, the sections were deparaffinized in xylene, followed by immersion in absolute alcohol, 90% ethanol, 70% ethanol, 50% ethanol and water before staining with hematoxylin for 5-10 minutes. The sections were immersed in above mentioned solutions in reverse order before counter-staining in eosin for 15 seconds. Then the samples were dipped in absolute ethanol and xylene before mounting with DPX.

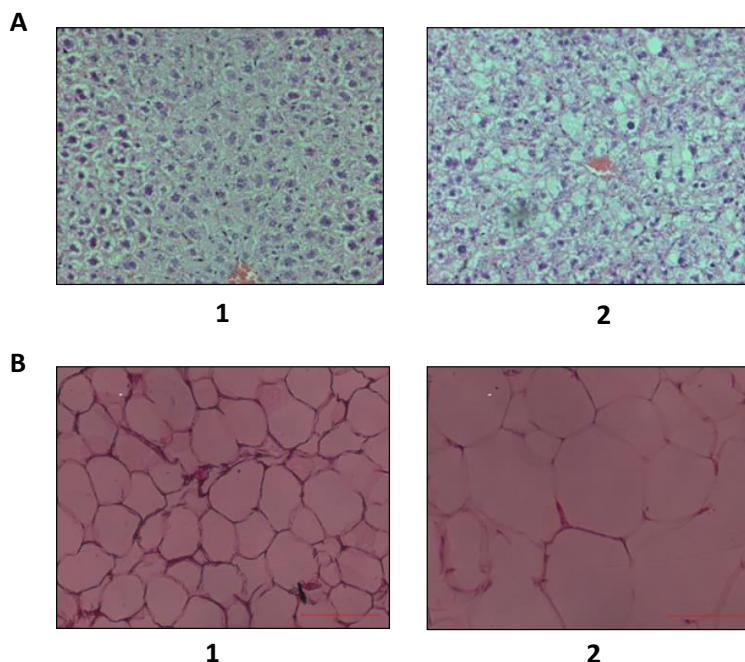


Figure 13: Representative images of hematoxylin and eosin stained liver (A) and epididymal fat pad (B) of lean (1) and obese (2) mice.

2.12.4 Picrosirius Red staining of liver

Sirius Red Staining was performed on paraffin embedded sections of liver having the thickness of 5 μm . The sections were deparaffinized in xylene, followed by immersion in absolute alcohol, 90% alcohol, 70% alcohol, 50% alcohol and water before staining with Sirius Red solution (0.5 gm in 500 ml of saturated aqueous solution of picric acid) for 1.5 hours. The samples were then thoroughly washed in acidified water (5 ml glacial acetic acid in 1 liter distilled water) for 30 minutes. Then the samples were dehydrated in absolute ethanol, cleared in xylene and mounted with DPX.



Figure 14: Representative images of Sirius Red stained liver showing very low and mild fibrosis in periportal regions.

2.12.5 Immunofluorescence staining of liver

Collected liver tissue samples were stored in 4% paraformaldehyde for 24 hours after which they were cryoprotected in 30% sucrose solution for two weeks. Cryosections were performed at 7 μ m sections using Cryostat LeicaCM1850 UV. For staining, the tissue sections were washed with PBS followed by antigen retrieval with 0.01 M citrate buffer (pH 6). The tissues were then permeabilised with 0.3% Triton X-100/PBS (PBST) and blocked with 2% serum followed by incubation with primary antibodies overnight at 4°C. The next day, secondary antibody incubation was carried out for one hour at room temperature followed by staining of the nuclei with Hoechst 33342 and mounting with 70% glycerol. Images were acquired by confocal microscopy. For quantitation, intensity of each modification specific staining was normalized with respect to the Hoechst staining intensity.

2.13 Mass spectrometry

2.13.1 Targeted analysis of butyryl CoA by Ultra-performance liquid chromatography coupled with time-of-flight mass spectrometer (Q-TOF LC/MS)

The cultured cells were washed with ice cold PBS and then collected in a solution of 50% autoclaved water and 50% methanol. The cells were then lysed by sonication, the debris were spun down at 4°C and the supernatant was collected

and snap frozen in liquid nitrogen followed by lyophilization. Targeted analysis of butyryl CoA was performed on an Agilent 1290 Infinity LC system coupled to Agilent 6545 Accurate-Mass Quadrupole Time-of-Flight (QTOF) with Agilent Jet Stream Thermal Gradient Technology. The UPLC system was assembled with a Diode array detector (DAD) and autosampler. The Chromatographic separation was achieved on Agilent ZORBAX SB- C18 column (2.1 × 100 mm, 1.8 μm) as stationary phase. The mobile phase consisted of a linear gradient of 100mM ammonium formate (A) and Acetonitrile (B): 0–5.0 min, 0–50% B (v/v); 5.0–6.5 min, 50–100% B (v/v); 6.5–8.0 min, 100% B (v/v); 8.0–9.0 min, 100–0% B (v/v); 9.0–15.0 min, 100% A. The sample was dissolved in 1 ml solution containing 50% acetonitrile and 50% water with 0.1% formic acid, centrifuged and supernatant was taken for UPLC-QTOF-MS analysis. The column was reconditioned for 5 minutes prior to the next injection. The flow rate was 0.5 mL/min, and the injected volume was 20 μL. The UPLC was connected to the MS analysis was performed on an Agilent 6545 Accurate-Mass Q-TOF/MS system with an electrospray ionization (ESI) source. Considering the MS conditions, positive ion mode was used to obtain high-resolution mass spectra. The ESI source parameters were: drying gas (N₂) flow, 8 L/min; drying gas temperature, 200°C. Other parameters were set as nebuliser gas, 35 psig; capillary voltage, 3000 V; skimmer voltage, 65 V; nozzle voltage 1000 V and fragmentor voltage 150 V. The data acquisition on the LC-QTOF was performed using Agilent MassHunter Acquisition software (Agilent Technologies, Santa Clara, CA, USA). The data were deconvoluted into individual chemical peaks with Agilent MassHunter Qualitative Analysis (MassHunterQual, Agilent Technologies). For comparison of butyryl CoA levels under different conditions, the peak area of butyryl CoA fraction was normalised to that of all other metabolites and this area sum percent was used as a measure of the abundance level of butyryl CoA.

2.13.2 Untargeted analysis of intracellular metabolites by Ultra-performance liquid chromatography coupled with time-of-flight mass spectrometer (Q-TOF LC/MS)

The cultured cells were washed with ice cold PBS and then collected in a solution of 50% autoclaved water and 50% methanol. The cells were then lysed by sonication, the debris were spun down at 4°C and the supernatant was collected and snap frozen in liquid nitrogen followed by lyophilization. Profiling of intracellular metabolites was performed on an Agilent 1290 Infinity LC system coupled to Agilent 6545 Accurate-Mass Quadrupole Time-of-Flight (QTOF) with Agilent Jet Stream Thermal Gradient Technology. The UPLC system was assembled with a Diode array detector (DAD) and autosampler. The Chromatographic separation was achieved on Agilent ZORBAX SB- C18 column (2.1 × 100 mm, 1.8 μm) as stationary phase. The mobile phase consisted of a linear gradient of 100mM ammonium formate (A) and Acetonitrile (B): 0–10.0 min, 30-80% B (v/v); 10.0–15.0 min, 80–100% B (v/v); 15.0–20.0 min, 100% B (v/v); 20.0–21.0 min, 100–30% B (v/v); 21.0–25.0 min, 30% B. The sample was dissolved in 1 ml solution containing 50% acetonitrile and 50% water with 0.1% formic acid, centrifuged and supernatant was taken for UPLC-QTOF-MS analysis. The column was reconditioned for 5 min prior to the next injection. The flow rate was 0.5 mL/min, and the injected volume was 20 μL. The UPLC was connected to the MS analysis was performed on an Agilent 6545 Accurate-Mass Q-TOF/MS system with an electrospray ionization (ESI) source. Considering the MS conditions, positive ion mode was used to obtain high-resolution mass spectra. The ESI source parameters were: drying gas (N₂) flow, 8 L/min; drying gas temperature, 200°C. Other parameters were set as nebuliser gas, 35 psig; capillary voltage, 3000 V; skimmer voltage, 65 V; nozzle voltage 1000 V and fragmentor voltage 150 V. The data acquisition on the LC-QTOF was performed using Agilent MassHunter Acquisition software (Agilent Technologies, Santa Clara, CA, USA). The data were deconvoluted into individual chemical peaks with Agilent MassHunter Qualitative Analysis (MassHunterQual, Agilent Technologies).

2.14 Generation and characterization of H4K5 butyrylation antibody

The peptide sequence that was used for generating H4K5 butyrylation antibody is given below-

SGRG(K-Bu)GGKGLGKGGAKRHRKV

The KLH-conjugated peptide was received in a lyophilized form and then it was reconstituted in water to a final concentration of 1 mg/ml. The peptide solution (750 microlitres) was mixed with complete adjuvant in a 1:1 ratio by volume, with the help of a syringe. The emulsion was injected subcutaneously in 2-3 months old New Zealand white rabbits. After this, booster doses were prepared using the peptide solution and incomplete adjuvant. The scheme that was followed for antibody generation is given below-

DAY 0 - Primary Injection

DAY 16 – First booster injected

DAY 27 – Test bleed collected

DAY 31 – Second booster injected

DAY 38 – Minor bleed collected

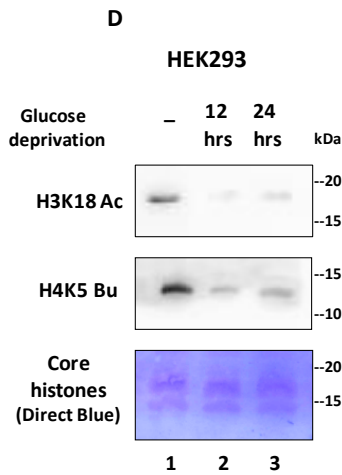
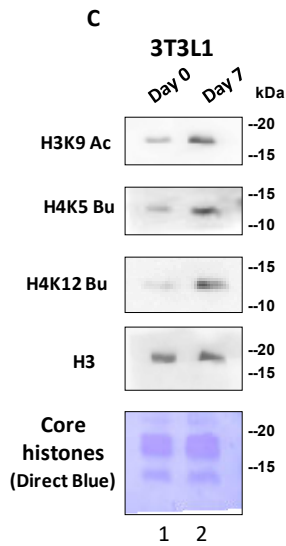
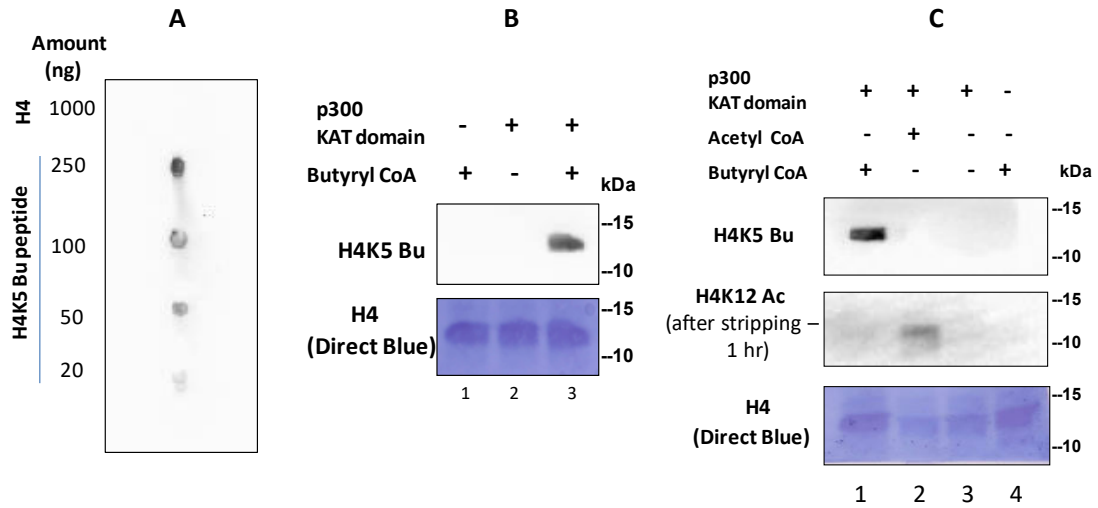
DAY 64 – Third booster injected

DAY 84 – Fourth booster injected

DAY 101 – Major bleed collected

The ability of the raised antibody to detect butyrylation was initially tested by dot blot assay with the supplied H4K5 butyrylated unconjugated peptide and immunoblotting with *in vitro* butyrylated histone H4. Possible cross-reactivity of the antibody was tested by performing immunoblotting with *in vitro* acetylated histone H4. The antibody was also tested for its ability to detect butyrylation in cultured cells by immunoblotting with acid extracted histones from cell lines. Finally, the antibody was tested for its ability to detect butyrylation in tissues by

performing immunofluorescence staining with paraffin embedded mice liver sections as well as immunofluorescence staining with acid extracted histones from mice epididymal fat pads.



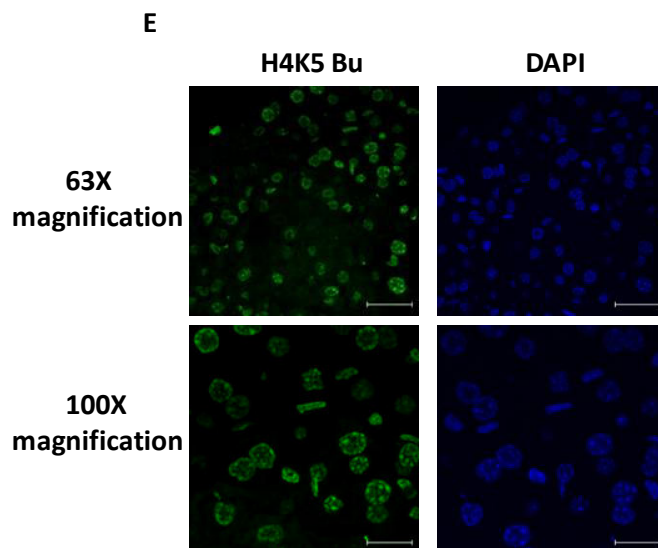


Figure 15: (A) Dot blot assay with H4K5Bu antibody and different substrates as indicated. The experiment demonstrates the reactivity of the antibody towards butyrylated peptide without recognizing the unmodified histone H4. (B) Immunoblotting with H4K5Bu antibody and *in vitro* butyrylated recombinant histone H4. (C) Testing for possible cross-reactivity of H4K5Bu specific antibody using different *in vitro* acylated recombinant histone H4 as substrates. The antibody did not cross-react with acetylated histone, the acetylation of which was proved by reprobing the blot with acetylation specific antibody (H4K12Ac). (D) Immunoblotting with H4K5Bu antibody and acid extracted histones from glucose deprived HEK293 cells, showing that like acetylation (H3K9Ac), H4K5 butyrylation level gets reduced with decreasing glucose concentrations. (E) Immunoblotting with H4K5Bu antibody an acid extracted histones from pre-adipocytes and differentiated 3T3L1 adipocytes, showing that like acetylation (H3K18 Ac), H4K5 butyrylation level rises upon adipogenesis. (F) Immunofluorescence staining of liver sections from high fat diet fed C57BL6/J mice with H4K5Bu specific antibody.

p300 mediated histone butyrylation is critical for adipogenesis

**p300 mediated histone butyrylation is critical
for adipogenesis**

p300 mediated histone butyrylation is critical for adipogenesis

The following chapter starts with an introduction on adipogenesis and obesity along with the epigenetic mechanisms involved in the processes, including the essential role of p300. It discusses in detail about the currently available small molecule modulators of p300 acetyltransferase activity. Finally, it presents results on the discovery of a small molecular modulator of p300 acyltransferase activity along with its implications in obesity control by inhibition of adipogenesis.

3.1 Background

- 3.1.5** Adipose tissue and obesity
- 3.1.6** Molecular origins of adipose tissue
- 3.1.7** Chromatin landscape of adipogenesis
- 3.1.8** Inhibitors of p300 acetyltransferase activity
 - 3.1.8.4** Bisubstrate inhibitors
 - 3.1.8.5** Inhibitors from natural sources
 - 3.1.8.6** Synthetic inhibitors
 - 3.1.8.7** Bromodomain inhibitors

3.2 Results

- 3.2.1 Search for a selective inhibitor of p300 butyryltransferase activity
- 3.2.2 Understanding the structural basis for selective inhibition of EP300 catalysed butyrylation by LTK-14A by molecular docking
- 3.2.3 Validation of molecular docking by site directed mutagenesis
- 3.2.4 Butyryl CoA levels are higher in adipocytes compared to pre-adipocytes
- 3.2.5 Histone butyrylation increases during adipogenesis
- 3.2.6 Histone butyrylation increases in the promoters of pro-adipogenic genes during adipogenesis

3.2.7 LTK-14A is metabolically stable, cell permeable and inhibits adipogenesis without causing toxic effects

3.2.8 LTK-14A inhibits adipogenesis by mainly repressing the expression of lipogenic genes including the master regulators of adipogenesis

3.2.9 LTK-14A represses gene expression by specific inhibition of histone butyrylation without affecting acetylation

3.2.10 LTK-14A prevents obesity and adipocyte hypertrophy in mice fed with high fat diet by specific inhibition of histone butyrylation without affecting acetylation in adipose tissues

3.2.11 LTK-14A reverses obesity and adipocyte hypertrophy in genetically obese mice by specific inhibition of histone butyrylation without affecting acetylation in adipose tissues

3.2.12 LTK-14A prevents adipocyte hypertrophy by repression of lipogenic genes and not by browning of fat

3.1 Background

3.1.1 Adipose tissue and obesity

In the last few decades, obesity has become a major health concern in various places all over the globe. Obesity has also been linked to other clinical disorders such as type 2 diabetes and insulin resistance. Moreover, uncontrolled obesity can also lead to other organ related diseases such as hepatic steatosis, cardiovascular disease and even certain types of cancer (Afshin *et al*, 2017; Nyberg *et al*, 2018; Castellano-Castillo *et al*, 2018). Obesity has been principally associated with increased adipose tissue mass that leads to greater body weight along with metabolic dysfunctions of the enlarged tissue (Figure 1) (Pellegrinelli *et al*, 2016; Carobbio *et al*, 2017).

There are three types of adipose tissue- white, brown and beige or brite (brown-to-white). The white adipose tissue serves as a storage depot for excess energy after feeding in the form of lipids (triglycerides) and mobilizes them during fasting to meet the energy demands of other tissues (Li *et al*, 1993; Blüher *et al*, 2013). But new research indicates that the white adipose tissue is much more than just a storehouse of energy since it can release bioactive molecules called adipokines, which include various hormones, cytokines and miRNAs that are involved in regulating insulin sensitivity, inflammation, energy balance and vascular haemostasis by cross-talk with other organs such as liver, gut, muscle and brain. In this way metabolic signals are integrated to serve the body energy requirements based on environmental cues (Lee *et al*, 2019; Scherer *et al*, 2019; Villarroya *et al*, 2017). White adipose tissues are characterized by the presence of large quantities of lipids and are distributed in various stereotypical depots throughout the body (Kissebah *et al*, 1989; Gesta *et al*, 2006). Depending on their location, they can be either visceral (lining internal organs) or subcutaneous (below the skin) (Pellegrinelli *et al*, 2016). Accordingly, they display distinct molecular and physiological properties, with the visceral adipose tissue being more hormonally active and primarily responsible for inflammation and metabolic complications (Hayashi *et al*, 2008).

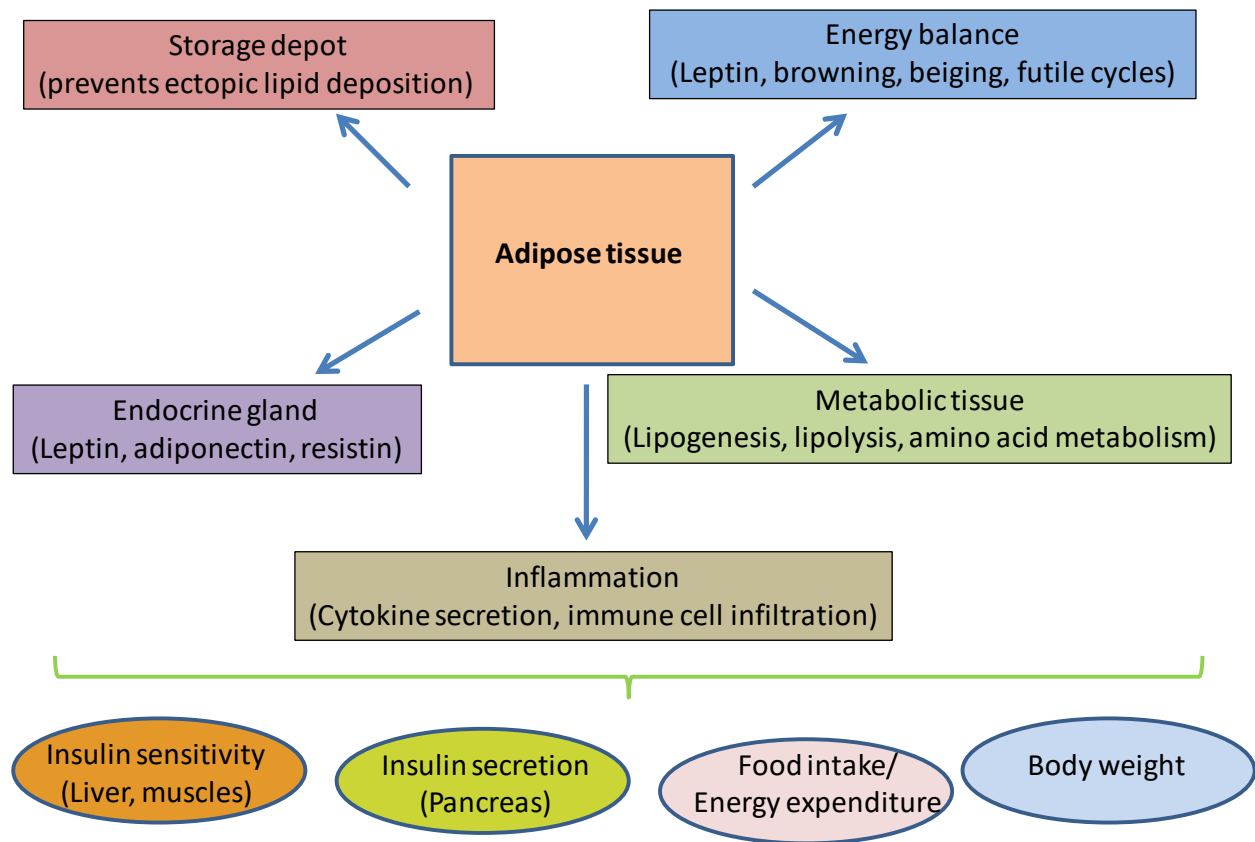


Figure 1: Diverse biological functions of adipose tissue and its cross-talk with other organs with their implications. (Adapted and modified from Kahn *et al*, Diabetes, 2019)

The brown adipose tissue is mainly found in the intrascapular region of humans and rodents. It is characterized by the presence of smaller multilocular lipid droplets compared to white adipocytes, large number of mitochondria and also the expression of a specific protein called Uncoupling Protein 1 (UCP1). As a result, it is capable of generating heat by metabolizing fatty acids and hence it has been associated more with energy expenditure (Cannon *et al*, 2004). The brown adipose tissue is responsible for non-shivering thermogenesis in hibernating animals and newborn mammals, and it has rarely been considered to be of functional importance in adult humans (Farmer *et al*, 2008). However, new evidences are emerging which point out to the role of brown adipose tissue in energy homeostasis in adults especially in colder climates (Nedergaard *et al*, 2007; Cypess *et al*, 2009). An inverse correlation has also been observed between

the amount of brown adipose tissue and body mass index in older human beings (Tiraby *et al*, 2003).

In order to store surplus energy, white adipose tissue expansion occurs by hypertrophy i.e. increase in size of pre-existent adipocytes by intracellular accumulation of triglycerides and hyperplasia i.e. increase in adipocyte number by proliferation of adipocytes and formation of new adipocytes from pre-adipocytes (adipogenesis). The two processes are not mutually exclusive events during obesity manifestation. New vasculature gets formed around the expanding adipose tissue for providing oxygen and nutrients (Hammerstedt *et al*, 2018). Accordingly, the extracellular matrix also remodels itself for accommodating changes in the adipose tissue size and shape (Crewe *et al*, 2017). The hypertrophic adipocytes exhibit stress associated with endoplasmic reticulum, mitochondria and oxidation which lead to activation of several inflammatory pathways (Malagon *et al*, 2014). These distressed adipocytes have poor lipogenic capacity and an altered pro-inflammatory cytokine secretion profile which in turn affects the local insulin signaling (a process essential for regulating the transcriptional programme which controls adipogenesis as well as nutrient uptake and lipid storage by adipocytes). They also recruit pro-inflammatory immune cells near the vicinity and promote tissue fibrosis by maladaptive extracellular matrix remodeling. On the other hand, the hyperplastic adipocytes are associated with low hypoxic stress and inflammation, as a result of which they can partially serve as a conduit for storing the excess energy that the hypertrophied, dysfunctional adipocytes are unable to store (Vishvanath *et al*, 2019).

Therefore, it is the larger adipocytes that have been associated with impaired glucose metabolism while the smaller adipocytes are less prone to give rise to metabolic alterations such as diabetes. Obesity along with increased white adipose tissue mass has been linked with various co-morbidities (Chouchani *et al*, 2019). However, many individuals have been found to remain overall healthy despite having high blood glucose and triglyceride levels, low HDL-cholesterol levels and insulin resistance (Barbarroja *et al*, 2010; Reaven *et al*, 2005; Karelis *et*

al, 2004; Clemente-Postigo *et al*, 2015). On the contrary, many non-obese individuals have also been found to be at risk of cardiovascular diseases, normally associated with obesity (Schulze *et al*, 2019; Stefan *et al*, 2017). There are also many patients with lipodystrophy (partial or total loss of adipose tissue and abnormal tissue distribution) who have similar metabolic complications as obese patients (Akinci *et al*, 2018). Due to these paradoxical observations, the new hypothesis is that it is not just the total mass of the white adipose tissue but rather the lipogenic capacity of the adipose tissue to properly expand that determines the metabolic status of the individual (Virtue *et al*, 2008).

3.1.2 Molecular origins of adipose tissue

The adipose tissue, along with the muscle and bone are considered to have originated from mesenchymal stem cells present in the mesoderm of embryo. However, lineage tracing studies have shown that a small subset of adipocytes may also have been derived from mesenchymal cells of neuroectoderm (Billon *et al*, 2007). A mixed origin of adipose tissue may explain the differences in properties and functions of adipose tissue in various depots (Billon *et al*, 2008).

The mesenchymal stem cells are pluripotent in nature, which in response to specific environmental cues can give rise to cells of different lineage. The first step of adipogenesis is called lineage determination which involves the conversion of mesenchymal cells into pre-adipocytes. These pre-adipocytes are morphologically similar to mesenchymal stem cells, but are only committed to become cells of a specific type. Pre-adipocytes exhibit fibrous morphology and have high expression of Pre-adipocyte factor 1 (Pref1) that distinguishes them from the differentiated adipocytes (Wang *et al*, 2010). The second step of adipogenesis is called terminal differentiation, in which the pre-adipocytes acquire all the necessary features of mature adipocytes which include the necessary machinery for lipid biosynthesis and transport as well as expression of markers such as leptin and adiponectin.

There are a myriad of transcription factors which can promote the differentiation of mesenchymal stem cells into a specific cell type and suppress the conversion to

other lineages. The master regulator transcription factor PPAR γ (peroxisome proliferator activated receptor γ) is responsible for directing adipogenesis and preventing bone cell formation by osteoblastogenesis. Similarly, inducers of canonical Wnt/ β -catenin signaling pathway in osteoblastogenesis suppress the transactivation of PPAR γ by promoting the expression of histone methyltransferase SETDB1 (Bennett *et al*, 2005; Takada *et al*, Nat Cell Biol, 2007; Takada *et al*, Ann NY Acad Sci, 2007). The SETDB1 together with NLK (Nemo-like kinase) and CHD7 (chromodomain helicase DNA binding protein 7) form a repressor complex that downregulate the expression of PPAR γ through H3K9 dimethylation of its target promoter. Moreover, the histone deacetylase Sirt1 in association with NcoR/SMRT complex bind to the promoter of PPAR γ and repress its expression. Simultaneously, Wnt-5a promotes the expression of Runx2 that induces osteoblastogenesis (Takada *et al*, Nat Cell Biol, 2007; Takada *et al*, Ann NY Acad Sci, 2007).

Similarly, a group of proteins belonging to a family of transcription factors called tension inducible/inhibited proteins (TIPs) are responsible for fate determination of mesenchymal stem cells by differentiation into either adipocytes or myocytes (Jakkaraju *et al*, 2005). These proteins have the unique property of their expression being regulated by mechanical forces. One of the members Tip-1 is induced by stretch and promotes myogenesis by binding to the promoter of serum responsive factor (srf). On the other hand, another member of the family Tip-3 is repressed by stretch and induces adipogenesis by binding to the promoter of *Pparg* gene (Jakkaraju *et al*, 2005).

Brown fat cells can develop from Myf-5 expressing myogenic precursor cells (Seale *et al*, 2008). Moreover, transcription factor PRDM16 is also essential for the development of adipocytes in brown adipose tissue (Kajimura *et al*, 2008). It has been observed in white adipose tissue, that there are brown fat like cells, with morphology intermediate between those of white and brown adipocytes, interspersed within the white adipose tissue. These are commonly referred to as brite cells (**brown in white**) or beige cells (Enerback *et al*, 2009). Their formation is

highly simulated by β 3-adrenergic stimulation, chronic activation of PPAR γ or due to exposure to very low temperatures (Huttunen *et al*, 1981; Cousin *et al*, 1992; Ghorbani *et al*, 1997; Guerra *et al*, 1998; Xue *et al*, 2005; Petrovic *et al*, 2010). Interestingly, fully developed and mature white adipocytes can also be transdifferentiated to brown fat like cells by overexpression of PRDM16 (Seale *et al*, 2011) (Figure 2).

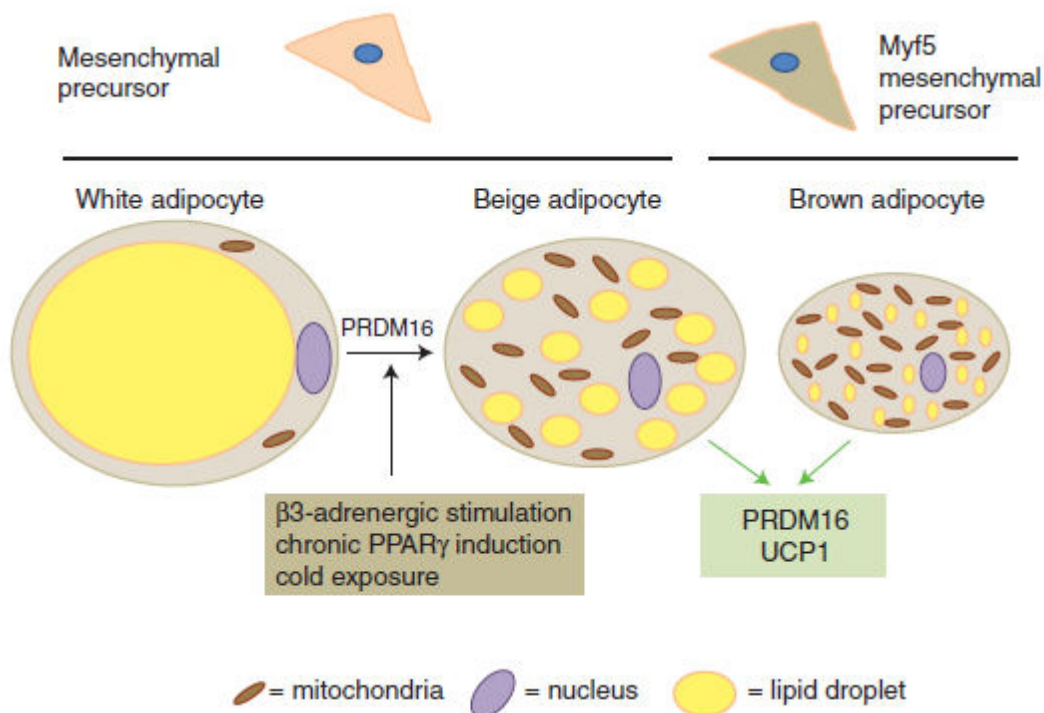


Figure 2: Diagram depicting different morphologies of white, brown and beige adipocytes and their different origins. (Source- Sarjeant *et al*, Cold Spring Harb Perspect Biol, 2012).

3.1.3. Chromatin landscape of adipogenesis

The promoters associated with genes involved in differentiation into adipocytes are characterized by the presence of large stretches of H3K27 trimethylation involved in gene silencing and smaller stretches of H3K4 trimethylation which are involved in gene activation (Bracken *et al*, 2006; Noer *et al*, 2009). These bivalent histone marks are actually a signature of genes that are transcriptionally silent,

but are poised for transcription based on inductive signals. The H3K27 trimethylation mark is deposited by polycomb group proteins (PcG), a family of transcriptional repressors that are required for maintenance of pluripotency in cells by keeping the expression of differentiation related genes in check (Fouse *et al*, 2008). It has been reported that in the absence of the H3K27 methyltransferase Eed and the H3K4 methylation regulator PTIP, aberrant expression of lineage specific genes occur leading to uncontrolled differentiation (Kim, D. *et al*, 2009). In addition to histone marks, a further layer of regulation is added to these genes by DNA methylation in the vicinity of the promoters, which is again responsible for transcriptional silencing (Mohn *et al*, 2008).

In the pre-adipocytes, another histone mark H3K4 dimethylation is enriched in the promoters of transcriptionally silent genes such as adiponectin and is localized predominantly around the nuclear periphery (Musri *et al*, 2006). Upon differentiation to adipocytes, the modification is found to relocalize to the interior of nucleoplasm. In fact, the critical pro-adipogenic transcription factors PPAR γ and C/EBP α (CCAAT/enhancer binding protein α) have also been found to be located around the nuclear envelope in pre-adipocytes and shift to interior of nucleus in adipocytes (Szczerbal *et al*, 2009). Hence there seems to be a correlation between histone modifications and higher order chromatin dynamics in regulating gene expression during adipogenesis.

For adipogenesis to take place, the two most crucial transcription factors are PPAR γ and C/EBP α (Lefterova *et al*, 2008; Nielsen *et al*, 2008). In fact, PPAR γ is known as the master regulator of adipogenesis because, the process gets completely abolished in its absence and no other transcription factor can play a substituting role (Barak *et al*, 1999; Rosen *et al*, 1999; Rosen *et al*, 2002). Two other transcription factors C/EBP β and C/EBP δ are responsible for stimulating the expression of C/EBP α and PPAR γ . The latter two factors, after being expressed can induce the transcription of each other (Rosen *et al*, 2006; Farmer *et al*, 2006). In pre-adipocytes, C/EBP β and C/EBP δ already remain bound to the promoters of *Cebpa* and *Pparg* (Salma *et al*, 2006) (Figure 3). But C/EBP β is unable to induce

their expression, as it remains associated with mSin3A/HDAC1 repressor complex (Zuo *et al*, 2006). Similarly, PPAR γ also remains bound to its cognate promoters in association with repressor complex comprised of pRb and HDAC3 (Fajas *et al*, 2002). Upon induction of differentiation, pRb gets phosphorylated and dissociates, leaving PPAR γ free to promote transcription of its target pro-adipogenic genes by recruiting transcriptional coactivator p300 and CARM1 (Chen *et al*, 2000; Gelman *et al*, 1999). Moreover, PPAR γ is able to free C/EBP β from the repressor HDAC1 by targeting HDAC1 to 26S proteasomal complex for degradation (Zuo *et al*, 2006). Glucocorticoids can exert a similar effect by stimulating the activation of GCN5 acetyltransferase which acetylates a cluster of lysine residues on C/EBP β that leads to its dissociation from HDAC1 (Wiper-Bergeron *et al*, 2003). Thus C/EBP β is able to induce transcription of C/EBP α , which at the later stages of adipogenesis displaces C/EBP β from its cognate promoters of important adipocyte marker genes like leptin, adiponectin and also PPAR γ (Salma *et al*, 2006). It takes up the important role of keeping the transcriptionally active genes firing by recruiting the SWI/SNF chromatin remodeling complex (Pedersen *et al*, 2001).

Histone acetylation has been regarded as one of the most important epigenetic marks associated with adipogenesis. The process of adipogenesis is accompanied by decrease in levels of histone deacetylases HDAC 1, -2 and -5 along with increased level of p300 which results in increased acetylation of histones at several sites (Yoo *et al*, 2006). Ligands that promote interaction between PPAR γ and p300 have also been found to promote adipogenesis (Gelman *et al*, 1999). Another acetyltransferase known to transactivate PPAR γ and induce adipogenesis is SRC1 (Nolte *et al*, 1998). The importance of acetylation in adipogenesis is further underlined by the fact that knockdown of ATP citrate lyase, responsible for generation of nucleocytosolic pool of acetyl CoA, leads to inhibition of adipogenesis with concomitant loss of histone acetylation (Wellen *et al*, 2009).

The evidences of histone acetylation promoting adipogenesis may indicate that simply inhibiting histone deacetylases using HDAC inhibitors would increase the

rate of adipogenesis (Yoo *et al*, 2006). However that is not the case, with reports of differential effects of various HDAC inhibitors on adipogenesis (Kim, S.N. *et al*, 2009; Lagace *et al*, 2004; Haberland *et al*, 2010). These contradictions do make drawing a conclusion difficult about the effect of HDAC inhibitors on adipogenesis. In fact, one HDAC inhibitor apicidin can also bring about de-differentiation of mature adipocytes (Kim *et al*, 2009). A possible explanation for the diverse effects of these inhibitors could be the differences in their affinity for different HDACs. Moreover, certain HDACs promote adipogenesis by silencing anti-adipogenic genes which remain highly expressed in pre-adipocytes. As for example, HDAC3 is recruited by the transcription factor KLF6 in the promoter of pre-adipocyte marker *dlk1* during adipogenesis, leading to deacetylation of the promoter and transcriptional repression (Li *et al*, 2005). Interestingly, short chain fatty acids acetate, propionate and butyrate have been shown independently by different groups to have a positive effect on adipogenesis on a consistent basis (Nolte *et al*, 1998; Haberland *et al*, 2010). Amongst them butyrate has been known to serve as an HDAC inhibitor at micromolar concentrations, but the fact that acetate and propionate do not have such properties, indicates that there could be some other mechanism behind this pro-adipogenic effect. Recently, a new finding shows that these short chain fatty acids can induce p300 autoacetylation, enhancing its activity, leading to higher acetylation of histones (Thomas *et al*, 2021). This could be one among several additional effects of HDAC inhibitors, yet to be discovered, that are responsible for promoting adipogenesis.

Histone methylation is another modification that has been well documented for its role in adipogenesis. CARM1 is an arginine methyltransferase that serves as a coactivator for PPAR γ and promotes adipogenesis. Suppression of CARM1 activity leads to inhibition of adipogenesis along with reduced H3R17 dimethylation mark deposited by it (Yadav *et al*, 2008). H3K4 dimethylation is associated with genes poised for transcription in pre-adipocytes, characterized by high RNA polymerase II loading (Musri *et al*, 2006) while H3K4 trimethylation, deposited by MLL3 and MLL4 is associated with gene activation (Lee, J. *et al*, 2008). Lysine methyltransferases SUV39H1 and SETDB1 both repress PPAR γ target gene

expression in association with different factors (Takada *et al*, Nat Cell Biol, 2007; Takada *et al*, Ann NY Acad Sci, 2007; Fu *et al*, 2005). G9a is another methyltransferase that represses UCP1 expression by H3K9 dimethylation of its promoter and prevents brown adipose tissue formation (Kiskinis *et al*, 2007). Along similar lines the histone demethylase JMJD1A is required for histone demethylation in the promoter of *ucp1*, thereby promoting brown fat formation (Tateishi *et al*, 2009). On the other hand H4K20 monomethylation, deposited by Set7/Set8, promotes adipogenesis (Wakabayashi *et al*, 2009).

DNA methylation at cytosine (5-methylcytosine) can serve as a biphasic mark in regulation of adipogenesis, since it can either have a promoting or repressive effect depending on temporal circumstances. Knockdown of DNMT1 using a novel miRNA (miRNA 148a) led to promotion of adipogenesis (Londono Gentile *et al*, 2013) while chemical inhibition of DNA methylation by 5-azacytidine at early stage promotes adipogenesis and at later stage represses adipogenesis (Yang *et al*, 2016). Another DNA methylation mark is N⁶-methyladenine deposited by METTL4 that has been recently found to promote adipogenesis (Zhang *et al*, 2012). Amongst the enzymes responsible for DNA methylation marks, TET2 has been recognized as an anti-adipogenic enzyme because knockdown of *tet2* gene leads to promotion of adipogenesis (Hou *et al*, 2020).

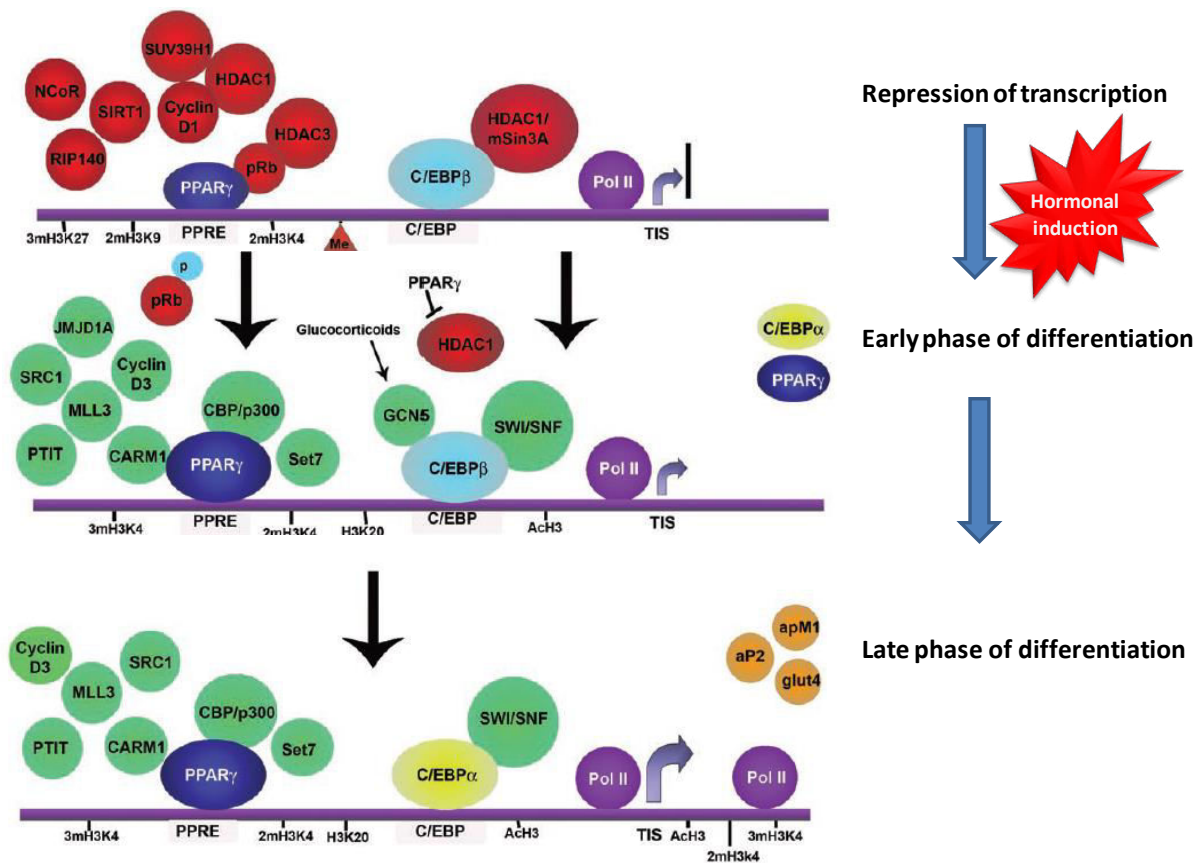


Figure 3: Schematic representation of the different transcription factors and histone post-translational modifications involved in adipogenesis (Adapted and modified from Musri *et al*, Organogenesis, 2009)

3.1.4 Small molecule modulators of p300 acetyltransferase activity

Despite a lot of research behind design and development of inhibitors of p300 and other KATs, the area is still not as developed as other aspects of pharmacological research such as modulators of HDACs (histone deacetylases). However, with modernization of screening methods and computational modeling studies, significant progress has been made in the last few decades. The KAT inhibitors can be mainly divided into four classes- bisubstrate inhibitors,

bromodomain inhibitors, synthetic inhibitors and inhibitors derived from natural sources.

3.1.4.1 Bisubstrate inhibitors

The first KAT inhibitor to be published for p300 was the bisubstrate inhibitor lysyl CoA (Figure 5) in which the lysine residue mimics the substrate lysine to be modified, and it is linked by a methylene bridge to Coenzyme A, mimicking the cofactor by being a part of acetyl CoA (Lau *et al*, 2000). The rationale behind the design was the Theorell Chance mechanism of p300 catalysed acetylation whereby p300 forms a transient ternary complex with both the substrate and cofactor, with a strong interaction with the cofactor and a weaker one with the substrate (91). Lysyl CoA showed greater specificity towards p300 compared to PCAF with an IC_{50} value of 0.5 μ M. This method has also been adopted for designing such inhibitors for other KATs as well as improving the efficiency of p300 inhibition. In fact Boc-C5-CoA, containing a tertiary butyl oxycarbonyl group with an optimized linker length that is capable of fitting inside the p300 active site, was an improved version of lysyl CoA with an IC_{50} value of 0.07 μ M (Kwie *et al*, 2011) (Figure 5). Due to the presence of the polar phosphate moieties in the Coenzyme A part and peptidic nature of the bisubstrate inhibitors, these compounds do not have high membrane permeability and metabolic stability and are therefore unsuitable for wider applications. Cellular permeability issues were overcome by conjugating the inhibitor's amino acid backbone to TAT protein or arginine rich peptide sequences that improved cellular uptake of the compounds (Wadia *et al*, 2005; Zheng *et al*, 2005). However, the elaborate nature of the compound preparation serves as an obstacle. Further improvement has been done in this regard by linking the Coenzyme A with the polyamine spermidine to generate (Spd(N¹)-CoA) which was readily taken up by cells through the polyamine transporter (Bandyopadhyay *et al*, 2009; Cullis *et al*, 1982) (Figure 5). The catalytic activity of the compound was improved by truncating the Coenzyme A moiety to cysteamine- β alanine core that showed greater activity inside cells (Bandyopadhyay *et al*, 2009). These compounds were able to inhibit histone

acetylation dependant DNA damage repair that led to better radio- and chemosensitization of cancer cells.

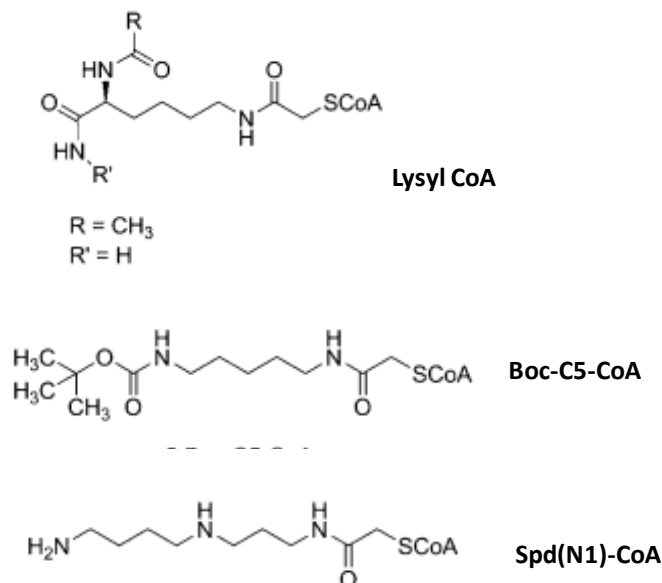


Figure 5: Structures of a few bisubstrate inhibitors of p300 acetyltransferase (Source- Simon *et al*, J Med Chem, 2016)

3.1.4.2 Inhibitors from natural sources (semisynthetic modulators of p300)

Plant and microbial sources have served as a treasure trove for several KAT inhibitors including those of p300. However, they have high reactivity to other enzymes and proteins as well, making their effects non-specific. Modifications have been made in the structures of these naturally occurring compounds to produce derivatives that have improved specificity. In fact, derivatization has even led to the discovery of activators of KATs using these natural compounds as synthons.

Anacardic acid, obtained from cashew nut shells, was discovered during a screening of plant extracts for anti-cancer activity (Balasubramanyam *et al*, 2003) (Figure 6). It was initially found to be a non-competitive inhibitor of p300/CBP and PCAF, but later on it was also found to inhibit Tip60 (Ghizzoni *et al*, 2012). At cellular level, it represses NFκB signaling by inhibiting acetylation of p65 subunit.

Derivatization of anacardic acid led to the discovery of a p300 activator CTPB, which is a benzamide analogue of the compound and has more specificity towards p300 compared to PCAF (Balasubramanyam *et al*, 2003) (Figure 6). Removal of the long alkyl chain of CTPB produced TTK21 (Figure 6) which retained its histone acetyltransferase activator property and upon conjugation with carbon nanospheres, it could safely cross the blood brain barrier and ameliorate several pathophysiological conditions by activating p300 (Chatterjee *et al*, 2013). Another derivative called LoCAM, which has a long chain alkylidenmalonate substituent, serves as a PCAF activator while it inhibits p300 (Sbardella *et al*, 2008).

Curcuma longa rhizome which is used in Indian and Chinese traditional medicine and cooking, was the source of the compound curcumin which could specifically inhibit p300 (IC₅₀ value of 25 μM) without any effect on PCAF (Balasubramanyam, Varier *et al*, 2004) (Figure 6). Structural studies have revealed that curcumin forms covalent bonds to interact with p300 at a site other than the active site with the double bonds in its cinnamoyl structure serving as Michael reaction acceptors (Neckers *et al*, 2006). Despite showing specificity amongst KATs, curcumin has been found to also affect other epigenetic enzymes – HDACs, DNMT1, LSD1 as well as several non-epigenetic proteins (Fu *et al*, 2010). Open chain and cyclic cinnamoyl analogues of curcumin have also shown similar properties as the main compound (Costi *et al*, 2007). Moreover, CTK7A, a sodium salt of hydrazinocurcumin has been found to be a potent inhibitor of p300 with high water solubility (Arif *et al*, 2010) (Figure 6). Despite the fact that curcumin and some of its derivatives are being used in clinical application studies, it can affect many other factors besides p300. Moreover, it has also been found to be a membrane disruptor, which raises concerns about its potential as a drug (Ingolfsson *et al*, 2014).

Garcinol from *Garcinia indica* (kokum) is a polyisoprenylated benzophenone that can inhibit both p300 (IC₅₀ value of 7 μM) and PCAF (IC₅₀ value of 5 μM) (Balasubramanyam, Altaf *et al*, 2004). The catechol hydroxyl groups interact with the cofactor binding pocket of p300, while its isoprenoid moieties interact with

the substrate binding site. LTK-14, a monomethylated derivative of its internal cyclised product isogarcinol, has more specificity towards p300 acetyltransferase activity (Mantelingu *et al*, 2007). Isosteric replacement of the benzophenone core of garcinol led to the synthesis of a benzylidene barbituric acid derivative EML425 that exhibited improved efficiency at inhibition of p300 (IC₅₀ value of 2.9 µM) and CBP (IC₅₀ value of 1.1 µM) acetyltransferase activity (Milite *et al*, 2009).

Plumbagin is a hydroxynaphthoquinone obtained from *Plumbago rosea* that has been shown to inhibit p300 catalysed acetylation without targeting other KATs (Ravindra *et al*, 2009). Structural studies have shown that the hydroxyl group in its C5 position is critical for forming hydrogen bonds with a lysine residue at 1358 position in the active site of p300. However, the compound has a non-specific nature to other proteins due to its thiol reactivity, which can be overcome by methylation at its C3 position (Vasudevarao *et al*, 2014).

As far as KAT inhibitors from microbial sources are concerned, two secondary metabolites from *Penicillium* strain have shown promise. They are NK13650A and NK13650B, both of which have a peptidic structure with a citric acid moiety (Tohyama *et al*, 2012). Both have been found to be specific inhibitors of p300 with IC₅₀ values of 11 and 22 nM respectively. Moreover, they have also been shown to be capable of repressing androgen and estrogen dependent gene transcription as well as being cytotoxic to various cancer cell lines owing to their acetyltransferase inhibitory property. However, because the compounds have a peptidic nature they are relatively less cell permeable and are also low on metabolic stability. Still, they are promising candidates for future drug development from microbial sources by derivatization and modification of the already existent structures.

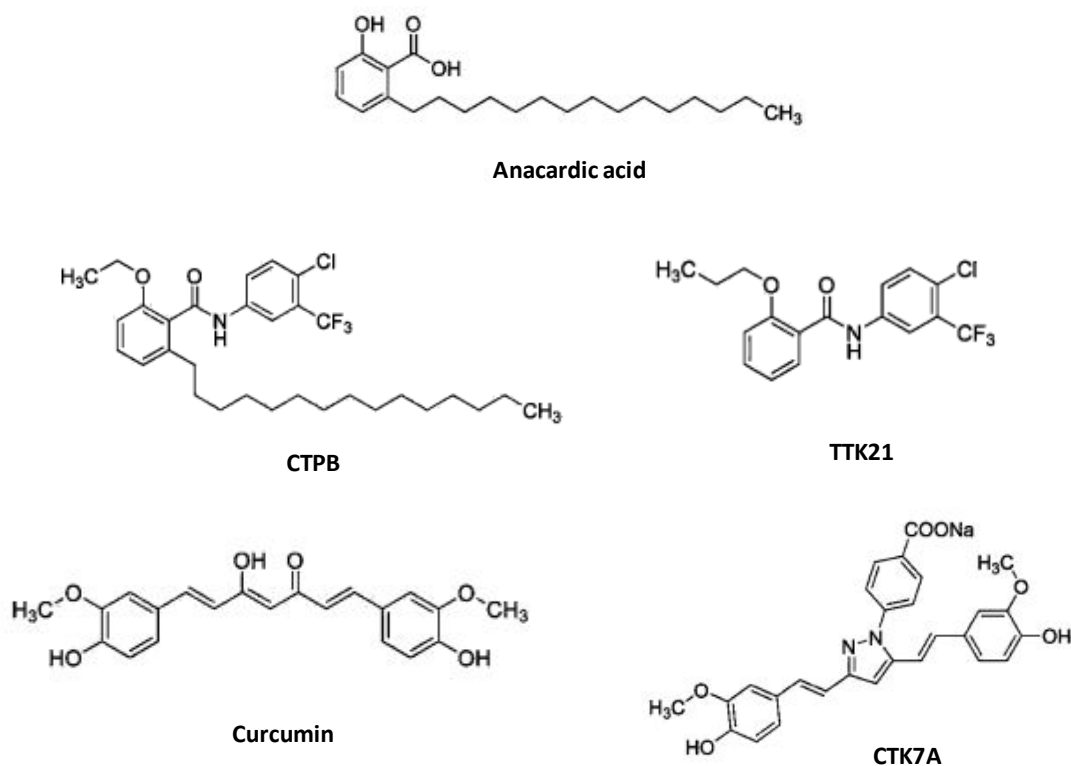


Figure 6: Structures of anacardic acid, curcumin and a few of their important derivatives (Source- Simon *et al*, J Med Chem, 2016)

3.1.4.3 Synthetic inhibitors

Various KAT inhibitors have been discovered by synthetic means with the use of high throughput assays, rational design and *in silico* screening. One of the most prominent p300 inhibitors that have found widespread applications is the pyrazolone containing synthetic inhibitor C646 (Bowers *et al*, 2010) (Figure 7). It was basically designed using a virtual screening approach by molecular docking whereby it could bind in the same pocket of p300 as the bisubstrate inhibitor lysyl CoA. The free carboxylic acid and nitro group of C646 enables it to form several hydrogen bonds and salt bridges with critical amino acid residues in the p300 active site, while the planarity of the pyrazolone structure allows it to efficiently dock into the active site. However, despite its specificity towards p300 amongst the different KATs, C646 has also been found to form conjugates with different

cysteine containing proteins (Shrimp *et al*, 2015). The extended conjugated system of C646 makes it unsuitable for fluorescence based assays, which was circumvented by replacing the furan with a phenyl ring (Dancy *et al*, 2012). The new derivative could also inhibit p300 acetyltransferase activity and also prevent cell growth in various cancer cell lines by histone hypoacetylation (Gao *et al*, 2013).

Recently, another new synthetic inhibitor A-485 has been developed that has shown remarkable specificity as well potency for inhibiting p300 acetyltransferase activity at nanomolar concentration (IC_{50} value of 73 nM) (Lasko *et al*, 2017) (Figure 7). It has shown high promise in preventing cell proliferation in several cancer cell lines as well as tumor growth in mice models by inhibition of H3K27 acetylation. Since its discovery, A-485 has been extensively used in various other model systems for highlighting the role of p300 in different physiological processes. Its administration has been successful in attenuating lipogenesis and weight gain in mice on high fat diet by inhibition of p300 catalysed acetylation (Zhou *et al*, 2020). In a similar manner, it has also shown promise in treatment of neurodegenerative diseases such as Parkinson's, by ameliorating α -Synuclein aggregation in the brain through p300 inhibition (Hluschchuk *et al*, 2021).

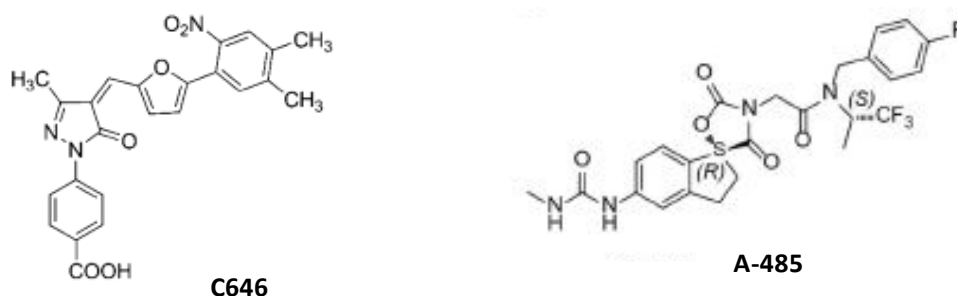
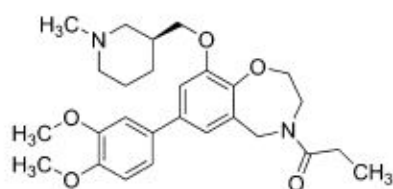


Figure 7: Structures of two of the most prominent synthetic inhibitors of p300 acetyltransferase (Source- Simon *et al*, J Med Chem, 2016 and Lasko *et al*, Nature, 2017)

3.1.4.4 Bromodomain inhibitors

In addition to directly targeting the catalytic activity of p300 or any other KAT, a new strategy for enzyme inhibition has been to disrupt its protein-protein interactions. The bromodomain of p300 is essential for recognizing acetylated substrate as well as for binding chromatin. Therefore, abrogation of the bromodomain interaction would prevent the assembly of p300 and other transcriptional coactivator complexes and repress the downstream acetylation dependant signaling processes. Most of the bromodomain inhibitors designed till date are specific for CBP. One such inhibitor I-CBP112, which has been designed on a benzoxazepine scaffold, not only inhibited CBP but could also bind the bromodomain of p300 with a slightly higher binding constant (Picaud *et al*, 2015) (Figure 8). The compound has even shown activity in leukemia cell lines, causing cell cycle arrest at G1 phase and altering cellular morphology.



I-CBP112

Figure 8: Structure of two of the bromodomain inhibitor of p300- I-CBP112 (Source- Simon *et al*, J Med Chem, 2016)

3.2 Results

3.2.1 Search for a selective inhibitor of p300 butyryltransferase activity

Previously, research had been carried out on garcinol, a polyisoprenylated benzophenone (Figure 1) obtained from *Garcinia indica* (popularly known as kokum in India), for its effect on different histone acetyltransferase activities including EP300. It was observed that garcinol non-specifically inhibits various enzymes and is also toxic to cells. The non-specificity and cytotoxicity could be attributed to the free phenolic –OH groups present in the structure of garcinol, leading to its high reactivity (Mantelingu *et al*, 2007).

In order to prepare compounds with more specificity towards EP300, a series of derivatives were synthesized using the structure of garcinol as the main scaffold (Figure 1)(108). Internal cyclisation of garcinol produced isogarcinol (IG) which had one of its –OH groups blocked. Isogarcinol also retained the properties of a non-specific and cytotoxic inhibitor. Further addition of one or two functional groups to the remaining free -OH groups gave rise to various mono and di-substituted derivatives. Two of these mono-substituted derivatives having an additional isopropyl and methyl group were named LTK-13 (14-isopropoxy IG) and LTK-14 (14-methoxy IG) respectively.

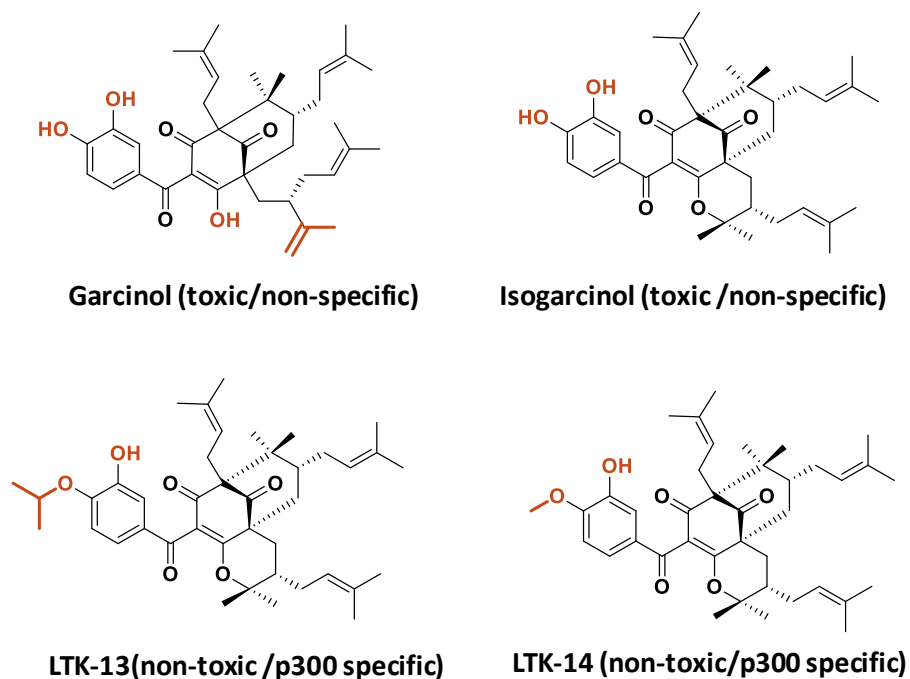


Figure 1: Structures of g Garcinol and its cyclised and mono-substituted derivatives. The site of internal cyclisation and the site of mono-substitution are shown in brown colour.

Their corresponding disubstituted counterparts in which both the –OH groups were blocked were named LTK-13A (13, 14-diisopropoxy IG) and LTK-14A respectively (13,14-dimethoxy IG). Two more disubstituted derivatives synthesized were LTK-15 (13,14-diacetoxy IG) and LTK-19 (13,14-disulfoxy IG) (Figure 2).

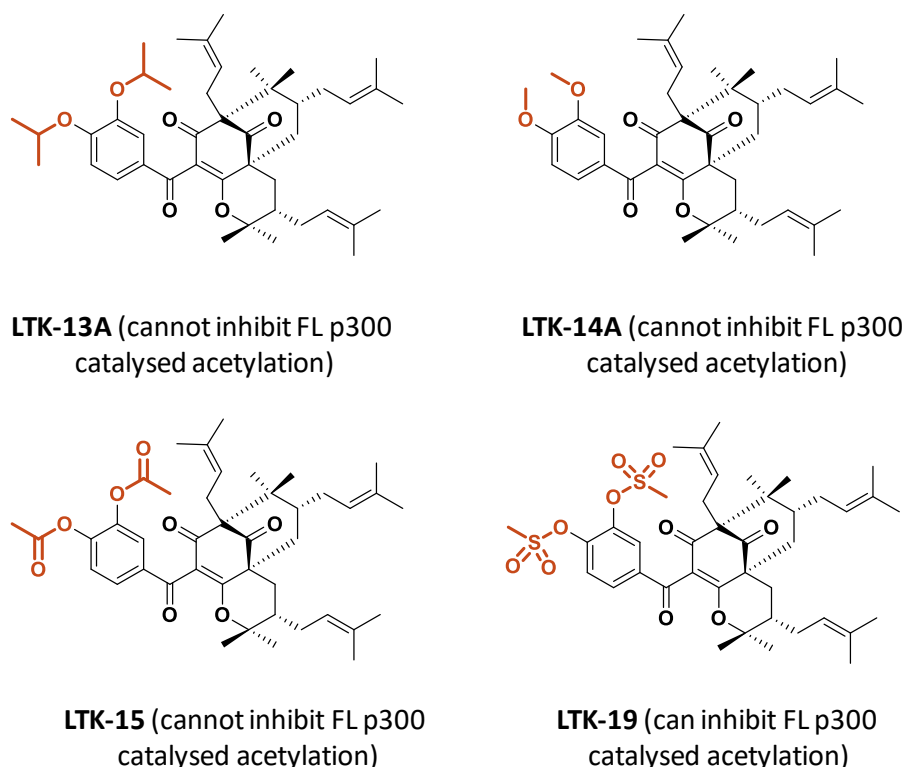


Figure 2: Structures of different disubstituted derivatives of isogarcinol. The added substituents are shown in red.

It had been previously reported that amongst these compounds, the monosubstituted derivatives LTK-13 and LTK-14 could potentially inhibit EP300 catalysed acetylation, while their disubstituted counterparts LTK-13A and LTK-14A were unable to do so. This was probably due to increased steric hindrance brought about by the addition of an extra functional group that interfered with the interaction between the compounds and EP300. An inverse correlation between catalytic rates of acylation reactions by EP300 and increasing acyl chain length had already been established previously. This led to our hypothesis that since butyrylation is catalysed by EP300 at a much slower rate compared to acetylation, one of the compounds which could not inhibit EP300 catalysed acetylation, might be able to inhibit the slower butyrylation reaction.

To start with the proceedings, at first *in vitro* acetylation assays were performed with the different derivatives using recombinant full length p300 and histone H3

as the substrate. The results obtained were in confirmation with the previous report, as it was observed that garcinol, isogarcinol, LTK-13, LTK-14 and LTK-19 strongly inhibited acetylation while LTK-13A, LTK-14A and LTK-15 could not (Figure 3A). When *in vitro* butyrylation assays were performed with these compounds, most of them could inhibit the butyrylation reaction (Figure 3B).

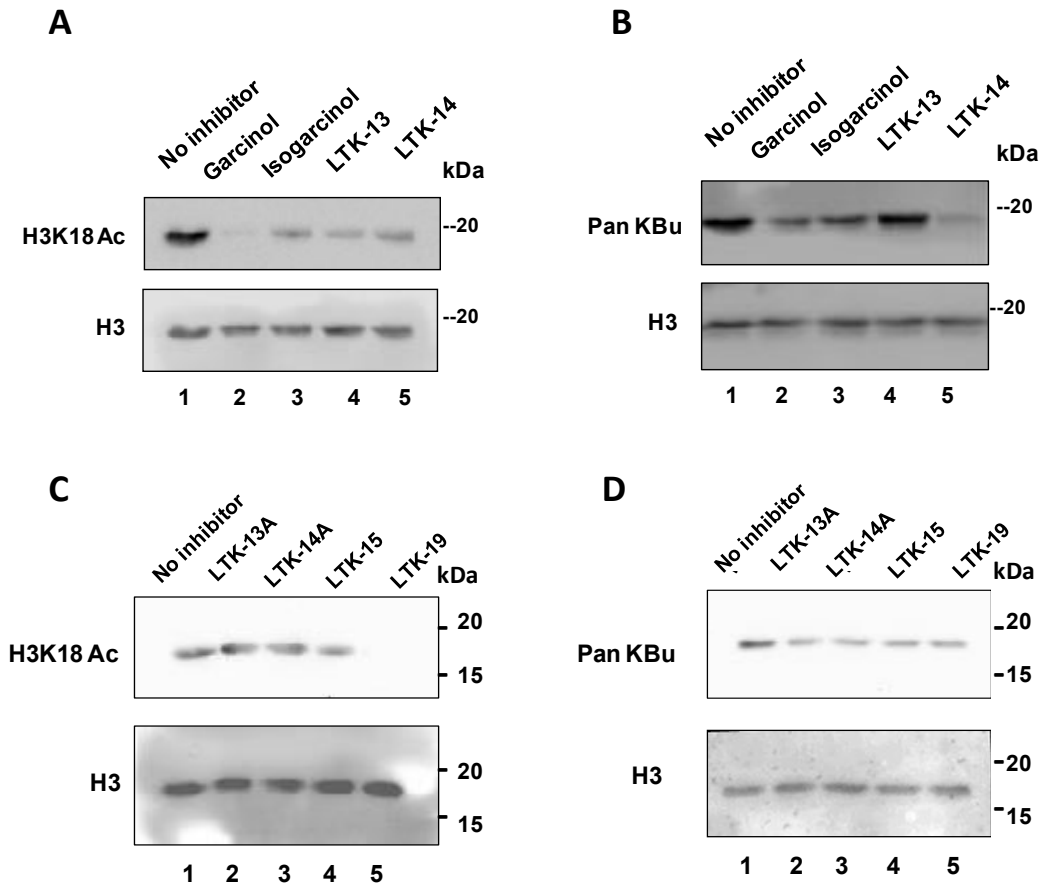


Figure 3: Immunoblotting with antibodies against acetylated H3K18 (A) and pan-butyryl lysine (B) to check for the relative inhibition of acetyltransferase and butyryltransferase activities of full length p300 by garcinol and its derivatives. Lane 1, enzyme alone; Lane 2, enzyme + garcinol; Lane 3, enzyme + isogarcinol; Lane 4, enzyme + LTK-13; Lane 5, enzyme + LTK-14. All the compounds were used at a concentration of 10 μ M. Recombinant *Xenopus* histone H3 was used as loading control. (C, D) Initial screening for the different disubstituted compounds for their differential effect on p300 catalysed acetylation (C) and butyrylation (D) on histone H3. Lane 1, enzyme alone; Lane 2, enzyme + LTK-13A; Lane 3, enzyme + LTK-14A; Lane 4,

enzyme + LTK-15; Lane 5, enzyme + LTK-19. All the compounds were used at a concentration of 25 μ M.

Our aim was to screen for a compound that could inhibit butyrylation but would not be able to inhibit the acetylation reaction. LTK-13A, LTK-14A and LTK-15 matched this criterion (Figure 3C and D). Since extensive characterization studies had already been performed with LTK-14, and LTK-14A was its disubstituted counterpart, comparative structural and biological studies with this compound seemed more feasible. Hence LTK-14A was finalized as the selective butyrylation inhibitor for the purpose of downstream analysis.

3.2.2 Understanding the structural basis for selective inhibition of EP300 catalysed butyrylation by LTK-14A by molecular docking

When *in vitro* acetylation and butyrylation assays were performed simultaneously with different doses of LTK-14 and LTK-14A it was observed that LTK-14 could not only inhibit both the reactions, but while it inhibited acetylation at 10 μ M concentration (Figure 4A), it could inhibit butyrylation at a much lower concentration i.e. 2 mM (Figure 4B). On the other hand, LTK-14A could most prominently inhibit butyrylation at 25 μ M concentration (Figure 4D,F), while acetylation remained uninhibited (Figure 4 C,E) . Thus, LTK-14A was able to inhibit only the slower butyrylation reaction, LTK-14 could inhibit both the acylation reactions with greater inhibitory effect on butyrylation.

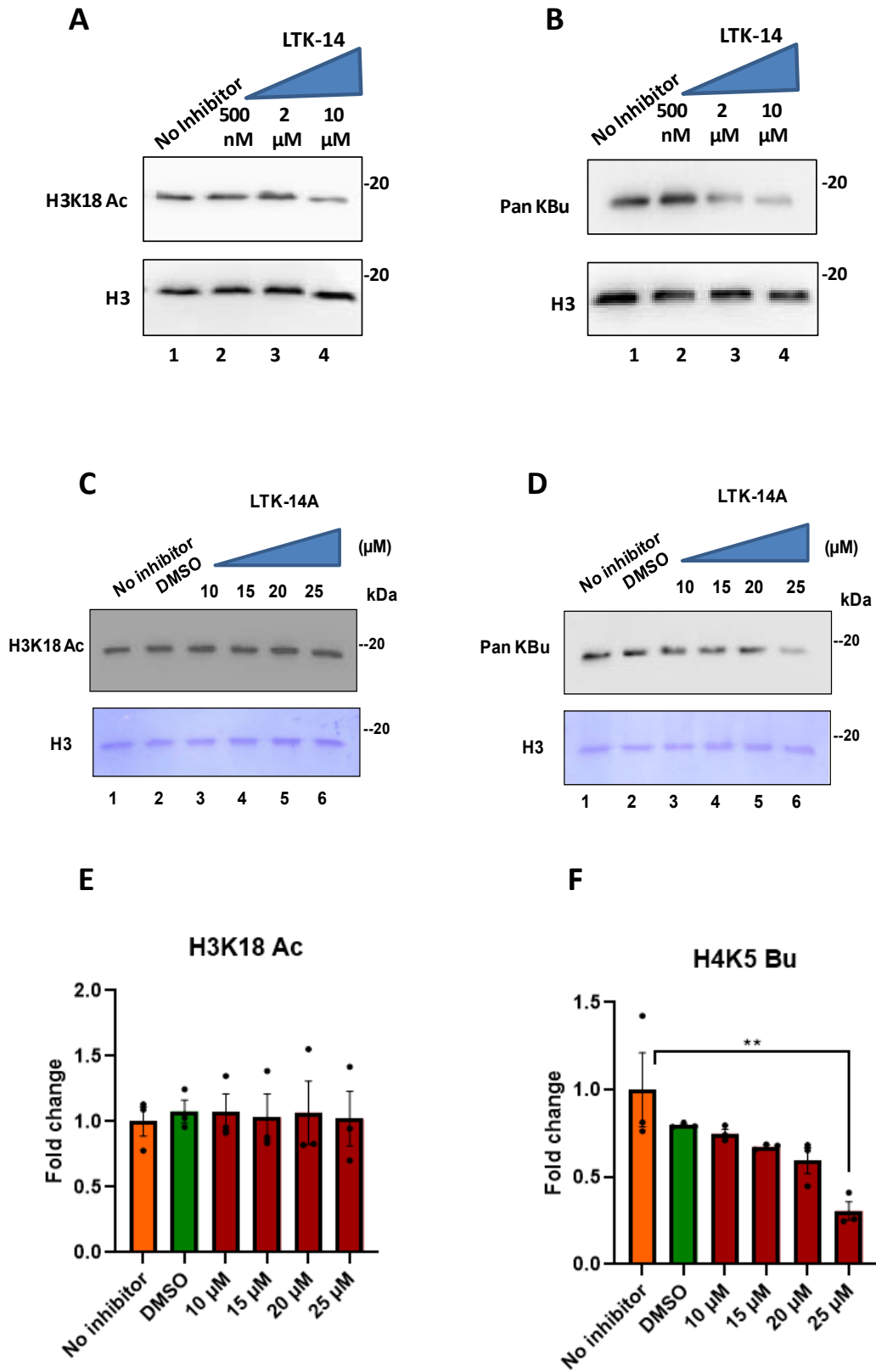


Figure 4: Immunoblotting with antibodies against acetylated H3K18 (A) and pan-butyryl lysine (B) to check for the relative inhibition of acetyltransferase and butyryltransferase activities of full length p300 by LTK-14 at different concentrations. Lane 1, enzyme alone; Lane 2-4 enzyme + LTK-14 at concentrations 500 nM, 2 μ M and 10 μ M respectively. (C, D) Immunoblotting with antibodies against acetylated H3K18 (A) and pan-butyryl lysine (B) to check for the relative inhibition of acetyltransferase and butyryltransferase activities of full length p300 by LTK-14A at different concentrations. Lane 1, enzyme alone; Lane 2, enzyme + DMSO; Lane 3-6, enzyme + LTK-14A at concentrations 10, 15, 20 and 25 μ M respectively. The quantitations are given in panels E and F. Error bars denote mean \pm SEM of three biological replicates, one-way ANOVA with Bonferroni's multiple comparison; * $P < 0.05$, ** $P < 0.01$, * $P < 0.001$, ns: not significant.**

In order to understand the mechanism behind this selective inhibition by LTK-14A, we performed molecular docking analysis of LTK-14 and LTK-14A with the EP300 lysine acetyltransferase catalytic domain. For this purpose, the crystal structure of LTK-14A was solved. The crystal structure of LTK-14 had already been solved and it was taken for comparative analysis. The energy minimized analysis revealed that both LTK-14 and LTK-14A could potentially bind with the active site of EP300 catalytic domain forming several hydrophobic interactions (Figure 5). LTK-14, due to the presence of a free phenolic –OH group, could hydrogen bond with a carbonyl oxygen atom present in the peptide backbone of S1396 residue. However, LTK-14A has all of its phenolic –OH groups blocked and so it is incapable of forming such an interaction. This hydrogen bonding by LTK-14 could imply a stronger binding to the enzyme, while LTK-14A, by interacting with lesser number of residues presumably inhibits only the slower butyrylation reaction, although the interaction may not be strong enough for inhibiting the faster acetylation reaction.

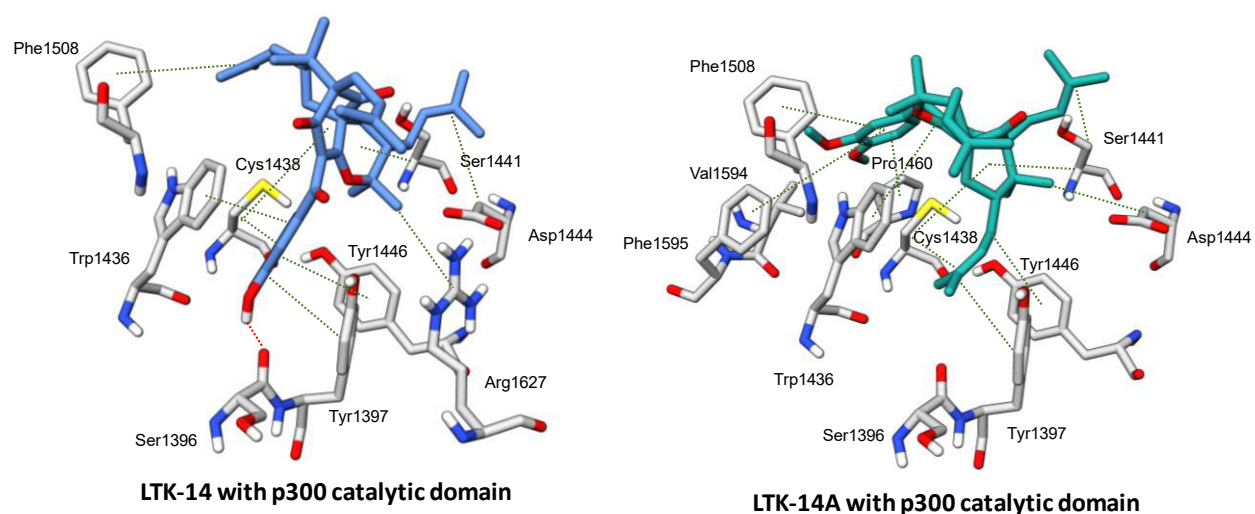


Figure 5: Molecular docking studies for studying comparative interaction of LTK-14 and LTK-14A with the amino acid residues of p300 catalytic domain. The predicted interactions are denoted by tick lines. Hydrogen bonding is shown in red and hydrophobic interaction is shown in green.

3.2.3 Validation of molecular docking by site directed mutagenesis

Some of the residues with which LTK-14A could form hydrophobic interaction have already been reported before as being critical for targeting inhibition of enzymatic activity of EP300. These residues include C1438, Y1446, Y1397 and W1436 (Figure 5). To verify the molecular docking result, a point mutant of the EP300 catalytic domain was generated in which the mutation was introduced at one of the predicted positions C1438. This particular residue was chosen for downstream analysis as it was predicted to have the highest propensity for interaction with LTK-14A. The large Van der Waal's radius of sulfur in the side chain of cysteine residue might be responsible for the close proximity between the amino acid and the isoprenyl group of LTK-14A. Hence it was assumed that mutating the cysteine to alanine would reduce the proximity by curbing the length of the side chain at the C β atom and thereby affect the interaction of LTK-14A with the EP300 catalytic domain.

In vitro filter binding assay showed that both wild type and mutant p300 catalytic domain had similar acetyltransferase activity (Figure 6A). *In vitro* histone acylation

assays were simultaneously performed using wild type and C1438A mutant of EP300 catalytic domain with different doses of LTK-14A. It was observed that the wild type EP300 KAT domain catalysed butyrylation was inhibited by LTK-14A most prominently at 25 μ M concentration (Figure 6 C, E) while acetylation was not inhibited (Figure 6 B,D) . In contrast, neither acetylation (Figure 7 A,B) nor butyrylation (Figure 7 C, D) modification catalysed by the mutant EP300 catalytic domain could be inhibited by LTK-14A even at 25 μ M concentration. Taken together these data suggested that LTK-14A indeed interacts with C1438 within the active site of EP300 catalytic domain and this residue is critical for butyrylation reaction inhibition by the compound.

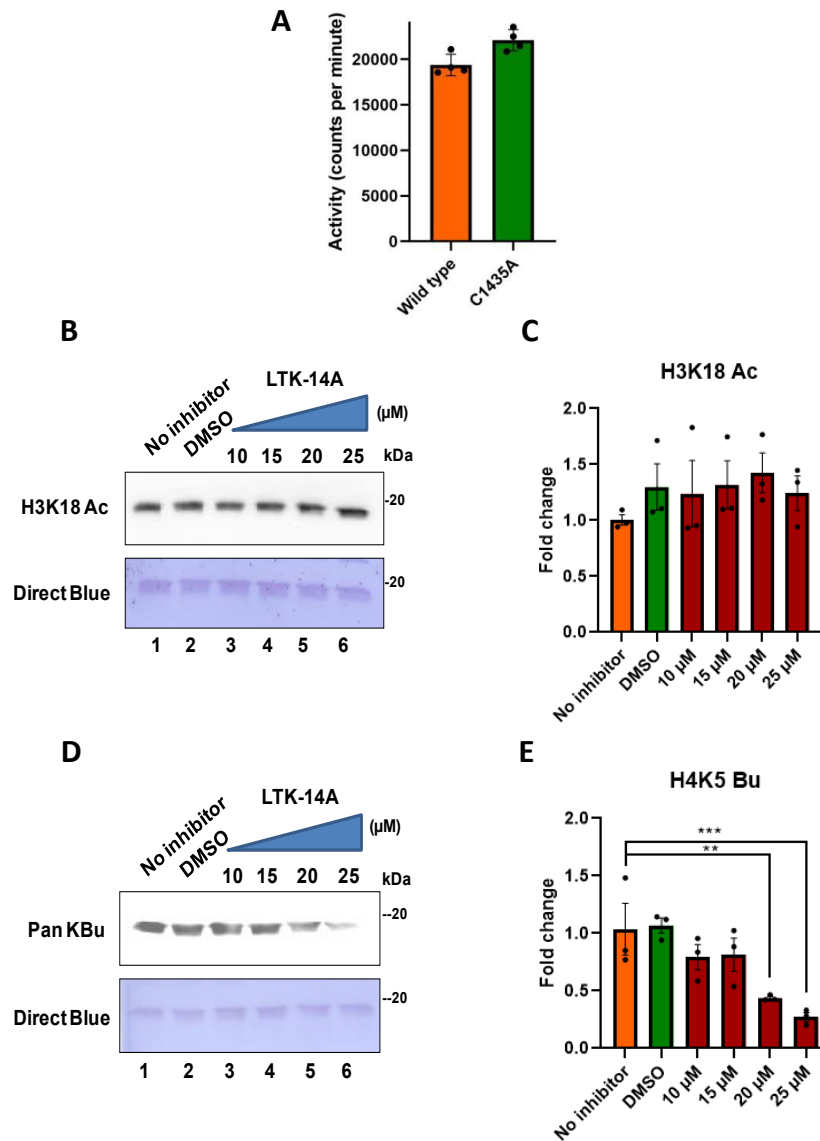


Figure 6: (A) Filter binding assay to compare the relative canonical acetyltransferase activity of wild type and mutant p300 catalytic domain. (B,D) Immunoblotting with antibodies against acetylated H3K18 (B) and pan-butyryl lysine (D) to check for the relative inhibition of acetyltransferase and butyryltransferase activities of wild type p300 catalytic domain by LTK-14A at different concentrations. Lane 1, enzyme alone; Lane 2, enzyme + DMSO; Lane 3-6, enzyme + LTK-14A at concentrations 10, 15, 20 and 25 μM respectively. The quantitations are given in panels C and E. Error bars denote mean \pm SEM of three biological replicates, one-way ANOVA with Bonferroni's multiple comparison; * $P < 0.05$, ** $P < 0.01$, *** $P < 0.001$, ns: not significant.

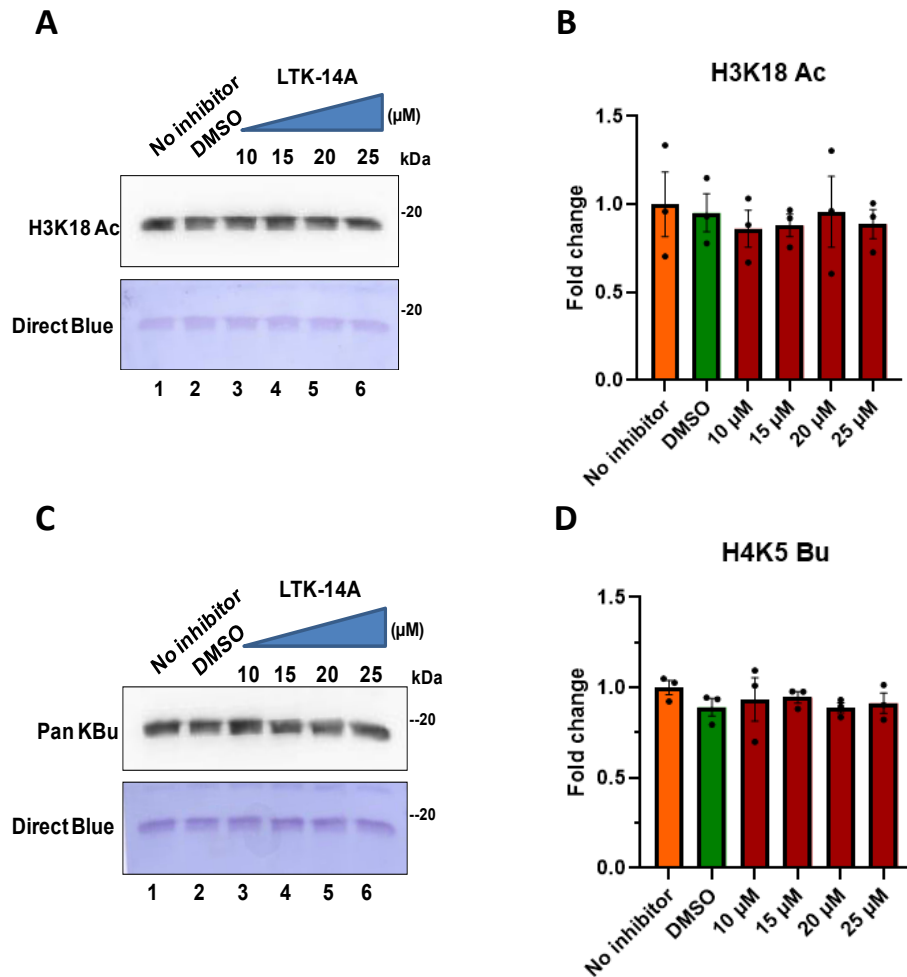


Figure 7: Immunoblotting with antibodies against acetylated H3K18 (A) and pan-butryl lysine (C) to check for the relative inhibition of acetyltransferase and butyryltransferase activities of catalytically active p300 catalytic domain with point mutation C1438A by LTK-14A at different concentrations. Lane 1, enzyme alone; Lane 2, enzyme + DMSO; Lane 3-6, enzyme + LTK-14A at concentrations 10, 15, 20 and 25 μ M respectively. The quantitations are given in panels B and D. Error bars denote mean \pm SEM of three biological replicates, one-way ANOVA with Bonferroni's multiple comparison; * $P < 0.05$, ** $P < 0.01$, *** $P < 0.001$, ns: not significant.

3.2.4 Butyryl CoA levels are higher in adipocytes compared to pre-adipocytes

After obtaining a butyrylation specific inhibitor, it was imperative to use it as a chemical biology based tool to highlight the importance of this modification in a physiological context.

Under normal circumstances, the cellular levels of certain coenzyme A derivatives are much less than acetyl CoA. The situation may alter in specific cases where metabolic pathways promoting the production of other acyl CoA derivatives become more predominant. It was surmised that one such possible scenario could be the process of adipogenesis in which even chained fatty acid synthesis and breakdown can give rise to several intermediate products like butyryl CoA.

The possible causal relationship of butyryl CoA and adipogenesis was investigated using the 3T3L1 pre-adipocyte cell line as model system. The cells were subjected to adipogenesis process and on seventh day it was confirmed by Oil Red-O staining. The expression of the molecular markers of adipogenesis such as *Pparg* and *Cebpa* further confirmed the differentiation process (Figure 8A). Interestingly, a significant increase in the expression of *Acss2* (acyl-CoA synthetase short chain family member 2) upon differentiation could also be observed. Previously, ACSS2 had been established as the enzyme responsible for generation of acyl-CoA derivatives from their corresponding short chain fatty acids.

In order to investigate the metabolic state (especially concentration of butyryl CoA) of the cells during differentiation, metabolites were extracted from undifferentiated and differentiated 3T3L1 cells and the stoichiometric levels of butyryl CoA were estimated by mass spectrometry analysis (Figure 8B). A near two-fold increase in the levels of butyryl CoA was observed upon differentiation. The enhanced transcript level of *Acss2* and stoichiometric level of butyryl CoA suggested that ACSS2 could possibly play a critical role in increased conversion of butyric acid to butyryl CoA, which in turn may lead to a more pronounced physiological role of butyryl CoA during adipogenesis.

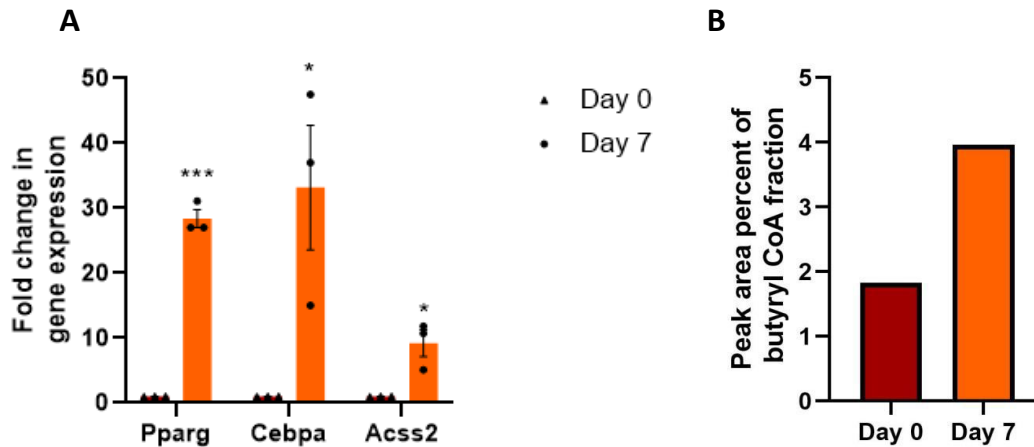


Figure 8: (A) qRT-PCR analysis was performed to check for transcript levels of *Acss2* in undifferentiated and differentiated 3T3L1 cells. Error bars denote mean \pm SEM of three biological replicates; two-tailed unpaired Student's t-test: * $P < 0.05$, ** $P < 0.01$, *** $P < 0.001$, ns: not significant. **(B)** Stoichiometric levels of butyryl CoA in pre-adipocytes and differentiated adipocytes as estimated by LC-ES-MS analysis of metabolites extracted from 3T3L1 cells. The levels were determined by measuring the area under the curve for the eluted fractions in which butyryl CoA was the predominant molecular ion species and normalising it with peak area for all metabolites

3.2.5 Histone butyrylation increases during adipogenesis

The enhanced butyryl CoA levels with adipogenesis prompted us to find out whether this was also reflected in the butyrylation status of histones. For this purpose, histones were acid extracted from undifferentiated and differentiated 3T3L1 cells followed by immunoblotting (Figure 9). We observed that in accordance with previous report, there was indeed an increase in histone acetylation level (H3K9 Ac) in the differentiated cells as compared to the undifferentiated cells. Interestingly, we also observed enhanced global histone butyrylation levels upon differentiation. Immunoblotting analysis with site-specific antibodies against histone butyrylation marks (H3K9, H3K23, H3K27, H4K5, H4K8 and H4K12 Butyrylation) also revealed that butyrylation at each of these sites

increased upon differentiation. Amongst these modifications, H4K8 butyrylation was barely detectable in the undifferentiated pre-adipocytes and showed a dramatic increase in adipocytes. Collectively these results showed that during adipogenesis, EP300 catalysed butyrylation of histones could be an important epigenetic signature.

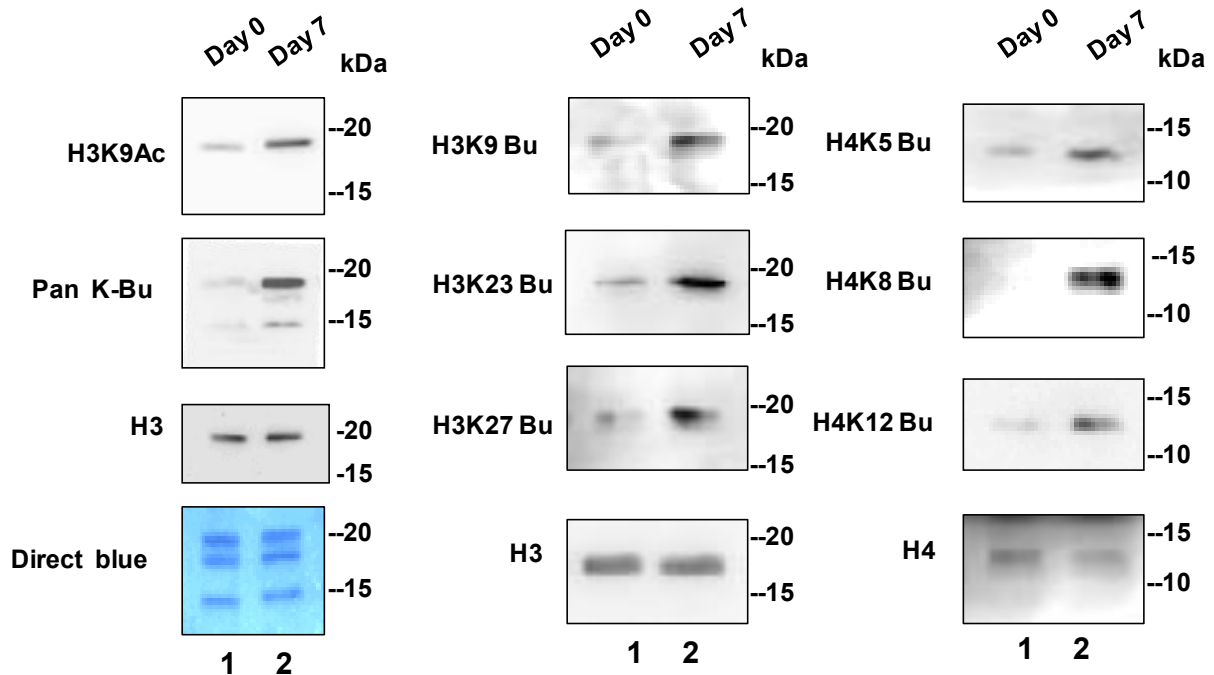


Figure 9: Histone acetylation and butyrylation levels in 3T3L1 cells in undifferentiated and differentiated state were analysed by immunoblotting with antibodies specific for acetylated H3K9, butyrylated H3K9, H3K23, H3K27, H4K5, H4K8, H4K12 and pan-butyryl lysine antibody . H3 and H4 were used as loading controls along with Direct Blue staining of all four core histones. Lane 1- undifferentiated pre-adipocyte (Day 0) and Lane 2 - differentiated adipocyte (Day 7) in each of the panels.

3.2.6 Histone butyrylation increases in the promoters of pro-adipogenic genes during adipogenesis

Since immunoblotting with extracted histones only gives a picture of the post-translational modification pattern changes occurring globally, chromatin immunoprecipitation (ChIP) was performed with H4K5 butyrylation specific antibody for a more comprehensive idea about the butyrylation changes occurring at the promoters of genes relevant to adipogenesis. We selected three genes for this study – the master regulator of adipogenesis *Pparg*, mature adipocyte marker *Lep* and *Cebpd*, a transcription factor required at the early stage of adipogenesis. Moreover, ChIP was carried out at three different time points – day 0 (undifferentiated pre-adipocyte), day 2 (initial stage of adipogenesis) and day 3 (terminal stage of adipogenesis) to investigate the temporal pattern of histone modification change in the selected gene promoters.

In the undifferentiated pre-adipocytes there was hardly any enrichment of H4K5 butyrylation in the promoters of any of the three genes, which is concurrent with the fact that global levels of histone butyrylation, as seen by immunoblotting, were also very low on day 0. However, on day 2 after induction of differentiation, there was a significant increase in the butyrylation at the promoter of *Pparg* while there was no detectable increase in the promoters of the other two genes. At day 6, there was a marked increase in H4K5 butyrylation in the promoters of all the three genes. PPAR γ is the most important transcription factor without which adipogenesis cannot proceed. Since butyrylation of histones is generally an inducer of increased transcription (Goudarzi et al, 2016), an increase in its enrichment in *Pparg* promoter at day 2 indicates that this modification might possibly play a role in inducing the transcription of this factor. The fact that the *Lep* gene encodes the adipocyte marker leptin which gets expressed only in mature adipocytes, might explain why there was no increase in H4K5 butyrylation in its promoter in the initial stage of differentiation and there was detectable enrichment at the terminal stage only. At day 6, however, both the genes

exhibited an increased enrichment of butyrylation in their promoters indicating that these genes are being even more actively transcribed at this state.

Interestingly, for *Cebpd*, which also encodes a transcription factor for adipogenesis, only had an increased enrichment of H4K5 butyrylation at day 6 and not at day 2.

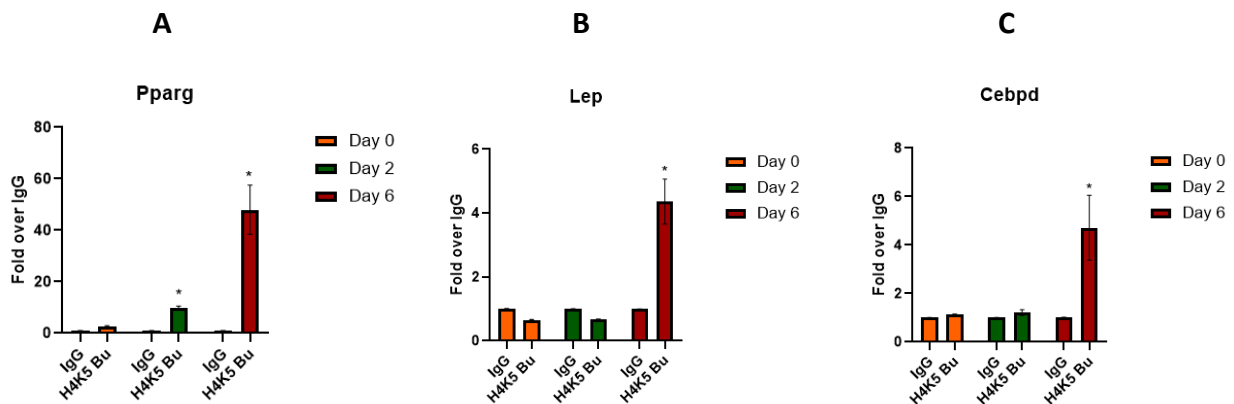


Figure 10: Enrichment of H4K5 butyrylation in the promoters of (A) *Pparg*, (B) *Lep* and (C) *Cebpd* represented in the form of fold change over IgG. Error bars denote mean \pm SEM of three biological replicates; one-way ANOVA with Dunnett's multiple comparison was performed: * P < 0.05, **P < 0.01, *P < 0.001, ns: not significant.**

3.2.7 LTK-14A is metabolically stable, cell permeable and inhibits adipogenesis without causing toxic effects

Upon establishing that the semi-synthetic derivative of garcinol, LTK-14A is an EP300 acylation specific inhibitor *in vitro*, its cellular effects were tested using 3T3L1 cells. First we checked the cellular permeability and metabolic stability of the compound. It was found the LTK14A is highly cell-permeable and also metabolically stable as it could be detected by mass spectrometry of metabolites extracted from LTK-14A treated cells after 6 days (Figure 11A).

MTT assay data showed that LTK-14A at 25 μ M concentration did not have any adverse effect on the cellular oxidoreductase activity, a signature of metabolic output of cells, suggesting that LTK-14A is non-toxic to 3T3L1 even after 6 days (Figure 11B). The effect of LTK-14A on the adipogenesis process was tested in the

next step. The 3T3L1 cells were induced to undergo adipogenesis in the presence and absence of LTK-14A. Treatment with DMSO was taken as solvent control. The result shows that although there was minimal reduction in adipogenesis upon DMSO treatment, almost 60% inhibition in adipogenesis was observed in presence of LTK-14A as revealed by Oil Red-O staining, followed by spectrophotometric quantitation (Figure 11 C, D).

The above data clearly establishes that although LTK-14A, is nontoxic to cells, it could inhibit the differentiation of the 3T3L1 cells.

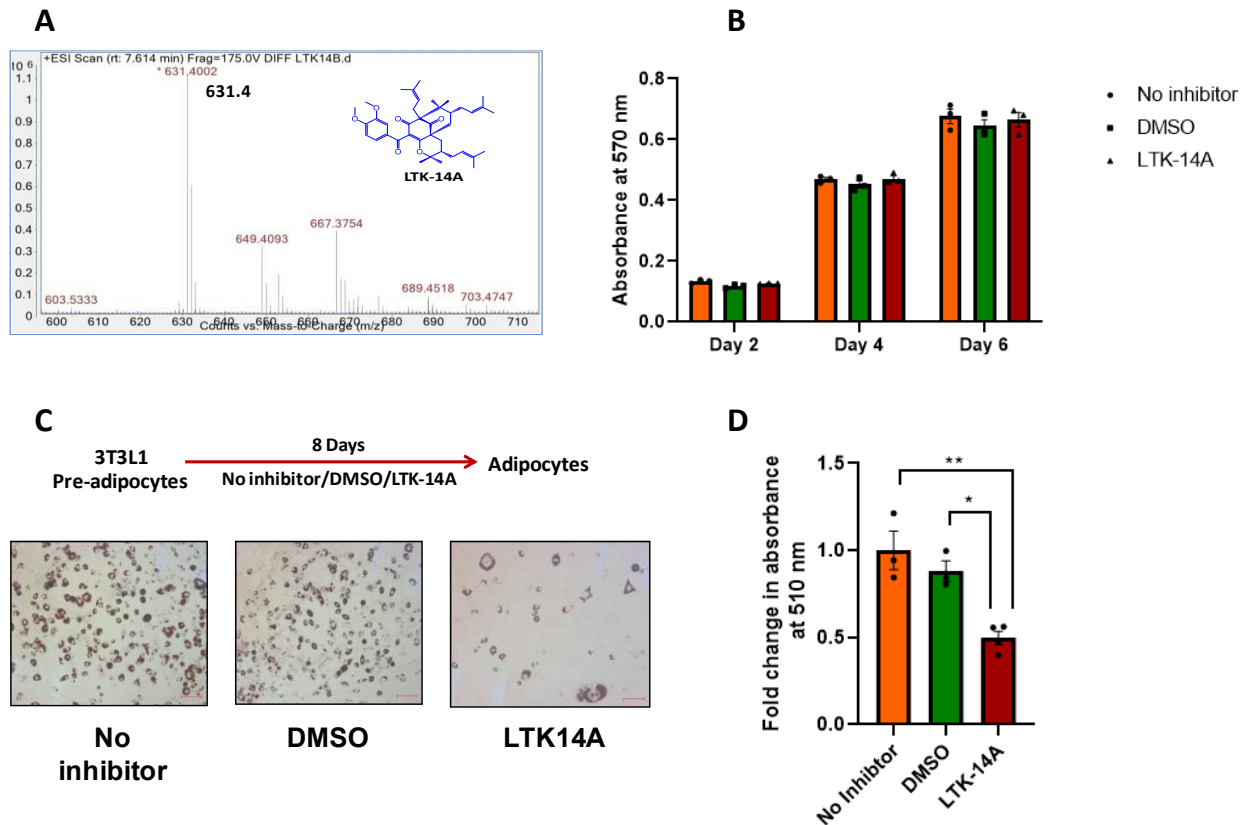


Figure 11: (A) The permeability and stability of LTK-14A in 3T3L1 was tested by LC-ESI-MS analysis of metabolites, extracted from compound treated 3T3L1 cells to detect the protonated LTK-14A in the ESI spectra of the eluted fraction. (B) MTT assay was performed to check for any possible cellular toxicity effect of LTK-14A, using 25 μ M concentration of the compound on 3T3L1 cells upon incubation for varying lengths of time (2, 4 and 6 days).

Comparison was done with cells that were left untreated or treated with DMSO as solvent control. (C, D) The effect of LTK-14A (25 μ M) treatment on adipogenesis was tested by Oil Red-O staining of the adipocytes (C) and the quantitation of staining is represented graphically in (D). Error bars denote mean \pm SEM of three biological replicates, one-way ANOVA with Bonferroni's multiple comparison; * $P < 0.05$, ** $P < 0.01$, *** $P < 0.001$, ns: not significant.

3.2.8 LTK-14A inhibits adipogenesis by mainly repressing the expression of lipogenic genes including the master regulators of adipogenesis

Since treatment with the butyrylation inhibitor LTK-14A inhibited adipogenesis, we presumed that the inhibition of differentiation might be taking place by repression of pro-adipogenic genes. In order to understand the mechanism of LTK14A-mediated inhibition of adipogenesis, cells treated with LTK-14A were subjected to transcriptome analysis. The untreated and solvent treated cells were taken as control. The volcano plot (Figure 12 A) and heat map (Figure 12B) analysis revealed that upon incubation with the compound, a large number of genes were found to be differentially expressed compared to DMSO treatment and untreated conditions.

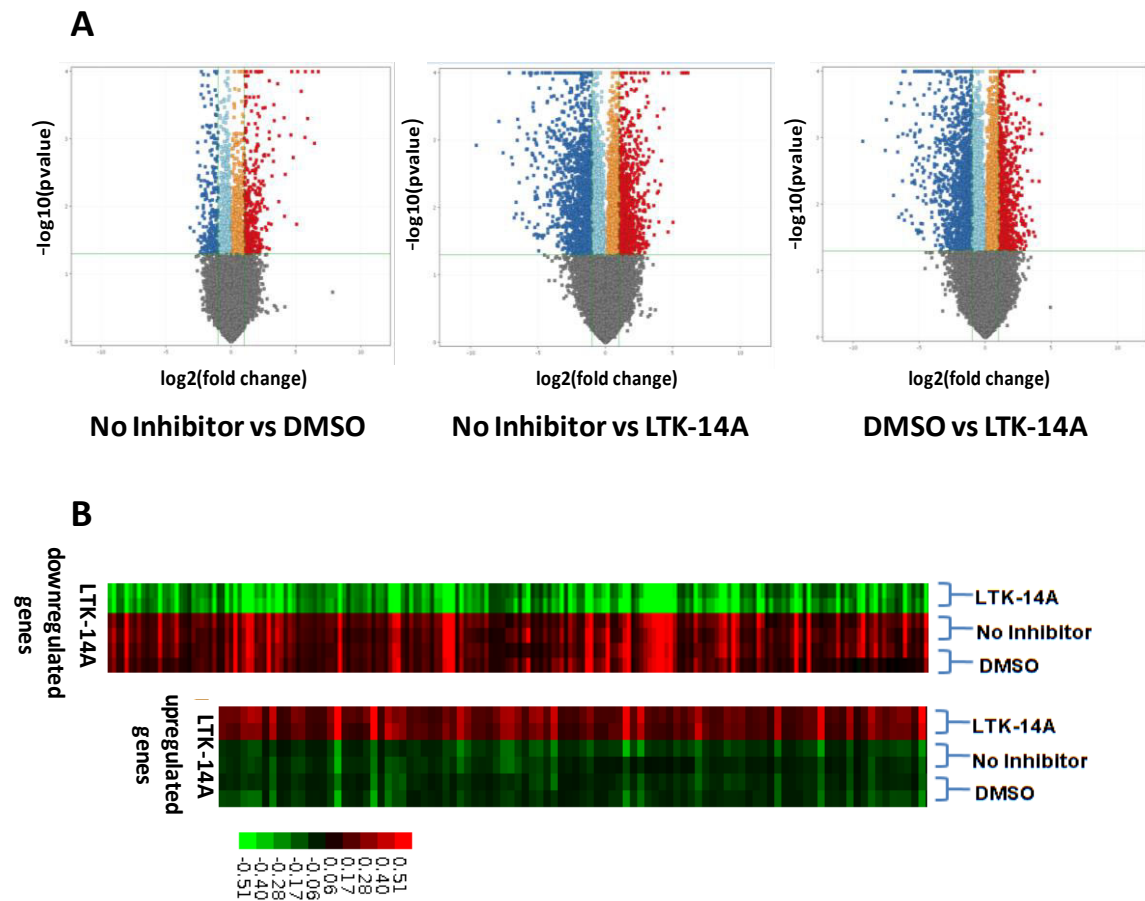


Figure 12: (A) Differential gene expression pattern of three conditions compared with each other depicted in volcano plots- No Inhibitor versus DMSO, No Inhibitor versus LTK-14A and DMSO versus LTK-14A. Downregulated and upregulated genes are shown in blue and red respectively. (B) Heat maps showing the differential gene expression pattern between LTK-14A treated cells and DMSO treated or untreated cells.

In order to gain a better understanding of LTK-14A affected genes we focused on the common genes that were differentially expressed in the two cases- (1) LTK-14A versus no inhibitor and (2) LTK-14A versus DMSO (Figure 13). Amongst these common genes 2200 genes were found to be downregulated and 1309 genes

were upregulated with a majority of them to be protein coding genes.

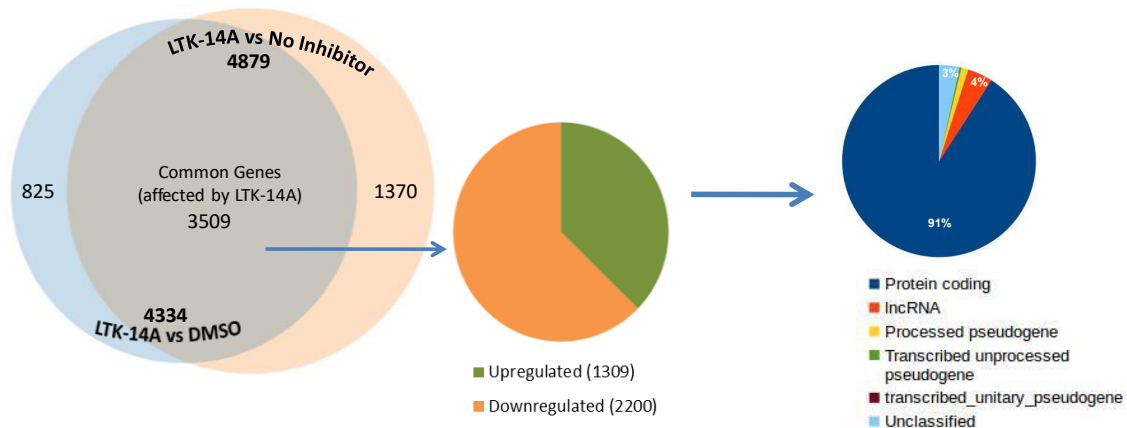
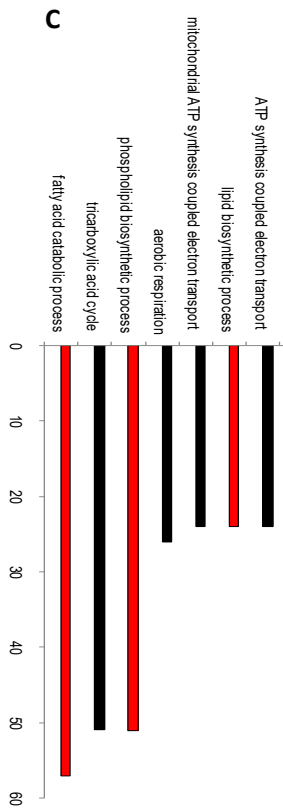
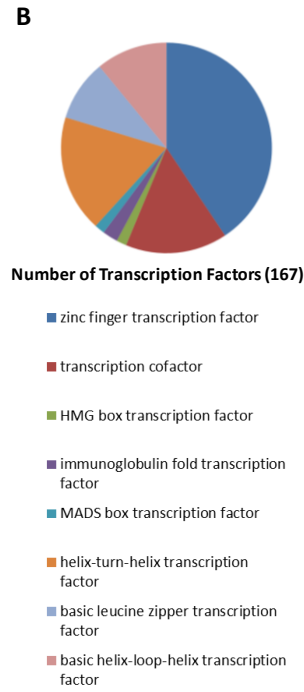
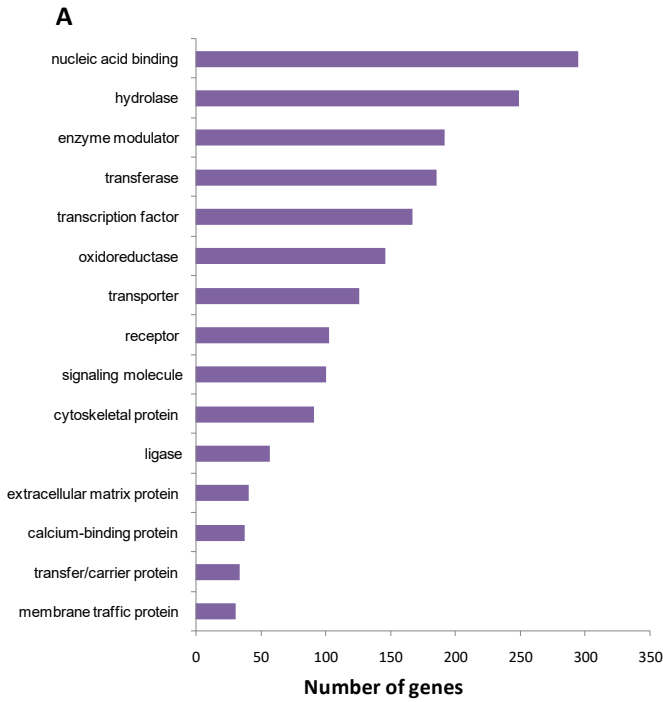


Figure 13: Venn diagram showing the number of differentially expressed genes upon LTK-14A treatment with respect to untreated and DMSO treated conditions. Pie chart showing the classification of the common differentially expressed genes.

A large proportion of these genes encoded for nucleic acid binding proteins such as transcription factors (TFs) (Figure 14 A). Interestingly, the major class of TFs affected was found to be zinc finger proteins (Figure 13B). The gene ontology analysis revealed that LTK14A treatment predominantly affected the genes involved in lipid metabolism pathways (Figure 14 C, D) which were minimally affected by DMSO alone (Figure 14 E).



D

Major pathways affected by LTK-14A

Biological processes	Fold enrichment	P-value
fatty acid beta-oxidation using acyl-CoA dehydrogenase	6.93	0.0000556
positive regulation of cholesterol biosynthetic process	6.06	0.00129
positive regulation of cholesterol metabolic process	6.06	0.00129
positive regulation of sterol biosynthetic process	6.06	0.00129
acetyl-CoA biosynthetic process from pyruvate	6.06	0.00129

E

Major pathways affected by DMSO

Biological process	Fold enrichment	P-value
receptor localization to synapse	4.78	0.0000625
protein localization to synapse	4.37	0.0000078
regulation of synaptic plasticity	3.55	1.25E-09
signal release	2.97	0.0000189
exocytosis	2.83	0.00000493

Figure 14: (A) Classification of the differentially expressed protein coding genes upon LTK-14A treatment according to their functionality. (B) Pie-chart depicting the classification of different transcription factors whose expression was perturbed upon LTK-14A treatment. (C, D, E) Gene ontology analysis was performed to study the different biological pathways that were affected by LTK-14A in 3T3L1 compared to DMSO treated as well as untreated conditions, as predicted by Panther software. The pathways were ranked in the order of those with maximum number of genes affected (C). A different ranking order was created on the basis of fold enrichment i.e. the pathways in which the ratio of number of observed affected genes over number of expected genes to be affected was the highest (D). A similar analysis was also performed for genes differentially expressed in DMSO versus untreated conditions (E).

Further analysis revealed that out of 97 pro-adipogenic genes (Table 1), as curated by us, a significant 41 were found to be downregulated (Table 2), 22 of which encoded for transcription factors upon LTK-14A treatment (Figure 15 A). This highlighted that LTK-14A was probably affecting the adipogenesis programme predominantly at the transcriptional level. A similar analysis for anti-adipogenic factors revealed that only 19 such factors out of 71 (Table 3) were upregulated upon LTK-14A treatment (Table 4, Figure 15 B). This indicated that the inhibition of adipogenesis by LTK-14A was more through repression of pro-adipogenic genes than through upregulation of anti-adipogenic genes. Interestingly, out of the 19 anti-adipogenic genes, 13 were found to be transcription factors. The gene regulatory networks and the respective pathways were constructed with the major genes that were affected by LTK-14A treatment compared to DMSO treated and untreated conditions (Figure 15 C). They collectively depict how LTK-14A, by inhibiting expression of a large number of genes that are interconnected via several pathways associated with lipid metabolism, brings about a collapse in the adipogenesis process as a whole.

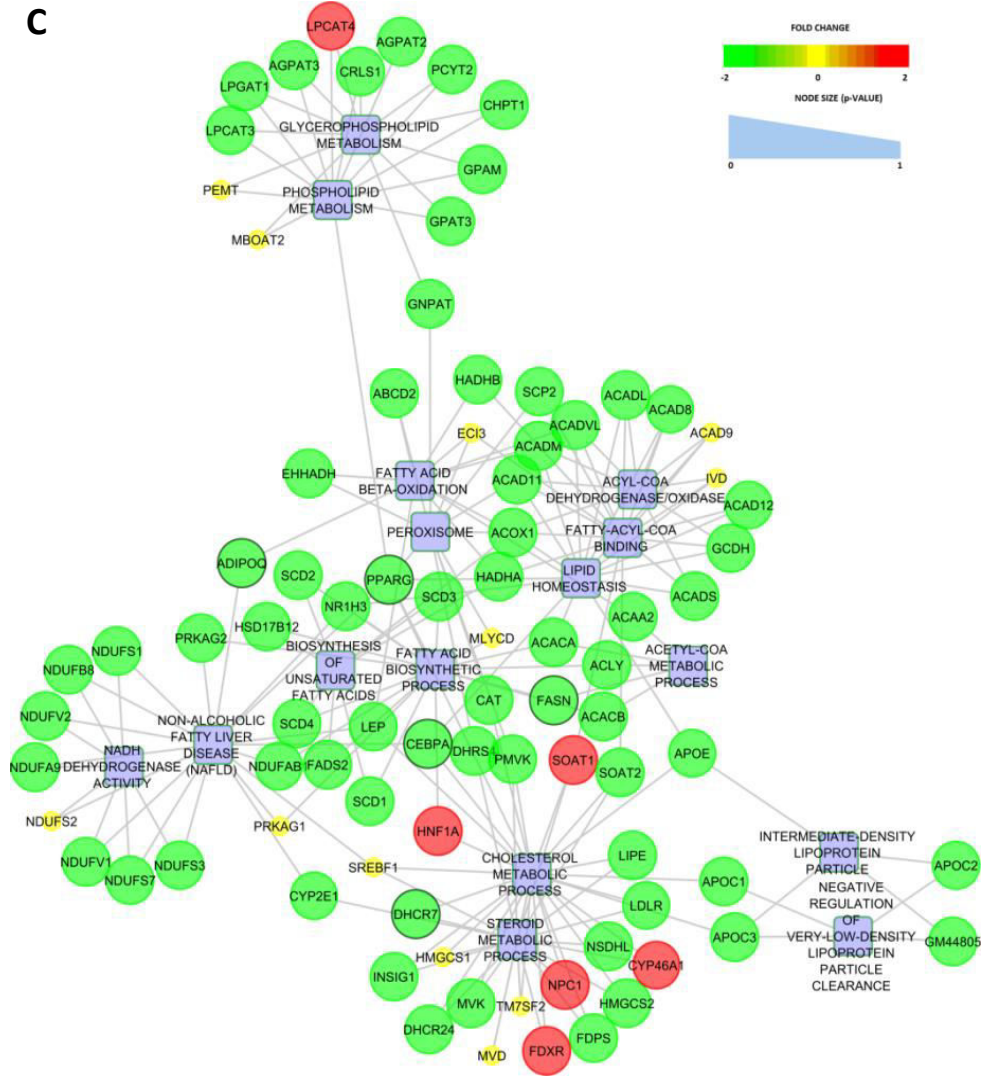
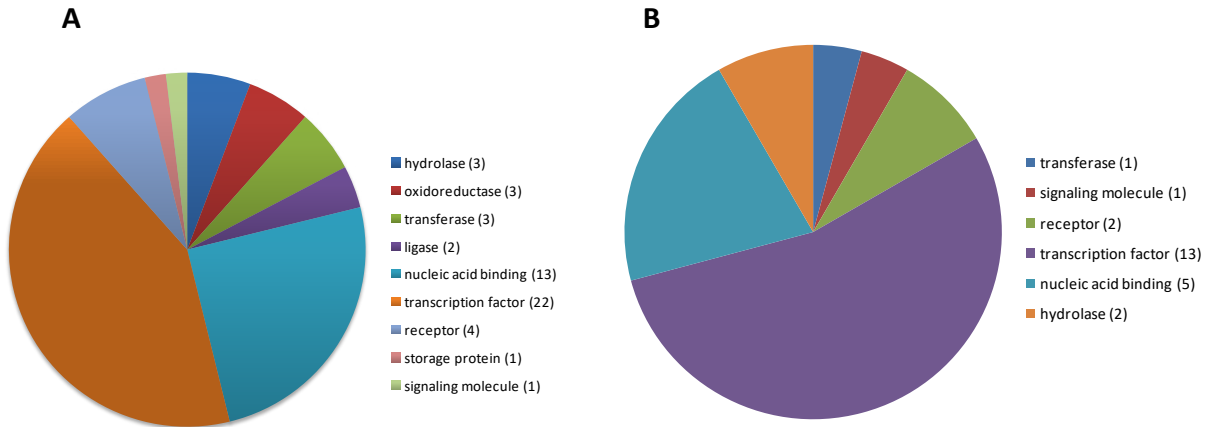


Figure 15: (A, B) Pie chart depicting the different classes of pro-adipogenic factors (A) and anti-adipogenic factors (B) whose expression was downregulated and upregulated respectively by LTK-14A treatment. (C) A molecular network was constructed to depict the interconnectivity between the lipid metabolism related genes and pathways that were affected upon their dysregulation by LTK-14A compared to DMSO treated conditions.

A few of the pro-adipogenic genes downregulated by LTK-14A, as indicated by RNA sequencing, were selected for further validation. These included the transcription factors such as *Cebpd* and master regulators of adipogenesis *Pparg* and *Cebpa*, adipocyte markers like *Adipoq* and *Lep*, genes encoding lipid metabolism associated genes such as *Fasn*, *Fabp4* and *Slc2a4*. Quantitative PCR analysis corroborated that the prominent pro-adipogenic genes (*Pparg*, *Cebpa*, *Adipoq*, *Lep*, *Slc2a4*, *Fasn* and *Fabp4*) showed a marked downregulation upon LTK-14A treatment (Figure 16 A). *Acss2*, the gene encoding the enzyme speculated to generate butyryl CoA from butyrate, was also downregulated by LTK-14A (Figure 14B). The upregulation of anti-adipogenic genes was also verified by performing qRT-PCR analysis for two such candidate genes- *Kdm4c* and *Tead4* (Figure 16 B). Interestingly, it was observed that the expression of *Cebpd* was not affected by LTK-14A (Figure 16B).

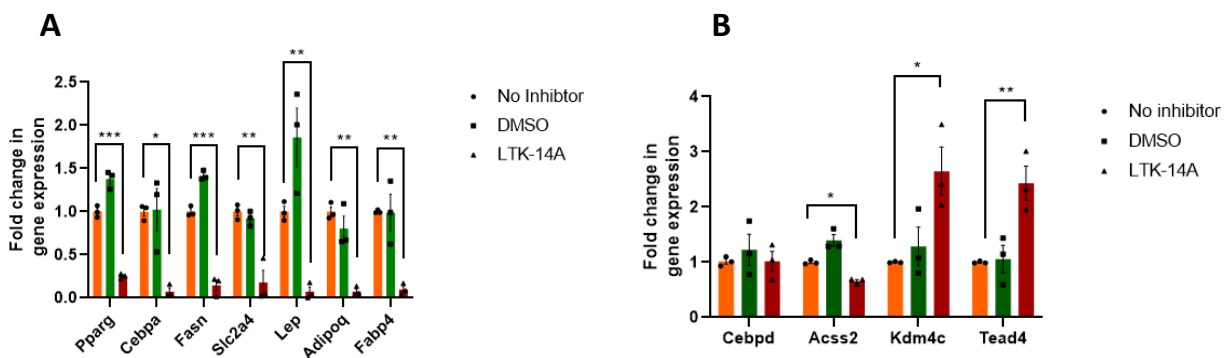


Figure 16 : (A,B) qRT-PCR analysis was performed to validate the putative target genes that were downregulated (A) or partially upregulated or unaffected (B) by LTK-14A. Error bars denote mean +/- SEM of three biological replicates; one-way ANOVA with Bonferroni's multiple comparison: * P < 0.05, **P < 0.01, ***P < 0.001, ns: not significant.

Collectively, the RNA-sequencing analysis along with the validation of gene targets further convincingly suggest that LTK-14A is capable of inhibiting the adipogenesis process in 3T3L1 cells, mainly by repressing the expression of important pro-adipogenic genes.

3.2.9 LTK-14A represses gene expression by specific inhibition of histone butyrylation without affecting acetylation

Since gene expression is epigenetically regulated by histone post-translational modifications, we were interested to find out whether LTK-14A mediated downregulation of adipogenesis is causally linked to the inhibition of histone butyrylation. Histones were acid extracted from 3T3L1 cells under treated/untreated conditions with the compound and subjected to immunoblotting analysis. It was found that treatment with LTK-14A inhibited overall butyrylation of histones (Figure 17 A,B). Among the specific modification sites tested, H3K23 and H4K5 butyrylation showed a significant decrease upon treatment with LTK-14A while butyrylation at other tested sites were affected minimally. Acetylation of histones (H3K9, H3K18 and H4K12) was also found to be unaffected upon LTK-14A treatment (Figure 17 C, D). To establish the specificity of the LTK14A, the effect of LTK-14A on lysine and arginine methylation along with phosphorylation of histones were also investigated. We chose to study the effect of LTK-14A on H3R17 dimethylation (specific mark for PRMT4/CARM1), H3K9 dimethylation (specific mark for G9a) and H3S10 phosphorylation (deposited by Aurora kinase). We observed no significant changes in these marks upon the compound treatment (Figure 17 E, F), thereby indicating that in the 3T3L1 cells, LTK-14A specifically inhibits butyrylation without affecting other modifications, to inhibit adipogenesis.

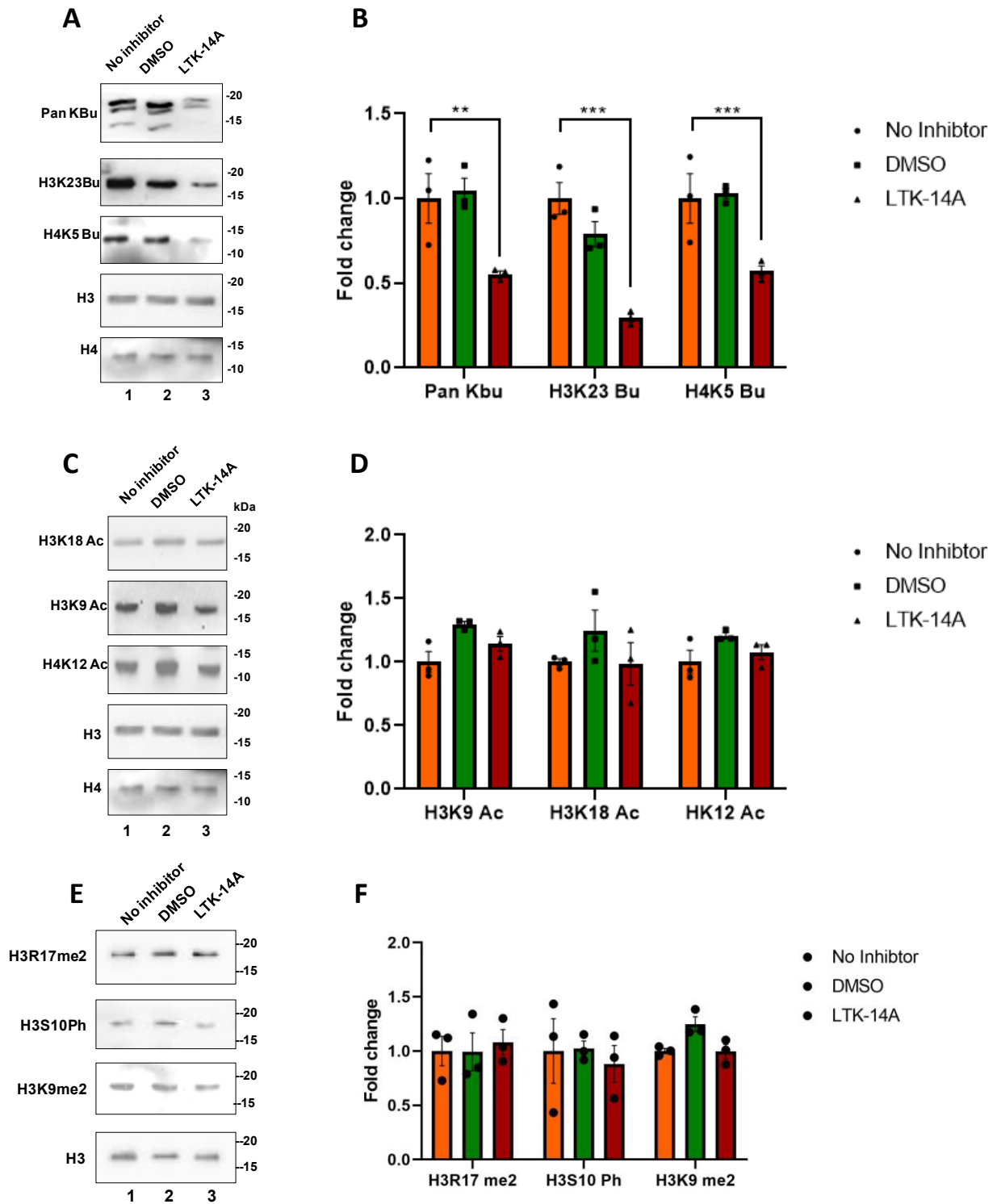


Figure 17: (A,B) Histone butyrylation levels in 3T3L1 cells that were treated with LTK-14A were compared with that in DMSO treated and untreated conditions by immunoblotting with antibodies against butyrylated histone H3K23, H4K5 and pan-butyryl lysine. Histones H3 and H4 were used as loading controls (A). The fold change of quantified band intensity is graphically represented in panel (B) in which the error bars denote mean \pm SD of three biological replicates. (C,D) Under similar conditions histone acetylation levels were compared by immunoblotting using antibodies against acetylated histones H3K18, H3K9 and H4K12 (C). The result is graphically represented in panel (D) in which error bars denote mean \pm SEM of three biological replicates. (E, F) Immunoblotting was also performed with antibodies against histone H3R17 dimethylation, H3S10 Phosphorylation and H3K9 dimethylation. The result is graphically represented in panel (F) in which error bars denote mean \pm SEM of three biological replicates. For all data one-way ANOVA with Bonferroni's multiple comparison was performed: * $P < 0.05$, ** $P < 0.01$, * $P < 0.001$, ns: not significant.**

3.2.10 LTK-14A prevents obesity and adipocyte hypertrophy in mice fed with high fat diet by specific inhibition of histone butyrylation without affecting acetylation in adipose tissues

After observing the anti-adipogenic effect of LTK-14A on 3T3L1 cells, we investigated whether this compound could also affect adipogenesis at organismal level. For this purpose, C57BL6/J mice were maintained either on normal diet or on a high fat diet with or without LTK-14A. In due course of time, it was observed that the mice maintained on a high fat diet showed a significant increase in weight gain compared to those on chow diet, as expected (Figure 18 A, B). Interestingly, the mice maintained on a high fat diet along with LTK-14A had a weight gaining trend intermediate between the normal diet and high fat diet fed mice (Figure 18 A, B). The diet consumption pattern of the mice showed that the two groups on high fat diet with or without LTK-14A, had a similar consumption rate (Figure 18 C) indicating that the reduced weight gain of the compound treated mice is not due to discrepancy in diet consumption.

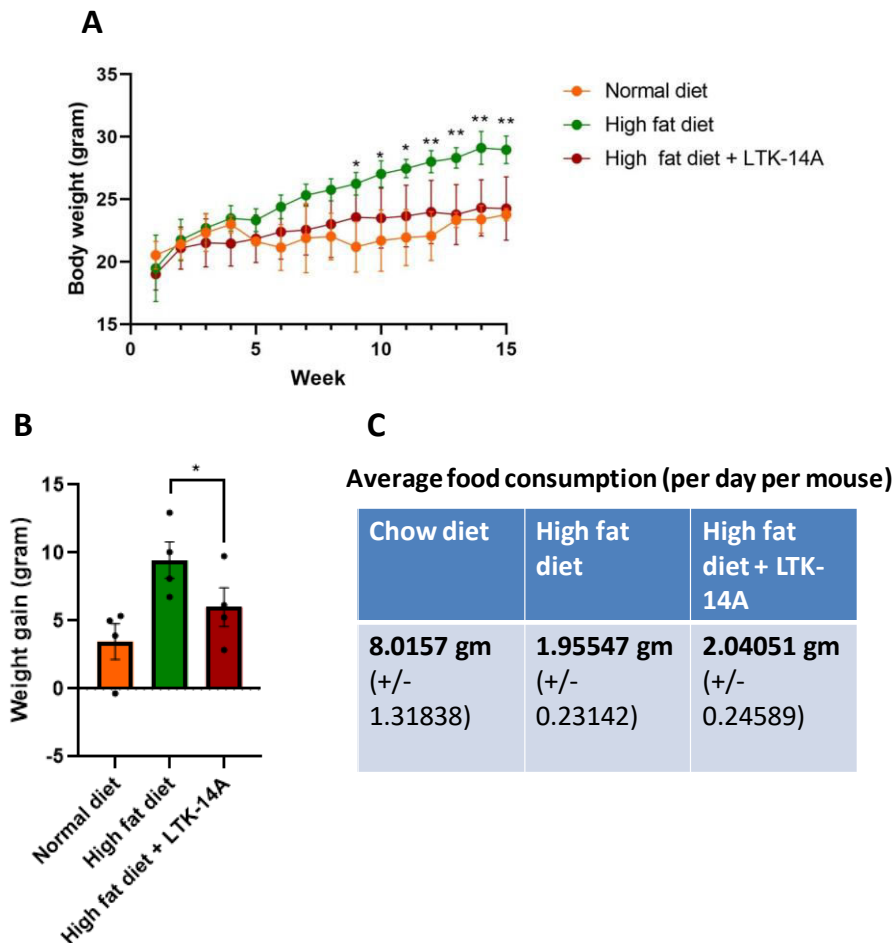


Figure 18: Trend of weight gaining (A) and average body weight gained after 16 weeks (B) of C57BL6/J mice maintained on normal chow diet, high fat diet and high fat diet mixed with LTK-14A was plotted ; n=4 in each group, one-way ANOVA with Dunnett's multiple comparison was performed: * P < 0.05, **P < 0.01, ***P < 0.001, ns: not significant. The comparative diet consumption pattern of the mice maintained on high fat diet only and high fat diet with LTK-14A has been shown in tabulated form (C).

Dissection of the mice revealed that the fat accumulation in high fat diet maintained mice was the highest, followed by those on high fat diet and LTK-14A, and then by those on normal diet (Figure 19 A) .The epididymal fat pads were separately weighed and the weights of the three groups showed the same trend as was seen for total body weights of the mice (Figure 19 B, C). Adipose tissues in mice undergo increased weight gain due to- (1) adipocyte hypertrophy (enlargement of already existent adipocytes) and (2) adipocyte hyperplasia

(increase in number of adipocytes by differentiation of pre-existent pre-adipocytes). The harmful effects of inflammation in adipose tissues occur mainly in the hypertrophied adipocytes in which endoplasmic reticulum stress, mitochondrial dysfunction and oxidative stress activate the inflammatory pathways. Hyperplastic adipocytes serve as a lipid sink for the excess lipids that cannot be stored by the hypertrophied adipocytes. Hematoxylin and eosin staining of epididymal fat pads (the main adipose tissue depot in mice) revealed morphology in high fat diet maintained mice typically carrying symptoms of onset of obesity i.e. the adipocytes were enlarged owing to lipid accumulation, a phenomenon known as adipose tissue hypertrophy (Figure 19 D). The morphology of the tissues obtained from normal diet fed mice and the mice fed with compound treated high fat diet were closely similar to one another, as they both exhibited smaller adipocyte size. Taken together these data indicate that LTK-14A could inhibit adipogenesis even in the *in vivo* context, and thereby the development of obesity.

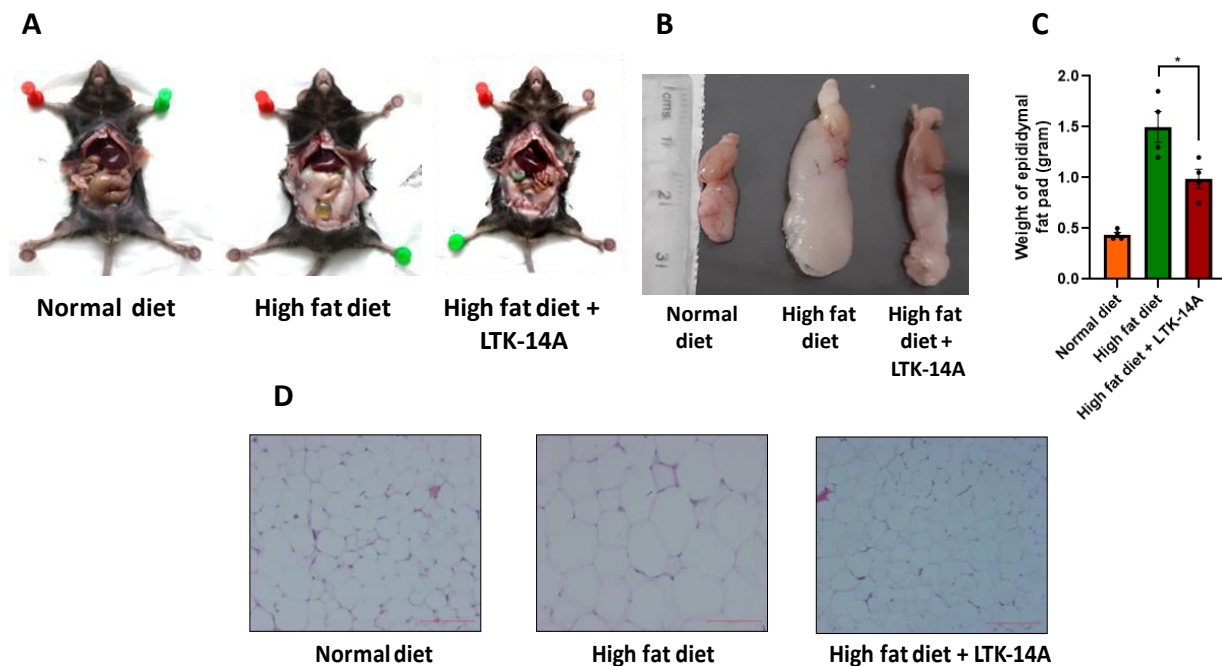


Figure 19: Representative images of dissected bodies showing fat accumulation (A) and epididymal fat pads (B) of the mice from three groups. The average weight of the fat pads is represented graphically (C); n=4 in each group, one-way ANOVA with Dunnett's multiple comparison was performed: * P < 0.05, **P < 0.01, *P < 0.001, ns: not significant. (D) Representative images of morphology of adipose tissue from the mice of the three groups, as studied by hematoxylin and eosin staining.**

In order to verify whether histone butyrylation had any functional relationship with adipogenesis and obesity in mice, the modification pattern in the adipose tissues was studied with acid extracted histones from the epididymal fat pads. H4K5 butyrylation was reduced in the LTK-14A treated samples compared to those of high fat diet fed mice (Figure 20 A, C). H3K14 acetylation levels were relatively unchanged across all the three different groups (Figure 20 A, B).

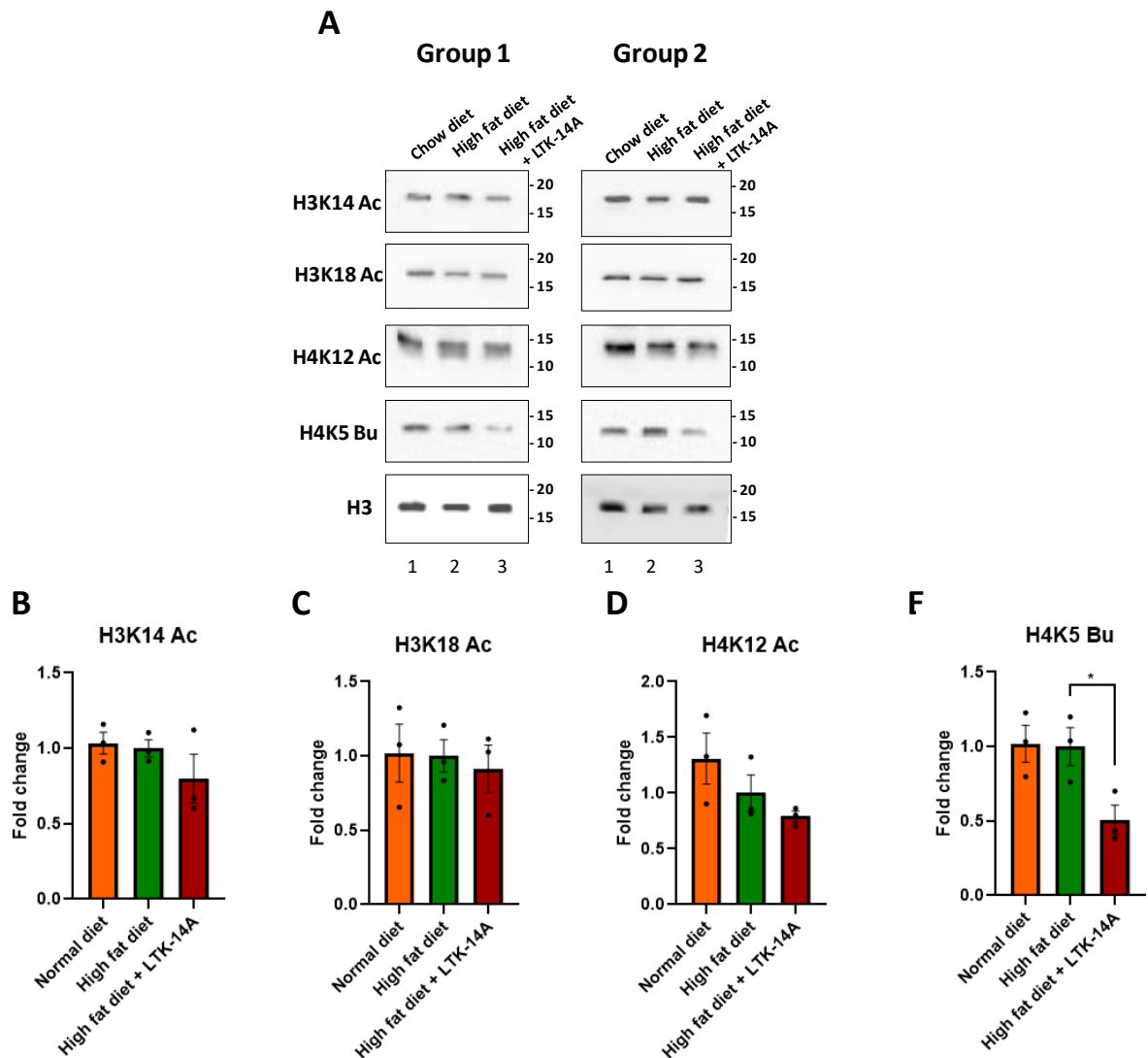
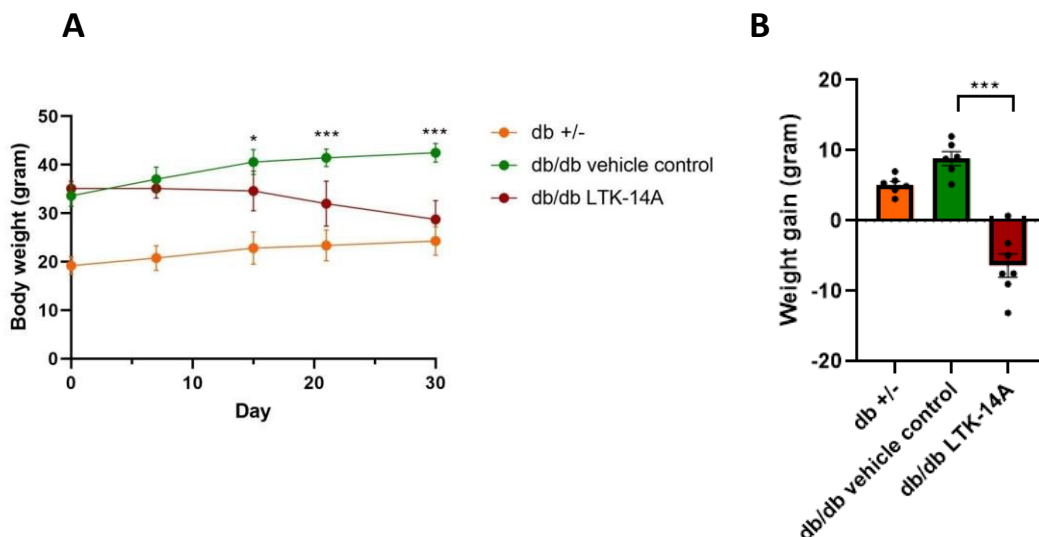


Figure 20: (A) Histone H3K14 acetylation, H3K18 acetylation, H4K12 acetylation and H4K5 butyrylation levels in epididymal fat pads of mice were estimated by immunoblotting. Histone H3 was used as loading control. The fold change of quantified band intensity is graphically represented in (B),(C), (D) and (E); n=3 in each group; one-way ANOVA with Dunnett's multiple comparison: * P < 0.05, **P < 0.01, ***P < 0.001, ns: not significant.

3.2.11 LTK-14A reverses obesity and adipocyte hypertrophy in genetically obese mice by specific inhibition of histone butyrylation without affecting acetylation in adipose tissues

The attenuation of weight gain in C57BL6/J mice had been achieved with LTK-14A being added within the high fat diet from the very initiation point of the experiment. We then proceeded with a different approach to test whether LTK-14A could also prevent weight gain in mice that were already obese. Genetically obese db/db mice were taken as the model system for this purpose. Heterozygous mutants db +/- mice were taken as control for the homozygous mutant db/db mice. These hyperphagic db/db mice were orally administered with LTK-14A daily at the same dosage as before (50 mg/Kg body weight). Since db/b mice were already highly obese before compound administration, oral gavaging of LTK-14A was done for more effectiveness and accurate dosing. We observed that upon oral gavaging of LTK-14A, the overweight mice not only showed an arrest in weight gain, but their body weights were significantly reduced by the end of one month of treatment (Figure 21 A, B). The food intake of LTK-14A treated mice was marginally less than that of the vehicle treated mice while both groups had significantly greater energy intake compared to the db+/- mice (Figure 21C).



C

Average food consumption (per week per mouse)

db +/-	db/db vehicle control	db/db LTK- 14A
25.8 gm (+/-1.04)	37.8 gm (+/- 1.64)	34.5 gm (+/- 0.64)

Figure 21: Trend of weight gaining (A) and average body weight gained after 30 days (B) of db +/- and db/db mice orally administered with either LTK-14A or vehicle solution ; n=6 to 7 in each group, one-way ANOVA with Dunnett's multiple comparison: * P < 0.05, **P < 0.01, ***P < 0.001, ns: not significant. The comparative diet consumption pattern of the three groups of mice has been shown in tabulated form (C).

Dissection of the mice revealed much greater accumulation of fat in the vehicle control treated db/db mice compared to the other two groups (Figure 22 A). Average weight of the epididymal fat pads was the highest for db/db mice given vehicle control and least for the db+/- mice, while that for the compound treated db/db mice was intermediate (Figure 22 B, C). *In vivo* Echo MRI of live mice revealed that total adiposity i.e. fat mass of the mice was significantly lowered upon LTK-14A treatment while lean mass was marginally affected (Figure 22 D). The negligible reduction in lean mass (Figure 22 E) could be due to the slightly lower feed intake of the compound treated mice that led to the lowering of both fat mass and muscle mass. However, LTK-14A treatment showed much more significant effect on lipid accumulation i.e. fat mass compared to muscle mass development. Moreover, hematoxylin and eosin staining of the epididymal fat pads showed greatest degree of adipocyte hypertrophy for the vehicle treated db/db mice, followed by compound treated db/db mice and db+/- mice in decreasing order (Figure 22 F)

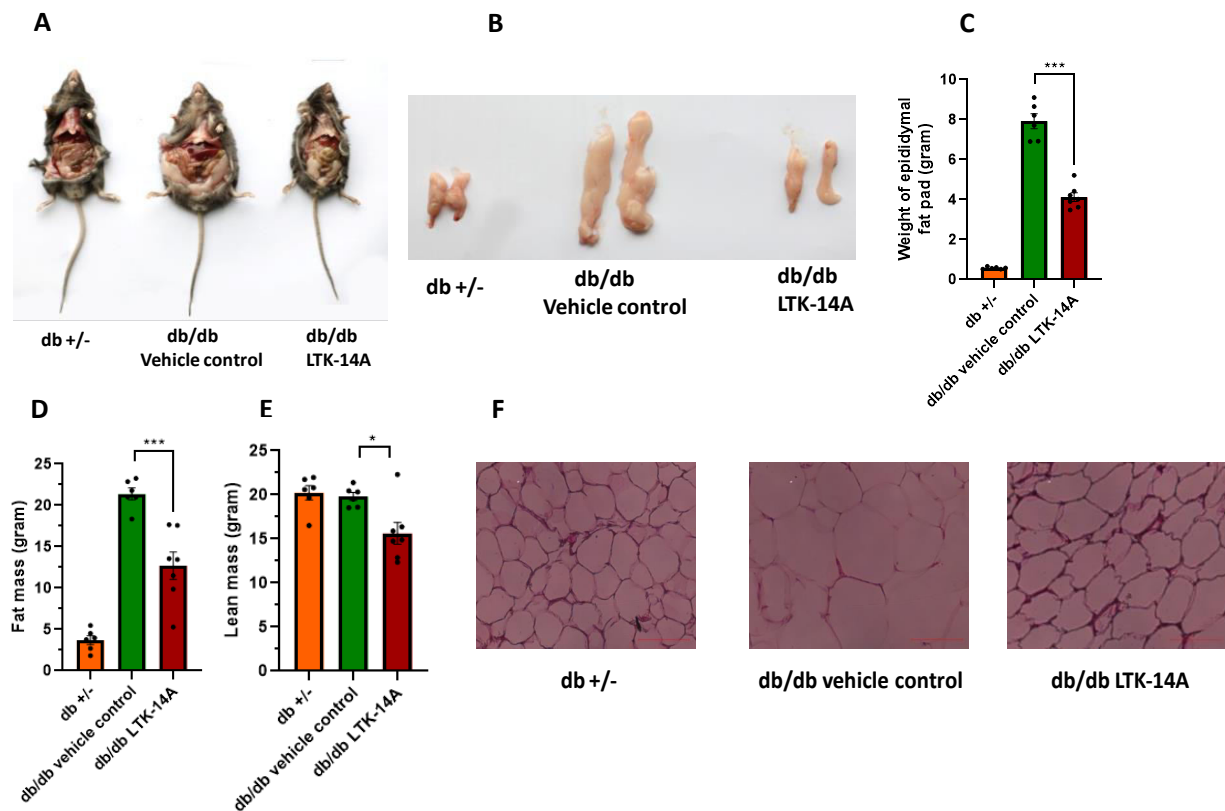


Figure 22: (A) Representative images of dissected bodies showing fat accumulation of the mice from three groups. Representative images of epididymal fat pads (B) from the mice of three groups and average weight of fat pads (C) depicted graphically; $n = 6$ to 7 in each group. Total fat mass (D) and total lean mass (E) of mice from three groups are depicted graphically; $n = 6$ to 7 in each group. (F) Representative images of morphology of adipose tissue from the mice of the three groups, as studied by hematoxylin and eosin staining. For all data one-way ANOVA with Dunnett's multiple comparison was performed: * $P < 0.05$, ** $P < 0.01$, *** $P < 0.001$, ns: not significant.

Immunoblotting with acid extracted histones from epididymal fat pads showed that H4K5 butyrylation was reduced in the adipose tissues of LTK-14A treated mice compared to vehicle control treated obese mice (Figure 23 A, C). H3K14 acetylation was not significantly altered in any of the three groups (Figure 23 A, B).

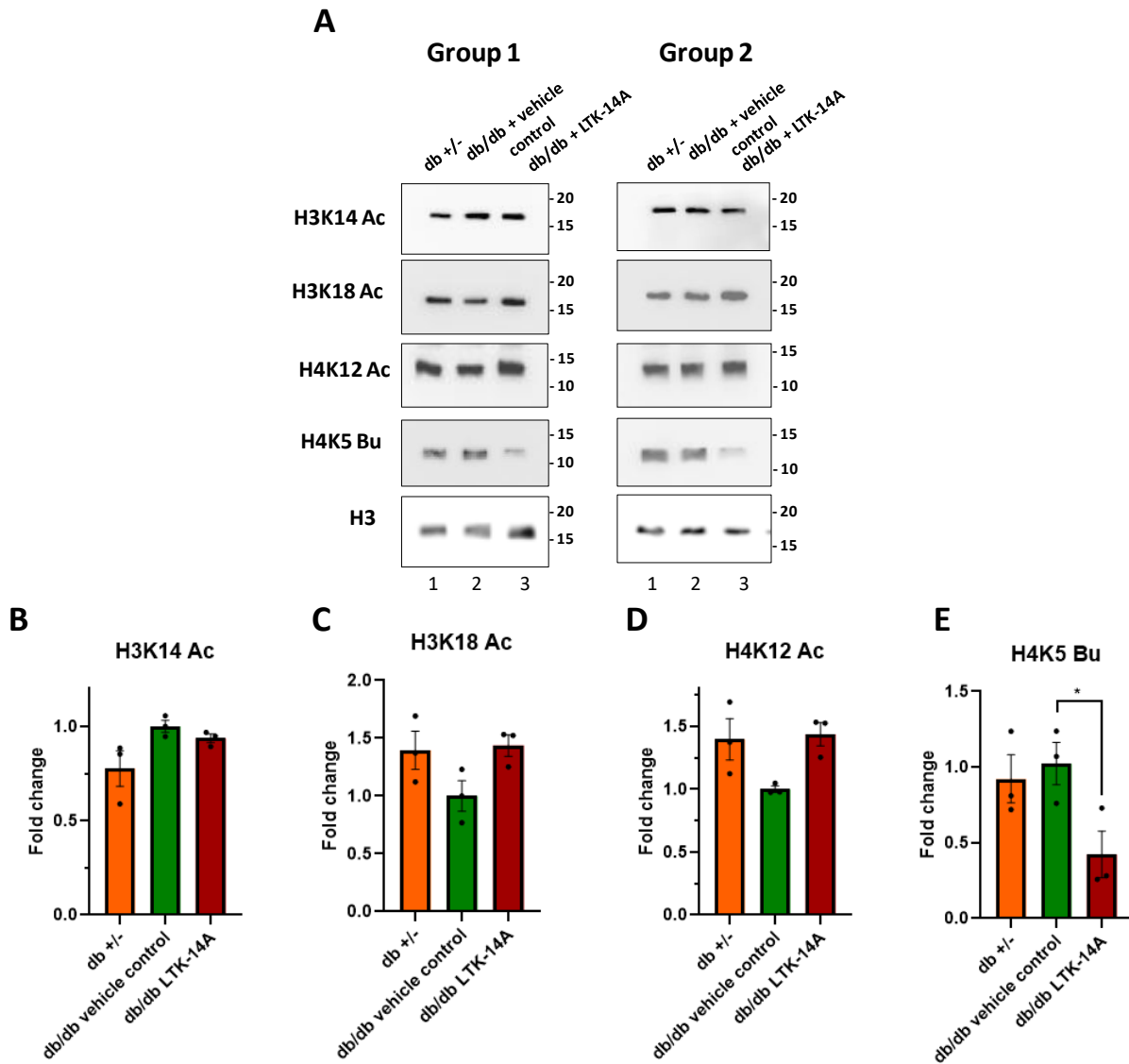


Figure 23: (A) Histone H3K14 acetylation, H3K18 acetylation, H3K14 acetylation and H4K5 butyrylation levels in epididymal fat pads of mice were estimated by immunoblotting. Histone H3 was used as loading control. The fold change of quantified band intensity is graphically represented in (B), (C), (D) and (E); $n=3$ in each group; one-way ANOVA with Dunnett's multiple comparison: * $P < 0.05$, ** $P < 0.01$, *** $P < 0.001$, ns: not significant.

Collectively these data establish that obesity can not only be prevented but also reverted by specific inhibition of H4K5 butyrylation, thereby highlighting the importance of this modification in the context of adipogenesis.

3.2.12 LTK-14A prevents adipocyte hypertrophy by repression of lipogenic genes and not by browning of fat

Previously, gene expression analysis was performed in cultured 3T3L1 adipocytes to investigate the effect of LTK-14A on expression pattern of pro-adipogenic genes. While it indicated that LTK-14A predominantly inhibited the expression of important transcription factors of adipogenesis as well as adipocyte markers, its effect in the organismal context was yet to be explored. Therefore, RNA was isolated from the epididymal fat pads of db +/-, db/db vehicle treated and db/db LTK-14A treated mice for transcriptome analysis. It was observed, that there was a marked upregulation in the expression of the master regulator of adipogenesis *Pparg* along with adipocyte markers *Lep*, *Slc2a4* and *Adipoq* in the fat pads of obese db/db mice compared to the lean db +/- mice. On the other hand, these genes had a very low expression in the adipose tissues of LTK-14A treated db/db mice. Thus, in both cell line and animal models of adipogenesis LTK-14A prevented lipid accumulation by repression of pro-adipogenic genes (Figure 24 A).

Unlike cell line models, the animal models of obesity are more complicated as the process of obesity manifestation not only involves the adipose tissue but also organ to organ cross-talk. Moreover, in the organismal context there are various mechanisms by which a compound serving as a small molecule modulator could bring about its effects for attenuation of obesity. One of these effects, in addition to inhibition of pro-adipogenic genes, is a phenomenon called induction of browning of fat. White adipocytes can undergo morphological changes to form a different type of adipocytes having features intermediate between white and brown fat. These adipocytes are characterized by high expression of the mitochondrial protein UCP1 (Uncoupling Protein 1) and are sometimes referred to as beige adipocytes. A number of brown adipocyte specific genes were selected for checking their expression pattern upon LTK-14A treatment. These genes included *Prdm16* (a critical transcription factor required for inducing transcription of brown fat specific genes) (Seale *et al*, 2008), *Cebpb* (binding partner for PRDM16 in transcription induction) (Kajimura *et al*, 2009), *Ppargc1a* (displaces

the corepressor CtBP from PRDM16 for the later to carry out its function) (Kajimura *et al*, 2008) and *Ppara* (maintains the expression of *Ucp1* in mature brown adipocytes) (Bargut *et al*, 2017). Moreover, analysis was also done for the expression pattern of factors whose downregulation promotes browning of fat. These genes were *Nrip1* (nucleates a repressive complex of HDAC1, HDAC3, G9a and Dnmt1 to the promoter of *Ucp1*) (Kiskinis *et al*, 2007) and *Foxp1* (represses *ADRB3* expression which encodes the β adrenergic receptor required for adaptive thermogenesis upon cold exposure) (Liu *et al*, 2019). Finally, the expression pattern of the highly expressed brown adipocyte markers *Ucp1* and *Cox5a* was also investigated. It was observed that some of the genes required for browning of fat were selectively induced while others were unaffected upon LTK-14A treatment (Figure 24 B, C). While there was no significant change in the expression pattern of *Cebpb* and *Ppara*, there was indeed a significant upregulation in the expression of *Prdm16* and *Ppargc1a*. Furthermore, *Nrip1* was downregulated while *Foxp1* expression was unaltered. Most importantly, there was no increased expression of *Ucp1* and *Cox5a* in the LTK-14A treated adipose tissue, implying that browning of fat did not occur in the adipose tissues upon LTK-14A treatment. Even though certain brown adipogenesis related genes were not upregulated by LTK-14A, the enhanced expression of *Prdm16*, the most critical transcription factor for inducing expression of genes involved in brown adipogenesis programme, should had promoted the development of beige fat. Yet, the unchanged expression of brown fat markers *Ucp1* and *Cox5a* indicate that the upregulation of *Prdm16* was not enough for inducing browning of fat. A possible explanation for this could be the fact in the same LTK-14A treated tissue samples, *Pparg* was also significantly downregulated. PPAR γ is the master regulator which is essential for recruiting PRDM16 to its cognate promoters for inducing expression of brown fat related genes (Qiang *et al*, 2012). Despite the increased levels of *Prdm16*, brown adipogenesis programme could not be induced due to the decreased expression of *Pparg*. Hence, it could be said that LTK-14A attenuates obesity by primarily repressing lipogenic gene expression and does not

induce brown fat formation; and mechanistically this is achieved mainly by downregulation of the master regulator *Pparg*.

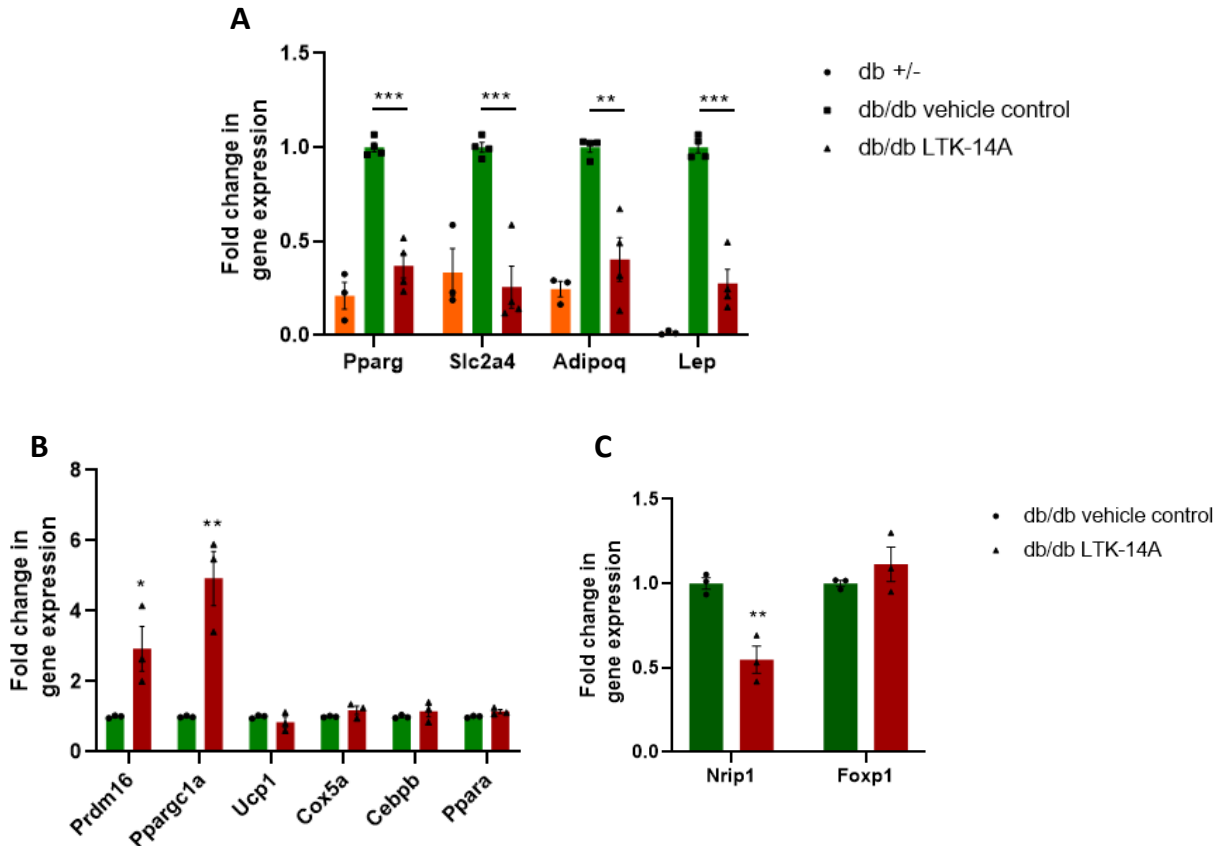


Figure 24: (A) qRT-PCR with RNA isolated from epididymal fat pads of genetically obese mouse model to check the expression pattern of lipogenesis related pro-adipogenic genes upon LTK-14A treatment; n=3/4 in each group; one-way ANOVA with Dunnett's multiple comparison: * P < 0.05, **P < 0.01, ***P < 0.001, ns: not significant. qRT-PCR was also performed to check the expression pattern of genes that promote (B) or repress browning of fat; n=3 in each group, two-tailed unpaired Student's t-test: * P < 0.05, **P < 0.01, ***P < 0.001, ns: not significant.

TABLES

Table 1 – List of pro-adipogenic factors that were curated for checking their expression pattern under the effect of LTK-14A

Gene	Reference	Gene	Reference	Gene	Reference
Aamdc	J:265628	Frzb	J:78619	Sh3pxd2b	J:235640
Acsl1	PMID:24269233	Gdf39	J:239199	Slc2a4	PMID:28916720
Acss2	PMID:28003429	Hic12	PMID:28546992	Snai2	J:130039
Adig	J:83859	Hoxa5	PMID:29439250	Spry4	PMID:25790378
Adipoq	PMID:15834118	Hr	PMID:22964757	Stk3	J:184223
Akt1	J:164563	Htr2a3	J:182833	Stk4	J:184223
Ankra	PMID:23949615	Htr2c	J:182833	Sult1e1	J:164563
Asxl2	J:164563	Id1	PMID:28270523	Syap1	J:255333
Atoh8	PMID:25163748	Id2	J:138276	Tbx2	PMID:24516689
Bmp2	J:91833	Igf16	J:155856	Tecr	PMID:12482854
Carm1	J:168191	Itpk1	PMID:11909533	Tle3	PMID:21459326
Ccdc3	J:220560	Klf15	PMID:15664998	Tle6	PMID:23555558
Cebpa	J:125420	Klf5	J:182833	Tmem64	J:221949
Cebpb	J:148702	Lmo3	J:199236	Tph1	J:182833
Cebpd	PMID:19233245	Lpl	J:164563	Trpm4	J:155856
Cers4	PMID:23530041	Lrp5	J:164563	Uchl3	J:158204
Cmklr1	J:125389	Lypla1	PMID:22399288	Wdfy2	J:225490
Creb1	J:180535	Maf	PMID:23229156	Wif1	J:78619
Crebl2	J:180535	Med14	PMID:20194623	Wnt5b	J:97443
Dact1	J:146933	Medag	J:188082	Wt1	PMID:26257994
Dgat1	PMID:9756920	Mxd3	PMID:24254064	Xbp1	J:198494
Dkk1	J:78619	Noct	J:161288	Zbtb16	J:164563
Elf4	PMID:22307523	Nr1h3	PMID:15060163	Zbtb7c	J:184939
Epas1	PMID:15258146	Pbx1	PMID:21922607	Zc3h12a	J:228414
Esr1	PMID:29196658	Pnpla2	PMID:15550674	Zfp36	J:233569
Esrra	PMID:17512501	Pparg	J:167907	Zfp36l1	J:233569
Ets2	PMID:21989915	Ppargc1b	PMID:24049736	Zfp385a	J:136258
Fabp4	PMID:23047894	Rarres2	2 J:125389	Zfp423	PMID:27238639
Fads2	PMID:9867867	Rb1	PMID:23315497	Zfp69	PMID:19578398
Far2	PMID:15220348	Sav1	J:184223		
Fasn	PMID:7567999	Scd1	PMID:12177411		
Fndc	J:94268	Scd2	PMID:16443825		
Fosl1	PMID:28747725	Sfrp1	J:78619		
Fosl2	PMID:22326952	Sfrp2	J:78619		

Table 2 – List of curated pro-adipogenic factors that were downregulated by LTK-14A

Gene	Fold Change LTK-14A vs No Inhibitor	Fold Change LTK-14A vs DMSO	Gene	Fold Change LTK-14A vs No Inhibitor	Fold Change LTK-14A vs DMSO
Adig	-44.07924552	39.5013483	Acss2	2.932285581	2.296786919
Esr1	-28.3040834	-22.845503	Id2	2.808199913	7.235019785
Slc2a4	26.61502535	24.7401678	Esrra	2.765565624	2.258865273
Scd1	24.33143107	22.9995046	Fads2	2.642474922	2.376192775
Adipoq	-19.1222549	18.6192333	Dgat1	2.609323417	-2.53556226
Cebpa	18.69657309	14.0306643	Aamdc	2.509190104	1.963307824
Klf15	14.42249043	13.4748839	Cers4	2.507992418	1.929948398
Fasn	11.23366607	9.08087688	Tle3	2.254334931	1.864610622
Spry4	10.05519276	7.77070921	Zfp69	2.191487737	1.685032634
Nr1h3	8.853427111	7.79580024	Atoh8	2.164757135	2.375094068
Fabp4	6.413318485	6.73289277	Hr	2.108480011	1.627569899
Scd2	6.209651835	5.44208554	Hic1	1.955299193	1.694416755
Ppargc1b	5.632303232	-4.251853	Zc3h12a	-1.84802901	1.674901672
Pnpla2	5.433561195	-5.4583894	Lypla1	1.804525996	2.157247024
Mxd3	3.676677433	3.46761505	Tbx2	1.754108858	1.515771526
Pparg	3.232215435	3.36220561	Hoxa5	1.730900563	1.687554804
Id1	3.118198389	2.54384533	Tecr	1.678655232	-1.53451369
Epas1	3.114669593	2.86259045	Lpl	-1.66952705	1.726717099
Fosl1	3.084361284	2.03216351	Zfp423	1.631814888	1.656391264
Rarres2	2.971486582	-2.8421224	Rb1	1.578192999	-1.63095676

Table 3 - List of anti-adipogenic factors that were curated for checking their expression pattern under the effect of LTK-14A

Gene	Reference	Gene	Reference	Gene	Reference
Ahr	PMID:9788873	Id4	J:162236	Sod2	J:102322
Ankrd26	J:243390	Ing1	PMID:28992291	Sort1	J:216244
Arntl	J:187450	Insig1	J:84786	Stat1	PMID:23735217
Asxl1	J:183204	Irx2	PMID:23150689	Tcf7l2	J:125420
Atf3	PMID:22475484	Jag1	J:89916	Tead4	PMID:30209132
Axin1	J:125420	Jdp2	J:139241	Tgfb1	J:164563
Bbs12	J:189019	Kdm4c	PMID:21637537	Tgfb1i1	J:95883
C1ql4	J:203503	Klf10	PMID:30026232	Tnf	J:155856
Cand2	PMID:29717274	Lrp6	J:127355	Trib2	J:124706
Ccdc85b	J:98010	Mir448	J:182833	Trib3	J:124706
Ccn4	J:273517	Mmp11	J:142976	Trio	J:243390
Ddit3	J:204800	Msx2	J:91833	Vegfa	J:191431
Dlk1	J:21435	Ncor2	J:142665	Vgll3	PMID:23152581
E2f1	J:72330	Nod1	PMID:23712977	Wnt1	J:125420
Egr1	PMID:19229250	Nr4a1	PMID:30044048	Wnt10b	J:125420
Enpp1	J:265628	Nucb2	J:155856	Wnt3a	J:97443
Fam57b	J:197105	Rora	J:148702	Wnt5a	J:164563
Fhl3	PMID:12556451	Runx1	PMID:30391794	Wwtr1	J:100164
Foxc2	PMID:15277530	Runx1t1	J:229306	Zadh2	J:200769
Foxo1	J:129943	Sertad2	PMID:29654510	Zfp36l2	J:233569
Gata2	J:100710	Sirt1	J:91106	Zfpm1	J:172935
Gata3	J:164563	Sirt2	J:129943	Zfpm2	J:172935
Gper1	J:201910	Smad3	J:164563		

Table 4 - List of curated anti-adipogenic factors that were upregulated by LTK-14A

Gene	Fold Change LTK-14A vs No Inhibitor	Fold Change LTK-14A vs DMSO
Mmp11	4.96535	5.288891
Ahr	3.191657	3.437679
Tead4	3.040762	2.46436
Runx1	2.516034	2.087697
Trib2	2.326059	1.928203
Vgll3	2.190575	1.685392
Ddit3	2.117421	2.786076
Foxc2	1.903257	2.711413
Cand2	1.880214	1.984744
Kdm4c	1.8494	1.583173
Enpp1	1.808645	2.95298
Sertad2	1.724761	1.695539
Smad4	1.679714	1.694661
Rora	1.663496	1.555649
Irx2	1.61498	1.577194
Zfpm1	1.613167	2.121497
Atf3	1.594914	2.311616
Ing1	1.541016	1.686796
Dlk1	1.507563	1.751258

p300 mediated histone butyrylation is critical for hepatic steatosis

**p300 mediated histone butyrylation is critical
for hepatic steatosis**

p300 mediated histone butyrylation is critical for hepatic steatosis

The following chapter starts with an introduction on non-alcoholic fatty liver disease along with the epigenetic mechanisms involved in the process of liver steatosis and inflammation, with special emphasis given on the role of p300. It then presents results on the application of a small molecule modulator of p300 acyltransferase activity in attenuation of hepatic steatosis in different cell line and animal models.

1.2 Background

1.2.1 Non-alcoholic fatty liver disease

1.2.2 Pathways leading to fatty liver disease manifestation

1.2.2.1 Increased release of fatty acids into liver from direct excessive food consumption and from adipose tissue stores

1.2.2.2 Increased de novo synthesis of fatty acids and triacylglycerides

1.2.2.3 Impaired export of lipids

1.2.2.4 Impaired β oxidation of fatty acids

1.2.2.5 Oxidative stress and inflammatory response

1.2.3 Epigenetic regulation of NAFLD

1.2.3.1 Lysine methylation and demethylation in hepatic steatosis

1.2.3.2 Lysine acetylation in hepatic steatosis

1.2.3.3 Lysine deacetylation in hepatic steatosis

4.2 Results

4.2.1 Histone butyrylation increases with hepatic steatosis in HepG2

4.2.2 LTK-14A inhibits glucose induced steatosis in HepG2 cells without having any toxic effect

4.2.3 LTK-14A inhibits steatosis of HepG2 by repressing the expression of lipogenic genes

4.2.4 LTK-14A represses gene expression by specific inhibition of histone butyrylation without affecting acetylation in HepG2

4.2.5 LTK-14A prevents hepatic steatosis in mice fed with high fat diet by specific inhibition of histone butyrylation without affecting acetylation in liver

4.2.6 LTK-14A prevents hepatic steatosis in genetically obese mice by specific inhibition of histone butyrylation without affecting acetylation in liver

4.2.7 LTK-14A is metabolically stable and is bio-available in its intact form in liver

4.2.8 Application of LTK-14A for prevention of liver fibrosis

4.1 Background

4.1.1 Non-alcoholic fatty liver disease

Non-alcoholic fatty liver disease (NAFLD) is a clinico-pathological disease of the liver defined as excessive lipid deposition in liver cells without alcohol consumption. It is the most prominent form of chronic liver disease plaguing large parts of the world and is considered to be one of the major factors contributing to hepatocellular carcinoma and end stage liver disease that requires liver transplantation. NAFLD involves a spectrum of disorders starting with simple steatosis i.e. lipid accumulation in liver, followed by steatohepatitis, fibrosis, cirrhosis and ultimately culminating in carcinoma. Non-alcoholic steatohepatitis (NASH) is characterized by not only steatosis, but it also carries symptoms of hepatocellular ballooning and high degree of inflammation with a centrilobular distribution (Kleiner *et al*, 2016). These pathophysiological conditions are reversible till the stage of fibrosis, but once advanced stages of fibrosis set in leading to cirrhosis, the condition becomes almost irreversible and requires consideration for liver transplant (Figure 1). NAFLD has often been found to occur along with obesity (excessive adiposity, high intake of energy rich foods such as fructose added drinks and very little physical activity), dyslipidemia, insulin resistance and type 2 diabetes (Chalasani *et al*, 2018).

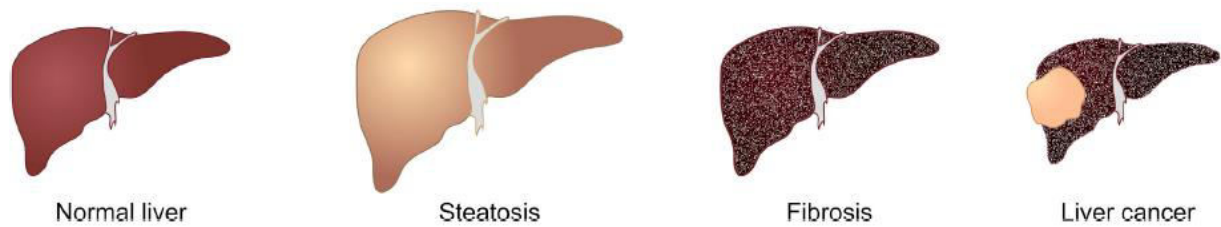


Figure 1: Diagrammatic depiction of different stages of non-alcoholic fatty liver disease (Adapted from Romeo *et al*, Cell Metab, 2020)

NAFLD could be caused by various genetic and environmental factors. These are not mutually exclusive and their co-occurrence could further aggravate liver conditions. There are a few observations indicating that inherited factors do contribute to NAFLD (Eslam *et al*, 2018). Twin studies have shown that 25-50% of hepatic fat variability could be due to heritable factors (Loomba *et al*, 2015). Moreover, there exists interethnic variability for susceptibility to this disease with high occurrence in Hispanic races, intermediate occurrence in European Caucasians and lowest incidences in African populations (Guerrerio *et al*, 2012). It has also been observed in many cases that the offsprings of parents with fatty liver disease generally also develop similar complications (Long *et al*, 2019). In fact a genome wide association study had revealed a particular variant I148M mutant of PNPLA3 is highly associated with NAFLD (Eslam *et al*, 2018) and accounted for the pre-disposition of specific ethnic communities to the disease (Romeo *et al*, 2010). However, these genetic factors have been found to co-occur with environmental insults to health as well, making it difficult to delineate the exact contribution of genetics to NAFLD.

A “two hit hypothesis” had been first proposed to describe the stages of NAFLD pathogenesis (Day *et al*, 1998). The first “hit” is steatosis which involves lipid accumulation in liver cells and insulin resistance, sensitizing the liver to the second “hit” involving high inflammation and necrosis of cells due to oxidative stress and lipid peroxidation. This hypothesis has been further revised to a “multi

hit hypothesis” which takes into account the combination of genetic and environmental factors leading to NAFLD manifestation (Day *et al*, 2002).

4.1.2 Pathways leading to fatty liver disease manifestation

The liver plays a principal role in metabolism of lipids and carbohydrates within the body. Steatosis, the first “hit” for NAFLD, begins happening inside the liver when the lipid biosynthesis or import exceeds lipid catabolism or export (Bradbury *et al*, 2004). There are four ways by which this can occur- excessive nutrient intake, excessive synthesis of free fatty acids and triglycerides, impaired lipid export and impaired lipid degradation (Figure 2).

4.1.2.1 Increased release of fatty acids into liver from direct excessive food consumption and from adipose tissue stores

Hepatic steatosis has often been correlated with cases of obesity characterized by high adiposity in the omental and mesenteric regions of the body. With increasing load of lipids within the hypertrophied adipocytes in obese individuals, some of the lipids are released into the portal circulation as long chain free fatty acids upon the action of hormone sensitive lipase (HSL). Moreover, the adipose tissue is a highly bioactive organ that releases several important regulators of carbohydrate metabolism (leptin, adiponectin, resistin), lipid metabolism (apolipoprotein E, lipoprotein lipase) and inflammatory cytokines or adipokines (TNF α , IL-6, TGF β) (Brunt *et al*, 2004). The secretion of TNF α from adipocytes gets markedly increased in obesity. This cytokine acts in a paracrine as well as autocrine fashion on itself to activate I κ B kinase β (I κ k β) and inhibits phosphorylation of insulin receptor substrates 1 and 2 (IRS-1 and IRS-2). This disrupts the insulin signaling pathway that is required for keeping the activity of HSL in check (Day *et al*, 2002; Shoelson *et al*, 2003). Therefore, with no attenuation of HSL activity, even more free fatty acids are released that end up accumulating inside the liver. Moreover, TNF α released by the adipocytes upregulate the expression of fatty acid translocase in the liver which promotes further uptake of liver, thereby contributing to steatosis (Memon *et al*, 1998).

4.1.2.2 Increased *de novo* synthesis of fatty acids and triacylglycerides

The increased levels of glucose and insulin in blood after a carbohydrate rich meal can promote *de novo* lipid biosynthesis in the liver via ChREBP and SREBP1-c (Dentin *et al*, 2005). Both are membrane bound transcription factors that are sensitive to blood glucose and insulin levels that bind to their cognate promoters and induce transcription of various lipogenic genes. Elevated insulin levels also promote GLUT4 dependant uptake of glucose by adipocytes, increased lipogenesis and decreased lipolysis. Interestingly, in obese conditions the GLUT4 activity is lower which leads to postprandial hyperglycemia that causes more insulin release from the pancreas (Carvalho *et al*, 2001). This, along with increased secretion of TNF α by the adipose tissue leads to insulin resistance and drives further long chain fatty acid synthesis in the liver from acetyl CoA. The first step in triacylglycerol synthesis by glycerol phosphate acyl transferase is non rate limiting, as a result of which a slight build up in fatty acid levels inside the liver leads to immediate conversion to triglycerides, further compounding the steatosis conditions (Bradbury *et al*, 2004).

4.1.2.3 Impaired export of lipids

Hepatic clearance of fatty acids takes place by their esterification to form triglycerides and their export in the form of very low density lipoprotein (VLDL). The transfer of lipid to apolipoprotein E by microsomal triglyceride transfer protein (MTT) in endoplasmic reticulum is the rate limiting step in VLDL synthesis. Autosomal recessive mutation in the gene encoding this enzyme has been observed in cases leading to abetalipoproteinemia and severe steatosis (Berriot-Varoqueaux *et al*, 2000).

4.1.2.4 Impaired β oxidation of fatty acids

The mitochondria, peroxisomes and endoplasmic reticulum are the three sites of fatty acid oxidation with the mitochondria playing the main role (Reddy *et al*, 2001). Any disruption in the steps of fatty acid oxidation in mitochondria would lead to an overload of fatty acids and the catabolism responsibility is then taken up by the other organelles. The enzyme carnitine palmitoyl transferase 1 (CPT1) is

involved in the esterification and import of fatty acids into the mitochondrial matrix. This particular step is the rate limiting step in fatty acid oxidation and the enzyme is inhibited by malonyl CoA, the first product of fatty acid synthesis (Mcgarry *et al*, 2002). Once inside the mitochondria, the fatty acids go through a sequence of four reactions for degradation. The final three of these steps are catalysed by the multisubunit complex of mitochondrial trifunctional protein which is an octamer four α subunits and four β subunits. Autosomal recessive mutation in the gene encoding this enzyme has been implicated in steatotic Reye like syndrome, cardiomyopathy and even sudden death (Ibdah *et al*, 2001; Ibdah *et al*, 2005). Such mutation in the foetus can lead to HELLP (hemolysis, elevated liver enzymes, low platelet count) syndrome and fatty liver pregnancy.

4.1.2.5 Oxidative stress and inflammatory response

The above stated four mechanisms contribute the first “hit” required for sensitizing the liver to steatotic conditions. The progression of steatosis to steatohepatitis happens by the second “hit” which involves hepatocellular injury and cell death due to high degree of oxidative stress and inflammation. The principal site of fatty acid catabolism within the liver cells is the mitochondria, in which β oxidation of fatty acids takes place (Reddy *et al*, 2001). Within the mitochondria, most of the electrons that are generated through β oxidation are safely released via the electron transport chain. But during hyperactivity of the mitochondria, some of these electrons may react to produce singlet oxygen molecules, superoxide anions, hydrogen peroxide and hydroxyl radicals. The enzymes involved in mitochondrial β oxidation are regulated by PPAR α (peroxisome proliferator activated receptor α), a ligand inducible transmembrane transcription factor. However, PPAR α preferentially stimulates fatty acid oxidation in peroxisomes and endoplasmic reticulum (Reddy *et al*, 2001). In fact, when mitochondria are overloaded with fatty acids, the other two organelles take over as the major sites of fatty acid degradation. The pathway of β oxidation of fatty acids in peroxisomes is not connected to the electron transport chain and hence generates hydrogen peroxide as a byproduct. Moreover, the endoplasmic reticulum generates dicarboxylic acid and other reactive oxygen species (ROS) by cytochrome P450 enzyme -4A and -2E1 catalyzed ω oxidation of fatty acids. When

the ROS production inside the hepatocytes exceeds the antioxidative capacity of the cells, severe damage occurs in the nuclear and mitochondrial DNA along with phospholipid disruption by free radicals and secretion of pro-inflammatory cytokines such as TNF α (Pessayre *et al*, 2002; Browning *et al*, 2004). The stress is further compounded due to the impairment of electron transport chain caused by mitochondrial damage and loss of cytochrome c, resulting in more ROS production (McClain *et al*, 2004). Lipid peroxidation of polyunsaturated fatty acids produces several toxic aldehyde products such as malondialdehyde and hydroxynonemal. These products are far more persistent than ROS and cause greater damage to more cell organelles that can lead to necrosis of cells. They can also activate the stellate cells of liver, leading to fibrosis. They can further strengthen the pro-inflammatory response by serving as chemotactic agent for neutrophils, recruiting more immune cells in the process (George *et al*, 2003). ROS could also induce Fas ligand expression in hepatocytes, triggering apoptotic cell death (Pessayre *et al*, 2002).

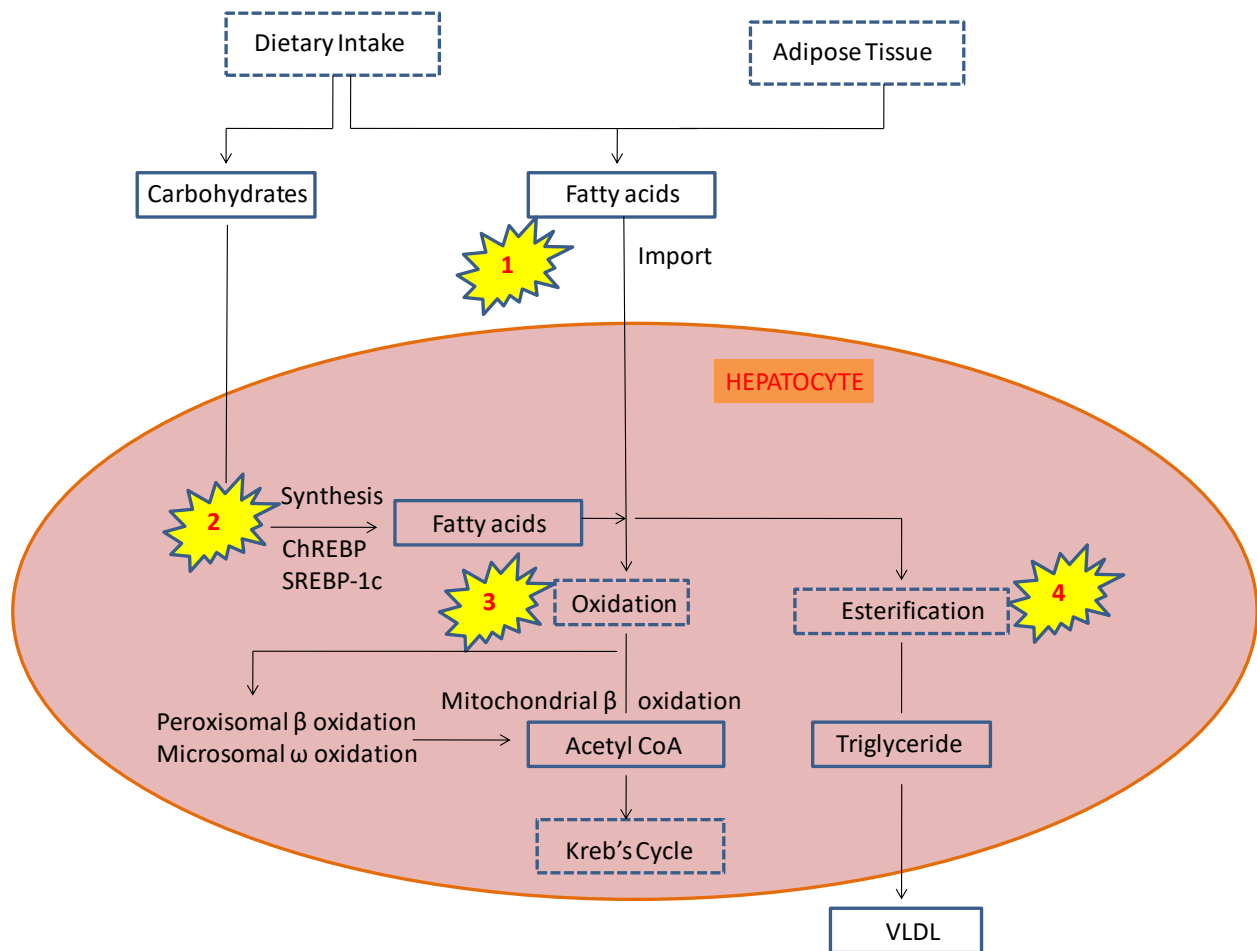


Figure 2: Different pathways by which lipid accumulation occurs in the liver. The critical steps affected during steatosis are numbered as (1), (2), (3) and (4). (Source- Adapted from Anstee *et al*, Int J Exp Path, 2006)

4.1.3 Epigenetic regulation of NAFLD

At the core of pathogenesis of fatty liver disease lies the epigenetic regulation of lipogenic gene expression. There are three groups of histone modifiers that have been found to play important regulatory roles in hepatic steatosis not only by modifying histones with different chemical groups, but also by interacting with and recruiting important transcription factors to their target promoters.

4.1.3.1 Lysine methylation and demethylation in hepatic steatosis

The methylation mark H3K4 trimethylation is associated with transcription activation. Mixed-lineage leukemia protein 3/4 (MLL3/4) is an H3K4 methyltransferase that associates with the transcription factor LXR with the help of the adaptor protein activating signal co-integrator 2 (ASC2) and deposits activation marks in the promoters of important lipogenic genes such as FASN and SREBP1-c (Lee, S. *et al*, 2008). Genetic ablation of the enzyme leads to downregulation of these target genes, while activation of the enzyme with its agonist T1317 promotes their expression (Lee *et al*, 2008).

Another methylation modification H3K9 dimethylation is a repressive mark that is involved in the downregulation of several lipogenic genes. Hence lysine demethylases play the role of promoting lipogenesis by removing the repressive mark at H3K9 position. Amongst them the Jmj domain containing demethylases have been found to play the most prominent role. These enzymes use α -ketoglutarate as a cofactor which itself is a metabolic product generated by oxidation of isocitrate and also from glutamine through the intermediate glutamate. JMJD1C, a member of the KDM3 family of Jmj domain containing demethylases, associates with the transcription factor USF1 in the promoters of many lipogenesis related genes like FASN (Fatty acid synthase), ACL (ATP citrate lyase), ACC (Acetyl CoA carboxylase) and SREBP1-c (Sterol regulatory element binding protein 1c) (Khamzina *et al*, 2005). Moreover, JMJD1C has been found to remove the repressive mark H3K9 dimethylation from various lipogenic promoters upon feeding or insulin stimulation. Another member of the KDM3 family – JHDM2A removes mono- and dimethylation marks at H3K9 position and keeps the chromatin in an open state for transcription (Inagaki *et al*, 2009). In fact, mice in which JHDM2A is deleted become obese within 8 weeks; develop hyperlipidemia and insulin resistance, implying the importance of the enzyme in obesity.

The plant homeodomain finger protein 2 (Phf2) is another demethylase that removes H3K9 dimethylation mark. It also associates with the transcription factor ChREBP and helps in promoting expression of its target genes such as FASN and

SCD-1 (Stearoyl CoA desaturase) (Bricambert et al, 2018). Despite its apparent role in fatty liver disease manifestation, Phf2 overexpressing mice are protected from liver fibrosis. A possible explanation could be that Phf2, by promoting SCD1 expression, increases the levels of monounsaturated fatty acids over saturated fatty acids. Therefore the liver is spared from the effects of oxidative stress and pro-inflammatory response which prevents fibrosis from taking place.

Although there may seem to be redundancy in the functioning of Phf2 and JMJD1C since both are histone demethylases, there may be a specific pattern for their participation in gene expression regulation. Phf2 can only bind chromatin which already has H3K4 trimethylation mark deposited. Hence, before Phf2 can assemble at its target promoters in association with ChREBP, the H3K4 trimethylation is carried out by MLL3/4 after being recruited by LXR. Then again, neither ChREBP nor LXR has been known to bind to repressed chromatin. Therefore, even preceding their assembly, the transcription factor USF1 would have to recruit JMJD1C to remove the H3K9 dimethylation and change the chromatin to a more open state, for the subsequent steps of transcriptional activation to occur.

4.1.3.2 Lysine acetylation in hepatic steatosis

The acetyltransferase p300 plays a very important role in regulating expression of genes for lipid homeostasis by not only acetylating histones but also by helping in recruitment of important transcription factors to their cognate promoters. Two of these factors are SREBP1c and ChREBP (Dentin *et al*, 2005) (Figure 3). SREBP1c is a basic helix-loop-helix –leucine zipper motif containing transcription factor that binds to its target promoters as dimers upon high nutrient stimulation (Horton *et al*, 2002). Acetylation of SREBP1c by p300 stabilizes it under high glucose and insulin conditions (Giandomenico et al, 2003; Ponugoti *et al*, 2010) that enable its recruitment to its gene promoters leading to lipid accumulation (Jang *et al*, 2017).

ChREBP is another transcription factor stimulated by high glucose uptake, that promotes expression of lipogenic genes like ACC (acetyl CoA carboxylase), FASN (Fatty acid synthase), SCD-1 (Stearoyl CoA desaturase) and ACLY (ATP citrate lyase) (Huang *et al*, 2017; Izuka *et al*, 2004). In low glucose conditions, it is

phosphorylated by protein kinase A that prevents it from entering the nucleus (Kabashima *et al*, 2003; Mendez-Lucas *et al*, 2017). In fed state, it gets dephosphorylated that leads to its translocation into the nucleus (Mendez-Lucas *et al*, 2017). Furthermore, acetylation of ChREBP by p300 leads to proper recruitment of the transcription factor to its target promoters (Bricambert *et al*, 2010). During lipogenesis stimulating conditions, p300 acetylates FXR (Farnesoid X receptor) which increases its stability and inhibits its heterodimerization with RXRa (retinoic acid receptor), DNA binding and transactivation activity (Kemper *et al*, 2009). Inactivated FXR induces hyperlipidemia and hyperglycemia by stimulating the expression of SHP (small heterodimer partner). Increased SHP expression decreases levels of PLTP (phospholipid transfer protein) and VLDL (very low density lipoprotein) which are required for efficient clearance of lipids and also increases expression of G6Pa (Glucose 6 phosphatase) and PEPCK (phosphoenol pyruvate carboxykinase, both of which are enzymes for gluconeogenesis that increase glucose production from non-carbohydrate sources (Fang *et al*, 2008). Another acetyltransferase PCAF has been found to acetylate USF1 to help in its recruitment to lipogenic gene promoters and induce steatosis.

The onset of hepatic steatosis is not only affected by the rate of lipid synthesis but also by the rate of lipid clearance by export or β oxidation. MTP (microsomal triglyceride transfer protein) is a crucial factor that helps in the assembly and secretion of lipoproteins from the liver (Hussain *et al*, 2011). Its expression is regulated by hepatocyte nuclear factor 4 (HNF4) which binds with increased affinity to the MTP promoter upon high nutrient intake. It has been observed that p300 can interact with an RNA helicase DDX3 which in turn also interacts with HNF4 (Hadzopoulou-Cladaras *et al*, 1997; Hayhurst *et al*, 2001; Soutoglou *et al*, 2000; Yang *et al*, 2009). This leads to acetylation of HNF4 which enhances its binding to the promoter of MTP gene, leading to greater expression of MTP and increased lipid export.

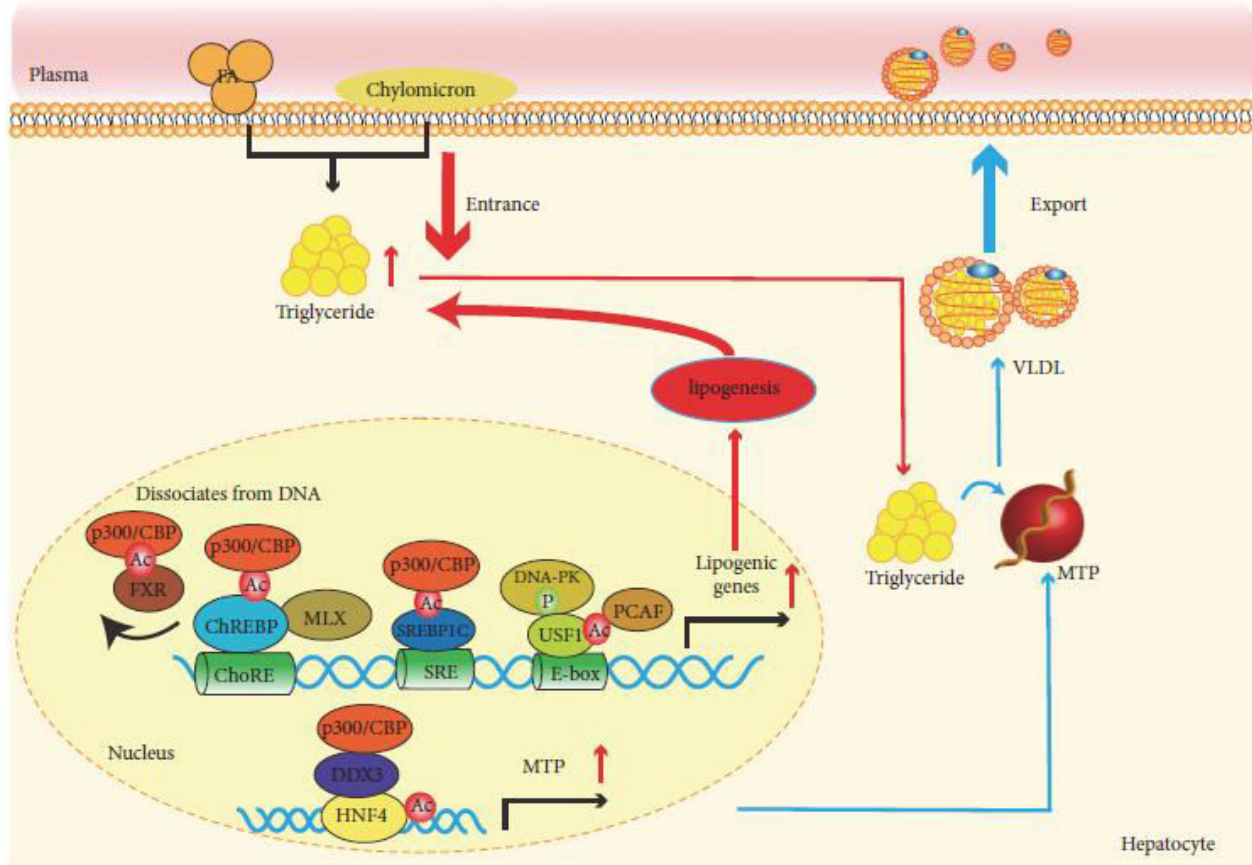


Figure 3: A summarized diagram depicting the molecular mechanisms by which p300 regulates lipid homestasis in liver (Source – Yao et al, Biomed Res Int, 2018)

As hepatic steatosis progresses to more harmful stages, high inflammation occurs and collagenous fibres get deposited in the liver leading to fibrosis. p300 has been found to promote fibrosis by its involvement in various signaling pathways. In nutrient surplus conditions, p300 acetylates SMAD3 which is a transcription factor involved in TGF β induced fibrosis in the liver (Kondou *et al*, 2003; Tian *et al*, 2016; Fan, Z. *et al*, 2015). The activity of SMAD3 is regulated by post-translational modifications p such as phosphorylation which is required for its dimerization and entry into the nucleus (Moustakas *et al*, 2001). Similarly, its acetylation by p300 helps in its binding to its target promoters that induce fibrogenesis (Inoue *et al*, 2007). Simultaneously, PIAS4 downregulates the expression of deacetylase SIRT1 whose action is antagonistic to p300, that acetylates SMAD3 (Sun *et al*, 2016). Hypoxia inducible factor 1 alpha (HIF-1 α), an important transcription factor that modulates oxygen homestasis, has also been implicated in hepatic fibrosis. Under

hypoxic conditions, HIF-1 α heterodimerises with HIF-1 β and forms a complex with p300 inside the nucleus that activates various pro-fibrogenic genes by binding to the hypoxia responsive elements (HRE) in their promoters (Freedman *et al*, 2002).

The activity of p300 itself can be regulated by post-translational modifications of its own polypeptide sequence. It gets phosphorylated by Salt Inducible Kinase 2 (SIK2) at Serine 89 position that reduces its acetyltransferase activity (Bricambert *et al*, 2010). Reducing the SIK2 activity either by its knockdown or overexpression of a catalytically defective mutant leads to increased p300 acetyltransferase activity that activates NF κ B signaling pathway downstream to induce fibrosis. It has been observed in cultured hepatocytes that high glucose and insulin causes p300 to assemble at the promoters of several lipogenic genes such as FASN, ACC and ACLY and increase the H3K9 and H4K8 acetylation levels (Bricambert *et al*, 2010). High fat diet induced and homozygous mutant ob/ob mice that are obese, also exhibit reduced SIK2 expression in their liver indicating increased p300 acetyltransferase activity (Bricambert *et al*, 2010).

In high fat diet induced obese Sprague-Dawley rats, hepatic acetyl CoA levels are increased along with increased hepatic glucose production and lipolysis in white adipose tissue (Perry *et al*, 2015). However, a contradictory observation has been seen in the high fat diet induced obese C57BL6/J mice in which high fat diet consumption reduced acetyl CoA levels by downregulation of ACLY and ACSS2 genes (Carrer *et al*, 2017). The global acetylation levels of histones at different sites, as studied by immunoblotting, however did not get significantly altered. The discrepancies in the observations could be due to differences in the metabolic states of the two animal species. It further highlights the fact that more in depth analysis is required for understanding the metabolic changes occurring across different organisms under various nutritional conditions and their effect on post-translational modifications of enzymes that could alter their activities as well as histone modifications at promoter as well as global levels.

Nevertheless, there are several other observations indicating that hepatic steatosis can be induced by increased acetyl CoA levels. In cultured hepatocyte cell line HepG2, external addition of acetate leads to increased acetylation at

H3K9, H3K27 and H3K56 positions (Gao *et al*, 2016). p300 has been shown to form a complex with CEBP α and CEBP β at the promoters of lipogenic genes diglyceride acyltransferase (DGAT) 1 and 2 with increased H3K9 acetylation (Jin *et al*, 2013). Moreover, patient liver samples of NAFLD also exhibit increased levels of p300 and DGAT1, further highlighting its role in the pathogenesis of the disease (Jin *et al*, 2013).

4.1.3.3 Lysine deacetylation in hepatic steatosis

There are two types of histone deacetylases- the classical zinc ion dependant HDACs and the NAD⁺ dependant sirtuins. Members of both classes have been found to play inhibitory roles in lipogenesis.

The sirtuins use NAD⁺ as their cofactor which is also required to drive many metabolic reactions. During fasting, the levels of NAD⁺ substantially increase in the liver due to the action of sirtuins. One of the sirtuins- SIRT1 downregulates lipogenic gene expression by reducing H3 acetylation at their promoters (Cao *et al*, 2013). Moreover, it antagonizes the function of pro-lipogenic transcription factor LXR by interacting with it through the adaptor protein Men1 (menin) (Cao *et al*, 2013; Cheng *et al*, 2015). This disrupts the interaction of LXR with other transcriptional coactivators. SIRT1 also interacts with another transcription factor SREBP1-c and deactivates it by deacetylating it (Ponugoti *et al*, 2010). Another sirtuin- SIRT6 also prevents lipogenesis by deacetylation of histones at H3K9 in the promoters of lipogenic genes such as FASN, ACC and SCD1 (Kim *et al*, 2010). The protein levels of SIRT6 in the liver decrease during feeding and increase during fasting, indicating that the upregulation of SIRT6 in fasting state acts in a feed-forward loop to promote lipolysis and inhibit lipogenesis (Kim *et al*, 2010).

Unlike sirtuins, the classical HDAC activity is not driven by any metabolites and they perform their role by associating with different repressor complexes such as nucleosome remodeling deacetylase (NuRD), corepressor element 1 silencing transcription factor (CoREST) and nuclear receptor corepressor/silencing mediator for retinoid or thyroid hormone receptor (NCoR/SMRT) complex (Hayakawa *et al*,

2015). One of the members of this family- HDAC3 represses lipogenesis by reducing the acetylation at H4K5, H4K8 and H4K12 positions at promoters of target genes such as acetyl CoA carboxylase β (Acab) (Knutson *et al*, 2008). Two other deacetylases HDAC1 and HDAC2 deacetylate H3K9 and H3K27 at lipogenic gene promoters through their interaction with snail family transcriptional repressor (Snail1) and suppress lipogenesis (Liu, Y. *et al*, 2018).

4.2 Results

4.2.3 Histone butyrylation increases with hepatic steatosis in HepG2

In order to study the epigenetic modifications involved in hepatic steatosis, the liver cell line HepG2 was taken as the cellular model. HepG2 cells were cultured in low glucose conditions (5 mM) all the time and steatosis was induced by increasing the glucose concentration to 25 mM along with the supplementation of 100 nM insulin for 24 hours. Histones were acid extracted from the cells under either low or high glucose conditions and immunoblotting was performed with antibodies against acetylation and butyrylation modifications.

There was not much observable change in the acetylation (H3K9 and H4K12) levels in the two conditions (Figure 1). However, butyrylation at different sites – H3K9, H3K23, H4K5 and H4K12 were all found to be increased upon steatosis (Figure 1).

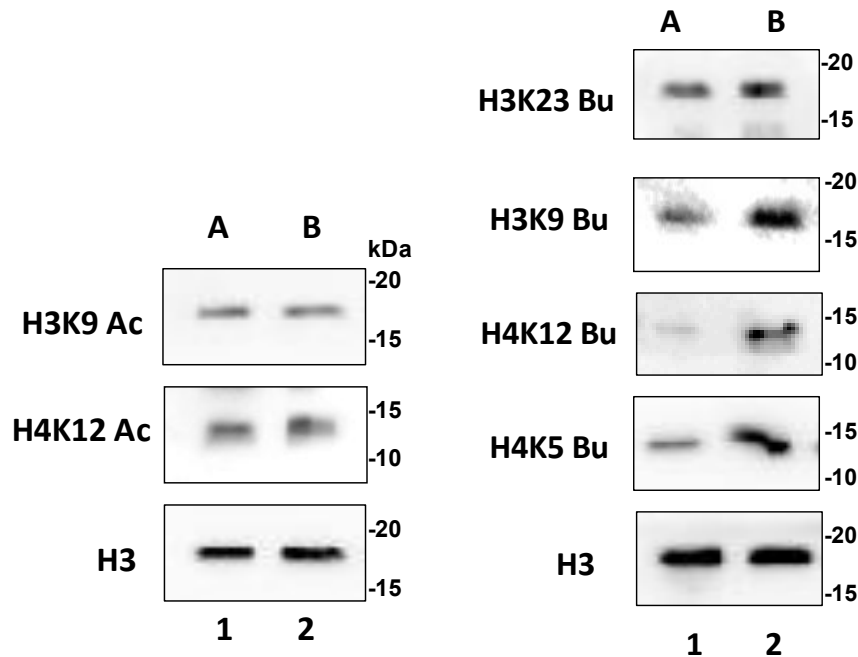


Figure 1: Histone acetylation and butyrylation levels in HepG2 cells under high and low glucose conditions were analysed by immunoblotting with antibodies specific for acetylated H3K9, H4K12 and butyrylated H3K9, H3K23, H4K5 and H4K12. H3 was used as loading control. Lane 1- low steatosis with 5 mM glucose and Lane 2 – high steatosis with 25 mM glucose and 100 nM insulin

Since the technique of immunoblotting can only reflect the modification changes happening at a global level, the possibility of acetylation increasing at specific sites of promoters cannot be ruled out. Moreover, unlike in the case of adipogenesis, which involves lineage change of cells through the participation of a plethora of transcription factors and chromatin modifiers in a concerted manner over a period of 6-8 days, the process of steatosis in a cellular model is a lot faster, spanning over 24 hours during which the transcription of required lipogenic genes that were already being transcribed is further enhanced for more lipid biosynthesis. Therefore, in the smaller time frame, the changes in the predominant acetylation modification may not have been too significant to be observed by immunoblotting. Since butyrylation is a much rarer modification under normal conditions, its enhancement under conditions of fatty acid

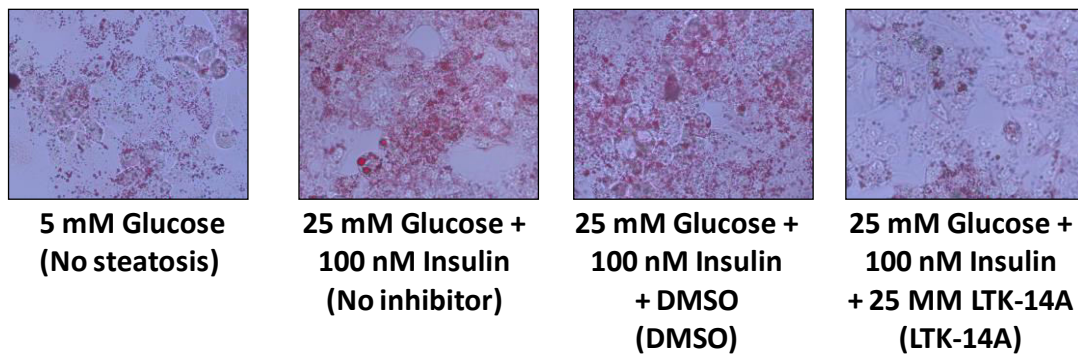
synthesis was more prominent, indicating that it could become a critical epigenetic modification during steatosis.

4.2.4 LTK-14A inhibits glucose induced steatosis in HepG2 cells without having any toxic effect

Since LTK-14A had been found to repress adipogenesis by histone butyrylation inhibition, it was hypothesized that the role of butyrylation in hepatic steatosis could also be highlighted using a similar chemical biology based approach. If butyrylation indeed plays an important role in steatosis then administration of butyrylation inhibitor LTK-14A should prevent lipid accumulation in HepG2.

Therefore, HepG2 cells were treated with LTK-14A at 25 μ M concentration for 24 hours under high glucose conditions that promote steatosis. This particular concentration was chosen because LTK-14A had significant inhibitory effect on adipogenesis at the same concentration. By Oil Red-O staining of hepatocytes (Figure 2A) followed by spectrophotometric estimation of absorbed dye (Figure 2B) it was observed that in this case also, LTK-14A could inhibit steatosis of HepG2 cells after 24 hours of treatment.

A



B

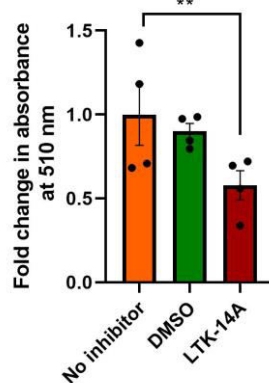


Figure 2: (A) The effect of LTK-14A (25 μ M) treatment on steatosis was tested by Oil Red-O staining of the hepatocytes and the quantitation of staining is represented graphically in (B). Error bars denote mean \pm SEM of three biological replicates, one-way ANOVA with Bonferroni's multiple comparison; * $P < 0.05$, ** $P < 0.01$, *** $P < 0.001$, ns: not significant.

In order to rule out any possibility that the steatosis inhibition did not occur because of any toxic side effect of the compound, an MTT assay was performed by incubating HepG2 cells with LTK-14A at a wide concentration range from 10 μ M to 50 μ M (Figure 3). No change in the metabolic output of the cells was observed in any of these conditions, indicating that the attenuation of lipid accumulation did not occur because of any undesirable toxicity from the compound.

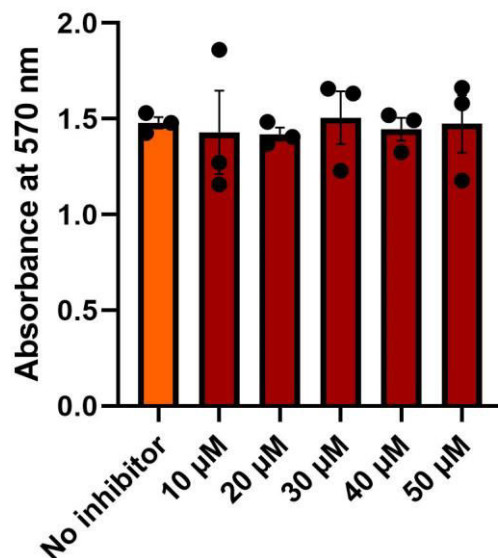


Figure 3: MTT assay was performed to check for any possible cellular toxicity effect of LTK-14A at a concentration range from 10 μ M to 50 μ M on HepG2 cells. Comparison was done with cells that were left untreated. Error bars denote mean \pm SEM of three biological replicates, one-way ANOVA with Bonferroni's multiple comparison; * $P < 0.05$, ** $P < 0.01$, *** $P < 0.001$, ns: not significant.

4.2.3 LTK-14A inhibits steatosis of HepG2 by repressing the expression of lipogenic genes

The inhibition of steatosis by LTK-14A might have been due to downregulation of expression of genes important for lipogenesis in HepG2. To verify this, RNA was isolated from LTK-14A treated HepG2 cells maintained under steatosis inducing conditions and gene expression pattern was compared with untreated and DMSO treated conditions. Two of the candidate genes chosen were the two transcription factors *ChREBP* and *SREBP1c*, which have been previously reported to be acetylated by p300 for their recruitment to their cognate promoters of genes required for synthesis of triglycerides. The other candidate gene was *Scd1* which is required for fatty acid biosynthesis. All three genes were found to be downregulated by LTK-14A (Figure 4). Even though the extent of downregulation was not as drastic as that seen in the case of adipogenesis inhibition, this observation still indicated that LTK-14A could be inhibiting steatosis by repressing the expression of important lipid metabolism related genes

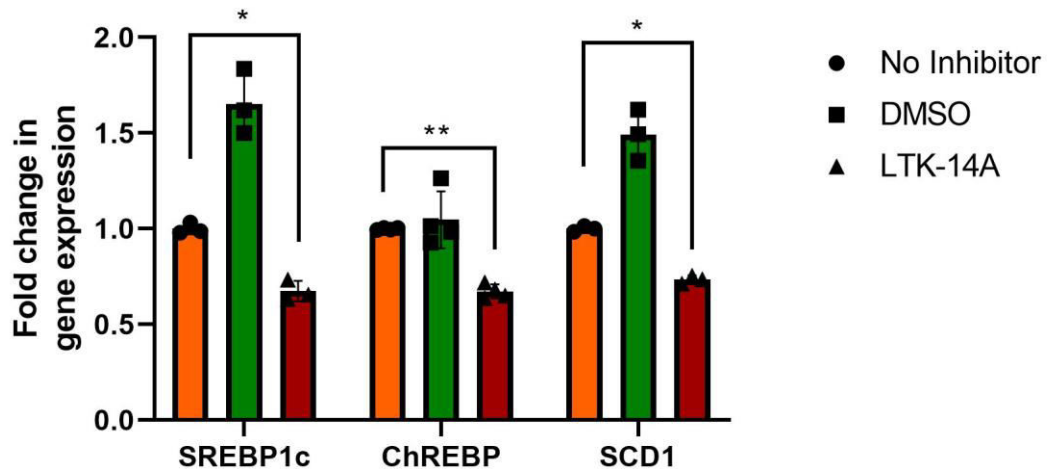


Figure 4: Q-PCR analysis was performed to check the expression pattern of lipogenic genes in HepG2 upon treatment with LTK-14A. Error bars denote mean \pm SEM of three/four biological replicates; one-way ANOVA with Bonferroni's multiple comparison: * $P < 0.05$, ** $P < 0.01$, *** $P < 0.001$, ns: not significant.

4.2.4 LTK-14A represses gene expression by specific inhibition of histone butyrylation without affecting acetylation in HepG2

Since LTK-14A treatment had resulted in downregulation of lipogenic gene expression, investigation was carried out to see whether there was any change in histone modification pattern that affected the gene expression. Histones were acid extracted from LTK-14A treated HepG2 cells maintained in high glucose conditions and immunoblotting was performed with acetylation and butyrylation specific antibodies to check for any change in the modifications compared to untreated and DMSO treated conditions. It was observed that none of the tested acetylation marks at the sites H3K14, H3K18 and H4K12 were affected upon LTK-14A treatment (Figure 5). However, amongst the tested butyrylation marks, although H3K23 Bu did not change, there was a reduction in H4K5 Bu level with LTK-14A treatment (Figure 5).

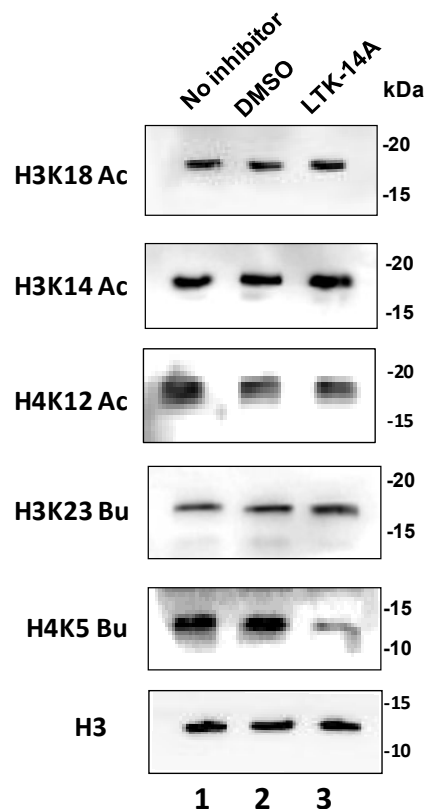


Figure 5: Histone acetylation and butyrylation levels in HepG2 cells that were treated with LTK-14A were compared with that in DMSO treated and untreated conditions by

immunoblotting with antibodies against acetylated histones H3K18, H3K14 and H4K12 and butyrylated histones H3K23 and H4K5. Histone H3 was used as loading control.

This same site-specific modification had shown a consistent pattern of being reduced with LTK-14A treatment in adipocytes of both cellular and mice models. This indicated that H4K5 Bu may be an important mark for epigenetic regulation of lipid metabolism related processes.

4.2.5 LTK-14A prevents hepatic steatosis in mice fed with high fat diet by specific inhibition of histone butyrylation without affecting acetylation in liver

After observing that LTK-14A could prevent glucose induced steatosis in cultured hepatocytes, we wanted to see whether similar effects could be achieved in animal models of steatohepatitis as well. Previous reports suggest that the same mice models of high fat diet induced or genetically induced obesity exhibited symptoms of liver steatosis, in addition to adipose tissue enlargement. Therefore, at first, we checked the morphology of the liver from the high fat diet maintained mice and compared with that of the LTK-14A treated mice by hematoxylin and eosin staining (Figure 6). The liver of mice maintained on high fat diet exhibited characteristic features of lipid accumulation, while no such features could be observed in the liver samples of mice maintained either on normal chow diet or on LTK-14A mixed high fat diet.

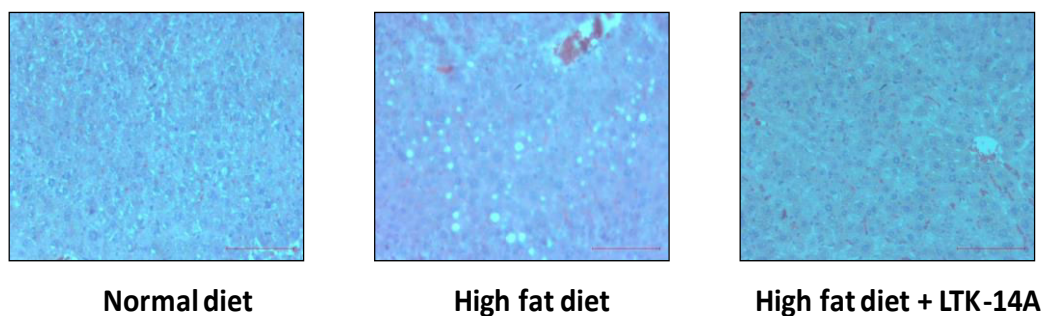
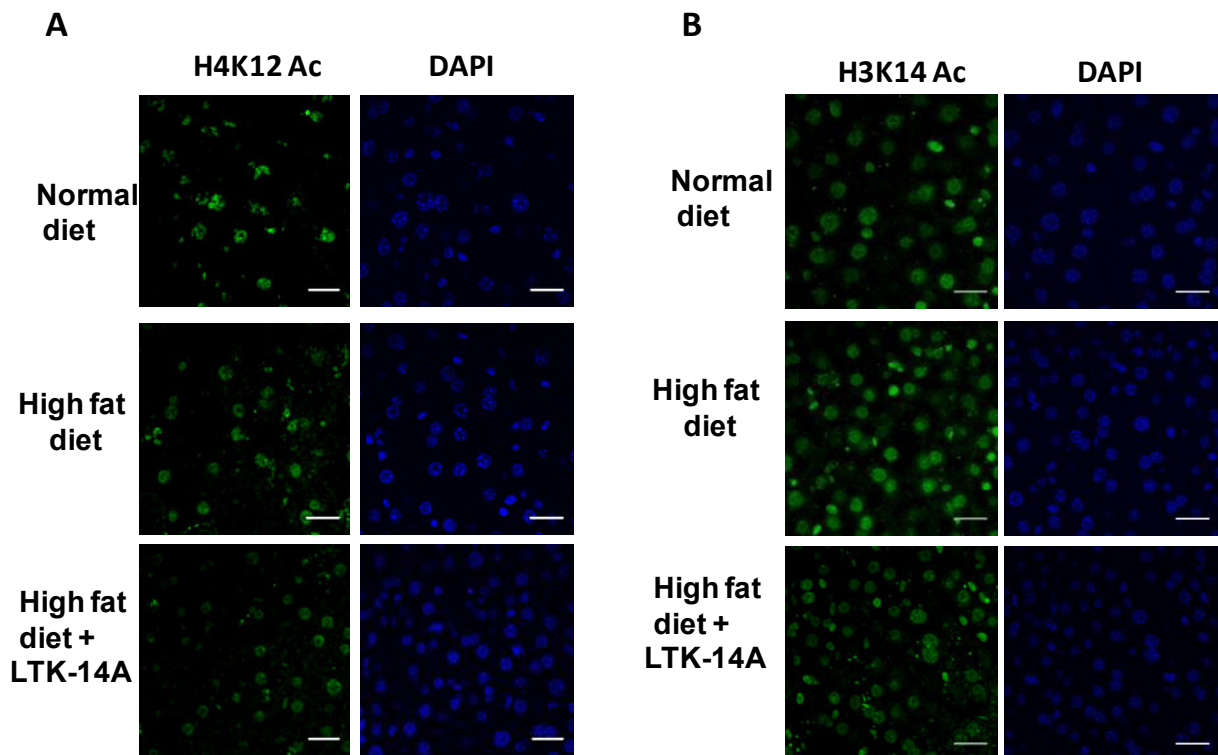


Figure 6: Representative images of morphology of adipose tissue from the mice of the three groups, as studied by hematoxylin and eosin staining.

We also wanted to check whether there were any changes in epigenetic modifications in the liver of LTK-14A treated mice. Immunofluorescence staining of the liver samples was carried out using antibodies against H3K14 Ac, H4K12 Ac

and H4K5 Bu. It was observed that neither high fat diet consumption alone nor the additional administration of LTK-14A had any effect on the two acetylation marks and the levels of both these modifications seemed to be consistently similar across the three groups of mice (Figure 7A, B, C, and D). However, H4K5 Bu was barely detectable in the liver of normal diet maintained mice, while it was definitively increased in high fat diet maintained mice (Figure 8 A and B). Interestingly, H4K5 Bu was again reduced to barely detectable levels in the liver of mice maintained on LTK-14A mixed high fat diet. This change in the pattern of butyrylation at H4K5 site once again corroborated the hypothesis that this site specific modification could be critical for regulating steatosis.



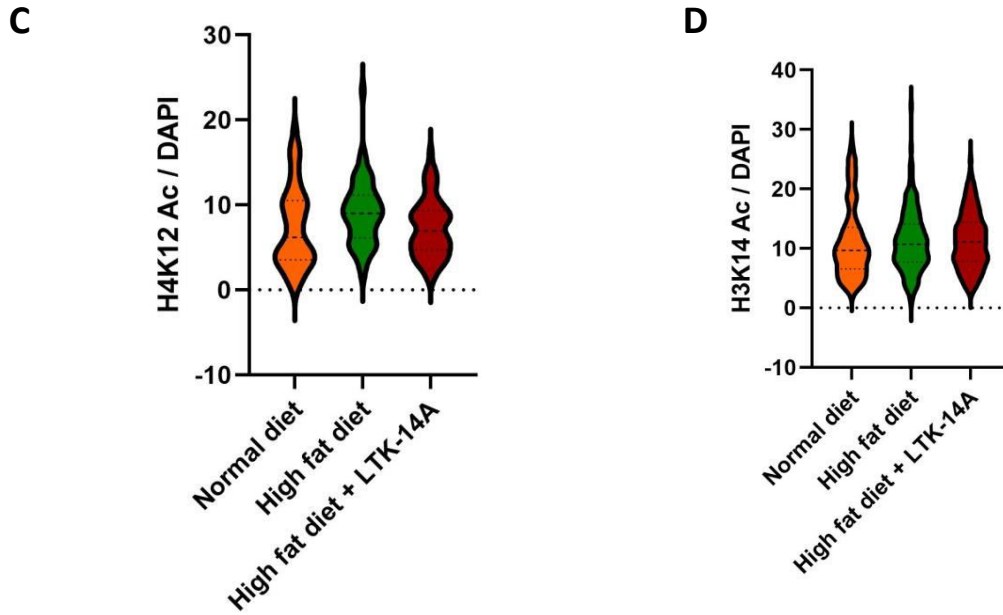


Figure 7: Immunofluorescence microscopy of liver sections stained with antibodies against histone H4K12 acetylation (panel A) and histone H3K14 acetylation (panel B). The fluorescence intensity of the modified histone marks was normalised against DAPI staining of whole nuclei for quantitation which is graphically depicted in panel C and D ;n=3 in each group; one-way ANOVA with Dunnett's multiple comparison: * P < 0.05, **P < 0.01, ***P < 0.001, ns: not significant. Magnification is 40X and scale bar is 21 μ M.

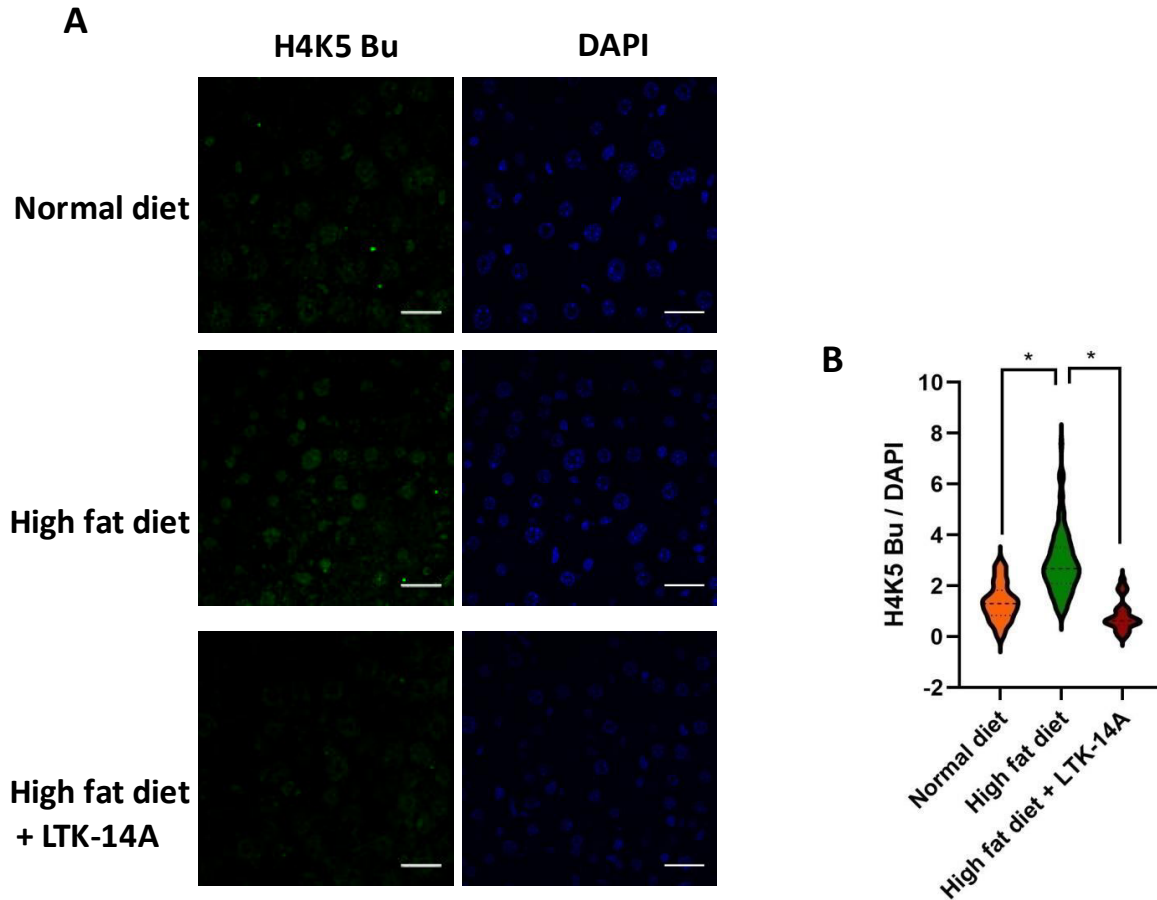


Figure 8: Immunofluorescence microscopy of liver sections stained with antibody against histone H4K5 butyrylation. The fluorescence intensity of the modified histone mark was normalised against DAPI staining of whole nuclei for quantitation which is graphically depicted in panel B ;n=3 in each group; one-way ANOVA with Dunnett's multiple comparison: * P < 0.05, **P < 0.01, ***P < 0.001, ns: not significant. Magnification is 40X and scale bar is 21 μ M.

4.2.6 LTK-14A prevents hepatic steatosis in genetically obese mice by specific inhibition of histone butyrylation without affecting acetylation in liver

The successful attenuation of hepatic steatosis by LTK-14A in high fat diet maintained mice encouraged us to investigate whether the compound had similar effects in the genetically obese db/db mouse model. The db/db mice were even more obese and had greater body weights than the high fat diet maintained

C57BL6/J mice. Average weight of the liver was the highest for db/db mice given vehicle control and least for the db+/- mice, while that for the compound treated db/db mice was intermediate (Figure 9 A and B). Hematoxylin and eosin staining of liver tissues indicated a high degree of hepatocyte ballooning in db/db mice given vehicle control, a signature of high inflammatory response due to excessive lipid accumulation and peroxidation (Figure 9 C). Such features were absent in the liver tissues of db+/- mice and db/db mice treated with LTK-14A.

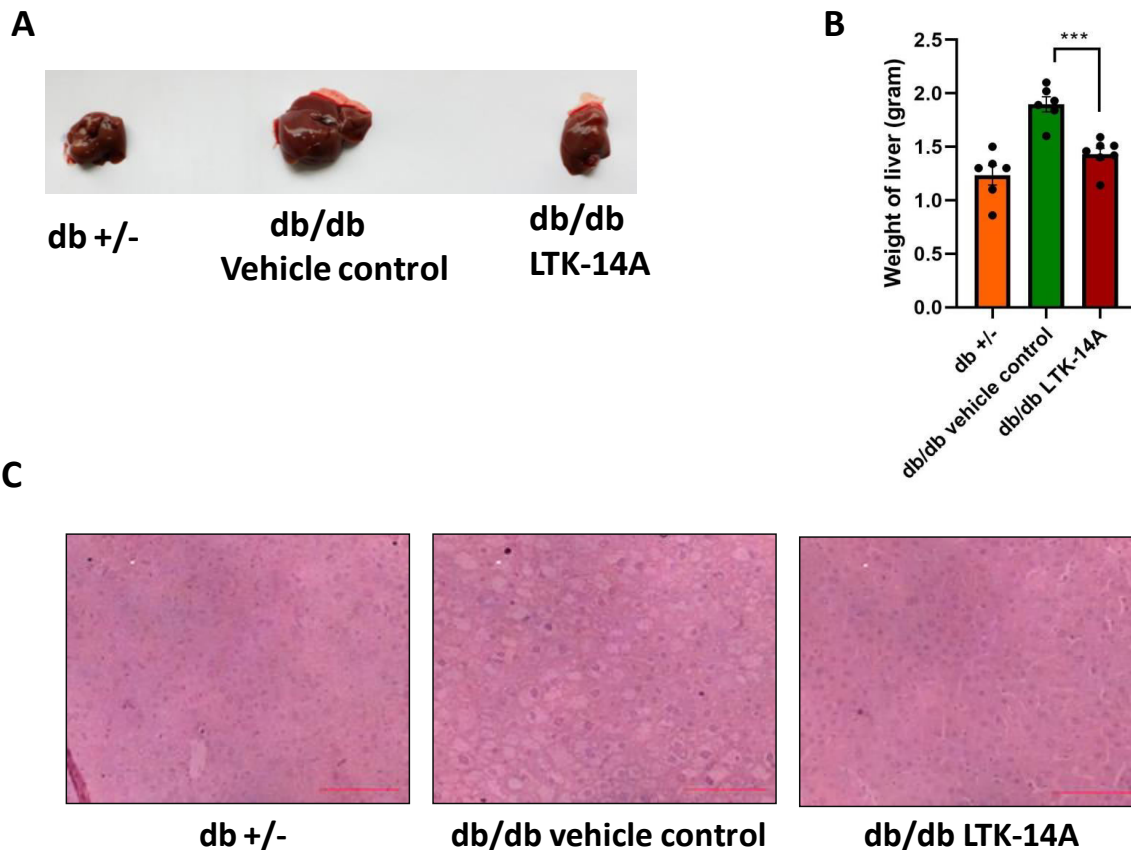


Figure 9: Representative images of liver (panel A) from the mice of three groups and average weight of liver (panel B) depicted graphically; n= 6 to 7 in each group; ; one-way ANOVA with Dunnett's multiple comparison: * P < 0.05, **P < 0.01, ***P < 0.001, ns: not significant. (C) Representative images of morphology of liver from the mice of the three groups, as studied by hematoxylin and eosin staining.

Immunofluorescence staining revealed that similar to the high fat diet induced obesity model, the more obese homozygous leptin receptor mutant mice (db/db) liver had greater level of H4K5 butyrylation compared to leaner heterozygous mutant mice (db +/-) (Figure 10 A and B). Moreover, LTK-14A treated db/db mice liver showed a decrease in H4K5 butyrylation compared to vehicle control treated mice liver. In contrast, H4K12 and H3K14 acetylation were only partially upregulated in the db/db mice and did not get significantly reduced upon LTK-14A treatment (Figure 11 A, B, C and D).

Thus, collectively it could be said that H4K5 butyrylation is a key epigenetic signature for not only adipogenesis but also hepatic steatosis, and obesity in mice could be attenuated by administration of LTK-14A, which prevented lipid accumulation in liver and adipose tissue by inhibiting H4K5 butyrylation.

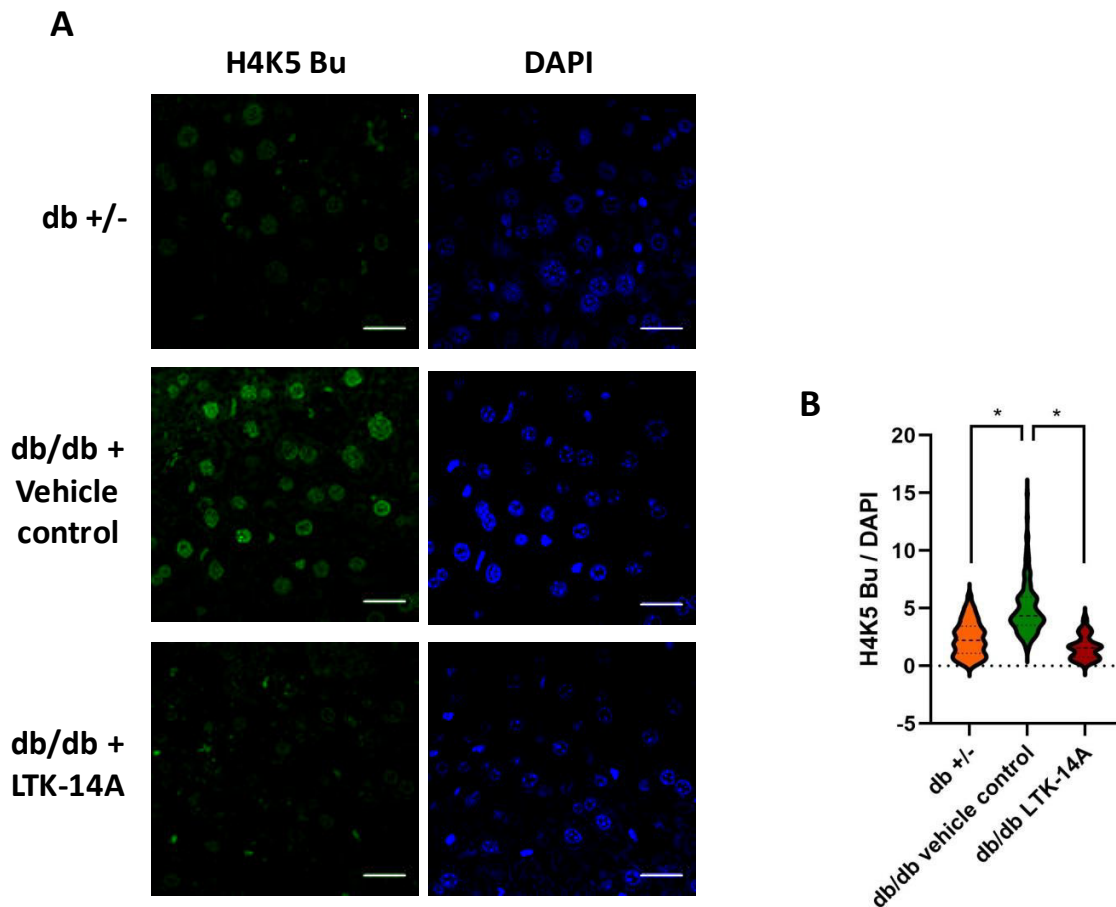
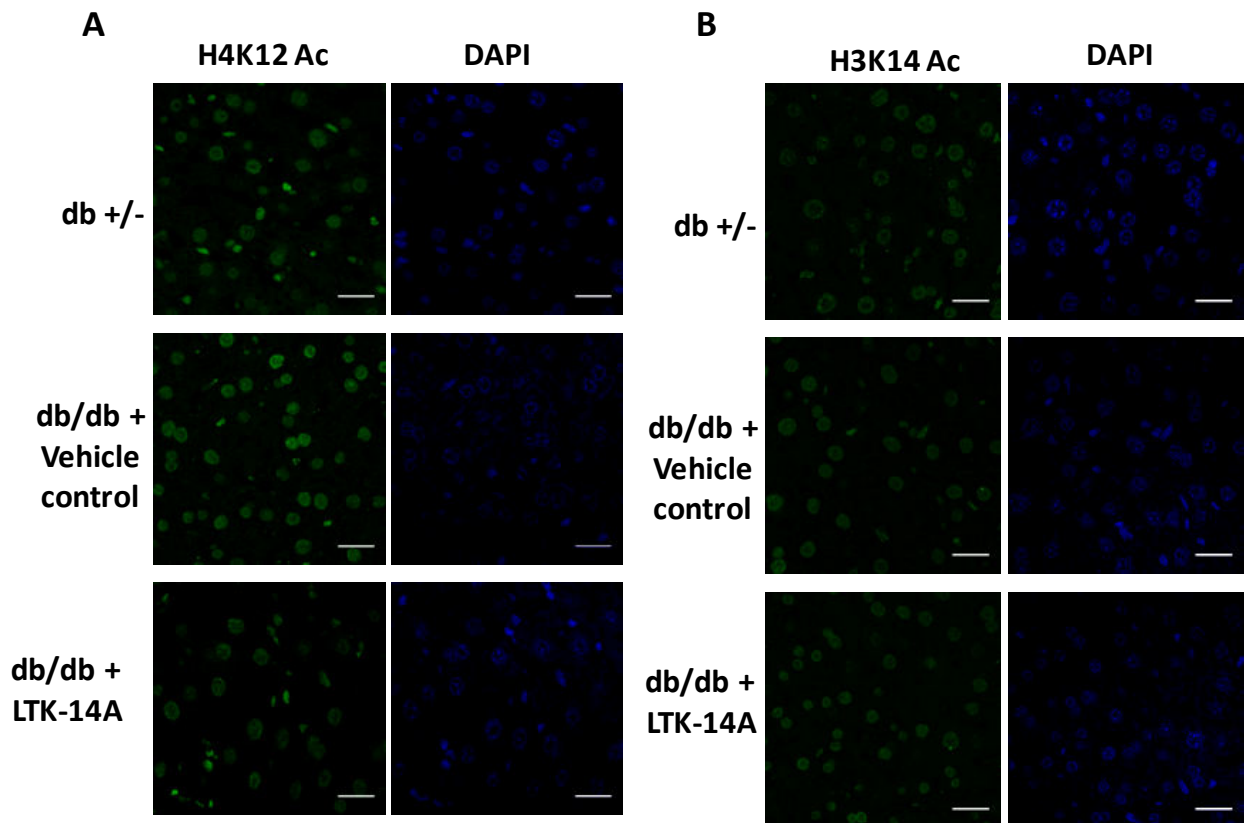


Figure 10: Immunofluorescence microscopy of liver sections stained with antibody against histone H4K5 butyrylation. The fluorescence intensity of the modified histone mark was normalised against DAPI staining of whole nuclei for quantitation which is graphically depicted in panel B ;n=3 in each group; one-way ANOVA with Dunnett's multiple comparison: * P < 0.05, **P < 0.01, ***P < 0.001, ns: not significant. Magnification is 40X and scale bar is 21 μ M.



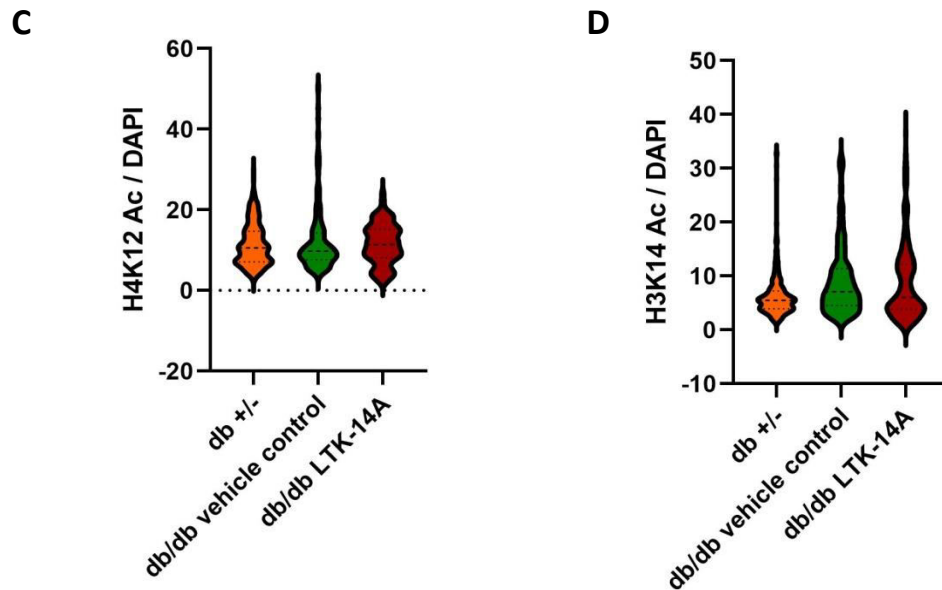
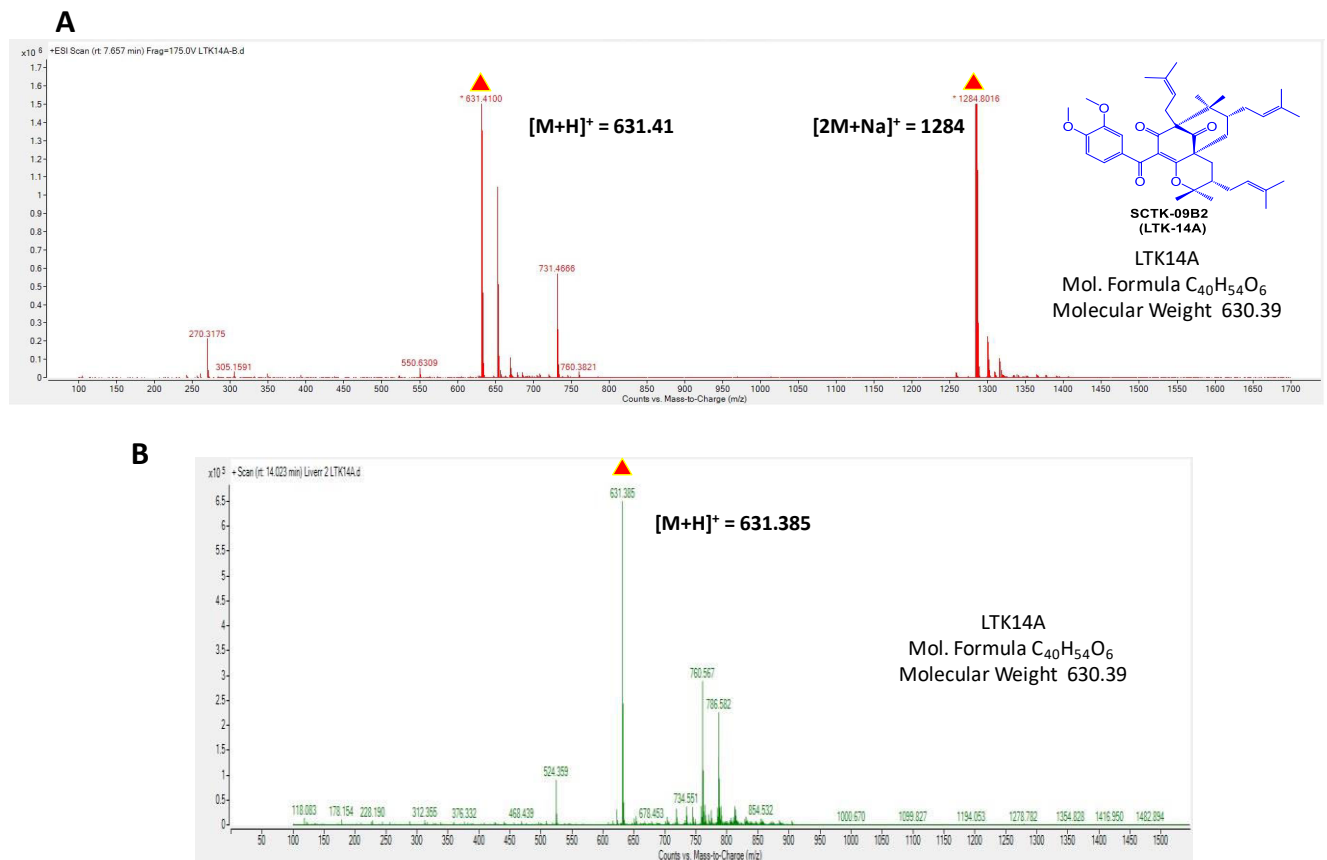


Figure 11: Immunofluorescence microscopy of liver sections stained with antibodies against histone H4K12 acetylation (panel A) and histone H3K14 acetylation (panel B). The fluorescence intensity of the modified histone marks was normalised against DAPI staining of whole nuclei for quantitation which is graphically depicted in panel C and D ;n=3 in each group; one-way ANOVA with Dunnett's multiple comparison: * P < 0.05, **P < 0.01, ***P < 0.001, ns: not significant. Magnification is 40X and scale bar is 21 μ M.

4.2.7 LTK-14A is metabolically stable and is bio-available in its intact form in liver

Although LTK-14A had prevented obesity in both high fat diet induced and genetically obese mice models, it was imperative to check whether the compound had indeed been available in its intact form in the liver, after its passage through the gastrointestinal tract and being acted upon by the digestive enzymes. Metabolites were extracted from the liver of the mice fed with high fat diet mixed with LTK-14A and LC-ES-MS analysis was performed. LTK-14A was indeed detected in the liver extracts of all the compound treated mice as proved by the presence of its characteristic protonated molecular ion peak in the ESI spectra of the analytes (Figure 12 A and B). LTK-14A exhibits UV absorbance at 254 nm and the UV chromatogram of the extracts showed a peak in the elution fraction

containing LTK-14A whereas no such peak could be seen for the extracts of normal diet and high fat diet fed mice at the same elution time point (Figure 12 C). The position of this peak coincided with the position of the peak in the UV chromatogram of pure LTK-14A, thereby indicating that this peak is due to the presence of LTK-14A in the elution fraction. Overall, the mass spectrometry results proved that LTK-14A could still be available in its intact state in the liver cells to perform its downstream steatosis inhibitory action.



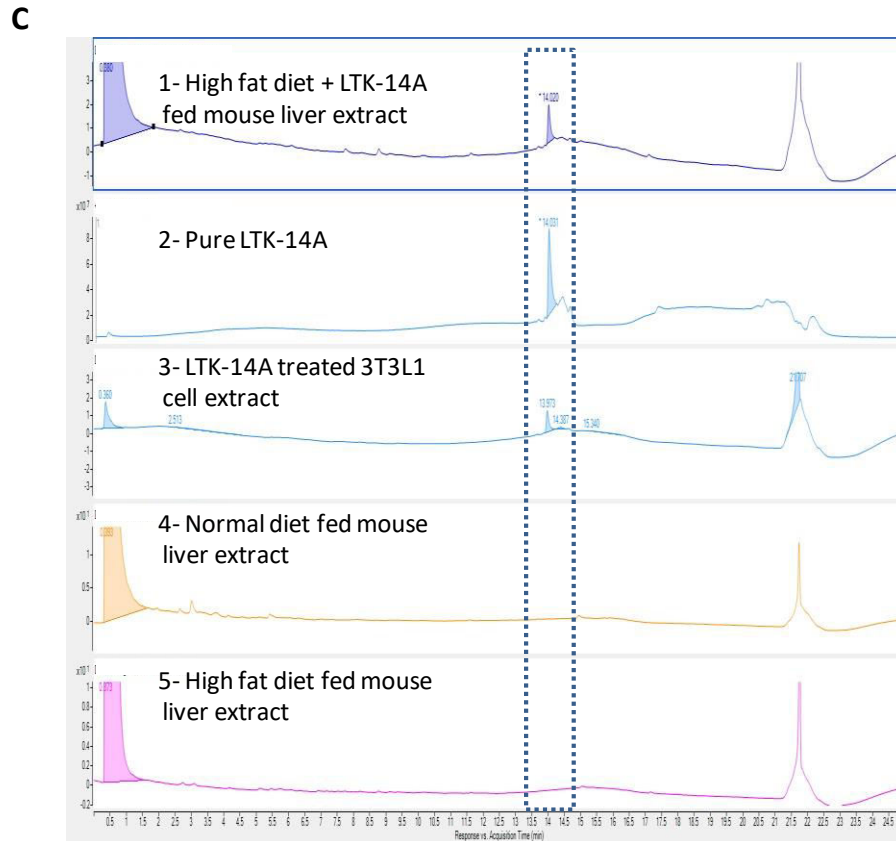


Figure 12: (A) ESI spectra of pure LTK-14A. (B) The presence of LTK-14A in the physiological system upon administering the compound was verified by LC-ESI-MS analysis of the metabolite extracts of liver. (C) Comparative UV chromatogram of (1) liver extracts of LTK-14A treated mouse, (2) pure LTK-14A, (3) LTK-14A treated 3T3L1 cell extracts, (4) liver extracts of normal diet fed mouse and (5) high fat diet fed mouse.

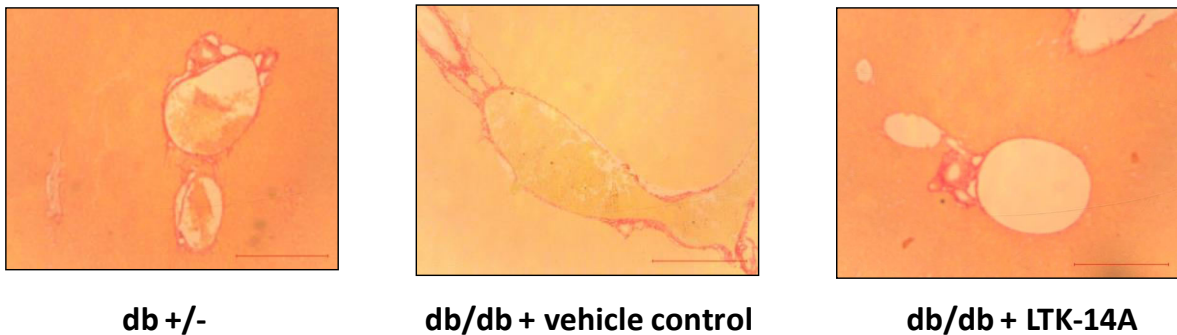
4.2.8 Application of LTK-14A for prevention of liver fibrosis

During obesity manifestation, if the process of ectopic lipid accumulation goes on unhindered within the liver, excessive reactive oxygen species and free radicals get produced in the hepatocytes due to the action of the lipid peroxidation enzymes involved in lipid catabolism. This sets off a high inflammation response in the liver that ultimately damages the cells. Although the damaged cells are replaced by new healthy liver cells in due course of time, repeated damage to the liver through high degree of steatosis leads to deposition of collagenous matrices by the exhausted regenerative liver stem cells. The deposited collagen fibres are an indication of liver fibrosis which is still reversible, but if the fibre formation

continues unabated, the liver is permanently and irreversibly damaged by cirrhosis.

Since LTK-14A showed good potential in preventing hepatic steatosis in both mice models of obesity, we surmised that it might be effective for prevention of liver fibrosis as well. For this purpose, picosirius red staining of collagen fibres was performed with the liver samples from genetically obese db/db mice experiment (Figure 13 A). Most of the staining was found to occur near the periportal regions of the liver with almost no perisinusoidal fibrosis observed. Upon quantitation of the area of each fibrotic lesion it was observed that the average area of these lesions was the highest in the liver samples of vehicle control treated db/db mice (Figure 13 B). Although the average lesion area was less for the db +/- and LTK-14A treated db/db mice, the differences were not high enough to make the result statistically significant.

A



B

Animal type	db +/-	db/db + vehicle control	db/db + LTK-14A
Percent area covered by lesion (+/- SD)	7.294 (+/- 4.3)	12.13 (+/- 3.77)	7.87 (+/- 4.52)

Figure 13: (A) Representative images of Sirius Red stained liver samples of mice from the three different groups. The average area of the fibrotic lesion has been given in tabulated form in panel (B).

Since the fibrotic lesion area in db/db mice was only slightly greater than that of db +/- mice, the leptin receptor deficient mouse model did not serve as a suitable model for studying fibrosis in the first place. A new theory of “two hit hypothesis” has been gaining ground in this aspect which suggests that more than one “hit” or causal factor will be required for the liver fibrosis to manifest in mice. The first “hit” such as excessive energy (lipid) intake through high fat diet or excessive *de novo* synthesis of lipids due to high consumption of normal chow diet owing to leptin receptor deficiency, would lead to hepatic steatosis. An additional second “hit” would be required for a high enough inflammation that would result in fibrosis. In spite of the shortcomings of the two models used, the trend of fibrosis reduction in LTK-14A treated db/db mice liver indicates that the compound may find potential in preventing fibrosis in more severe disease models.

DISCUSSION

Discussion

The following chapter provides a summary of the results from each of the two previous sections and also provides an insight on possible future directions.

In the recent years, several rare modifications of histones have been discovered, possibly due to advancements in mass spectrometry technology. Concomitantly the writers, readers and erasers that are regulating these modifications are also being identified and characterized. All these acylation modifications are brought about by acyl CoA moieties derived from different endogenous analytes produced from various metabolic pathways. Under normal circumstances, the stoichiometric levels of these acyl CoA species are much lower relative to that of acetyl CoA (King *et al*, 1985; Hosokawa *et al*, 1986). Therefore acetylation of histones predominates over other acylation modifications. However, new evidences indicate that under specific circumstances, if there is an increased availability of precursor metabolites that serve as sources for acyl CoAs, then the chance for acylation of substrates increases (Sabari *et al*, 2015; Zhang *et al*, 2019). This event alone may not be enough (Kebede *et al*, 2017) as it may also require increased expression or catalytic activity of the corresponding writer enzyme to bring about enhanced acylation of histones. *In vitro* transcription assays with certain selected acyl CoAs have demonstrated that acylation of histones generally increase the transcription rate by having a similar positive charge neutralization effect on lysine as acetylation (Sabari *et al*, 2015, Goudarzi *et al*, 2016). In fact, their bulkier size could have an even more profound effect compared to acetylation. Still, more research is required to understand the regulatory roles of these modifications.

We investigated about histone butyrylation to find out its possible physiological role. Butyric acid, the source of butyryl CoA, is largely produced by microbiota residing in the intestine. But it is also found in adipose tissues as well as animal products rich in fat such as butter. We hypothesized that since butyric acid is a short chain fatty acid, its stoichiometric levels could increase in lipid metabolism associated processes such as fatty acid synthesis or oxidation. Adopting this

hypothesis we decided to study the pattern of histone butyrylation in two cellular processes in which lipid metabolism is predominant- adipogenesis and liver steatosis.

At the time of initiation of this study, p300 was the only known acetyltransferase that could promiscuously perform other acylation modifications such as butyrylation. The role of p300 catalysed acetylation in adipogenesis and hepatic steatosis was already well known (Gelman *et al*, 1999; Yoo *et al*, 2016; Jang *et al*, 2017; Bricambert *et al*, 2010). In order to delineate the functional role of butyrylation from acetylation, we adopted a chemical biology based approach by using a small molecule modulator that could selectively inhibit butyrylation without inhibiting acetylation. We hypothesized that if p300 catalysed butyrylation is not just a “metabolic noise” but rather indeed important for regulating gene expression during adipogenesis or steatosis, then inhibition of butyrylation should be enough to attenuate lipid biosynthesis or accumulation that are strongly associated with these two processes.

1) Understanding the importance of histone butyrylation in adipogenesis

Using a cellular model of adipogenesis, we began with the observation that just like acetylation, as reported before, butyrylation also increases globally at several sites on the histones along with increased gene expression of butyryl CoA producing *Acss2*. Chromatin immunoprecipitation with H4K5 butyrylation specific antibody also revealed an increased enrichment of the modification in the promoters of the pro-adipogenic genes *Pparg* and *Lep* at terminal stage of differentiation compared to the pre-adipocyte stage. However, the increase did not follow the same pattern in the two gene promoters. While, there was a continuous increase in the butyrylation enrichment in the promoter of the master regulator *Pparg* after induction till the terminal stage, the *Lep* gene promoter exhibited an increased enrichment only in the mature adipocyte stage. In the time course of adipogenesis, *Pparg* needs to be expressed at the early stage and it remains in a highly transcribed state even at the late stage of differentiation. On the other hand, *Lep* gets expressed only towards the end as a marker of adipocytes and this might explain the difference in the enrichment pattern of histone butyrylation in the two promoters.

We screened for a potential selective butyrylation inhibitor amongst a class of derivatives prepared from a naturally occurring molecule in *Garcinia indica*. Molecular docking and supportive mutagenesis studies were performed to develop a better understanding of the selective nature of our compound. These *in vitro* studies were followed by experiments performed with the compound in cell line to test its permeability, toxicity and ability to repress adipogenesis. Mechanistically, it was found that the compound downregulated a large number of pro-adipogenic genes possibly through inhibition of histone butyrylation at specific sites. Under these conditions, histone acetylation and other post-translational modifications were found to be relatively unaffected.

Amongst the important adipogenesis related genes that were found to be downregulated by LTK-14A were the master regulator transcription factor *Pparg* and *Cebpa*, both of which are essential for adipogenesis. In the pre-adipocyte stage the expression of these factors in turn are regulated by C/EBP β and C/EBP δ (Cao *et al*, 1991; Yeh *et al*, 1995). It was surprising to observe that in both the RNA sequencing analysis as well as in the qRT-PCR analysis for validation, *Cebpd* was not downregulated by LTK-14A. This indicated that *Cebpd* may be less prone to be regulated by histone butyrylation compared to the other genes tested in our experiments. Indeed, chromatin immunoprecipitation study indicated that in the initial stage of induction of differentiation in pre-adipocytes, there was no enrichment of H4K5 butyrylation in the promoter of *Cebpd*. This could explain why the butyrylation inhibitor LTK-14A treatment at the induction stage did not inhibit *Cebpd* expression, since there was no butyrylation mark enrichment for inhibition in its promoter to begin with. An increased butyrylation in its promoter at the terminal stage could be either through p300 catalysed modification or non-enzymatic means with greater availability of butyryl CoA, or both. Currently, we have not been able to verify this. However our preliminary observations with promoter specific studies indicate that H4K5 butyrylation plays a role in regulating the expression of the critical transcription factor *Pparg*. Inhibition of butyrylation by LTK-14A repressed the

expression of the master regulator which further led to the inhibition of downstream genes like *Lep*, whose expression is dependent on PPAR γ .

While cell line based studies indicate that C/EBP δ regulates the expression of a cascade of transcription factors like C/EBP α and PPAR γ , this fact has been questioned in knockout mice which have poorly differentiated adipose tissue but still express *Pparg* and *Cebpa* (Tanaka *et al*, 1997). This indicates that there could be other factors playing a redundant function like C/EBP δ in the initiation stage of adipogenesis. Moreover, an additional function of C/EBP δ may seem to be downstream of C/EBP α and PPAR γ at the terminal stage of adipogenesis. It has been speculated that this could involve inducing the expression of ligands that activate PPAR γ (Hamm *et al*, 2001). Therefore, the increased butyrylation in the promoter of *Cebpd* on day 6 of adipogenesis might be responsible for its role in the terminal stage. The expression of *Cebpd* is independent of *Pparg* and hence repression of *Pparg* by butyrylation inhibition with LTK-14A did not repress *Cebpd*.

Among the different site-specific butyrylation modifications tested, we observed that H4K5 butyrylation was consistently reduced in LTK-14A treated conditions, both in cell lines as well as in mice adipose tissues while the other butyrylation sites were not as affected. This specifically highlights the importance of H4K5 butyrylation in regulation of adipogenesis.

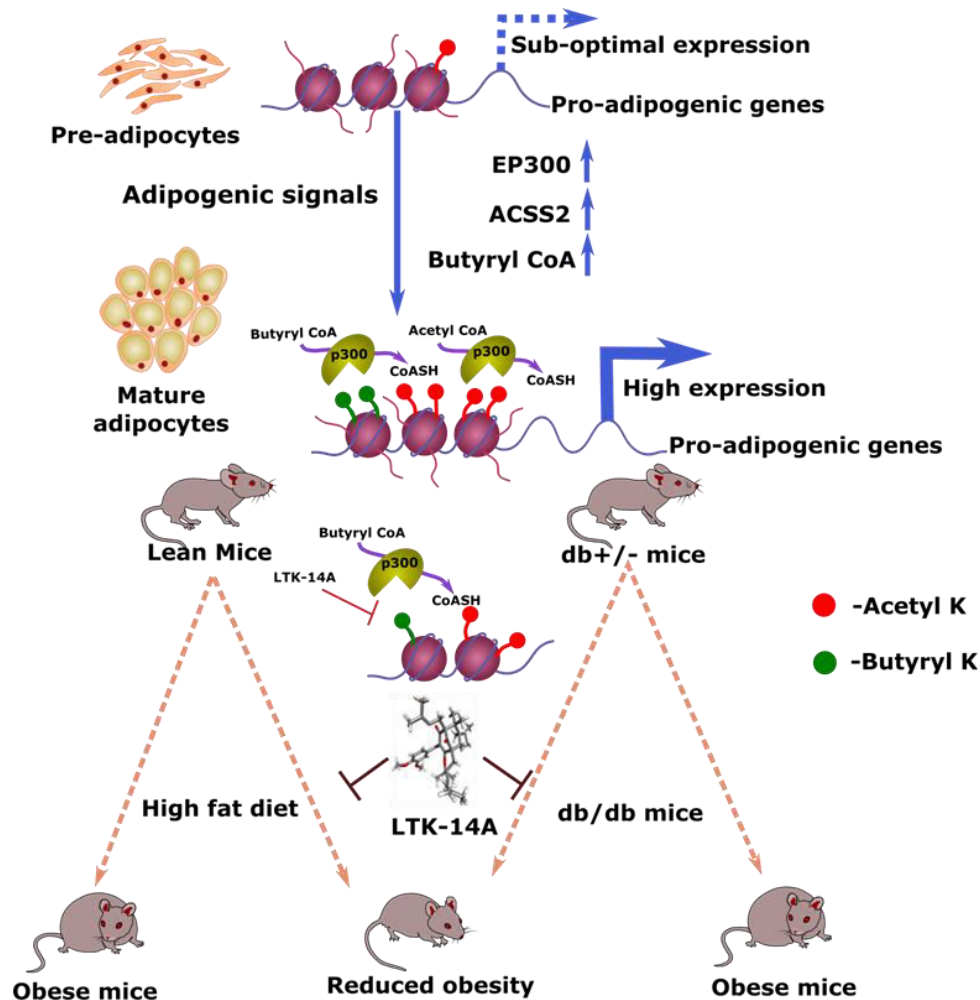
H4K5 butyrylation has been found to be a modification of physiological importance in the context of spermatogenesis wherein it marks the histones in those genomic loci where the histones are retained throughout the process of development and are not replaced by protamines (Goudarzi *et al*, 2016). Moreover, this particular modification is efficiently carried out by p300 and has a role in opening up the chromatin and making it more conducive for transcription.

While our work was in progress, a new report was published in which it was demonstrated that inhibition of fatty acid synthesis as well as oxidation leads to reduction in H4K5 butyrylation while acetylation remains unaffected (Gao *et al*, 2021). This further reinforces our own hypothesis that fatty acid metabolism is an important source for certain acyl CoAs such as butyryl CoA, derived from the short chain fatty acid butyric acid. Another work published

during this period revealed HBO1, a member of MYST family of acetyltransferase, also possesses the ability to catalyse acylation reactions including butyrylation (Xiao *et al*, 2021). Mass spectrometry studies of histone modifications altered by knockdown of HBO1 in HeLa cells showed that H4K5 butyrylation does not get affected by depletion of HBO1 indicating that it is a p300 specific mark.

We have also tested the potency of our molecule in arresting obesity in two different mouse models of obesity. Used as a prophylactic, it prevented further weight gain in mice maintained on a high fat diet. Furthermore, it reduced the weight of genetically obese mice that had already gained a lot of weight, thereby showing its efficacy as a cure. In both the mice models, our compound had a profound effect on the adipose tissue hypertrophy and total fat mass of the mice. As seen in cell line model, LTK-14A treatment also inhibited *Pparg* expression in the mice adipose tissue along with other lipogenic genes. More importantly, in both mice models the reduced adiposity could be attributed to reduced histone H4K5 butyrylation in the adipose tissues while acetylation was unaffected. Enhanced H4K5 butyrylation was not observed in mature adipose tissues of obese mice possibly due to predominance of adipocyte population in the tissues of mice from all the groups. In our cell line model of adipogenesis we had detected an increase in histone modification in highly differentiated adipocytes compared to pre-adipocytes because majority of the pre-adipocytes had differentiated to adipocytes and the comparison of histone modification was done with a homogenous culture of pre-adipocytes. On the other hand, in mice adipose tissues, due to the heterogeneity of cell population and predominance of adipocytes over pre-adipocytes and other cell types (Burgeois *et al*, 2019), the contribution of H4K5 butyrylation, as seen by immunoblotting, might have been mainly from the adipocytes in all three groups of mice in both experimental models. Nevertheless, H4K5 butyrylation could be playing an important role in regulating gene expression related to lipid metabolism, because inhibiting this modification led to attenuation of weight gain and adipocyte hypertrophy.

Based on our observations we propose the following model on the role of p300 catalysed butyrylation in adipogenesis-



Schematic diagram illustrating the importance of p300 catalysed butyrylation in adipogenesis and obesity, highlighted by the butyrylation specific inhibitor LTK-14A

In pre-adipocytes, there exists a basal level of histone acetylation while butyrylation is present to a much lesser extent owing to low stoichiometric levels of butyryl CoA. Induction of adipogenesis causes a simultaneous upregulation of histone acetylation and butyrylation marks leading to increased rate of adipogenesis and concomitant transcriptional activation of pro-adipogenic genes.

One major issue that will always be associated with acylation studies is that whether these acylation modifications have a synergistic or antagonistic effect compared to acetylation of histones. In our cell line model of adipogenesis we have observed that both acetylation and butyrylation marks are upregulated, indicating synergism for gene expression activation. An interesting question in

this context would be that if acetylation of histones is already activating gene expression, why should butyrylation of histones be necessary, that too on overlapping lysine residues? A similar issue has already been addressed by Saadi Kochbin's group which stated that both the modifications can co-occur dynamically on histones, especially if the cofactor concentrations are no longer limiting (Goudarzi *et al*, 2016). The dynamicity in the co-occurrence of acetylation and butyrylation on histones is due to the high turnover rate of acetylation and deacetylation. In a specific physiological context, when a certain subset of genes is being highly transcribed, the histones in their corresponding promoters are highly acetylated. Due to the high turnover rate of acetylation (Jackson *et al*, 2015), those promoters will be continuously undergoing repeated cycles of acetylation and deacetylation, leading to a decrease in the local concentration of acetyl CoA in the vicinity of the promoters. Kochbin and his colleagues had postulated that in order to maintain the high expression level of these transcriptionally active genes, the writer enzyme (in this case p300) will utilize other cofactors similar to acetyl CoA for maintaining the open state of the chromatin. Along similar lines, we assume that during the initial stage of adipogenesis, acetylation of histones is increased to induce the expression of pro-adipogenic genes. As the fatty acid synthesis begins, there is increased generation of butyric acid which is converted to butyryl CoA by ACSS2. This butyryl CoA is then utilized by p300 to butyrylate the histones and keep the already transcriptionally active genes firing. Depending on the site being modified, certain site specific modifications might have a more profound effect on gene regulation than others. Based on previously published reports, H4K5 butyrylation could be one such important histone acylation site because modification at this very site has a significance in the context of reader protein Brdt binding to the histones during spermatogenesis (Goudarzi *et al*, 2016). Moreover, it seems to be highly responsive to fatty acid levels, as inhibition of fatty acid synthesis specifically inhibits H4K5 butyrylation without inhibiting acetylation (Gao *et al*, 2021). Our studies also indicate that H4K5 butyrylation could play a special role in gene expression regulation in adipogenesis.

Onset of obesity in mice, either due to excess energy intake through high fat diet consumption or increased *de novo* synthesis of fatty acids due to leptin receptor gene mutation leading to hyperphagic behavior, is accompanied by adipocyte hyperplasia and hypertrophy. LTK-14A, a butyrylation specific inhibitor could efficiently prevent the processes of adipogenesis and adipocyte hypertrophy due to inhibition of H4K5 butyrylation in the epididymal fat pads, the major adipose tissue depot in mice. Thus the compound could attenuate weight gain by selective inhibition of butyrylation without affecting acetylation, thereby highlighting the importance of histone butyrylation in adipogenesis and obesity.

For several decades, various kinds of therapeutic intervention of obesity are being developed. However, only a few of these have been approved by the FDA because of limited safety and efficacy. With the advancement of our understanding of the molecular mechanisms of adipogenesis and thereby the identification of new targets to combat obesity, a large number of new chemical entities (NCE) have been invented which are in different phases of the drug development. There are mainly four ways by which a drug could bring about reduction in obesity – (1) reducing food consumption by controlling the appetite, (2) reducing nutrient assimilation, (3) promoting fatty acid oxidation and (4) inhibiting *de novo* lipogenesis. The drugs which affect the appetite modulate the action of monoamine neurotransmitters such as serotonin and norepinephrine. One such appetite suppressant is sibutramine which prevents the reuptake of serotonin and norepinephrine in the hypothalamus, thereby reducing its concentration (Astrup *et al*, 1998). Although it was widely used as an anti-obesity therapeutic measure, it has been withdrawn recently due to several reports of cardiovascular issues arising as side effects of the drug use (James *et al*, 2010). Fenfluramine is another such drug which could target the serotonergic 5HT-2 agonist and σ_1 receptor antagonist and was used initially for obesity treatment but had to be withdrawn due to heart valve damage caused by it (Smith *et al*, 2006; Connolly *et al*, 1997). Phentermine is a drug that is structurally similar to amphetamine and it can stimulate the release of norepinephrine into the hypothalamus that not only reduces the appetite but

also increases blood pressure (Rothman *et al*, 2001). Due to these undesirable side effects, phentermine in combination with fenfluramine is prescribed as a medication against obesity for short term usage only. Another drug that has been successful in attenuating obesity by application along with phentermine is topiramate that is normally used for treating migraine. It inhibits the gluconeogenesis enzyme fructose 1,6 biphosphatase that leads to reduction of glucose levels in the blood. It also has a suppressive effect on obesity by reducing the appetite (Colman *et al*, 2012), but it has not been FDA approved yet due to its side effects of drowsiness and coordination problems. Amongst the drugs targeting assimilation of nutrients, orlistat has been approved in USA as well as Europe. It inhibits the triacylglycerol lipase in the gastrointestinal tract that reduces dietary fat uptake and weight gain. However, for this compound too, there have been a few reports of undesirable side effects of stomach pain and irregular bowel movement (Ballinger *et al*, 2000). Amongst the drugs that reduce obesity through fatty acid oxidation, rimonabant had shown the greatest promise and was also used in clinical practice in Europe for some time. It increases adiponectin production in the adipocytes which leads to enhanced fatty acid uptake and oxidation (Pagotto *et al*, 2005). However, it is also an inhibitor of the receptor CB1, which is widely expressed in the central nervous system, and therefore causes side effects of anxiety, depression and even sometimes induces suicidal tendencies. The fourth method of pharmaceutically managing obesity is by inhibiting lipid synthesis and adipogenesis. In this aspect HDAC inhibitors like sodium butyrate and Trichostatin A have been found to successfully reduce diet induced obesity in experimental mice models (Gao *et al*, 2009). Short chain fatty acids such as butyrate are produced by the gut microbiota and transported across the gut epithelial barrier via monocarboxylate transporter 1 to reach the portal circulation. Thereafter they could reach other tissues such as adipose tissue and liver and reduce the inflammatory signals associated with obesity (Samuel *et al*, 2008; Kimura *et al*, 2013). By inhibiting HDACs butyrate can make the chromatin conducive for transcription and alter the expression of cholesterol, a precursor for bile acids (Hara *et al*, 1999) as well as restore the expression of glucagon receptor 1 which has been observed to be reduced in murine models

of obesity (Zhou *et al*, 2018). However, clinical trials using butyrate has given inconsistent results wherein it could improve glucose tolerance in healthy individuals but could not improve glucose tolerance or reduce excess weight in patients with obesity associated metabolic syndrome (Bouter *et al*, 2018). In fact, contradictory observations have been made with respect to the detailed mechanistic actions of butyrate and other short chain fatty acids. Cell line based studies of adipogenesis have revealed that while trichostatin A inhibits the process, butyrate actually dose dependently enhances adipogenesis (Haberland *et al*, 2010; Yoo *et al*, 2006). This implies that there could be additional modes of action of butyrate which are context and concentration dependent. Moreover, a recent study has shown that short chain fatty acids such as butyrate can promote autoacylation of p300 by its rapid conversion to butyryl CoA and enhance its catalytic function (Thomas *et al*, 2021). p300 has been known to promote adipogenesis and obesity via its acetyltransferase function. So it appears that butyrate may have different effects depending on its concentration and therefore more research is required to understand its mode of action and effect on obesity. There are other small molecules targeting epigenetic regulators that could also be developed as anti-obesity drugs. p300 acetyltransferase inhibitors such as curcumin (Ejaz *et al*, 2009) and A-485 (Zhou *et al*, 2020) have all been demonstrated to have weight reducing effects. Despite showing promise in specific models of obesity, it cannot be ruled out that there could be collateral damage caused by these drugs in clinical trials due to their targets playing important roles in several other processes besides the disease manifestation.

Name of drug	Mechanism of action	Side effects
DNP (Dinitrophenol)	Mitochondrial uncoupler, browning of fat	Hyperthermia, tachycardia, fever, tachypnoea, death
Diethylpropion/afepromone	Sympathomimetic	Nausea, constipation, insomnia, headache, tension and irritation, seizures
Methamphetamine	Sympathomimetic	High risk for abusiveness and addiction
Phenmetrazine	Sympathomimetic	Nausea, diarrhoea, dry mouth
Phenylpropanolamine	Sympathomimetic	Haemorrhagic stroke
Fenfluramine and dexfenfluramine	Sympathomimetic	Cardiac valvular insufficiency and pulmonary hypertension
Cathine	Sympathomimetic	Tachycardia, increase in blood pressure, restlessness, sleep disorder, depression
Sibutramine	Sympathomimetic	Non-fatal myocardial infarction and stroke (in individuals with pre-existing cardiovascular disorder)
Phentermine	Sympathomimetic	Palpitations, elevated blood pressure
Rimonabant	CB1 receptor blocker	Depression, suicidal ideation
Orlistat	Pancreatic lipase inhibitor	Liver injury, gastrointestinal symptoms
Lorcaserin	5-HT serotonin agonist	Depression, suicidal ideation, palpitations, gastrointestinal symptoms, increased cancer risk
Phentermine/Topiramate ER	Sympathomimetic/anticonvulsant	Depression, suicidal ideation, cardiovascular events, memory loss, birth defects
Naltrexone SR/ Bupropione SR	Dopamine and norepinephrine reuptake inhibitor	Seizures, palpitations, transient blood pressure elevations
Liraglutide	GLP1 receptor agonist	Nausea/vomiting, diarrhoea, constipation, pancreatitis, gallstones
Semaglutide	GLP1 receptor agonist	Nausea/vomiting, diarrhoea, constipation

Table 1: List of anti-obesity drugs that have been removed from the market due to undesirable side effects

Our studies conducted till date, indicate that LTK-14A attenuates obesity principally by reducing the expression of pro-adipogenic genes through inhibition of p300 catalysed histone butyrylation, specifically at H4K5 position. Since butyrylation is a rarer modification compared to acetylation and becomes physiologically relevant only in specific contexts, the butyrylation specific inhibitor LTK-14A might pose less threat for having non-specific effects. Oral administration of LTK-14A in db/db mice led to a slight reduction in food consumption as well, which was reflected in the small reduction in lean mass, indicating that it may have weight reducing effects by inducing calorie

restriction also. But the later effect might be a minor one since the fat mass was much more profoundly impacted by the compound. Improvements could be made in the efficacy of LTK-14A by preparing formulations of this compound for better controlled release and bioavailability of the compound in the targeted tissues.

2) Understanding the importance of histone butyrylation in hepatic steatosis

The mouse models of obesity not only served the purpose of studying the role of butyrylation in adipose tissue but were also used for studying its role in hepatic steatosis. It was observed that our selective inhibitor of butyrylation could prevent ectopic lipid accumulation and hepatocyte ballooning within the liver of these obese mice. Bioavailability of the compound was tested by performing mass spectrometry analysis with metabolites extracted from the liver. Detection of intact LTK-14A in liver extracts indicated that the compound is metabolically stable. Moreover, immunohistochemical analysis revealed that histone H4K5 butyrylation was specifically reduced in the liver by compound treatment while other acetylation modifications were unaffected. Global histone acetylation has previously been reported to remain unchanged in liver and adipose tissues of C57BL6/J mice even after high fat diet consumption (Carrer *et al*, 2017), which was consistent with the observations we made in both mice models studied. Since acetyl CoA is highly abundant, fluctuations in its levels did not lead to major changes in histone acetylation pattern. Because the usual butyryl CoA levels are far less than their corresponding Michaelis Menten constant for p300, an increase in butyryl CoA levels due to excess lipid consumption through high fat diet or *de novo* lipid synthesis through excess food consumption might have resulted in a concomitant increase in butyrylation by p300 which served as the nutritional sensor for butyryl CoA.

We also observed a global increase in histone butyrylation at several sites in a cell line model of glucose induced steatosis of HepG2. Increase in different acetylation marks could not be observed, possibly because immunoblotting gives a reflection of global changes in modification pattern. Previous reports of site specific increased histone acetylation upon glucose induced steatosis had gene specific promoter based studies using chromatin immunoprecipitation.

Treatment with our butyrylation inhibitor LTK-14A repressed the lipid accumulation in HepG2 by downregulating lipogenic gene expression without having any deleterious side effects of toxicity. Just as in organism level, this compound could selectively inhibit histone H4K5 butyrylation in the cell line as well, without affecting acetylation.

Since the butyrylation inhibitor LTK-14A has been effective in preventing ectopic lipid accumulation in liver, the compound could be applied in other more challenging models of hepatic steatosis to test its potential for being developed as a therapeutic option for non-alcoholic fatty liver disease.

Significance and future perspectives

Through our work we have managed to establish the fact that histone butyrylation is causally linked to adipogenesis and hepatic steatosis. We developed a selective inhibitor of p300 catalysed butyrylation to highlight the importance of this modification in processes involving lipid metabolism. To the best of our knowledge, this is the first ever report of a small molecule modulator that selectively inhibits the acyltransferase activity of p300, without affecting its canonical acetyltransferase activity. Our inhibitor was cell permeable and could efficiently repress adipogenesis and hepatic steatosis without having any adverse toxicity effects. It could downregulate the expression of several pro-adipogenic and lipogenic genes by inhibiting histone butyrylation without affecting other epigenetic modifications. This unique inhibitor prevented the weight gain of high fat diet fed mice and reduced the weight of genetically obese mice by preventing adipose tissue hypertrophy and hepatic steatosis. As had been observed *in vitro*, this compound specifically inhibited histone butyrylation without affecting acetylation in both adipose tissue and liver as well.

Based on our findings, butyrylation has been established as a new epigenetic signature in the context of adipogenesis and steatohepatitis. Selective inhibition of butyrylation could be a new target for treatment of obesity and non-alcoholic fatty liver disease.

In this aspect, single dose toxicity test has already been performed in Sprague Dawley rats as a part of preclinical studies for LTK-14A. The maximum tolerated dose of the rats was found to be 1000 mg/Kg body weight which was much higher than the animal equivalent dose used in our mice experiments. No changes in overall body weight, food and water consumption pattern was observed in the compound administered rats compared to the vehicle control treated rats. The general health of the rats was also not affected as the fur coat, nasal mucosa, eyes and conjunctivae remained normal with no discharge. Along this line, due to the promising results shown by our own selective butyrylation inhibitor, developments could be made on its structure and formulations could be prepared for enhancing its efficacy as a possible anti-obesity drug without any compromise in its specificity.

Publications

- 1) **Bhattacharya, A.**, Chatterjee, S., Bhaduri, U., Singh, A.K., Vasudevan, M., Sashidhara, K.V., Guha, R., Natesh, N., Kundu, T.K. EP300 (p300) mediated histone butyrylation is critical for adipogenesis. (Manuscript under consideration)
- 2) Senapati, P., **Bhattacharya, A.***, Das, S*., Dey, S., Sudarshan, D., G., Shyla, Vishwakarma, J., Sudevan, S., Ramachandran, R., Maliekal, T.T., Kundu, T.K. Histone Chaperone Nucleophosmin Regulates Transcription of Key Genes Involved in Oral Tumorigenesis. *Mol Cell Biol* 2022 17; 42(2):e0066920.
(* contributed equally)
- 3) Behera, A.K., Kumar, M., Shanmugam, M.K., **Bhattacharya, A.**, Rao, V.J., Bhat, A., Vasudevan, M., Gopinath, K.S., Mohiyuddin, A., Chatterjee, A., Sethi, G., Kundu, T.K. Functional interplay between YY1 and CARM1 promotes oral carcinogenesis. *Oncotarget*. 2019; 4; 10(38):3709-3724.
- 4) Behera, A.K., **Bhattacharya, A.**, Vasudevan, M., Kundu, T.K. p53 mediated regulation of coactivator associated arginine methyltransferase 1 (CARM1) expression is critical for suppression of adipogenesis. *FEBS J*. 2018; 285(9):1730-1744.

Patents

Title of the invention: Small molecule modulator targeting a rare histone modification, regulating adipogenesis and pharmaceutical formulation thereof.

Inventors: Kundu T K, **Bhattacharya A**, Chatterjee S, Sashidhara K V, Singh S P, Mishra P R, Nazir A, Guha R.

Indian provisional patent application number: 202111024677

References

- Afshin, A. et al. Health effects of overweight and obesity in 195 countries over 25 years. *N. Engl. J. Med.* 2017; 377, 13–27.
- Aik, W. et al. Structural basis for inhibition of the fat mass and obesity associated protein (FTO). *J. Med.Chem.* 2013; 56, 3680–3688.
- Akinci, B., Meral, R., Oral, E.A. Phenotypic and Genetic Characteristics of Lipodystrophy: Pathophysiology, Metabolic Abnormalities, and Comorbidities. *Curr. Diab. Rep.* 2018; 18, 143.
- Albaugh, B. N., Kolonko, E. M. and Denu, J. M. Kinetic mechanism of the Rtt109–Vps75 histone acetyltransferase-chaperone complex. *Biochemistry* 2010; 49, 6375–6385.
- Ali, M. et al. Tandem PHD fingers of MORF/MOZ acetyltransferases display selectivity for acetylate histone H3 and are required for the association with chromatin. *J. Mol. Biol.* 2012; 424, 328–338.
- Allaman, I., Bélanger, M. and Magistretti, P. J. Methylglyoxal, the dark side of glycolysis. *Front. Neurosci.* 2015; 9, 23–34.
- Allis, C.D., Jenuwein, T. The molecular hallmarks of epigenetic control. *Nat Rev Genet.* 2016; 17:487–500.
- Anand, R. and Marmorstein, R. Structure and mechanism of lysine-specific demethylase enzymes. *J. Biol. Chem.* 2007; 282, 35425–35429.
- Andrews, F. H. et al. The Taf14 YEATS domain is a reader of histone crotonylation. *Nat. Chem. Biol.* 2016; 12,396–398.
- Arango, D. et al. Acetylation of cytidine in mRNA promotes translation efficiency. *Cell* 2018; 175, 1872–1886. e1824 .
- Arif, M. et al. Nitric oxide-mediated histone hyperacetylation in oral cancer: target for a water-soluble HAT inhibitor, CTK7A. *Chem. Biol.* 2010; 17, 903–913.

Astrup, A., Hansen, D. L., Lundsgaard, C., and Toubro, S. Sibutramine and energy balance. *Int. J. Obes. Relat. Metab. Disord.* 1998; 22 (Suppl. 1), S30-5;discussion S 36–37, S42.

Bai, P. and Cantó, C. The role of PARP-1 and PARP-2 enzymes in metabolic regulation and disease. *Cell Metab.* 2012; 16, 290–295.

Bailey, M. H. et al. Comprehensive characterization of cancer driver genes and mutations. *Cell* 2018; 173, 371–385.e1.

Balasubramanyam, K., Swaminathan, V., Ranganathan, A. and Kundu, T. K. Small molecule modulators of histone acetyltransferase p300. *J. Biol. Chem.* 2003; 278, 19134–19140.

Balasubramanyam, K. et al. Curcumin, a novel p300/ CREB-binding protein-specific inhibitor of acetyltransferase, represses the acetylation of histone/nonhistone proteins and histone acetyltransferase- dependent chromatin transcription. *J. Biol. Chem.* 2004; 279, 51163–51171.

Balasubramanyam, K. et al. Polyisoprenylated benzophenone, garcinol, a natural histone acetyltransferase inhibitor, represses chromatin transcription and alters global gene expression. *J. Biol. Chem.* 2004; 279, 33716–33726.

Ballinger, A. Orlistat in the treatment of obesity. *Expert Opin. Pharmacother.* 2000; 1, 841–847.

Bandyopadhyay, K., Baneres, J. L., Martin, A., Blonski, C., Parello, J. and Gjerset, R. A. Spermidinyl-CoA-based HAT inhibitors block DNA repair and provide cancer-specific chemo- and radiosensitization. *Cell Cycle* 2009, 8, 2779–2788.

Bao, X. et al. Glutarylation of histone H4 lysine 91 regulates chromatin Dynamics. *Mol. Cell* 2019; 76, 660–675.e9.

Barak, Y. et al. PPAR γ is required for placental, cardiac and adipose tissue development. *Mol Cell* 1999; 4:585-95.

Barbarroja, N. et al. The obese healthy paradox: is inflammation the answer? *Biochem. J.* 2010, 430, 141–9.

Bargut, T.C.L., Souza-Mello, V., Aguila, M.B. and Mandarim-de-Lacerda, C.A. Browning of white adipose tissue: Lessons from experimental models. *Horm. Mol. Biol. Clin. Investig.* 2017, 31.

Batie, M. et al. Hypoxia induces rapid changes to histone methylation and reprograms chromatin. *Science* 2019; 363, 1222–1226 .

Bazopoulou, D. et al. Developmental ROS individualizes organismal stress resistance and lifespan. *Nature* 2019; 576, 301–305.

Bedford, M.T., Frankel, A., Yaffe, M.B., Clarke, S., Leder, P. and Richard, S. Arginine methylation inhibits the binding of proline-rich ligands to Src homology 3, but not WW, domains. *J Biol Chem.* 2000; 26; 275(21):16030-6.

Belenky, P. et al. Nicotinamide riboside promotes Sir2 silencing and extends lifespan via Nrk and Urh1/Pnp1/Meu1 pathways to NAD⁺. *Cell* 2007; 129, 473–484.

Bennett, C.N. et al. Regulation of osteoblastogenesis and bone mass by Wnt10b. *Proc Natl Acad Sci USA* 2005; 102:3324-9.

Berndsen, C. E., Albaugh, B. N., Tan, S. and Denu, J. M. Catalytic mechanism of a MYST family histone acetyltransferase. *Biochemistry* 2007; 46, 623–629.

Berriot-Varoqueaux, N., Aggerbeck, L.P., Samson-Bouma, M. and Wetterau, J.R. The role of the microsomal triglyceride transfer protein in abetalipoproteinemia. *Annu. Rev. Nutr.* 2000; 20, 663–697.

Bhanu, N. A.-S., L. and Garcia, B. A. Quantification of lysine crotonylation during in vitro human myogenic differentiation. The 61st Annu. Am. Soc. Mass Spectrom. Conference Mass Spectrom. Allied Top. <https://www.abstracts.asms.org/pages/dashboard.html#/conference/253/toc/253/details> 2013.

Billon, N. et al. The generation of adipocytes by the neural crest. *Development* 2007; 134:2283-92.

Billon, N., Monteiro, M.C. and Dani, C. Developmental origin of adipocytes: new insights into a pending question. *Biol Cell* 2008; 100:563-75.

Blüher, M. Adipose tissue dysfunction contributes to obesity related metabolic diseases. *Best Pract. Res. Clin. Endocrinol. Metab.* 2013; 27, 163–177.

Bose, S., Ramesh, V. and Locasale, J. W. Acetate metabolism in physiology, cancer, and beyond. *Trends Cell Biol.* 2019; 29, 695–703.

Bouter, K. et al. Differential metabolic effects of oral butyrate treatment in lean versus metabolic syndrome subjects. *Clin Transl Gastroenterol.* 2018;9:155.

Boutaud, O., Andreasson, K. I., Zagol-Ikapitte, I. and Oates, J. A. Cyclooxygenase-dependent lipid-modification of brain proteins. *Brain Pathol.* 2005; 15, 139–142.

Bowers, E. M. et al. Virtual ligand screening of the p300/CBP histone acetyltransferase: identification of a selective small molecule inhibitor. *Chem. Biol.* 2010; 17, 471–482.

Bracken, A.P., Dietrich, N., Pasini, D., Hansen, K.H. and Helin, K. Genome-wide mapping of Polycomb target genes unravels their roles in cell fate transitions. *Genes Dev* 2006; 20:1123-36.

Bradbury, M.W. and Berk, P.D. Lipid metabolism in hepatic steatosis. *Clin. Liver Dis.* 2004; 8, 639–671, xi.

Bricambert, J., Miranda, J., Benhamed, F., Girard, J., Postic, C. and Dentin, R. Salt-inducible kinase 2 links transcriptional coactivator p300 phosphorylation to the prevention of ChREBP dependent hepatic steatosis in mice. *J Clin Invest* 2010; 120 (12) : 4316–4331.

Bricambert, J. et al. The histone demethylase Phf2 acts as a molecular checkpoint to prevent NAFLD progression during obesity. *Nat Commun* 2018; 9:2092.

Brown, K.D. et al. Activation of SIRT3 by the NAD⁺ precursor nicotinamide riboside protects from noise-induced hearing loss. *Cell Metab.* 2014; 20, 1059–1068.

Browning, J.D. and Horton, J.D. Molecular mediators of hepatic steatosis and liver injury. *J. Clin. Invest* 2004; 114, 147–152.

Brownell, J. E., and Allis, C. D. An activity gel assay detects a single, catalytically active histone acetyltransferase subunit in *Tetrahymena macronuclei*. *Proc. Natl. Acad. Sci. U. S. A.* 1995; 92, 6364–6368. doi: 10.1073/pnas.92.14.6364.

Brunt, E.M. Nonalcoholic steatohepatitis. *Semin. Liver Dis.* 2004; 24, 3–20.

Burgeois, C. et al. Specific Biological Features of Adipose Tissue, and their impact on HIV persistence. *Front Microbiol* 2019 17;10:2837.

Cabal-Hierro, L. et al. Chromatin Accessibility Promotes Hematopoietic and Leukemia Stem Cell Activity. *Nat. Commun.* 2020; 11.

Cannon, B. and Nedergaard, J. Brown adipose tissue: function and physiological significance. *Physiol Rev* 2004; 84:277-359.

Cao, Z., Umek, R.M., and McKnight, S.L. Regulated expression of three C/EBP isoforms during adipose conversion of 3T3-L1 cells. *Genes Dev.* 1991; 5, 1538–1552.

Cao, Y. et al. Hepatic menin recruits SIRT1 to control liver steatosis through histone deacetylation. *J Hepatol* 2013; 59:1299–1306.

Cao, J., Lou, S., Ying, M. and Yang, B. DJ-1 as a human oncogene and potential therapeutic target. *Biochem. Pharmacol.* 2015; 93, 241–250.

Cao, J. et al. HDAC11 regulates type I interferon signaling through defattyacylation of SHMT2. *Proc Natl Acad Sci U S A* 2019; 116, 5487.

Carey, B. W., Finley, L. W. S., Cross, J. R., Allis, C. D. and Thompson, C. B. Intracellular α -ketoglutarate maintains the pluripotency of embryonic stem cells. *Nature* 2015; 518, 413–416.

Carobbio, S., Pellegrinelli, V. and Vidal-Puig, A. Adipose Tissue Function and Expandability as Determinantsof Lipotoxicity and the Metabolic Syndrome. *In Advances in Experimental Medicine and Biology; Springer New York LLC, 2017; Vol. 960, pp. 161–196.*

Carrer, A. *et al.* Impact of a High-fat Diet on Tissue Acyl-CoA and Histone Acetylation Levels. *J Biol Chem* 2017;292:3312-3322.

Carrier, E. J., Zagol-Ikapitte, I., Amarnath, V., Boutaud, O. and Oates, J. A. Levuglandin forms adducts with histone h4 in a cyclooxygenase- 2-dependent manner, altering its interaction with DNA. *Biochemistry* 2014; 53, 2436–2441.

Carvalho, E., Jansson, P.A., Nagaev, I., Wentzel, A.M. and Smith, U. Insulin resistance with low cellular IRS-1 expression is also associated with low GLUT4 expression and impaired insulin-stimulated glucose transport. *FASEB J.* 2001; 15, 1101–1103.

Castellano-Castillo, D. *et al.* Adipose tissue inflammation and VDR expression and methylation in colorectal cancer. *Clin. Epigenetics* 2018; 10, 1–10.

Cervera, A.M. *et al.* Inhibition of succinate dehydrogenase dysregulates histone modification in mammalian cells. *Mol. Cancer* 2009; 8, 89.

Chakraborty, A. A. *et al.* Histone demethylase KDM6A directly senses oxygen to control chromatin and cell fate. *Science* 2019 363, 1217–1222.

Chalasani, N. *et al.* The diagnosis and management of nonalcoholic fatty liver disease: Practice guidance from the American Association for the Study of Liver Diseases. *Hepatology* 2018; 67, 328–357.

Chatterjee, S. *et al.* A novel activator of CBP/p300 acetyltransferases promotes neurogenesis and extends memory duration in adult mice. *J. Neurosci.* 2013; 33, 10698–10712.

Chen, S. *et al.* Both coactivator LXXLL motif dependent and -independent interactions are required for PPAR γ function. *J Biol Chem* 2000; 275:3733-6.

Chen, Y. *et al.* Lysine propionylation and butyrylation are novel post-translational modifications in histones. *Mol. Cell. Proteomics* 2007; 6, 812–819.

Chen, P.B. *et al.* Hdac6 Regulates Tip60-P400 Function in Stem Cells. *eLife* 2013, 2 :e01557..

Chen, Q., Chen, Y., Bian, C., Fujiki, R. and Yu, X. TET2 promotes histone O-GlcNAcylation during gene transcription. *Nature* 2013; 493, 561–564.

Cheng, X., Collins, R.E. and Zhang, X. Structural and sequence motifs of protein (histone) methylation enzymes. *Annu Rev Biophys Biomol Struct.* 2005; 34:267–294.

Cheng, P. et al. Tumor suppressor Menin acts as a corepressor of LXRA to inhibit hepatic lipogenesis. *FEBS Lett* 2015; 589:3079–3084.

Chick, J. M. et al. A mass-tolerant database search identifies a large proportion of unassigned spectra in shotgun proteomics as modified peptides. *Nat. Biotechnol.* 2015; 33, 743–749.

Chouchani, E.T. and Kajimura, S. Metabolic adaptation and maladaptation in adipose tissue. *Nat. Metab.* 2019; 1, 189–200.

Ciccarone, F., Zampieri, M. and Caiafa, P. PARP1 orchestrates epigenetic events setting up chromatin domains. *Semin. Cell Dev. Biol.* 2017; 63, 123–134.

Clemente-Postigo, M. and Tinahones, F.J. Do metabolically healthy obese subjects exist? *Overweight and obesity* 2015; pp. 175–187.

Cluntun, A.A., Huang, H., Dai, L., Liu, X., Zhao, Y. and Locasale, J.W. The rate of glycolysis quantitatively mediates specific histone acetylation sites. *Cancer Metab* 2015; 23;3:10.

Colman, E., Golden, J., Roberts, M., Egan, A., Weaver, J., and Rosebraugh, C. The FDA's assessment of two drugs for chronic weight management. *N. Engl. J. Med.* 2012; 367, 1577–1579. doi: 10.1056/NEJMp1211277.

Connolly, H. M. et al. Valvular heart disease associated with fenfluramine-phentermine. *N. Engl. J. Med.* 1997; 337, 581–588. doi: 10.1056/NEJM199708283370901.

Costi, R. et al. Cinnamoyl compounds as simple molecules that inhibit p300 histone acetyltransferase. *J. Med. Chem.* 2007; 50, 1973–1977.

Cousin, B. et al. Occurrence of brown adipocytes in rat white adipose tissue: Molecular and morphological characterization. *J Cell Sci* 1992; 103 (Pt 4): 931–942.

Crewe, C., An, Y.A. and Scherer, P.E. The ominous triad of adipose tissue dysfunction: Inflammation, fibrosis, and impaired angiogenesis. *J. Clin. Invest.* 2017; 127, 74–82.

Cullis, P. M., Wolfenden, R., Cousens, L. S. and Alberts, B. M. Inhibition of histone acetylation by N-[2-(S-coenzyme A)acetyl] spermidine amide, a multisubstrate analog. *J. Biol. Chem.* 1982; 257,12165–12169.

Cypess, A.M. et al. Identification and importance of brown adipose tissue in adult humans. *N Engl J Med* 2009; 360:1509-17.

Dai, L. Z. et al. Lysine 2-hydroxyisobutyrylation is a widely distributed active histone mark. *Nat. Chem.Biol.* 2014; 10, 365–370.

Dai, Z., Mentch, S. J., Gao, X., Nichenametla, S. N. and Locasale, J. W. Methionine metabolism influences genomic architecture and gene expression through H3K4me3 peak width. *Nat. Commun.* 2018; 9, 1955.

Dancy, B. M. et al. Live-cell studies of p300/CBP histone acetyltransferase activity and inhibition. *ChemBioChem* 2012; 13, 2113–2121.

Davegårdh, C. et al. DNA methylation in the pathogenesis of type 2 diabetes in humans. *Mol. Metab.* 2018; 14, 12–25.

Day, C.P. and James, O.F. Steatohepatitis: a tale of two ‘hits’? *Gastroenterology* 1998; 114, 842–845.

Day, C.P. Pathogenesis of steatohepatitis. *Best. Pract. Res. Clin. Gastroenterol.* 2002; 16, 663–678.

Deaton, A.M. and Bird, A. CpG islands and the regulation of transcription. *Genes Dev.* 2011; 25, 1010–1022.

Ddavecchio, M., Gaucher, J., Aguilar-Gurrieri, C., Ortega, E. and Panne, D. Structure of the p300 catalytic core and implications for chromatin targeting and HAT regulation. *Nat Struct Mol Biol* 2013 ;20(9):1040-6.

de Hoon, M. J. L., Imoto, S., Nolan, J. and Miyano, S. Open source clustering software. *Bioinformatics* 2004;9:1453-1454

den Besten, G. et al. The role of short-chain fatty acids in the interplay between diet, gut microbiota, and host energy metabolism. *J. Lipid Res.* 2013; 54, 2325–2340.

Dentin, R., Girard, J. and Postic, C. Carbohydrate responsive element binding protein (ChREBP) and sterol regulatory element binding protein-1c (SREBP-1c): two key regulators of glucose metabolism and lipid synthesis in liver. *Biochimie* 2005; 87, 81–86.

Deplus, R. et al. Dnmt3L is a transcriptional repressor that recruits histone deacetylase. *Nucleic Acids Res.* 2002; 30, 3831–3838.

Dhar, S. et al. Loss of the major type I arginine methyltransferase PRMT1 causes substrate scavenging by other PRMTs. *Sci. Rep.* 2013; 3, 1311.

Ding, W. et al. Stress-responsive and metabolic gene regulation are altered in low S-adenosylmethionine. *PLoS Genet.* 2018; 14, e1007812.

Doi, M., Hirayama, J., and Sassone-Corsi, P. Circadian regulator CLOCK is a histone acetyltransferase. *Cell* 2006; 125, 497–508. doi: 10.1016/j.cell.2006.03.033.

Dreveny, I. et al. The double PHD finger domain of MOZ/MYST3 induces α -helical structure of the histone H3 tail to facilitate acetylation and methylation sampling and modification. *Nucleic Acids Res.* 2014; 42,822–835.

Du, J. T. et al. Sirt5 is a NAD-dependent protein lysine demalonylase and desuccinylase. *Science* 2011; 334, 806–809.

Eissenberg, J.C. and Elgin, S.C.R. HP1a: a structural chromosomal protein regulating transcription. *Trends Genet.* 2014; 30, 103–110.

Enerback, S. The origins of brown adipose tissue. *N Engl J Med* 2009; 360:n2021–2023.

Eslam, M., Valenti, L., and Romeo, S. Genetics and epigenetics of NAFLD and NASH: Clinical impact. *J. Hepatol.* 2018; 68, 268–279.

Estève, P.O. et al. Direct interaction between DNMT1 and G9a coordinates DNA and histone methylation during replication. *Genes Dev.* 2006; 20, 3089–3103.

Fajas, L. et al. The retinoblastoma-histone deacetylase 3 complex inhibits PPAR γ and adipocyte differentiation. *Dev Cell* 2002; 3:903-10.

Fan, J. et al. Metabolic regulation of histone posttranslational modifications. *ACS Chem. Biol.* 2015; 10, 95–108.

Fan, Z. et al. MKL1 is an epigenetic modulator of TGF- β induced fibrogenesis . *Biochim Biophys Acta* 2015; 1849 (9): 1219–1228.

Fang, S. et al. The p300 acetylase is critical for ligand-activated farnesoid X receptor (FXR) induction of SHP. *J Biol Chem* 2008; 283 (50): 35086–35095.

Fang, F., Xu, Y., Chew, K.-K., Chen, X., Ng, H.-H. and Matsudaira, P. Coactivators P300 and CBP Maintain the Identity of Mouse Embryonic Stem Cells by Mediating Long-Range Chromatin Structure. *Stem Cells* 2014; 32, 1805–1816.

Farmer, S.R. Transcriptional control of adipocyte formation. *Cell Metab* 2006; 4:263-73.

Farmer, S.R. Molecular determinants of brown adipocyte formation and function. *Genes Dev* 2008; 22:1269-75

Farrelly, L. A. et al. Histone serotonylation is a permissive modification that enhances TFIID binding to H3K4me3. *Nature* 2019; 567, 535–539.

Feldman, J.L. et al. Sirtuin catalysis and regulation. *J. Biol. Chem.* 2012; 287, 42419–42427.

Feldman, J.L. et al. Activation of the protein deacetylase SIRT6 by long-chain fatty acids and widespread deacylation by mammalian sirtuins. *J. Biol. Chem.* 2013; 288, 31350–31356.

Fellows, R. et al. Microbiota derived short chain fatty acids promote histone crotonylation in the colon through histone deactylases. *Nat Commun* 2018; 9(1):105.

Feng, Q. et al. Methylation of H3-lysine 79 is mediated by a new family of HMTases without a SET domain *Curr Biol* 2002; 12(12):1052-8.

Flynn, E. M. et al. A subset of human bromodomains recognizes butyryllysine and crotonyllysine histone peptide modifications. *Structure* 2015; 23, 1801–1814.

Folmes, C. D. et al. Somatic oxidative bioenergetics transitions into pluripotency-dependent glycolysis to facilitate nuclear reprogramming. *Cell Metab.* 2011; 14, 264–271.

Fouse, S.D. et al. Promoter CpG methylation contributes to ES cell gene regulation in parallel with Oct4/Nanog, PcG complex, and histone H3 K4/K27 trimethylation. *Cell Stem Cell* 2008; 2:160-9.

Freedman, S. J. et al. Structural basis for recruitment of CBP/p300 by hypoxia-inducible factor-1 α . *Proc Natl Acad Sci U S A* 2002; 99 (8) : 5367–5372.

Fu, S. and Kurzrock, R. Development of curcumin as an epigenetic agent. *Cancer* 2010; 116, 4670–4676.

Fu, M. et al. Cyclin D1 inhibits PPAR γ -mediated adipogenesis through histone deacetylase recruitment. *J Biol Chem* 2005; 280:16934-41.

Fuks, F. et al. T. DNA methyltransferase Dnmt1 associates with histone deacetylase activity. *Nat. Genet.* 2000; 24, 88–91.

Galligan, J. J. et al. Stable histone adduction by 4-oxo-2-nonenal: a potential link between oxidative stress and epigenetics. *J. Am. Chem. Soc.* 2014; 136, 11864–11866.

Gao, Z. et al. Butyrate improves insulin sensitivity and increases energy expenditure in mice. *Diabetes* 2009; 58, 1509–1517. doi: 10.2337/db08-1637.

Gao, X. N. et al. A histone acetyltransferase p300 inhibitor C646 induces cell cycle arrest and apoptosis selectively in AML1-ETO-positive AML cells. *PLoS One* 2013; 8, e55481.

Gao, X. et al. Acetate functions as an epigenetic metabolite to promote lipid synthesis under hypoxia. *Nat Commun* 2016; 7:11960.

Gao, M. et al. Metabolically controlled histone H4K5 acylation/acetylation ratio drives BRD4 genomic distribution. *Cell Rep* 2021; 36(4):109460.

Gelman, L., Zhou, G., Fajas, L., Raspe, E., Fruchart and J.C., Auwerx, J. p300 interacts with the N- and C-terminal part of PPAR γ 2 in a ligand-independent and – dependent manner, respectively. *J Biol Chem* 1999; 274:7681-8.

Geoghegan, V., Guo, A., Trudgian, D., Thomas, B. and Acuto, O. Comprehensive identification of arginine methylation in primary T cells reveals regulatory roles in cell signalling. *Nat. Commun.* 2015; 6, 6758.

George, J., Pera, N., Phung, N., Leclercq, I., Yun Hou, J. and Farrell, G. Lipid peroxidation, stellate cell activation and hepatic fibrogenesis in a rat model of chronic steatohepatitis. *J. Hepatol.* 2003; 39, 756–764.

Gerken, T. et al. The obesity-associated FTO gene encodes a 2-oxoglutarate-dependent nucleic acid demethylase. *Science* 2007; 318, 1469–1472.

Gesta, S. et al. Evidence for a role of developmental genes in the origin of obesity and body fat distribution. *Proc Natl Acad Sci USA* 2006; 103:6676-81.

Ghizzoni, M., Wu, J., Gao, T., Haisma, H. J., Dekker, F. J. and George Zheng, Y. 6-alkylsalicylates are selective Tip60 inhibitors and target the acetyl-CoA binding site. *Eur. J. Med. Chem.* 2012; 47, 337–344.

Ghorbani, M. and Himms-Hagen, J. Appearance of brown adipocytes in white adipose tissue during CL 316,243-induced reversal of obesity and diabetes in Zucker fa/fa rats. *Int J Obes Relat Metab Disord* 1997; 21: 465–475.

Giandomenico, V., Simonsson, M., Grönroos, E., and Ericsson, J. Coactivator-dependent acetylation stabilizes members of the SREBP family of transcription factors. *Mol Cell Biol* 2003; 23 (7) 2587–2599.

Glozak, M.A. and Seto, E. Histone deacetylases and cancer. *Oncogene* 2007; 26:5420-32.

Goodman, R.H. and Smolik, S. CBP/p300 in cell growth, transformation, and development. *Genes Dev.* 2000; 14, 1553–1577.

Goudarzi, A. et al. Dynamic competing histone H4K5K8 acetylation and butyrylation are hallmarks of highly active gene promoters. *Mol. Cell* 2016; 62, 169–180.

Goudarzi, A., Hosseinmardi, N., Salami, S., Mehdikhani, F., Derakshan, S. and Amnishakib P. Starvation promotes histone lysine butyrylation in the liver of male but not female mice. *Gene* 2020; 30;745:144647.

Greenberg, M.V.C. and Bourc'his, D. The diverse roles of DNA methylation in mammalian development and disease. *Nat. Rev. Mol. Cell Biol.* 2019; 20, 590–607.

Guerra, C., Koza, R.A., Yamashita, H, Walsh, K. and Kozak, L.P. Emergence of brown adipocytes in white fat in mice is under genetic control. Effects on body weight and adiposity. *J Clin Invest* 1998; 102: 412–420.

Guerrerio, A.L. et al. Choline intake in a large cohort of patients with nonalcoholic fatty liver disease. *Am. J. Clin. Nutr.* 2012; 95, 892–900.

Haberland, M., Carrer, M., Mokalled, H.M., Montgomery, R.L. and Olson, E.R. Redundant control of adipogenesis by histone deacetylases 1 and 2. *J Biol Chem* 2010; 285(19):14663-70.

Hadzopoulou-Cladaras, M., Kistanova, E., Evagelopoulou, C., Zeng, S., Cladaras, C. and Ladias, J. A. A. Functional domains of the nuclear receptor hepatocyte nuclear factor 4. *J Biol Chem* 1997; 272 (1) 539–550.

Halim, A.B. et al. Expression and functional interaction of the catalytic and regulatory subunits of human methionineadenosyltransferase in mammalian cells. *J. Biol. Chem.* 1999; 274,29720–29725.

Hamed, M., Khilji, S., Chen, J. and Li, Q. Stepwise Acetyltransferase Association and Histone Acetylation at the Myod1 Locus during Myogenic Differentiation. *Sci. Rep.* 2013; 3, 2390.

Hamm, J.K., Park, B.H., and Farmer, S.R. A role for C/EBPbeta in regulating peroxisome proliferator-activated receptor gamma activity during adipogenesis in 3T3-L1 preadipocytes. *J. Biol. Chem.* 2001; 276, 18464–18471.

Hammarstedt, A., Gogg, S., Hedjazifar, S., Nerstedt, A. and Smith, U. Impaired adipogenesis and dysfunctional adipose tissue in human hypertrophic obesity. *Physiol. Rev.* 2018, 98, 1911–1941.

Han, Z. et al. Revealing the protein propionylation activity of the histone acetyltransferase MOF (males absent on the first). *J. Biol. Chem.* 2018; 293, 3410–3420.

Hara, H., Haga, S., Aoyama, Y. and Kiriya, S. Short-chain fatty acids suppress cholesterol synthesis in rat liver and intestine. *J Nutr.* 1999;129:942–8.

Haws, S.A. et al. Methyl-metabolite depletion elicit adaptive responses to support heterochromatin stability and epigenetic persistence. *Mol. Cell* 2020; 78, 210–223.

Hayakawa, T. and Nakayama, J. Physiological roles of class I HDAC complex and histone demethylase. *J Biomed Biotechnol* 2011; 2011:129383.

Hayashi, T., Boyko, E. J., McNeely, M. J., Leonetti, D. L., Kahn, S. E., and Fujimoto, W. Y. Visceral adiposity, not abdominal subcutaneous fat area, is associated with

an increase in future insulin resistance in Japanese Americans. *Diabetes* 2008; 57, 1269–1275.

Hayhurst, G. P., Lee, Y. H., Lambert, G., Ward, J. M. and Gonzalez, F. J. Hepatocyte nuclear factor 4alpha (nuclear receptor 2A1) is essential for maintenance of hepatic gene expression and lipid homeostasis. *Mol Cell Biol* 2001; 21 : 1393-403.

Hendrich, B. and Bird, A. Identification and characterization of a family of mammalian methyl-CpG binding proteins. *Mol. Cell. Biol.* 1998; 18, 6538–6547.

Hluschchuk, I., Ruskoaho, H., Domanskyi, A., Airavaara, M., Valimaki and M.J. Domain-Independent Inhibition of CBP/p300 Attenuates α -Synuclein Aggregation. *ACS Chem Neurosci.* 2021; 7;12(13):2273-2279.

Ho, C. et al. SIRT1 markedly extends replicative lifespan if the NAD⁺ salvage pathway is enhanced. *FEBS Lett.* 2009; 583, 3081–3085.

Holoch, D. and Margueron, R. Mechanisms regulating PRC2 recruitment and enzymatic activity. *Trends Biochem. Sci.* 2017 42, 531–542.

Horton, J.D. Sterol regulatory element-binding proteins: transcriptional activators of lipid synthesis. *Biochem Soc Trans* 2002; 30, 6:1091–1095.

Hosokawa, Y., Shimomura, Y., Harris, R.A. and Ozawa, T. Determination of short-chain acyl-coenzyme A esters by high-performance liquid chromatography. *Anal. Biochem.* 1986 153, 45–49.

Hou, Y. et al. 5mC profiling characterized TET2 as an anti-adipogenic demethylase. *Gene* 2020 733:144265. doi: 10.1016/j.gene.2019.144265

Hsieh, Y. J., Kundu, T. K., Wang, Z., Kovelman, R. and Roeder, R. G. The TFIIC90 subunit of TFIIC interacts with multiple components of the RNA polymerase III machinery and contains a histone-specific acetyltransferase activity. *Mol. Cell. Biol.* 1999, 19, 7697–7704.

Huang, Z., Cai, L. and Tu, B.P. Dietary control of chromatin. *Curr Opin Cell Biol.* 2015; 34:69–74.

Huang, K.-H., Hao, L., Smith, P. B., Rogers, C. J., Patterson, A. D. and Ross, A. C. Lipid emulsion added to a liquid high-carbohydrate diet and voluntary running exercise reduce lipogenesis and ameliorate early-stage hepatic steatosis in mice. *J Nutr* 2017; 147(5): 746–753.

Huang, H. et al. Lysine benzoylation is a histone mark regulated by SIRT2. *Nat. Commun.* 2018; 9, 3374.

Hubbard, B.P. and Sinclair, D.A. Small molecule SIRT1 activators for the treatment of aging and age-related diseases. *Trends Pharmacol. Sci.* 2014; 35, 146–154.

Hughes RM, Waters ML. Arginine methylation in a beta-hairpin peptide: implications for Arg-pi interactions, DeltaCp(o), and the cold denatured state. *J Am Chem Soc.* 2006; 128:12735–12742.

Huttunen, P., Hirvonen, J. and Kinnula, V. The occurrence of brown adipose tissue in outdoor workers. *Eur J Appl Physiol Occup Physiol* 1981; 46: 339–345.

Hussain, M. M., Nijstad, N., and Franceschini, L. Regulation of microsomal triglyceride transfer protein. *Clin Lipidol* 2011; 6 (3): 293–303.

Ibdah, J.A. et al. Lack of mitochondrial trifunctional protein in mice causes neonatal hypoglycemia and sudden death. *J. Clin. Invest* 2001; 107, 1403–1409.

Ibdah, J.A. et al. Mice heterozygous for a defect in mitochondrial trifunctional protein develop hepatic steatosis and insulin resistance. *Gastroenterology* 2005; 128, 1381–1390.

Iizuka, K., Bruick, R. K., Liang, G., Horton, J. D. and Uyeda, K. Deficiency of carbohydrate response element-binding protein (ChREBP) reduces lipogenesis as well as glycolysis. *Proc Natl Acad Sci U S A* 2004; 101(19):7281–7286.

Inagaki, T. et al. Obesity and metabolic syndrome in histone demethylase JHDM2a-deficient mice. *Genes Cells* 2009; 14:991–1001.

Infantino, S., Benz, B., Waldmann, T., Jung, M., Schneider, R. and Reth, M. Arginine methylation of the B cell antigen receptor promotes differentiation. *J. Exp. Med.* 2010; 207, 711–719.

Infantino, S. et al. Arginine methylation catalyzed by PRMT1 is required for B cell activation and differentiation. *Nat. Commun.* 2017; 8, 891.

Inoue, Y. et al. Smad3 is acetylated by p300/CBP to regulate its transactivation activity. *Oncogene* 2007; 26 (4) : 500–508.

Inoue, M. et al. Arginine methylation controls the strength of γ c- family cytokine signaling in T cell maintenance. *Nat. Immunol.* 2018; 19, 1265–1276.

Ishiguro, T. et al. Malonylation of histone H2A at lysine 119 inhibits Bub1-dependent H2A phosphorylation and chromosomal localization of shugoshin proteins. *Sci. Rep.* 2018; 8, 7671.

Ito, S. et al. Human NAT10 is an ATP-dependent RNA acetyltransferase responsible for *N*-4-acetylcytidine formation in 18 S ribosomal RNA (rRNA). *J. Biol.Chem.* 2014; 289, 35724–35730.

Jackson, V. et al. Studies on highly metabolically active acetylation and phosphorylation of histones. *J Biol Chem.* 1975; 250(13):4856–63.

Jakkaraju, S., Zhe, X., Pan, D., Choudhury,, R. and Schuger, L. TIPs are tension-responsive proteins involved in myogenic versus adipogenic differentiation. *Dev Cell* 2005; 9:39-49.

James, W. P. T. et al. Effect of sibutramine on cardiovascular outcomes in overweight and obese subjects. *N. Engl. J. Med.* 2010; 363, 905–917.

Jang, J. et al. Berberine activates AMPK to suppress proteolytic processing, nuclear translocation and target DNA binding of SREBP-1c in 3T3-L1 adipocytes. *Mol Med Rep* 2017; 15(6): 4139–4147.

Jiang, Y. et al. Iron-dependent histone 3 lysine 9 demethylation controls B cell proliferation and humoral immune responses. *Nat. Commun.* 2019; 10, 2935.

Jin, J. et al. Increased expression of enzymes of triglyceride synthesis is essential for the development of hepatic steatosis. *Cell Reports* 2013; 3:831–843.

Jin, J., He, B., Zhang, X., Lin, H. and Wang, Y. SIRT2 reverses 4-oxononanoyl lysine modification on histones. *J. Am. Chem. Soc.* 2016; 138, 12304–12307.

Jing, H. and Lin, H. Sirtuins in epigenetic regulation. *Chem. Rev.* 2015; 115, 2350–2375.

Jo, C. et al. Histone acylation marks respond to metabolic perturbations and enable cellular adaptation. *Exp Mol Med* 2020; 52(12):2005-2019.

Kaczmarek, Z. et al. Structure of p300 in complex with acyl-CoA variants. *Nat. Chem. Biol.* 2016; 13(1):21-29.

Kabashima, T., Kawaguchi, T., Wadzinski, B.E. and Uyeda, K. Xylulose 5-phosphate mediates glucose-induced lipogenesis by xylulose 5-phosphate-activated protein phosphatase in rat liver. *Proc Natl Acad Sci U S A* 2003 (100): 5107–5112.

Kajimura, S. et al. Regulation of the brown and white fat gene programs through a PRDM16/CtBP transcriptional complex. *Genes Dev* 2008; 22: 1397–1409.

Kajimura, S. et al. Initiation of myoblast to brown fat switch by a PRDM16-C/EBP β transcriptional complex. *Nature* 2009; 460:1154-8.

Kalkhoven, E. CBP and p300: HATs for different occasions. *Biochem. Pharmacol.* 2004; 68, 1145–1155. doi: 10.1016/j.bcp.2004.03.045.

Karelis, A.D., St-Pierre, D.H., Conus, F., Rabasa-Lhoret, R. and Poehlman, E.T. Metabolic and body composition factors in subgroups of obesity: what do we know? *J. Clin. Endocrinol. Metab.* 2004, 89, 2569–75.

Katz, J.E., Dlakic, M. and Clarke, S. Automated identification of putative methyltransferases from genomic open reading frames. *Mol Cell Proteomics.* 2003; 2:525–540.

Kebede, A.F. et al. Histone propionylation is a mark of active chromatin. *Nat. Struct. Mol. Biol.* 2017; 24, 1048–1056.

Keleher, M.R. et al. A high-fat diet alters genome-wide DNA methylation and gene expression in SM/J mice. *BMC Genomics* 2018; 19, 888.

Kemper, J. K. et al. FXR Acetylation Is Normally Dynamically Regulated by p300 and SIRT1 but Constitutively Elevated in Metabolic Disease States. *Cell Metab* 2009; 10 (5): 392–404.

Khamzina, L., Veilleux, A., Bergeron, S. and Marette, A. Increased activation of the mammalian target of rapamycin pathway in liver and skeletal muscle of obese rats: possible involvement in obesity-linked insulin resistance. *Endocrinology* 2005;146:1473–1481.

Khokhar, E.S., Borikar, S., Eudy, E., Stearns, T., Young, K. and Trowbridge, J.J. Aging-Associated Decrease in the Histone Acetyltransferase KAT6B Is Linked to Altered Hematopoietic Stem Cell Differentiation. *Exp. Hematol.* 2020; 82, 43–52.e4.

Kim, S. C. et al. Substrate and functional diversity of lysine acetylation revealed by a proteomics survey. *Mol. Cell* 2006; 23, 607–618.

Kim, D., Patel, S.R., Xiao, H. and Dressler, G.R. The role of PTIP in maintaining embryonic stem cell pluripotency. *Stem Cells* 2009; 27:1516-23.

Kim, S.N., Choi, H.Y. and Kim, Y.K. Regulation of adipocyte differentiation by histone deacetylase inhibitors. *Arch Pharm Res* 2009; 32:535-41.

Kim, H-S. et al. Hepatic-specific disruption of SIRT6 in mice results in fatty liver formation due to enhanced glycolysis and triglyceride synthesis. *Cell Metab* 2010;12:224–236.

Kim, M.S., Cho, H.I., Park, S.H., Kim, J.H., Chai, Y.G. and Jang, Y.K. The Histone Acetyltransferase *Myst2* Regulates *Nanog* Expression and Is Involved in Maintaining Pluripotency and Self-Renewal of Embryonic Stem Cells. *FEBS Lett.* 2015; 589, 941–950.

Kimura, I. et al. The gut microbiota suppresses insulin-mediated fat accumulation via the short-chain fatty acid receptor GPR43. *Nat Commun.* 2013;4:1829.

King, M.T. and Reiss, P.D. Separation and measurement of short-chain coenzyme-A compounds in rat liver by reversed-phase high-performance liquid chromatography. *Anal. Biochem.* 1985 146, 173–179.

Kiskinis, E. et al. RIP140 directs histone and DNA methylation to silence Ucp1 expression in white adipocytes. *EMBO J* 2007; 26:4831-40.

Kissebah, A.H. and Peiris, A.N. Biology of regional body fat distribution: relationship to non-insulin-dependent diabetes mellitus. *Diabetes Metab Rev* 1989; 5:83-109.

Kleiner, D. et al. Diagnostic pattern and disease activity are related to disease progression and regression in nonalcoholic fatty liver disease. Conference reports for NATAP (NDDK NASH CRN) 2016.

Knutson, S.K., Chyla, B.J., Amann, J.M., Bhaskara, S., Huppert, S.S. and Hiebert, S.W. Liver-specific deletion of histone deacetylase 3 disrupts metabolic transcriptional networks. *EMBO J* 2008; 27:1017–1028.

Kondou, H., Mushiake, S., Etani, Y., Miyoshi, Y., Michigami, T. and Ozono, K. A blocking peptide for transforming growth factor- β 1 activation prevents hepatic fibrosis in vivo. *J Hepatol* 2003; 39 (5) : 742–748.

Kooistra, S.M. and Helin, K. Molecular mechanisms and potential functions of histone demethylases. *Nat. Rev. Mol. Cell Biol.* 2012; 13, 297–311.

Kornberg, R.D. and Thomas, J.O. Chromatin structure; oligomers of the histones. *Science.* 1974; 184:865–868.

Krautkramer, K.A. et al. Diet-microbiota interactions mediate global epigenetic programming in multiple host tissues. *Mol. Cell* 2016; 64, 982–992.

Kwie, F. H. et al. New potent bisubstrate inhibitors of histone acetyltransferase p300: design, synthesis and biological evaluation. *Chem. Biol. Drug Des.* 2011, 77, 86–92.

Lachner, M. and Jenuwein, T. The many faces of histone lysine methylation. *Curr Opin Cell Biol* 2002; 14(3):286-98.

Lacoste, N., Utley, R.T., Hunter, J.M., Poirier, G.G. and Cote, J. Disruptor of telomeric silencing-1 is a chromatin-specific histone H3 methyltransferase. *J Biol Chem* 2002; 277(34):30421-4.

Lagace, D.C. and Nachtigal, M.W. Inhibition of histone deacetylase activity by valproic acid blocks adipogenesis. *J Biol Chem* 2004; 279:18851-60.

Lange, M. et al. Regulation of muscle development by DPF3, a novel histone acetylation and methylation reader of the BAF chromatin remodeling complex. *Genes Dev.* 2008; 22, 2370–2384.

Langer, M.R., et al. Modulating acetyl-CoA binding in the GCN5 family of histone acetyltransferases. *J Biol Chem.* 2002; 277(30):27337–44.

Lasko, L.M. et al. Discovery of a selective catalytic p300/CBP inhibitor that targets lineage-specific tumours. *Nature* 2017; 5;550(7674):128-132.

Lau, O. D. et al. HATs off: selective synthetic inhibitors of the histone acetyltransferases p300 and PCAF. *Mol. Cell* 2000, 5, 589–595.

Lauberth, S.M. et al. H3K4me3 interactions with TAF3 regulate preinitiation complex assembly and selective gene activation. *Cell* 2013; 152, 1021–1036.

Lee, J. et al. Targeted inactivation of MLL3 histone H3-Lys-4 methyltransferase activity in the mouse reveals vital roles for MLL3 in adipogenesis. *Proc Natl Acad Sci USA* 2008; 105:19229-34.

Lee, S., Lee, J., Lee, S.K. and Lee, J.W. Activating signal cointegrator-2 is an essential adaptor to recruit histone H3 lysine 4 methyltransferases MLL3 and MLL4 to the liver X receptors. *Mol Endocrinol* 2008; 22:1312–1319.

Lee, J.V. et al. Akt-Dependent Metabolic Reprogramming Regulates Tumor Cell Histone Acetylation. *Cell Metabolism* 2014; 20:306-19.

Lee, M.-W., Lee, M. and Oh, K.-J. Adipose Tissue-Derived Signatures for Obesity and Type 2 Diabetes: Adipokines, Batokines and MicroRNAs. *J. Clin. Med.* 2019; 8, 854.

Leemhuis, H., Packman, L. C., Nightingale, K. P. and Hollfelder, F. The human histone acetyltransferase P/CAF is a promiscuous histone propionyltransferase. *Chembiochem* 2008; 9, 499–503.

Lefterova, M.I. et al. PPAR γ and C/EBP factors orchestrate adipocyte biology via adjacent binding on a genome-wide scale. *Genes Dev* 2008; 22:2941-52.

LeGros, H.L. et al. Cloning, expression, and functional characterization of the β regulatory subunit of human methionine adenosyltransferase (MAT II). *J. Biol. Chem.* 2000; 275, 2359–2366.

Lepack, A. E. et al. Dopaminylation of histone H3 in ventral tegmental area regulates cocaine seeking. *Science* 2020; 368, 197–201.

Letouzé, E. et al. SDH mutations establish a hypermethylator phenotype in paraganglioma. *Cancer Cell* 2013; 23, 739–752.

Li, M., Yang, S., and Bjömtorp, P. Metabolism of different adipose tissues in vivo in the rat. *Obes. Res.* 1993; 1, 459–468.

Li, D. et al. Kruppel-like factor-6 promotes preadipocyte differentiation through HDAC3-dependent repression of DLK1. *J Biol Chem* 2005; 280:26941-52.

Li, H. et al. Molecular basis for site-specific read-out of histone H3K4me3 by the BPTF PHD finger of NURF. *Nature* 2006; 442, 91–95.

Li, X. et al. The Histone Acetyltransferase MOF Is a Key Regulator of the Embryonic Stem Cell Core Transcriptional Network. *Cell Stem Cell* 2012; 11, 163–178.

Li, L. et al. SIRT7 is a histone desuccinylase that functionally links to chromatin compaction and genome stability. *Nat. Commun.* 2016; 7, 12235.

Li, Y. et al. Molecular coupling of histone crotonylation and active transcription by AF9 YEATS domain. *Mol. Cell* 2016; 62, 181–193.

Li, S. et al. JMJD1B demethylates H4R3me2s and H3K9me2 to facilitate gene expression for development of hematopoietic stem and progenitor cells. *Cell Rep.* 2018; 23, 389–403.

Li, X., Egervari, G., Wang, Y., Berger, S. L. and Lu, Z. Regulation of chromatin and gene expression by metabolic enzymes and metabolites. *Nat. Rev. Mol. Cell Biol.* 2018; 19, 563–578.

Litzler, L. C. et al. PRMT5 is essential for B cell development and germinal center dynamics. *Nat. Commun.* 2019; 10, 22.

Liu, X. et al. The structural basis of protein acetylation by the p300/CBP transcriptional coactivator. *Nature* 2008; 451, 846–850.

Liu, H. et al. Clipping of arginine-methylated histone tails by JMJD5 and JMJD7. *Proc Natl Acad Sci U S A* 2017; 114(37):E7717-E7726.

Liu, X. et al. MOF as an evolutionarily conserved histone crotonyltransferase and transcriptional activation by histone acetyltransferase-deficient and crotonyltransferase-competent CBP/p300. *Cell Discov* 2017; 3, 17016.

Liu, P.-S. et al. α -Ketoglutarate orchestrates macrophage activation through metabolic and epigenetic reprogramming. *Nat. Immunol.* 2017; 18, 985–994.

Liu, X. et al. Acetate production from glucose and coupling to mitochondrial metabolism in mammals. *Cell* 2018; 175, 502–513.e513.

Liu, X., Xu, X., Shang, R. and Chen, Y. Asymmetric dimethylarginine (ADMA) as an important risk factor for the increased cardiovascular diseases and heart failure in chronic kidney disease. *Nitric Oxide* 2018; 78, 113–120.

Liu, Y. et al. Insulin/Snail1 axis ameliorates fatty liver disease by epigenetically suppressing lipogenesis. *Nat Commun* 2018; 9:2751.

Liu, P. et al. Foxp1 controls brown/beige adipocyte differentiation and thermogenesis through regulating β 3-AR desensitization. *Nat. Commun.* 2019, 10, 5070.

Londono Gentile, T. et al. DNMT1 is regulated by ATP-Citrate lyase and maintains methylation patterns during adipocyte differentiation. *Mol. Cell. Biol.* 2013 33, 3864–3878.

Long, E. K., Olson, D. M. and Bernlohr, D. A. High-fat diet induces changes in adipose tissue trans-4-oxo-2-nonenal and trans-4-hydroxy-2-nonenal levels in a depot-specific manner. *Free Radic. Biol. Med.* 2013; 63, 390–398.

Long, M.T. et al. Parental non-alcoholic fatty liver disease increases risk of non-alcoholic fatty liver disease in offspring. *Liver Int.* 2019; 39, 740–747.

Loomba, R. et al. Genetics of NAFLD in Twins Consortium. Heritability of Hepatic Fibrosis and Steatosis Based on a Prospective Twin Study. *Gastroenterology* 2015; 149, 1784–1793.

Luge, K., Mader, A.W., Richmond, R.K., Sargent, D.F. and Richmond, T.J. Crystal structure of the nucleosome core particle at 2.8 Å resolution. *Nature.* 1997; 389:251–260.

Luscombe, N.M., Laskowski, R.A. and Thornton, J.M. Amino acid-base interactions: a three-dimensional analysis of protein-DNA interactions at an atomic level. *Nucleic Acids Res.* 2001; 29:2860–2874.

Malagon, M. et al. Adipobiology for Novel Therapeutic Approaches in Metabolic Syndrome. *Curr. Vasc. Pharmacol.* 2014, 11, 954–967.

Manning, E.T., Ikehara, T., Ito, T., Kadonaga, J.T. and Kraus, W.L. p300 forms a stable, template-committed complex with chromatin: role for the bromodomain. *Mol. Cell Biol.* 2001; 21, 3876–3887.

Mantelingu, K. et al. Specific inhibition of p300-HAT alters global gene expression and represses HIV replication. *Chem. Biol.* 2007; 14, 645–657.

Markham, G.D. and Pajares, M.A. Structure-function relationships in methionine adenosyltransferases. *Cell. Mol. Life Sci.* 2018; 66, 636–648.

Mauer, J. et al. FTO controls reversible m6Am RNA methylation during snRNA biogenesis. *Nat. Chem.Biol.* 2019; 15, 340–347.

McClain, C.J. et al. Mechanisms of non-alcoholic steatohepatitis. *Alcohol* 2004; 34, 67–79.

McDonnell, E. et al. Lipids reprogram metabolism to become a major carbon source for histone acetylation. *Cell Rep.* 2016; 17, 1463–1472.

Mcgarry, J.D. Banting lecture 2001: dysregulation of fatty acid metabolism in the etiology of type 2 diabetes. *Diabetes* 2002; 51, 7–18.

Meehan, R.R. et al. Identification of a mammalian protein that binds specifically to DNA containing methylated CpGs. *Cell* 1989; 58, 499–507.

Meier, J.L. Metabolic mechanisms of epigenetic regulation. *ACS Chem. Biol.* 2013; 8, 2607–2621.

Memon, R.A., Feingold, K.R., Moser, A.H., Fuller, J. and Grunfeld, C. Regulation of fatty acid transport protein and fatty acid translocase mRNA levels by endotoxin and cytokines. *Am. J. Physiol.* 1998; 274, E210–E217.

Mendez-Lucas, A. et al. Glucose catabolism in liver tumors induced by c-MYC can be sustained by various PKM1/PKM2 ratios and pyruvate activities. *Cancer Res* 2017; 77 (16): 4355–4364.

Mentch, S. J. et al. Histone methylation dynamics and gene regulation occur through the sensing of one-carbon metabolism. *Cell Metab.* 2015; 22, 861–873.

Merson, T.D. et al. The Transcriptional Coactivator Querkopf Controls Adult Neurogenesis. *J. Neurosci.* 2006; 26, 11359–11370.

Messner, S. and Hottiger, M. O. Histone ADP-ribosylation in DNA repair, replication and transcription. *Trends Cell Biol.* 2011; 21, 534–542.

Mews, P. et al. Acetyl-CoA synthetase regulates histone acetylation and hippocampal memory. *Nature* 2017; 546, 381–386.

Mews, P. et al. Alcohol metabolism contributes to brain histone acetylation. *Nature* 2019; 574, 717–721.

Milite, C. et al. A novel cell-permeable, selective, and noncompetitive inhibitor of KAT3 histone acetyltransferases from a combined molecular pruning/classical isosterism approach. *J. Med. Chem.* 2015; 58, 2779–2798.

Mizzen, C. A. et al. The TAF(II)250 subunit of TFIID has histone acetyltransferase activity. *Cell* 1996; 87, 1261–1270.

Mohn, F. et al. Lineage-specific polycomb targets and de novo DNA methylation define restriction and potential of neuronal progenitors. *Mol Cell* 2008; 30:755–66.

Mont, S. et al. Accumulation of isolevuglandin-modified protein in normal and fibrotic lung. *Sci. Rep.* 2016; 6, 24919.

Mouchiroud, L. et al. The NAD⁺/sirtuin pathway modulates longevity through activation of mitochondrial UPR and FOXO signaling. *Cell* 2013; 154, 430–441.

Moustakas, A., Souchelnytskyi, S. and Heldin, C.-H. Smad regulation in TGF- β signal transduction. *J Cell Sci* 2001; 114 (24): 4359–4369.

Mujtaba, S. et al. Structural mechanism of the bromodomain of the coactivator CBP in p53 transcriptional activation. *Mol. Cell* 2004; 13, 251–263.

Musri, M.M., Corominola, H., Casamitjana, R., Gomis, R. and Parrizas, M. Histone H3 lysine 4 dimethylation signals the transcriptional competence of the adiponectin promoter in preadipocytes. *J Biol Chem* 2006; 281:17180-8.

Myant, K. et al. LSH and G9a/GLP complex are required for developmentally programmed DNA methylation. *Genome Res.* 2011; 21, 83–94.

Nagaraj, R. et al. Nuclear localization of mitochondrial TCA cycle enzymes as a critical step in mammalian zygotic genome activation. *Cell* 2017; 168, 210–223.e211.

Najt, C.P. et al. Lipid droplet-derived monounsaturated fatty acids traffic via PLIN5 to allosterically activate SIRT1. *Mol. Cell* 2020; 77, 810–824.

Neckers, L. et al. Curcumin is an inhibitor of p300 histone acetyltransferase. *Med. Chem.* 2006, 2, 169–174.

Nedergaard, J., Bengtsson, T. and Cannon, B. Unexpected evidence for active brown adipose tissue in adult humans. *Am J Physiol Endocrinol Metab* 2007; 293:444-52.

Nie, L. et al. The landscape of histone modifications in a high-fat diet-induced obese (DIO) mouse model. *Molecular & Cellular Proteomics* 2017; 16(7):1324e1334.

Nielsen, R. et al. Genome-wide profiling of PPAR γ :RXR and RNA polymerase II occupancy reveals temporal activation of distinct metabolic pathways and changes in RXR dimer composition during adipogenesis. *Genes Dev* 2008; 22:2953-67.

Nieumierzycka, A. and Clarke, S. S-Adenosylmethionine-dependent methylation in *Saccharomyces cerevisiae*. Identification of a novel protein arginine methyltransferase. *J Biol Chem* 1999; 274(2):814-24.

Noer, A., Lindeman, L.C. and Collas, P. Histone H3 modifications associated with differentiation and long-term culture of mesenchymal adipose stem cells. *Stem Cells Dev* 2009; 18:725-36.

Nolte, R.T. et al. Ligand binding and co-activator assembly of the PPAR γ . *Nature* 1998; 395:137-43.

Nyberg, S.T. et al. Obesity and loss of disease-free years owing to major non-communicable diseases: a multicohort study. *Lancet Public Heal.* 2018; 3, e490–e497.

Paik, W. K., Lee, H. W. and Kim, S. Non-enzymatic methylation of proteins with S-adenosyl-L-methionine. *FEBS Lett.* 1975; 58, 39–42.

Pagotto, U., Vicennati, V., and Pasquali, R. The endocannabinoid system and the treatment of obesity. *Ann. Med.* 2005; 37, 270–275.

Park, J. et al. SIRT5-mediated lysine desuccinylation impacts diverse metabolic pathways. *Mol. Cell* 2013; 50,919–930.

Pedersen, T.A., Kowenz-Leutz, E., Leutz, A. and Nerlov, C. Cooperation between C/EBP α TBP/TFIIB and SWI/SNF recruiting domains is required for adipocyte differentiation. *Genes Dev* 2001; 15:3208-16.

Pellegrinelli, V., Carobbio, S. and Vidal-Puig, A. Adipose tissue plasticity: how fat depots respond differently to pathophysiological cues. *Diabetologia* 2016; 59, 1075–1088.

Pendleton, K. E. et al. The U6 snRNA m6A methyltransferase METTL16 regulates SAM synthetase intron retention. *Cell* 2017; 169, 824–835.e14.

Peng, C. et al. The first identification of lysine malonylation substrates and its regulatory enzyme. *Mol. Cell. Proteomics* 2011; 10, M111.012658.

Peng, M. et al. Aerobic glycolysis promotes T helper cell differentiation through an epigenetic mechanism. *Science* 2016; 354, 481–484.

Perry, R.J. et al. Hepatic acetyl CoA links adipose tissue inflammation to hepatic insulin resistance and type 2 diabetes. *Cell* 2015; 160:745–758.

Pessayre, D., Mansouri, A. and Fromenty, B. Nonalcoholic steatosis and steatohepatitis. V. Mitochondrial dysfunction in steatohepatitis. *Am. J. Physiol. Gastrointest. Liver Physiol.* 2002; 282, G193–G199.

Petrovic, N., Walden, T.B., Shabalina, I.G., Timmons, J.A., Cannon, B. and Nedergaard, J. Chronic peroxisome proliferator-activated receptor γ (PPAR γ) activation of epididymally derived white adipocyte cultures reveals a population of thermogenically competent, UCP1-containing adipocytes molecularly distinct from classic brown adipocytes. *J Biol Chem* 2010; 285: 7153–7164.

Picaud, S. et al. Generation of a selective small molecule inhibitor of the CBP/p300 bromodomain for leukemia therapy. *Cancer Res.* 2015; 75, 5106–5119.

Ponugoti, B. et al. SIRT1 deacetylates and inhibits SREBP-1C activity in regulation of hepatic lipid metabolism. *J Biol Chem* 2010; 285 (44): 33959–33970.

Puri, P.L. et al. Differential Roles of P300 and PCAF Acetyltransferases in Muscle Differentiation. *Mol. Cell* 1997; 1, 35–45.

Qiang, L. et al. Brown remodeling of white adipose tissue by SirT1-dependent deacetylation of Ppar γ . *Cell* 2012, 150, 620–632.

Qiao, Y., Wang, R., Yang, X., Tang, K. and Jing, N. Dual Roles of Histone H3 Lysine 9 Acetylation in Human Embryonic Stem Cell Pluripotency and Neural Differentiation. *J. Biol. Chem.* 2015; 290, 2508–2520.

Qiu, Y. et al. Combinatorial readout of unmodified H3R2 and acetylated H3K14 by the tandem PHD finger of MOZ reveals a regulatory mechanism for HOXA9 transcription. *Genes Dev.* 2012; 26, 1376–1391.

Qiu, J. et al. Acetate promotes T cell effector function during glucose restriction. *Cell Rep.* 2019; 27, 2063–2074. e2065.

Ragvin, A. et al. Nucleosome binding by the bromodomain and PHD finger of the transcriptional cofactor p300. *J. Mol. Biol.* 2004; 337, 773–788.

Raijmakers, R. et al. Methylation of arginine residues interferes with citrullination by peptidylarginine deiminases in vitro. *J. Mol. Biol.* 2007; 367, 1118–1129.

Ravindra, K. C. et al. Inhibition of lysine acetyltransferase KAT3B/p300 activity by a naturally occurring hydroxynaphthoquinone, plumbagin. *J. Biol. Chem.* 2009; 284, 24453–24464.

Reaven, G. All obese individuals are not created equal: insulin resistance is the major determinant of cardiovascular disease in overweight/obese individuals. *Diabetes Vasc. Dis. Res.* 2005, 2, 105–112.

Reid, M. A., Dai, Z. W. and Locasale, J. W. The impact of cellular metabolism on chromatin dynamics and epigenetics. *Nat. Cell Biol.* 2017 19, 1298–1306.

Reddy, J.K. Nonalcoholic steatosis and steatohepatitis. III. Peroxisomal beta-oxidation, PPAR alpha, and steatohepatitis. *Am. J. Physiol. Gastrointest. Liver Physiol.* 2001; 281, G1333–G1339.

Revollo, J.R. et al. The NAD biosynthesis pathway mediated by nicotinamide phosphoribosyltransferase regulates Sir2 activity in mammalian cells. *J. Biol. Chem.* 2004; 279, 50754–50763.

Ringel, A. E. and Wolberger, C. Structural basis for acyl group discrimination by human Gcn5L2. *Acta Crystallogr. D Struct. Biol.* 2016; 72, 841–848.

Romeo, S. et al. Morbid obesity exposes the association between PNPLA3 I148M (rs738409) and indices of hepatic injury in individuals of European descent. *Int. J. Obes.* 2010; 34, 190–194.

Rosen, E.D. et al. PPAR γ is required for the differentiation of adipose tissue in vivo and in vitro. *Mol Cell* 1999; 4:611-7.

Rosen, E.D. et al. C/EBP α induces adipogenesis through PPAR γ : a unified pathway. *Genes Dev* 2002; 16:22-6.

Rosen, E.D. and MacDougald, O.A. Adipocyte differentiation from the inside out. *Nat Rev Mol Cell Biol* 2006; 7:885-96.

Roth, S.Y., Denu, J.M. and Allis, C.D. Histone acetyltransferases. *Annu Rev Biochem.* 2001; 70: 81–120.

Rothman, R. B. et al. Amphetamine-type central nervous norepinephrine more potently than they release dopamine and serotonin. *Synapse* 2001; 39, 32–41.

Roy, D. G. et al. Methionine metabolism shapes T helper cell responses through regulation of epigenetic reprogramming. *Cell Metab.* 2020; 31, 250–266. e259.

Ruiz-Andres, O. et al. Histone lysine crotonylation during acute kidney injury in mice. *Dis. Model. Mech.* 2016; 9, 633–645.

Rydberg, B. and Lindahl, T. Nonenzymatic methylation of DNA by the intracellular methyl group donor S-adenosyl-L-methionine is a potentially mutagenic reaction. *EMBO J.* 1982; 1, 211–216.

Sabari, B. R. et al. Intracellular crotonyl-CoA stimulates transcription through p300-catalyzed histone crotonylation. *Mol. Cell* 2015; 58, 203–215.

Salma, N., Xiao, H. and Imbalzano, A.N. Temporal recruitment of CCAAT/enhancer-binding proteins to early and late adipogenic promoters in vivo. *J Mol Endocrinol* 2006; 36:139-51.

Salomon, T. et al. Ketone body acetoacetate buffers methylglyoxal via a non-enzymatic conversion during diabetic and dietary ketosis. *Cell Chem. Biol.* 2017; 24, 935–943.e7.

Samuel, B.S. et al. Effects of the gut microbiota on host adiposity are modulated by the short-chain fatty-acid binding G protein-coupled receptor, Gpr41. *Proc Natl Acad Sci U S A.* 2008;105:16767–72.

Sanchez, R. and Zhou, M.M. The PHD finger: a versatile epigenome reader. *Trends Biochem. Sci.* 2011; 36, 364–372.

Sanderson, S.M. et al. Methionine metabolism in health and cancer: a nexus of diet and precision medicine. *Nat. Rev. Cancer* 2019; 19, 625–637.

Sbardella, G. et al. Identification of long chain alkylidenemalonates as novel small molecule modulators of histone acetyltransferases. *Bioorg. Med. Chem. Lett.* 2008, 18, 2788–2792.

Scherer, P.E. The many secret lives of adipocytes: implications for diabetes. *Diabetologia* 2019; 62, 223–232.

Schröter, D. and Höhn, A. Role of advanced glycation end products in carcinogenesis and their therapeutic implications. *Curr. Pharm. Des.* 2018; 24,5245–5251.

Schulze, M.B. Metabolic health in normal-weight and obese individuals. *Diabetologia* 2019; 62, 558–566.

Shoelson, S.E., Lee, J. and Yuan, M. Inflammation and the IKK beta/I kappa B/NF-kappa B axis in obesity- and diet-induced insulin resistance. *Int. J. Obes. Relat Metab Disord.* 27 (Suppl. 3) 2003; S49–S52.

Shrimp, J. H., Sorum, A. W., Garlick, J. M., Guasch, L., Nicklaus, M. C. and Meier, J. L. Characterizing the Covalent Targets of a Small Molecule Inhibitor of the Lysine Acetyltransferase P300. *ACS Med. Chem. Lett.* 2015; 7(2):151-5.

Seale, P. et al. PRDM16 controls a brown fat/skeletal muscle switch. *Nature* 2008; 454: 961–967.

Seale, P. et al. Prdm16 determines the thermogenic program of subcutaneous white adipose tissue in mice. *J Clin Invest* 2011; 121: 96–105.

Sebastián, C. and Mostoslavsky, R. The various metabolic sources of histone acetylation. *Trends Endocrinol. Metab.* 2017; 28, 85–87.

Shi, Y. et al. Histone demethylation mediated by the nuclear amine oxidase homolog LSD1. *Cell* 2004; 119, 941–953.

Shi, H. L., Wei, J. B. and He, C. Where, when, and how: context-dependent functions of RNA methylation writers, readers, and erasers. *Mol. Cell* 2019; 74, 640–650.

Shima, H. et al. S-adenosylmethionine synthesis is regulated by selective N⁶-adenosine methylation and mRNA degradation involving METTL16 and YTHDC1. *Cell Rep.* 2017; 21, 3354–3363.

Shiraki, N. et al. Methionine metabolism regulates maintenance and differentiation of human pluripotent stem cells. *Cell Metab.* 2014; 19, 780–794.

Shurubor, Y.I., et al. Determination of Coenzyme A and Acetyl-Coenzyme A in Biological Samples Using HPLC with UV Detection. *Molecule.* 2017; 22(9).

Shyh-Chang, N. et al. Influence of threonine metabolism on S-adenosylmethionine and histone methylation. *Science* 2013; 339, 222–226.

Simpson, R.T. Structure of the chromatosome, a chromatin particle containing 160 base pairs of DNA and all the histones. *Biochemistry.* 1978; 17:5524–5531.

Sin, H. S. et al. RNF8 regulates active epigenetic modifications and escape gene activation from inactive sex chromosomes in post-meiotic spermatids. *Genes Dev.* 2012; 26, 2737–2748.

Sinclair, L.V. et al. Antigen receptor control of methionine metabolism in T cells. *eLife* 2019; 8, e44210.

Singh, R., Barden, A., Mori, T. and Beilin, L. Advanced glycation end-products: a review. *Diabetologia* 2001; 44, 129–146.

Sivanand, S. et al. Nuclear acetyl-CoA production by ACLY promotes homologous recombination. *Mol. Cell* 2017; 67, 252–265.

Sivanand, S. et al. Spatiotemporal control of acetyl-CoA metabolism in chromatin regulation. *Trends Biochem. Sci.* 2018 43, 61–74.

Schoof, M. et al. The Transcriptional Coactivator and Histone Acetyltransferase CBP Regulates Neural Precursor Cell Development and Migration. *Acta Neuropathol. Commun.* 2019; 7.

Smith, B. M., Thomsen, W. J., and Grottick, A. J. The potential use of selective 5-HT_{2C} agonists in treating obesity. *Expert Opin. Investig. Drugs* 2006; 15, 257–266.

Somasundaram, V. et al. Molecular mechanisms of nitric oxide in cancer progression, signal transduction, and metabolism. *Antioxid. Redox Signal.* 2019; 30, 1124–1143.

Song, X. et al. Dynamic crotonylation of EB1 by Tip60 ensures accurate spindle positioning in mitosis. *Nat Chem Biol* 2021; 17(12):1314-1323.

Soutoglou, E., Katrakili, N. and Talianidis, I. Acetylation regulates transcription factor activity at multiple levels. *Mol Cell* 2000; 5 (4): 745–751.

Spencer, T. E. et al. Steroid receptor coactivator-1 is a histone acetyltransferase. *Nature* 1997; 389, 194–198. doi: 10.1038/38304.

Sperber, H. et al. The metabolome regulates the epigenetic landscape during naive-to-primed human embryonic stem cell transition. *Nat. Cell Biol.* 2015; 17, 1523–1535.

Stefan, N., Schick, F., Häring and H.-U. Causes, Characteristics, and Consequences of Metabolically Unhealthy Normal Weight in Humans. *Cell Metab.* 2017; 26, 292–300.

Sterner, D.E., and Berger, S.L. Acetylation of histones and transcription-related factors. *Microbiol. Mol. Biol. Rev.* 2000; 64, 435– 459.

Su, R. et al. R-2HG exhibits anti-tumor activity by targeting FTO/m6A/MYC/CEBPA signaling. *Cell* 2018; 172, 90–105.e23.

Sun, L. et al. Transcriptional repression of SIRT1 by protein inhibitor of activated STAT 4 (PIAS4) in hepatic stellate cells contributes to liver fibrosis. *Sci Rep* 2016; 6 : 28342.

Sutendra, G. et al. A nuclear pyruvate dehydrogenase complex is important for the generation of acetyl-CoA and histone acetylation. *Cell* 2014; 158, 84–97.

Szczerbal, I., Foster, H.A. and Bridger, J.M. The spatial repositioning of adipogenesis genes is correlated with their expression status in a porcine mesenchymal stem cell adipogenesis model system. *Chromosoma* 2009; 118:647-63.

Takada, I. et al. A histone lysine methyltransferase activated by non-canonical Wnt signalling suppresses PPAR γ transactivation. *Nat Cell Biol* 2007; 9:1273-85.

Takada, I., Suzawa, M., Matsumoto, K. and Kato, S. Suppression of PPAR transactivation switches cell fate of bone marrow stem cells from adipocytes into osteoblasts. *Ann NY Acad Sci* 2007; 1116:182-95.

Takubo, K. et al. Regulation of glycolysis by Pdk functions as a metabolic checkpoint for cell cycle quiescence in hematopoietic stem cells. *Cell Stem Cell* 2013; 12, 49–61.

Tan, M. J. et al. Identification of 67 histone marks and histone lysine crotonylation as a new type of histone modification. *Cell* 2011; 146, 1015–1027.

Tan, M. J. et al. Lysine glutarylation is a protein posttranslational modification regulated by SIRT5. *Cell Metab.* 2014; 19, 605–617.

Tanaka, T., Yoshida, N., Kishimoto, T., and Akira, S. Defective adipocyte differentiation in mice lacking the C/EBP β and/or C/EBP δ gene. *EMBO J.* 1997; 16, 7432–7443.

Tang, S. et al. Methionine metabolism is essential for SIRT1-regulated mouse embryonic stem cell maintenance and embryonic development. *EMBO J.* 2017; 36, 3175–3193.

Tanner, K. G., Langer, M. R. and Denu, J. M. Kinetic mechanism of human histone acetyltransferase P/CAF. *Biochemistry* 2000; 39, 11961–11969.

Tanner, K. G., Langer, M. R., Kim, Y. J. and Denu, J. M. Kinetic mechanism of the histone acetyltransferase GCN5 from yeast. *J. Biol. Chem.* 2000; 275, 22048–22055.

Tateishi, K., Okada, Y., Kallin, E.M. and Zhang, Y. Role of Jhdm2a in regulating metabolic gene expression and obesity resistance. *Nature* 2009; 458:757-61.

TeSlaa, T. et al. α -Ketoglutarate accelerates the initial differentiation of primed human pluripotent stem cells. *Cell Metab.* 2016; 24, 485–493.

Thienpont, B. et al. Tumour hypoxia causes DNA hyper-methylation by reducing TET activity. *Nature* 2016; 537, 63–68.

Thomas, P. D. et al PANTHER: a library of protein families and subfamilies indexed by function. *Genome Res* 2003;13:2129-2141

Thomas, S.P. and Denu, J.M. Short-chain fatty acids activate acetyltransferase p300. *Elife* 2021; 22;10:e72171.

Thompson, P. R., Kurooka, H., Nakatani, Y. and Cole, P. A. Transcriptional coactivator protein p300 — kinetic characterization of its histone acetyltransferase activity. *J. Biol. Chem.* 2001; 276, 33721–33729.

Tian, W. et al. Myocardin-related transcription factor A (MRTF-A) plays an essential role in hepatic stellate cell activation by epigenetically modulating TGF- β signaling. *Int J Biochem Cell Biol* 2016; 71 : 35–43.

Tiraby, C. and Langin, D. Conversion from white to brown adipocytes: a strategy for the control of fat mass? *Trends Endocrinol Metab* 2003; 14:439-41.

Tohyama, S. et al. Discovery and characterization of NK13650s, naturally occurring p300-selective histone acetyltransferase inhibitors. *J. Org. Chem.* 2012; 77, 9044–9052.

Trapnell, C. et al Differential gene and transcript expression analysis of RNA-seq experiments with TopHat and Cufflinks. *Nat Protoc* 2012;7:562-578

Triebel, R.C. et al. Crystal structure and mechanism of histone acetylation of the yeast GCN5 transcriptional coactivator. *Proc Natl Acad Sci U S A* 1999;96:8931–8936.

Tsogtbaatar, E., Landin, C., Minter-Dykhouse, K. and Folmes, C. D. L. Energy metabolism regulates stem cell pluripotency. *Front. Cell Dev. Biol.* 2020; 8, 87.

Tweedie-Cullen, R. Y. et al. Identification of combinatorial patterns of post-translational modifications on individual histones in the mouse brain. *PLoS ONE* 2012; 7, e36980.

Vasudevarao, M. D. et al. Naphthoquinone mediated inhibition of lysine acetyltransferase KAT3B/p300, basis for non-toxic inhibitor synthesis. *J. Biol. Chem.* 2014; 289, 7702–7717.

Verdin, E. NAD⁺ in aging, metabolism, and neurodegeneration. *Science* 2015; 350, 1208–1213.

Villarroya, F., Cereijo, R., Villarroya, J. and Giralt, M. Brown adipose tissue as a secretory organ. *Nat. Rev. Endocrinol.* 2017; 13, 26–35.

Virtue, S. and Vidal-Puig, A. It's Not How Fat You Are, It's What You Do with It That Counts. *PLoS Biol.* 2008; 6, e237.

Vishvanath, L., Gupta, R.K., Vishvanath, L. and Gupta, R.K. Contribution of adipogenesis to healthy adipose tissue expansion in obesity. *J Clin Invest* 2019; 129, 4022–4031.

Vollmuth, F. and Geyer, M. Interaction of propionylated and butyrylated histone H3 lysine marks with Brd4 bromodomains. *Angew. Chem. Int. Ed.* 2010; 49,6768–6772.

Wadia, J. S. and Dowdy, S. F. Transmembrane delivery of protein and peptide drugs by TAT-mediated transduction in the treatment of cancer. *Adv. Drug Delivery Rev.* 2005, 57, 579–596.

Wagner, G. R. and Hirschey, M. D. Nonenzymatic protein acylation as a carbon stress regulated by sirtuin deacylases. *Mol. Cell* 2014; 54, 5–16.

Wakabayashi, K. et al. The PPAR γ /RXR α heterodimer targets the histone modification enzyme PR-Set7/Setd8 gene and regulates adipogenesis through a positive feedback loop. *Mol Cell Biol* 2009; 29:3544-55.

Walport, L. J. et al. Arginine demethylation is catalysed by a subset of JmJc histone lysine demethylases. *Nat. Commun.* 2016; 7, 11974.

Wang, L., Tang, Y., Cole, P.A. and Marmostein, Y. Structure and chemistry of the p300/CBP and Rtt109 histone acetyltransferases: Implications for histone acetyltransferase evolution and function *Curr Opin Struct Biol.* 2008; 18(6): 741–747.

Wang, Y., Hudak, C. and Sook, S.-H. Role of preadipocyte factor 1 in adipocyte differentiation. *Clin Lipidol* 2010; 5(1): 109–115.

Wang, Y. et al. KAT2A coupled with the α -KGDH complex acts as a histone H3 succinyltransferase. *Nature* 2017; 552, 273–277.

Wellen, K.E., Hatzivassiliou, G., Sachdeva, U.M., Bui, T.V., Cross, J.R. and Thompson, C.B.. ATP-citrate lyase links cellular metabolism to histone acetylation. *Science* 2009; 324:1076-80; PMID:19461003.

Wiper-Bergeron, N., Wu, D., Pope, L., Schild-Poulter, C. and Hache, R.J. Stimulation of preadipocyte differentiation by steroid through targeting of an HDAC1 complex. *EMBO J* 2003; 22:2135-45.

Wu, T. P. et al. DNA methylation on N6-adenine in mammalian embryonic stem cells. *Nature* 2016; 532, 329–333 .

Wu, X. and Zhang, Y. TET-mediated active DNA demethylation: mechanism, function and beyond. *Nat. Rev. Genet.* 2017; 18, 517–534.

Wysocka, J. et al. A PHD finger of NURF couples histone H3 lysine 4 trimethylation with chromatin remodelling. *Nature* 2006; 442, 86–90.

Xiao, M. et al. Inhibition of α -KG-dependent histone and DNA demethylases by fumarate and succinate that are accumulated in mutations of FH and SDH tumor suppressors. *Genes Dev.* 2012; 26, 1326–1338.

Xiao, Y. et al. HBO1 is a versatile histone acyltransferase critical for promoter histone acylations. *Nucleic Acids Res* 2021;49(14):8037-8059.

Xie, Z. et al. Metabolic regulation of gene expression by histone lysine β -hydroxybutyrylation. *Mol. Cell* 2016; 62, 194–206.

Xiong, X. et al. Selective recognition of histone crotonylation by double PHD fingers of MOZ and DPF2. *Nat. Chem. Biol.* 2016; 12(12):1111-1118.

Xu, W. et al. Oncometabolite 2-hydroxyglutarate is a competitive inhibitor of α -ketoglutarate-dependent dioxygenases. *Cancer Cell* 2011; 19, 17–30.

Xue, B., Coulter, A., Rim, J.S., Koza, R.A. and Kozak, L.P. Transcriptional synergy and the regulation of Ucp1 during brown adipocyte induction in white fat depots. *Mol Cell Biol* 2005; 25: 8311–8322.

Yadav, N. et al. CARM1 promotes adipocyte differentiation by coactivating PPAR γ . *EMBO Rep* 2008; 9:193-8.

Yan, Y., Harper, S., Speicher, D.W. and Marmorstein, R. The catalytic mechanism of the ESA1 histone acetyltransferase involves a self-acetylated intermediate. *Nat Struct Biol* 2002;9:862–869.

Yan, K., et al. Deficient histone H3 propionylation by BRPF1-KAT6 complexes in neurodevelopmental disorders and cancer. *Sci. Adv.* 2020; 6,eaax0021.

Yang, J. et al. Activation of SIRT1 by resveratrol represses transcription of the gene for the cytosolic form of phosphoenolpyruvate carboxykinase (GTP) by deacetylating hepatic nuclear factor 4 α . *J Biol Chem* 2009; 284 (40) : 27042–27053.

Yang, X., Wu, R., Shan, W., Yu, L., Xue, B., and Shi, H. DNA methylation biphasically regulates 3T3-L1 preadipocyte differentiation. *Mol. Endocrinol.* 2016; 30, 677–687.

Yang, Z., He, M., Austin, J., Pflieger, J. and Abdellatif, M. Histone H3K9 butyrylation is regulated by dietary fat and stress via an Acyl-CoA dehydrogenase short chain-dependent mechanism. *Mol Metab* 2021; 53:101249.

Ye, C. Q., Sutter, B. M., Wang, Y., Kuang, Z. and Tu, B. P. A metabolic function for phospholipid and histone methylation. *Mol. Cell* 2017; 66, 180–193.e8.

Ye, C. and Tu, B.P. Sink into the Epigenome: Histones as repositories that influence cellular metabolism. *Trends Endocrinol Metab.* 2018; September ; 29(9): 626–637.

Ye, C. Q. et al. Demethylation of the protein phosphatase PP2A promotes demethylation of histones to enable their function as a methyl group sink. *Mol. Cell* 2019; 73, 1115–1126.e6

Yeh, W.C., Cao, Z., Classon, M., and McKnight, S.L. Cascade regulation of terminal adipocyte differentiation by three members of the C/EBP family of leucine zipper proteins. *Genes Dev.* 1995; 9, 168–181.

Yin, Y. et al. Impact of cytosine methylation on DNA binding specificities of human transcription factors. *Science* 2017; 5; 356(6337):eaaj2239.

Yoo, E. J., Chung, J. J., Choe, S. S., Kim, K. H., and Kim, J. B. Down-regulation of histone deacetylases stimulates adipocyte differentiation. *J Biol Chem* 2006; 281:6608-6615.

Yu, W. et al. One-carbon metabolism supports S-adenosylmethionine and histone methylation to drive inflammatory macrophages. *Mol. Cell* 2019; 75,1147–1160.e1145.

Yue, Y., Liu, J. and He, C. RNA N6-methyladenosine methylation in post-transcriptional gene expression regulation. *Gene Dev.*2015; 29, 1343–1355.

Zaccara, S., Ries, R. J. and Jaffrey, S. R. Reading, writing and erasing mRNA methylation. *Nat. Rev. Mol. Cell Biol.* 2019; 20, 608–624.

Zee, B.M. et al. In vivo residue-specific histone methylation dynamics. *J Biol Chem.* 2010; 285(5):3341–50.

Zeng, L., Zhang, Q., Gerona-Navarro, G., Moshkina, N. and Zhou, M.M. Structural basis of site-specific histone recognition by the bromodomains of human coactivators PCAF and CBP/p300. *Structure* 2008; 16, 643–652.

Zeng, L. et al. Mechanism and regulation of acetylated histone binding by the tandem PHD finger of DPF3b. *Nature* 2010; 466, 258–262.

Zhang, S., Roche, K., Nasheuer, H.-P. and Lowndes, N. F. Modification of histones by sugar β -N-acetylglucosamine (GlcNAc) occurs on multiple residues, including histone H3 serine 10, and is cell cycle-regulated. *J. Biol. Chem.* 2011; 286, 37483–37495.

Zhang, Q., Ramlee, M. K., Brunmeir, R., Villanueva, C. J., Halperin, D., and Xu, F. Dynamic and distinct histone modifications modulate the expression of key adipogenesis regulatory genes. *Cell Cycle* 2012; 11, 4310–4322.

Zhang, Q. et al. Structural Insights into histone crotonyl-lysine recognition by the AF9 YEATS domain. *Structure* 2016; 24,1606–1612.

Zhang, Q. et al. Elevated H3K79 homocysteinylation causes abnormal gene expression during neural development and subsequent neural tube defects. *Nat. Commun.* 2018; 9, 3436.

Zhang, D. et al. Metabolic regulation of gene expression by histone lactylation. *Nature* 2019; 574,575–580.

Zhang, H. et al. Ketogenesis-generated β -hydroxybutyrate is an epigenetic regulator of CD8+ T cell memory development. *Nat Cell Biol* 2020; 22(1):18-25.

Zhao, D. et al. YEATS2 is a selective histone crotonylation reader. *Cell Res.* 2016; 26, 629–632.

Zheng, Y. et al. Synthesis and evaluation of a potent and selective cell-permeable p300 histone acetyltransferase inhibitor. *J. Am. Chem. Soc.* 2005, 127, 17182–17183.

Zhou, D. et al. Sodium butyrate reduces high-fat diet-induced non-alcoholic steatohepatitis through upregulation of hepatic GLP-1R expression. *Exp Mol Med.* 2018;50:1–12.

Zhou, F. et al. Selective inhibition of CBP/p300 HAT by A-485 results in suppression of lipogenesis and hepatic gluconeogenesis. *Cell Death Dis.* 2020; 11;11(9):745.

Zhu, Z. et al. Identification of lysine isobutyrylation as a new histone modification mark. *Nucleic Acids Res* 2021; 11;49(1):177-189.

Zuo, Y., Qiang, L. and Farmer, S.R. Activation of CCAAT/ enhancer-binding protein alpha (C/EBPa) expression by C/EBPb during adipogenesis requires a PPARg associated repression of HDAC1 at the C/ebpa gene promoter. *J Biol Chem* 2006; 281:7960-7.

Annexure

Reagent information

All reagents for bacterial culture associated work were obtained from Himedia which include Luria Bertani Broth or LB (M575), agar (GRM206), IPTG (MB072), antibiotics kanamycin (MB105) and ampicillin (MB104). Additional reagents obtained from Himedia include skimmed milk powder (GRM1254) and various cell culture related reagents- Phosphate Buffered Saline or PBS (TL1104), Trypsin-EDTA solution (TCL070) and antibiotic antimycotic solution (A002A). Other cell culture reagents were procured from various sources like Sigma Aldrich – DMEM High Glucose (S5761) and sodium bicarbonate (D1152); Gibco – DMEM No Glucose (11966-025) and Grace's Insect Medium (11605-094); Biological Industries – Foetal Bovine Serum (04-121-1A).

All inorganic salts for making buffer preparations were obtained from Fisher Scientific. In addition, reagents associated with histological studies were also obtained from there which included Xylene (1330-207), Hematoxylin (38803), Eosin (17372-87-1) and DPX (Q18404).

Ni-NTA (70644) and LCMS grade methanol (67-56-1) were obtained from Merck-Millipore. Reagents procured from NEB include DpnI (R0176S), DNase I (M0303S) and DNase digestion buffer (B0303S). Reagents for SDM were obtained from Agilent Technologies – PFU Ultra High Fidelity DNA polymerase (600380-52) and PFU Ultra HF Reaction Buffer (200524-51).

Reagents for RNA isolation and transcriptomics studies were obtained from several sources like Ambion Life Technologies- Trizol (15596018), Sigma Aldrich- DEPC (D5758), MMLV Reverse Transcriptase (M1427); Reverse Transcriptase Buffer (B8559), anchored oligo dT (O4387); Invitrogen – RNase Out (P/N 100000840), Takara – SYBR Green Master Mix (A46110).

Tritiated acetyl CoA was obtained from Perckin Elmer (NET2900).

Several miscellaneous reagents were procure from Sigma Aldrich, namely – D-Glucose (G7021), Oil Red-O (O625), Coomassie Brilliant Blue (B0149), Direct Blue

71 (212407), Sirius Red (35872), Picric Acid (197378), Corn Oil (C8267), acetyl CoA sodium salt (A2056), butyryl CoA lithium salt hydrate (B1508), insulin from bovine pancreas (16634), IBMX (15879), dexamethasone (D4902), BSA (A7906), gelatin from porcine skin (G1890), DMSO molecular biology grade (D8418), DMSO cell culture grade (D2650), PPO (D210404), POPOP (P3754), MTT (M5665), Freund's Complete Adjuvant (F5881) and Freund's Incomplete Adjuvant (F5506).

All acetylation specific antibodies had been previously in the laboratory. The butyrylation specific antibodies were obtained from PTM Biolabs- Pan Butyryl lysine (PTM-301), H3K9 Bu (PTM-305), H3K23 Bu (PTM-307), H3K27 Bu (PTM-315), H4K5 Bu (PTM-313), H4K8 Bu (PTM-311) and H2K12 Bu (PTM-314).

Table 1: List of primers used for gene expression analysis

	Gene	Primer Sequence (5' to 3')
1)	Actin Fwd	CCACTGTCGAGTCGCGTCC
2)	Actin Rev	GTCATCCATGGCGAACTGGTG
3)	Pparg Fwd	TCCGTGATGGAAGACCACTC
4)	Pparg Rev	CCCTTGCATCCTTCACAAGC
5)	Cebpd Fwd	ATCGACTTCAGCGCCTACAT
6)	Cebpd Rev	GCTTTGTGGTTGCTGTTGAA
7)	aP2 Fwd	TCTCCAGTGAAAACCTTCGAT
8)	aP2 Rev	TTACGCTGATGATCAATGTT
9)	Slc2a4 Fwd	ACGACGGACTCCATCTGTTG
10)	Slc2a4 Rev	GGAGACATAGCTCATGGCTGGAA
11)	Lep Fwd	GAGCGGGATCAGGTTTTGTGGT
12)	Lep Rev	TGTCACTCTTTCCCGGTCTCTTCA
13)	Adipoq Fwd	CAGTGGATCTGACGACACCAA
14)	Adipoq Rev	GAACAGGAGAGCTTGCAACAGT
15)	Cebpa Fwd	TACCGAGTAGGGGGAGCAAA
16)	Cebpa Rev	TCATTTTTCTCACGGGGCCA
17)	TEAD4 Fwd	GCCACAGCCTTCCACAGTAA
18)	TEAD4 Rev	AAGCTCCTTGCCAAAACCCT
19)	Kdm4c Fwd	CAGTGCGGAACAAGTCTTCCAA
20)	Kdm4c Rev	CAGATGTTTCTGCGCCGCT
21)	Fasn Fwd	GGGTGTGAGTGGTTCAGAGG
22)	Fasn Rev	AGGGCAATGCTTGGTCCTTT
23)	Acsc2 Fwd	TCGGAACCTTGATGCGATGGG
24)	Acsc2 Rev	TTTCCCCAAAACCTCCCGTGG
25)	Ucp1 Fwd	GGGCCCTTGTAACAACAAA
26)	Ucp1 Rev	GTCGGTCCTTCCTTGGTGTA
27)	Prdm16 Fwd	AGGGCAAGAACCATTACACG
28)	Prdm16 Rev	AGAGGTGGTCGTGGGTACAG
29)	Cox5a Fwd	TGTCTGTTCCATTCGCTGCT
30)	Cox5a Rev	AACCGTCTACATGCTCGCAA
31)	Nrip1 Fwd	ATCGAAAGCCCCAGTACCAA
32)	Nrip1 Rev	TTCTCGGCTTGGGACTCTTT

33)	Ppargc1a Fwd	TCAGAACCATGCAGCAAACC
34)	Ppargc1a Rev	TTGGTGTGAGGAGGGTCATC
35)	Cebpb Fwd	TGCGGGGTTGTTGATGTTTT
36)	Cebpb Rev	TGCTCGAAACGGAAAAGGTT
37)	Ppara Fwd	ACCTTGTGTATGGCCGAGAA
38)	Ppara Rev	AAGGAGGACAGCATCGTGAA
39)	Foxp1 Fwd	CACACTCTAGGGACATGGCA
40)	Foxp1 Rev	ATCTTCCATGGCCACTGTGA

Table 2: List of primers used for CHIP qRT-PCR analysis

	Gene	Primer Sequence (5' to 3')
1)	Pparg Fwd	AGCTCGATGACCATAAGCCT
2)	Pparg Rev	ATAGGCAGTGCATCAGCGAA
3)	Lep Fwd	AGGTCATGTGGACAGCTTGG
4)	Lep Rev	CGTCCAGCCTTGCTTTTTCC
5)	Cebpd Fwd	CGCTTTTCAGCCTGGACAG
6)	Cebpd Rev	TGGAGTCAATGTAGGCGCTG